The Role of ASPP2 in Intestinal Homeostasis and Tumourigenesis

Xiao Qin

St. Cross College
University of Oxford

A thesis submitted for the degree of
Doctor of Philosophy

Trinity 2017

Abstract

The intestinal epithelium represents one of the most actively renewing tissues in the body, and is widely used as a model system to study epithelial cell biology. ASPP2, a member of the ASPP (apoptosis stimulating protein of p53) protein family, has been shown to act as a regulator of epithelial cell polarity and tumour suppressor. This study investigated whether the dual function of ASPP2 is involved in the regulation of intestinal homeostasis and tumourigenesis, with a particular interest in the distinction between epithelial cell autonomous and non-autonomous mechanisms.

Germline and intestinal epithelial cell-specific ASPP2 conditional knockout mice were employed in this study. Deficiency of ASPP2 in the intestinal epithelium resulted in delayed recovery from dextran sulfate sodium (DSS)-induced acute colitis, concurrent with a reduction in the expression of proinflammatory cytokines such as interleukin (IL)-1β and IL-6. Moreover, ASPP2-deficient mice showed increased susceptibility to Azoxymethane/DSS-induced colorectal tumourigenesis. While wild-type and ASPP2-deficient crypts showed similar incidence of tumour formation, the local immune microenvironment of ASPP2-deficient mice favoured tumour progression.

The intestinal organoid culture was established to supplement *in vivo* experiments. The feasibility of the system was demonstrated with small intestinal organoids, in the context of proliferation, differentiation, and cell death. Using the established workflow, a colonic organoid-based tissue regeneration model was developed. The intrinsic susceptibility of organoids to DSS-induced cell death was not affected by the loss of ASPP2. However, ASPP2-deficient colonic organoids were less responsive to the pro-proliferative effects of IL-6, but were more sensitive to tumour necrosis factor-α-induced cell death in the presence of IL-22.

In conclusion, this project undertook parallel examinations of animal models and organoids, demonstrating that a deficiency of ASPP2 in the intestinal epithelium results in dysregulated epithelial–immune cell interactions. This may partially explain the pathological conditions observed in ASPP2-deficient mice. Importantly, this study highlights the possibility of using organoids to investigate epithelial cell non-autonomous factors implicated in intestinal pathogenesis.

The Role of ASPP2 in Intestinal Homeostasis and Tumourigenesis



Xiao Qin

St. Cross College

University of Oxford

A thesis submitted for the degree of

Doctor of Philosophy

Trinity 2017

Declaration

This thesis is submitted to the University of Oxford in support of my application for the degree of Doctor of Philosophy in Clinical Medicine. The work described herein was performed while I was a graduate student at the Ludwig Institute for Cancer Research, under the supervision of Professor Xin Lu. All the work presented in this thesis is the result of my own work unless otherwise stated and has not been submitted in any previous application for any degree.

Acknowledgements

The work presented in this thesis would not have been possible without the inspiration and support of many people. It has been a long (and at times daunting) journey, but after all turned out unexpectedly fulfilling.

First of all, I would like to express my gratitude to my supervisor, Professor Xin Lu, who offered me invaluable guidance and encouragement over the years. I must also take this opportunity to thank the China Scholarship Council and the Nuffield Department of Clinical Medicine, to whom I am grateful for the opportunity to study at the University of Oxford.

I would like to thank Professor Fiona Powrie and Professor Simon Leedham, who were examiners for my transfer and confirmation of status examinations. Their kind advice and words of encouragement were truly appreciated.

I must also give credit to the lab support team of the Ludwig Institute for Cancer Research, as well as the animal facility at the Wellcome Trust Centre for Human Genetics. Special thanks are due to Mark Shipman for assistance with microscopy and image analysis, and Indrika Ratnayaka for histological sample preparation. I would also like to thank Veronica Counsell and Alexandra Ward for their day-to-day help with all the paper work. A special acknowledgement goes to Mary Muers and Claire Beveridge for their critical input into the thesis.

Big thanks are owed to all my past and present colleagues, in particular Ludovico Buti, Sofia Koch, Felix Zhou, Carlos Ruiz Puig, Elizabeth Slee, Zinaida Dedeić, Stefanie Žentelis, Kathryn Chung, Khatoun Al Moussawi, Imogen Roth, James Chan, and Paul Miller, for being incredibly helpful both inside and out of the lab. Special thanks go to Jingyi Ma, with whom I shared the most memories of my time in Oxford.

It is a pleasure to thank all my other friends outside the lab, particularly Pakavarin Louphrasitthiphol, Chen-Yi Wang, Hubert Lam, Sizhu Lu, Min Sun, Si Yuen Lee, George Qian, Ping Zhang, and Ruiying Li, for the time we spent together and their heartfelt joy and love. I am greatly in debt to Carol Leung, from whom I learnt a lot about friendship and the inspirational nature of science. I am also genuinely thankful to Jingyu Zhang and Xiang Yu, for always being there as my most trustworthy friends.

Last but never least, I wish to convey my deepest gratitude to my family, who have made every effort to understand my life and work from so far away. Whatever I achieve in my life, I owe it all to them.

Abstract

The intestinal epithelium represents one of the most actively renewing tissues in the body, and is widely used as a model system to study epithelial cell biology. ASPP2, a member of the ASPP (apoptosis stimulating protein of p53) protein family, has been shown to act as a regulator of epithelial cell polarity and tumour suppressor. This study investigated whether the dual function of ASPP2 is involved in the regulation of intestinal homeostasis and tumourigenesis, with a particular interest in the distinction between epithelial cell autonomous and non-autonomous mechanisms.

Germline and intestinal epithelial cell-specific ASPP2 conditional knockout mice were employed in this study. Deficiency of ASPP2 in the intestinal epithelium resulted in delayed recovery from dextran sulfate sodium (DSS)-induced acute colitis, concurrent with a reduction in the expression of proinflammatory cytokines such as interleukin (IL)-1β and IL-6. Moreover, ASPP2-deficient mice showed increased susceptibility to Azoxymethane/DSS-induced colorectal tumourigenesis. While wild-type and ASPP2-deficient crypts showed similar incidence of tumour formation, the local immune microenvironment of ASPP2-deficient mice favoured tumour progression.

The intestinal organoid culture was established to supplement *in vivo* experiments. The feasibility of the system was demonstrated with small intestinal organoids, in the context of proliferation, differentiation, and cell death. Using the established workflow, a colonic organoid-based tissue regeneration model was developed. The intrinsic susceptibility of organoids to DSS-induced cell death was not affected by the loss of ASPP2. However, ASPP2-deficient colonic organoids were less responsive to the pro-proliferative effects of IL-6, but were more sensitive to tumour necrosis factor-α-induced cell death in the presence of IL-22.

In conclusion, this project undertook parallel examinations of animal models and organoids, demonstrating that a deficiency of ASPP2 in the intestinal epithelium results in dysregulated epithelial–immune cell interactions. This may partially explain the pathological conditions observed in ASPP2-deficient mice. Importantly, this study highlights the possibility of using organoids to investigate epithelial cell non-autonomous factors implicated in intestinal pathogenesis.

Contents

List of Figures viii

List of Tables xi

List of Abbreviations xii

1 Introduction 1

1.1 Intestinal Homeostasis 1

1.1.1 The intestinal epithelium: structure and function 1

1.1.2 Signalling pathways in intestinal homeostasis 3

1.1.3 Cell turnover in the intestine 7

1.1.4 Intestinal tissue regeneration 9

1.2 Inflammation in the Intestine 12

1.2.1 The intestinal microenvironment 12

1.2.2 Innate and adaptive immunity of the intestine 14

1.2.3 Inflammatory bowel diseases 19

1.3 Tumourigenesis in the Intestine 19

1.3.1 Genetics of colorectal cancer 19

1.3.2 Colitis-associated colorectal cancer 24

1.3.3 Inflammatory networks underlying colorectal cancer 25

1.4 The Intestinal Organoid 27

1.4.1 Organoids: a brief history 27

1.4.2 Organoids in the study of intestinal physiology 29

1.4.3 Organoids as a model for human diseases 31

1.5 ASPP2 - A Key Regulator of Epithelial Cell Biology 34

1.5.1 The ASPP protein family 34

1.5.2 ASPP2 in tumourigenesis 36

1.5.3 ASPP2 in cell polarity and development 38

1.6 Aims of the Study 41

2 Materials and Methods **42**
2.1 Animal Work . . . 42
2.2 Tissue Culture and Cell-based Assays . . . 48
2.3 Primary Organoid Culture . . . 51
2.4 DNA and RNA Techniques . . . 58
2.5 Histology Techniques . . . 62
2.6 Biochemistry . . . 64
2.7 Antibodies . . . 71
2.8 Data Analysis . . . 74

3 Loss of ASPP2 Leads to Delayed Recovery from DSS-Induced Colitis **75**
3.1 Introduction . . . 75
3.2 Results . . . 77
3.2.1 DSS-induced colitis was not affected by the loss of ASPP2 in the intestinal epithelium . . . 77
3.2.2 ASPP2$^{\text{IEC-}\Delta\text{exon3}}$ mice showed delayed recovery from DSS-induced colitis . . . 81
3.2.3 ASPP2$^{\text{IEC-}\Delta\text{exon3}}$ mice showed reduced proliferation within regenerative crypts . . . 84
3.2.4 Hippo/YAP signalling was not affected by the loss of ASPP2 in the intestinal epithelium . . . 88
3.2.5 ASPP2 deficiency in the intestinal epithelium led to reduced expression of proinflammatory cytokines by LPMCs . . . 91
3.2.6 ASPP2$^{\Delta\text{exon3}}$ mice showed higher susceptibility to DSS-induced colitis than ASPP2$^{\text{IEC-}\Delta\text{exon3}}$ mice . . . 93
3.3 Summary and Brief Discussion . . . 95

4 ASPP2 Deficiency Predisposes Mice to Colorectal Tumourigenesis **98**
4.1 Introduction . . . 98
4.2 Results . . . 100
4.2.1 ASPP2$^{\text{IEC-}\Delta\text{exon3}}$ mice showed increased susceptibility to AOM/DSS-induced tumourigenesis . . . 100
4.2.2 Wild-type and ASPP2$^{\text{IEC-}\Delta\text{exon3}}$ crypts showed similar incidence of colorectal tumour initiation . . . 103
4.2.3 ASPP2$^{\text{IEC-}\Delta\text{exon3}}$ and wild-type tumours showed similar levels of proliferation and apoptosis . . . 106
4.2.4 The Wnt/β-catenin pathway was not affected by the loss of ASPP2 in the intestinal epithelium . . . 108

4.2.5 ASPP2$^{\text{IEC-}\Delta\text{exon3}}$ mice showed decreased phosphorylation of YAP at Ser127 in AOM/DSS-induced colorectal tumours . . 110
4.2.6 Tumours developed in ASPP2$^{\text{IEC-}\Delta\text{exon3}}$ mice showed increased ERK phosphorylation 112
4.2.7 Loss of ASPP2 in the intestinal epithelium resulted in a local immune microenvironment favouring tumour progression . . 116
4.2.8 ASPP2$^{\Delta\text{exon3}}$ mice were not more susceptible to AOM/DSS-induced tumourigenesis than wild-type mice 119
4.3 Summary and Brief Discussion 120

5 Organoids as a Model System to Study Intestinal Biology 124
5.1 Introduction 124
5.2 Results 126
5.2.1 ASPP2-deficient organoids recapitulated epithelial hyperproliferation observed *in vivo* 126
5.2.2 Loss of ASPP2 predisposed IECs to the secretory lineage . . 129
5.2.3 Organoids as an *ex vivo* system to study cell death 133
5.2.4 ASPP2-deficient colonic organoids showed increased expression of stem cell markers 137
5.2.5 Development of a colonic organoid-based tissue regeneration model 139
5.2.6 Colorectal tumour organoids as a supplement to *in vivo* tumour characterisation 144
5.3 Summary and Brief Discussion 146

6 Discussion and Future Perspectives 149
6.1 ASPP2: A Putative Role in the Restoration of Intestinal Barrier Function 149
6.2 ASPP2: At the Crossroad of Tumour Initiation and Progression . . 153
6.3 Organoids: A Potential Tissue Surrogate 157

References 161

List of Figures

1.1 Structure and cell turnover of the intestinal epithelium 2
1.2 WNT signalling pathways 4
1.3 BMP signalling pathways 7
1.4 Tissue restitution and regeneration 10
1.5 The Hippo/YAP pathway 12
1.6 Schematic overview of intestinal homeostasis 13
1.7 Breakdown of the intestinal barrier 15
1.8 Canonical and non-canonical NF-κB pathways 16
1.9 Common genetic alterations in SCC 20
1.10 Common genetic alterations in CAC 24
1.11 Pathways activating STAT3 signalling in cancer 27
1.12 The intestinal organoid culture system 28
1.13 The ASPP family of proteins 35
1.14 ASPP2 in the intestinal epithelium 40

3.1 EYFP positivity is an indicator of ASPP2 depletion in the Villin-CreER, ASPP2$^{\text{exon3-fl/fl}}$ mouse model 78
3.2 ASPP2$^{\text{IEC-}\Delta\text{exon3}}$ mice were equally susceptible to DSS-induced colitis as wild-type controls 80
3.3 ASPP2$^{\text{IEC-}\Delta\text{exon3}}$ mice showed delayed recovery after DSS treatment 82
3.4 ASPP2$^{\text{IEC-}\Delta\text{exon3}}$ mice showed delayed restoration of intestinal permeability 83
3.5 ASPP2$^{\text{IEC-}\Delta\text{exon3}}$ mice showed higher histological scores during recovery than wild-type animals 85
3.6 ASPP2$^{\text{IEC-}\Delta\text{exon3}}$ crypts were less proliferative than wild-type crypts 87
3.7 ASPP2$^{\text{IEC-}\Delta\text{exon3}}$ crypts showed a similar level of apoptosis as wild-type crypts 88
3.8 ASPP2 interacts with and dephosphorylates YAP 89
3.9 Hippo/YAP signalling was not affected by the loss of ASPP2 90
3.10 LPMCs of wild-type mice expressed higher levels of proinflammatory cytokines than those of ASPP2$^{\text{IEC-}\Delta\text{exon3}}$ mice 92
3.11 ASPP2$^{\Delta\text{exon3}}$ mice showed increased susceptibility to DSS-induced intestinal barrier breakdown 93

3.12 ASPP2$^{\Delta exon3}$ mice showed higher histological scores than ASPP2$^{IEC\text{-}\Delta exon3}$ animals 94

4.1 ASPP2$^{IEC\text{-}\Delta exon3}$ mice showed increased susceptibility to AOM/DSS treatment 101
4.2 AOM/DSS treatment induced colorectal tumourigenesis 102
4.3 ASPP2$^{IEC\text{-}\Delta exon3}$ mice showed increased tumour loads 103
4.4 ASPP2$^{IEC\text{-}\Delta exon3}$ crypts showed similar incidence of colon tumour formation as wild-type crypts 105
4.5 Tumours developed in ASPP2$^{IEC\text{-}\Delta exon3}$ mice showed similar levels of proliferation as those of wild-type animals 107
4.6 Tumours developed in ASPP2$^{IEC\text{-}\Delta exon3}$ mice showed similar levels of apoptosis as those of wild-type animals 108
4.7 Loss of ASPP2 in the intestinal epithelium did not affect cellular localisation of β-catenin 109
4.8 ASPP2$^{IEC\text{-}\Delta exon3}$ tumours showed reduced YAP activity 111
4.9 Loss of ASPP2 in IECs resulted in upregulated ERK phosphorylation in AOM/DSS-induced tumours 113
4.10 Loss of ASPP2 in IECs resulted in upregulated ERK phosphorylation in regenerative colonic epithelium 115
4.11 Loss of ASPP2 in IECs resulted in increased macrophage infiltration 117
4.12 ASPP2$^{IEC\text{-}\Delta exon3}$ mice showed increased presence of Tregs in the lamina propria 118
4.13 ASPP2$^{\Delta exon3}$ mice showed similar susceptibility to AOM/DSS-induced tumourigenesis as wild-type animals 119

5.1 Loss of ASPP2 in duodenal epithelial cells resulted in hyperproliferation 127
5.2 ASPP2-deficient small intestinal organoids showed increased proliferation 128
5.3 VPA/CHIR99021 treatment led to the expansion of the Lgr5^{+} stem cell population 131
5.4 Loss of ASPP2 predisposed intestinal epithelial cells to the secretory lineage 132
5.5 Loss of ASPP2 in duodenal epithelial cells led to increased apoptosis 134
5.6 Necroptosis occurs in intestinal organoids 135
5.7 DSS induces apoptosis and necroptosis in organoids 136
5.8 Stem cell markers were upregulated in ASPP2-deficient colonic crypts and organoids 138
5.9 ASPP2-deficient epithelial cells were overtaken by wild-type cells in colonic organoids 139

5.10 Establishment of a colonic organoid-based tissue regeneration model 140
5.11 DSS-induced cell death and recovery in colonic organoids 141
5.12 Effects of IL-22 treatment on organoid growth 143
5.13 Colorectal tumour organoids retained physiologically relevant morphology 144
5.14 Characterisation of STAT3 phosphorylation in colorectal tumours and tumour organoids 145

6.1 Epithelial cell autonomous and non-autonomous regulation of STAT3 signalling 153
6.2 Proposed model for the involvement of epithelial ASPP2 in colorectal tumourigenesis 156
6.3 Establishment of organoid-based co-culture systems 159

List of Tables

1.1 Sensors and Activators of Regenerative Inflammation 18
1.2 Regeneration-inducing Cytokines and Their Effectors 18
1.3 Consensus Molecular Subtypes of CRC 20

2.1 Disease Activity Index (DAI) Score 46
2.2 Histological Scoring System for Colitis 47
2.3 List of Plasmids 49
2.4 Reagents Used in the Establishment of Intestinal Organoids 51
2.5 PCR Programme for Mouse Genotyping 59
2.6 PCR Primers for Genotyping 59
2.7 Primers for Real-time Quantitative PCR 60
2.8 Real-time qPCR Reaction System 61
2.9 Real-time qPCR Programme 61
2.10 SDS-Polyacrylamide Gels 67
2.11 Primary Antibodies 71
2.12 Secondary Antibodies 73

List of Abbreviations

3D . . . . . Three-dimensional

4-OHT 4-hydroxytamoxifen

AMP . . . . . Antimicrobial peptide/protein

AOM . . . . . Azoxymethane

AP-1 . . . . . Activator protein 1

APC . . . . . Adenomatous polyposis coli/Anaphase-promoting complex

ASC . . . . . Adult stem cell

ASPP . . . . . Ankyrin repeat, SH3 domain, and proline-rich containing protein

BMP . . . . . Bone morphogenetic proteins

CAC . . . . . Colitis-associated colorectal cancer

CD . . . . . Crohn's disease

CF . . . . . Cystic fibrosis

CFTR . . . . . Cystic fibrosis transmembrane conductance regulator

CK1 . . . . . Casein kinase 1

CRC . . . . . Colorectal cancer

DAPI . . . . . 4',6-diamidino-2-phenylindole

DIC . . . . . Differential interference contrast

DSS . . . . . Dextran sulfate sodium

EdU . . . . . 5-ethynyl-2'-deoxyuridine

EGF . . . . . Epidermal growth factor

EGFR . . . . . Epidermal growth factor receptor

ENR . . . . . EGF, Noggin and R-spondin

ERK . . . . . Extracellular signal-regulated protein kinase

EYFP . . . . . Enhanced yellow fluorescent protein

FITC . . . . . Fluorescein isothiocyanate

GPCR . . . . . G protein-coupled receptor

H&E . . . . . Haematoxylin and Eosin

IBD . . . . . Inflammatory bowel disease

IEC . . . . . Intestinal epithelial cell

IEL . . . . . Intraepithelial lymphocyte

IF . . . . . Immunofluorescent

IFN . . . . . Interferon

IHC . . . . . Immunohistochemical

IKK . . . . . IκB kinase

IL . . . . . Interleukin

IP . . . . . Immunoprecipitation

IQR . . . . . Interquartile range

ISC . . . . . Intestinal stem cell

Lgr5 . . . . . Leu-rich repeat-containing G protein-coupled receptor 5

LPMC . . . . . Lamina propria mononuclear cell

LPS . . . . . Lipopolysaccharide

MAMP . . . . Microbe-associated molecular patterns

MAPK . . . . Mitogen-activated protein kinase

MMR . . . . . Mismatch repair

MSI . . . . . Microsatellite instability

MTT . . . . . 3-(4,5-dimethylthiazol-2-yl)-2,5-diphenyltetrazolium bromide

Nec-1s Necrostatin-1s

NF-κB . . . . . Nuclear factor-κB

NICD . . . . . Notch intracellular domain

Olfm4 . . . . . Olfactomedin-4

PFA . . . . . Paraformaldehyde

PP1 . . . . . Protein phosphatase 1

qPCR . . . . . Real-time quantitative PCR

SCC . . . . . Sporadic colorectal cancer

SDS . . . . . Sodium dodecyl sulfate

SDS-PAGE . . SDS-polyacrylamide gel electrophoresis

SEM . . . . . Standard error of the mean

SFK . . . . . Src family kinase

STAT . . . . . Signal transducer and activator of transcription

TA cell . . . . Transit-amplifying cell

TGF-β . . . . . Transforming growth factor-β

TNF . . . . . Tumour necrosis factor

Treg . . . . . Regulatory T cell

TUNEL . . . . Terminal deoxynucleotidyl transferase dUTP nick end labelling

UC . . . . . Ulcerative colitis

VPA . . . . . Valproic acid

YAP . . . . . Yes-associated protein

Z-VAD . . . . Z-VAD-fmk

1 Introduction

1.1 Intestinal Homeostasis

1.1.1 The intestinal epithelium: structure and function

The primary functions of the intestine include digestion, the absorption of nutrients, secretion, and immune responses. All segments of the intestine are composed of four tissue layers; from the outermost inwards are the serosa, the muscularis propria, the submucosa and the mucosa. Of the four, the mucosa is structurally and functionally the most important, and it is made up of three layers. The outermost is called the muscularis mucosae, on top of which is the lamina propria. The innermost layer facing the intestinal lumen is made up of a single layer of epithelial cells and is called the intestinal epithelium.

The intestinal epithelium constitutes the largest interface between the host and the environment. The intestinal tract can be divided into the colon and the small intestine, with the latter further divided into three parts: the duodenum, the jejunum, and the ileum. Morphologically, the small intestinal epithelium is characterised by its finger-shaped protrusions called villi and flask-like invaginations called crypts, which substantially increase the surface area of the epithelium and therefore its absorptive capacity. In contrast, the colonic epithelium only has crypts and villi are replaced by a flat-surfaced epithelium (Figure 1.1, A and B). In both

the small intestine and the colon, the surface area of the epithelium is further increased by the presence of microvilli on the epithelial brush border.

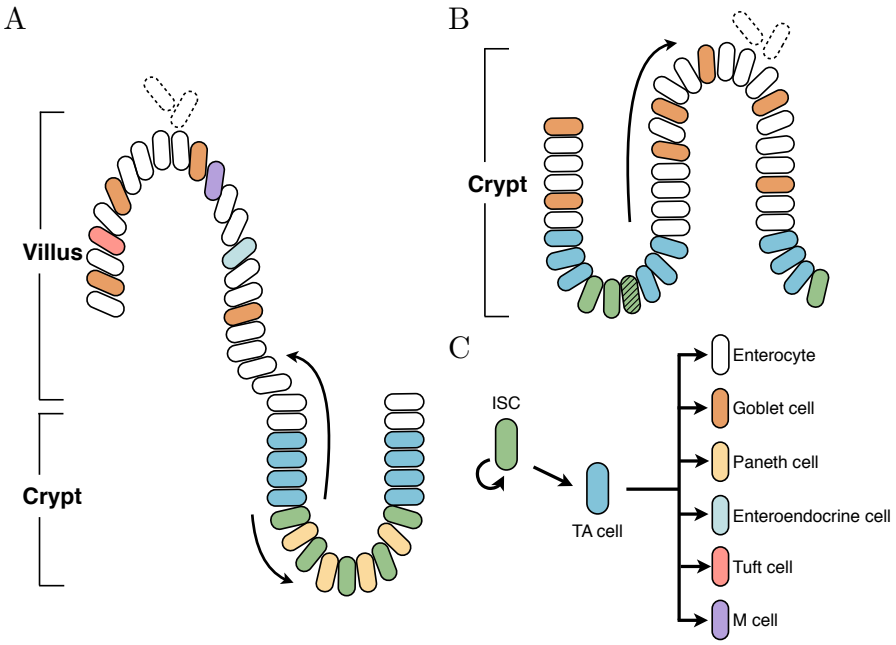


Figure 1.1: Structure and cell turnover of the intestinal epithelium. (A) Schematic illustration of the small intestinal epithelium, featured by the highly specialised structures of the villus and the crypt. Differentiated cells are distributed along the crypt–villus axis. While Paneth cells migrate downwards to the bottom of crypts, other differentiated cell types move upwards. Once they reach the tip of the villus, the cells are shed into the intestinal lumen and undergo anoikis due to the lack of attachment. (B) Schematic illustration of the colonic epithelium, in which the structure of villus is absent. Paneth cells are also absent in the colon, but deep crypt secretory cells (stripped) have been proposed to be the colon equivalent of Paneth cells (Sasaki et al. 2016). (C) Schematic overview of cell lineage commitment in the intestinal epithelium. Intestinal stem cells (ISCs) reside in the bottom of crypts and give rise to transit-amplifying (TA) cells, which differentiate into functionally distinct cell lineages, mainly including enterocytes, goblet cells, Paneth cells, enteroendocrine cells, tuft cells and M cells.

In the small intestine, the epithelium is simple, columnar, and composed of four major cell types (Figure 1.1C). The absorptive lineage comprises enterocytes, and the secretory lineage includes goblet cells, enteroendocrine cells, tuft cells, and Paneth cells. Enterocytes are the most abundant cell type present in the intestinal epithelium and are specialised for nutrient absorption. Goblet cells secrete mucus, which lubricates the epithelial surface and constitutes a protective barrier against the contents of the intestinal lumen (Specian et al. 1991). Enteroendocrine cells

of the intestine constitute an enteric endocrine system and produce a variety of hormones, such as serotonin and secretin (Rehfeld 1998). Tuft cells represent a small population within the small intestinal epithelium. In the presence of parasitic infection, tuft cells secret interleukin (IL)-25 and regulate type 2 immune responses (Gerbe et al. 2016). Lastly, Paneth cells are a source of anti-microbial compounds such as lysozyme and defensins, which are critical for the regulation of host–microbe interactions (Bevins et al. 2011). Together with mesenchymal, vascular, neural and hematopoietic cells, Paneth cells function as a critical component of the ISC niche, which is essential for the maintenance of the ISC pool (Morrison et al. 2008). Enterocytes and goblet cells are also present in the colonic epithelium.

1.1.2 Signalling pathways in intestinal homeostasis

Under normal conditions, the homeostasis of the intestine is maintained by an orchestrated network of signalling pathways. The biological processes involved include stem cell activity, TA cell proliferation, cell lineage determination, terminal differentiation, and cell death (Sancho et al. 2004). The Wnt, Notch, BMP, and Hedgehog pathways are essential for the development and homeostatic control of the intestinal epithelium.

Wnt signalling

The canonical Wnt signalling pathway is highly conserved across a wide range of species and plays critical roles in embryonic development and adult tissue homeostasis (Mah et al. 2016). In the absence of Wnt, a destruction complex consisting of glycogen synthase kinase 3 (GSK3), Anaphase-promoting complex (APC), casein kinase 1 (CK1) and Axin phosphorylates cytoplasmic β-catenin and targets it for proteasomal degradation (Clevers et al. 2014; Figure 1.2A). Wnt ligands act as short-range signals to induce the inhibition of the GSK3/APC/Axin/CK1 destruction complex, leading to the stabilisation of β-catenin in the cytoplasm (Farin et al. 2016; Clevers et al. 2014). The accumulated β-catenin will eventually translocate into the nucleus and activate transcriptional programs together with the T cell factor/lymphoid-enhancing factor (TCF/LEF) family transcription factors

(Daniels et al. 2005; Figure 1.2B). It is worth noting that non-canonical Wnt signalling also plays critical roles in development and tissue regeneration, via the regulation of transcription factors such as nuclear factor of activated T cells (NFAT) and activator protein 1 (AP1), as outlined in Figure 1.2C.

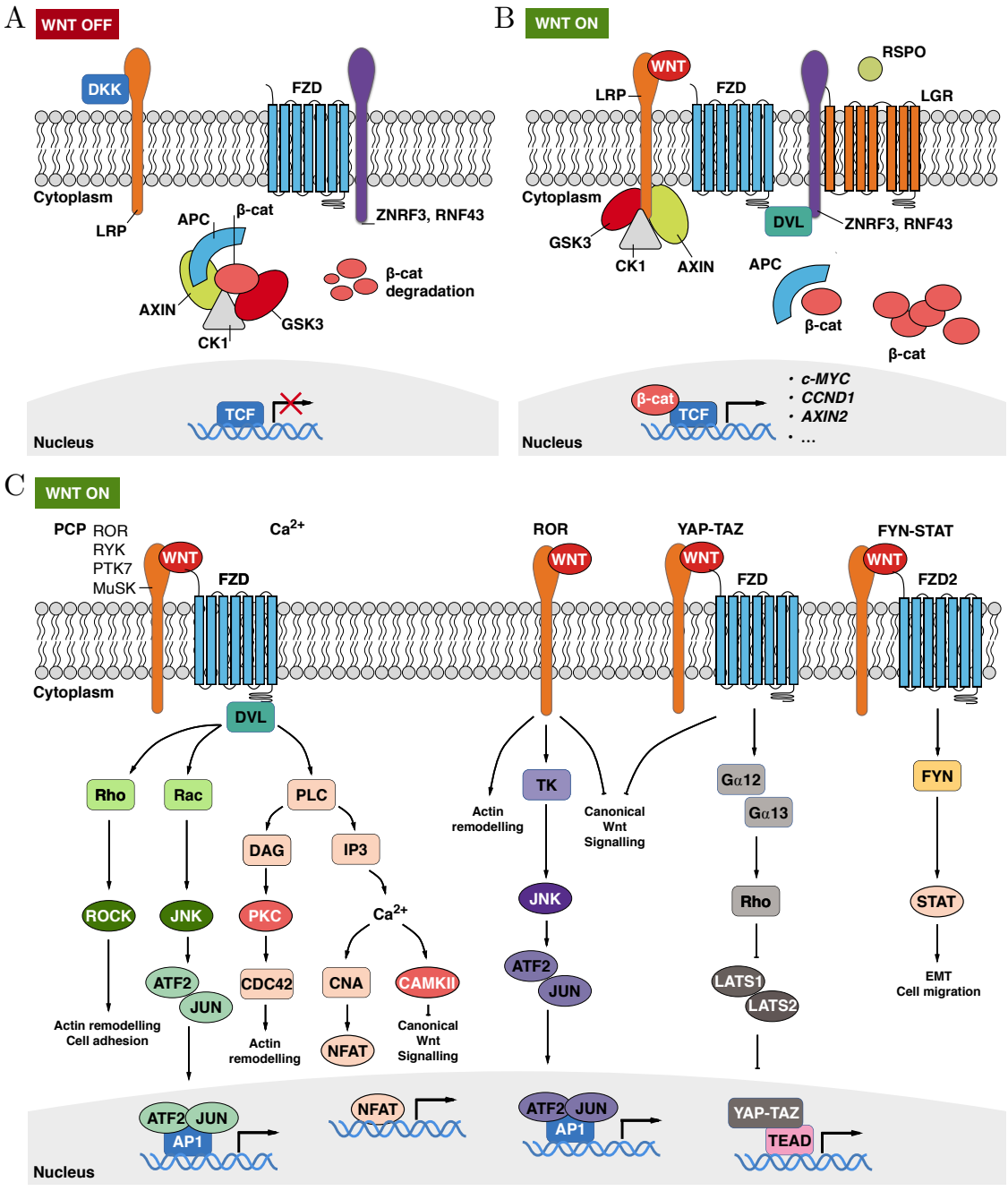


Figure 1.2: WNT signalling pathways

Wnt signalling pathways (adapted from Murillo-Garzón et al. 2017). (A) In the absence of Wnt ligands, β-catenin (β-cat) is targeted for proteasomal degradation by the GSK3/APC/Axin/CK1 destruction complex and the expression of Wnt target genes are repressed. (B) In canonical Wnt signalling, binding of Wnt ligands to frizzled (FZD) and either low-density lipoprotein receptor (LRP) 5 or LRP6 leads to stabilisation of β-catenin and activation of Wnt target genes, including c-MYC, CCND1, and AXIN2. ZNRF3 and RNF43 are transmembrane E3 ubiquitin ligases that inhibit Wnt signalling by targeting FZD for proteasomal degradation. (C) Non-canonical Wnt signalling activates small GTPases and various kinases, mobilises Ca^{2+}, and activates NFAT and AP1 family transcription factors. YAP and TAZ, the tyrosine protein kinase FYN and signal transducer and activator of transcription (STAT) family proteins are also activated by non-canonical Wnt signalling. CK1, casein kinase 1; DVL, dishevelled; EMT, epithelial–mesenchymal transition; GSK3, glycogen synthase kinase 3; LGR, leucine-rich repeat-containing G protein-coupled receptors; MuSK, muscle, skeletal receptor tyrosine-protein kinase; PCP, planar cell polarity; ROR, tyrosine protein kinase transmembrane receptor; RYK, tyrosine-protein kinase; PTK7, protein-tyrosine kinase 7.

Various *in vivo* evidence has implicated Wnt signalling in the proliferation of intestinal progenitor cells and the maintenance of the stem cell population (Pinto et al. 2003). Defective Wnt signalling resulting from either deletion of epithelial β-catenin in the intestine or overexpression of the Wnt inhibitor Dickkopf-1 (Dkk-1) leads to depletion of the proliferative cell compartment (Kuhnert et al. 2004; Ireland et al. 2004). The Wnt signalling is also required for the correct allocation of different intestinal cell lineages along the crypt–villus axis, partially via modulation of the expression of EphB (erythropoietin-producing human hepatocellular receptor B) and ephrinB (Eph family receptor interacting protein B) (Batlle et al. 2002).

Notch signalling

Notch is an evolutionarily conserved master regulator of tissue patterning and cell fate commitment (Artavanis-Tsakonas et al. 1999). It is activated when Notch ligands bind to their receptors on adjacent cells, leading to proteolytic cleavage of the receptor and translocation of the Notch intracellular domain (NICD) into the nucleus (Hori et al. 2013). There, NICD binds to the transcription factor CSL (CBF1–Suppressor of Hairless–Lag1) and activates target gene transcription (Mumm et al. 2000).

Several Notch target genes have been implicated in intestinal cell fate commitment, including Hes-1 (hairy and enhancer of split-type protein 1) and its downstream transcription factor Math1 (Jensen et al. 2000; Yang et al. 2001). Given that all the intestinal cell lineages arise from a common stem cell population, the mechanisms underlying cell proliferation and cell fate determination must be coordinated (Sancho et al. 2004). Indeed, along the crypt–villus axis, Notch-activated cells in the Wnt-activated tissue compartment give rise to enterocytes, whereas inactivation of Notch leads to secretory lineage differentiation (Nakamura et al. 2007).

BMP signalling

Bone morphogenetic proteins (BMPs) belong to the transforming growth factor-β (TGF-β) cytokine family. Depending on the cellular context, the BMP signalling is involved in a variety of biological processes, including differentiation, apoptosis and cell growth (Vanuytsel et al. 2013; R. N. Wang et al. 2014; Figure 1.3).

Notably, the BMP pathway has been shown to be intricately implicated in epithelial–stromal interactions, especially in the establishment and maintenance of the ISC niche (A. Tian et al. 2014). Mechanistically, BMP inhibits the stemness of Lgr5-positive stem cells through SMAD-mediated recruitment of the histone deacetylase HDAC1, thereby suppressing the expression of a number of stem cell signature genes, including Lgr5 (Qi et al. 2017). A disruption of the homeostatic intestinal BMP gradients results in intestinal epithelial cells acquiring stemness outside the ISC niche, as is demonstrated with a transgenic mouse model of GREM1, a mesenchymal BMP antagonist. This observation also implies the involvement of the BMP signalling in colonic tumourigenesis (Davis et al. 2014).

Hedgehog signalling

The Hedgehog family of secreted morphogenetic proteins is widely used by mammals to control differentiation and tissue patterning. There are three Hedgehog homologues, sonic hedgehog (Shh), indian hedgehog (Ihh), and desert hedgehog (Dhh) (Brink 2007). In the absence of Hedgehog ligands, the activity of the transmembrane

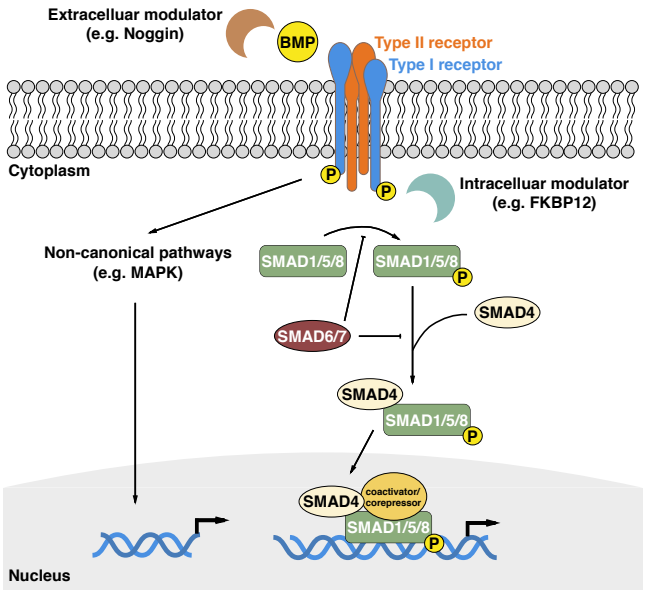


Figure 1.3: BMP signalling pathways. BMPs signal through the canonical, SMAD-dependent pathway and non-canonical pathways. In the canonical pathway, binding of BMPs to type I and II Ser/Thr kinase receptors initiates the signal transduction cascade. The type I receptor gets phosphorylated by the type II receptor, and in turn phosphorylates the receptor-regulated SMADs (SMAD1/5/8). Phosphorylated SMAD1/5/8 associates with the cooperating SMAD4 and translocates to the nucleus, where they interact with other coactivators or corepressors of transcription and regulate BMP target gene expression. In non-canonical BMP pathways, various signal pathways are activated, including the MAPK (mitogen-activated protein kinase) cascade. The BMP signalling is regulated by extracellular modulators such as Noggin and intracellular modulators such as FKBP12.

protein Smoothened (SMO) is inhibited by the Hedgehog receptor Patched (PTCH). Upon binding of Hedgehog proteins to PTCH, SMO is released and triggers a cascade of downstream events leading to the translocation of the Glioblastoma (GLI) transcription factors to the nucleus. There, they activate the expression of Hedgehog target genes and regulate the mesenchyme organisation (Vanuytsel et al. 2013). During the development of the small intestine, the combined signal between Shh and Ihh acts on the mesenchyme and contributes to the establishment and organisation of the crypt–villus axis (Madison et al. 2005).

1.1.3 Cell turnover in the intestine

The intestinal epithelium is the fastest self-renewing tissue compartment in mammals, both under steady-state conditions and in response to tissue damage. The homeostasis of the intestinal epithelium is maintained by a fine-tuned balance

between cell proliferation, differentiation, and cell death. Epithelial turnover occurs every 3–5 days in the small intestine and 5–7 days in the colon (Barker 2013).

Most of the differentiated cells in the small intestine are distributed along the villus, whereas Paneth cells only reside at the bottom of the crypt. Lgr5-positive ISCs are also located at the crypt base and are interspersed between Paneth cells (Barker et al. 2007). The remaining part of the crypt constitutes the proliferating progenitor compartment and harbours TA cells. TA cells spend around 2 days in the crypt, where they divide and differentiate into functionally distinct intestinal cell lineages (Flier et al. 2009). Newly differentiated Paneth cells move downwards and stay in the proliferative zone, whereas enterocytes and goblet cells migrate upwards along the crypt–villus axis (Flier et al. 2009). Once they reach the tip of the villus, the terminally differentiated epithelial cells will be shed into the lumen of the intestinal tract and undergo anoikis (Frisch et al. 1994).

The driving force of the intestinal renewal program is the ISC population, which is not a static entity but rather dynamic (Vermeulen et al. 2014). The working definition of a stem cell includes its capacity to self-renew and to differentiate into multiple cell lineages (Weiner 2008). Even with these criteria, the exact identity of the ISC population still remains unclear. It has been demonstrated that Lgr5-positive ($Lgr5^+$) crypt base columnar cells function as multipotent stem cells in both the small intestine and the colon (Barker et al. 2007). In support of that notion, a single $Lgr5^+$ stem cell can be propagated *in vitro* to form a fully differentiated crypt/villus-like structure, the organoid, suggesting that Lgr5 is a *bona fide* ISC marker (Sato et al. 2009). Lgr5 belongs to the Lgr family of G protein-coupled receptors (GPCRs). Together with Lgr4 and Lgr6, Lgr5 functions as a component of R-spondin receptors, thereby potentiating Wnt signals (Lau et al. 2014).

During the last decade, the application of lineage tracing techniques and mathematical modelling has greatly expanded our understanding of stem cell dynamics. The functionality of various ISC populations has been revealed, both under homeostasis conditions and conditions of tissue injury. The list of ISC markers includes, and may not be limited to, Lgr5, Ascl2, Olfm4, Rnf43, Znrf3, Smoc2,

Troy, Prom1, Sox9, Msi1, and Klf5 (Sailaja et al. 2016). Despite the fundamental importance of $Lgr5^+$ stem cells in the intestinal epithelium, genetic ablation of the $Lgr5^+$ population does not cause long-term defects in crypt homeostasis, suggesting the existence of reserve stem cell populations (H. Tian et al. 2011; Andersson-Rolf et al. 2017).

For a long time, the postulated quiescent stem cell populations were believed to be located at the +4 position in the crypt, with several +4 cell-specific markers being proposed (H. Tian et al. 2011; A. E. Powell et al. 2012). This hypothesis has been challenged by subsequent studies, since some of those markers are scattered along the crypt–villus axis and some are also expressed by $Lgr5^+$ stem cells (Muñoz et al. 2012). It was later demonstrated that, once the $Lgr5^+$ cell population is ablated, the +4 cells represent a population of Delta-like 1 (Dll1)-positive secretory progenitors that are able to dedifferentiate into a stem cell-like state (Buczacki et al. 2013). For example, Bmi1, a marker gene expressed by ISC and intestinal progenitor cells, labels a cell population that is quiescent under homeostasis but responsible for clonally repopulating the intestinal epithelium following radiation injuries (Sangiorgi et al. 2008; K. Yan et al. 2012). The potential of committed progenitor cells to be reprogrammed into stem cells is essential for epithelial regeneration in the intestine (Barker 2013; Andersson-Rolf et al. 2017).

1.1.4 Intestinal tissue regeneration

The intestinal epithelium is constantly confronted by a variety of environmental insults, such as acid, bacteria, and bacterial products (Podolsky 1999). In the event of intestinal tissue damage, a dynamic process of tissue repair is readily initiated, which requires epithelial restitution and regeneration (Taupin et al. 2003). Tissue restitution is the process that promotes the spreading and migration of epithelial cells, so that surface–cell continuity can be restored. Tissue regeneration, on the other hand, involves the proliferation and differentiation of epithelial cells followed by the remodelling of tissue architecture (Singer et al. 1999; Figure 1.4). It is worth noting that adaptive cellular reprogramming has also been proposed to be

responsible for tissue regeneration. In response to tissue damage, replacement cells were reprogrammed from differentiated cell types to compensate for the cell loss. This process is accompanied by the generation of transient cell states, known as repair cells, that promote the healing process (Jessen et al. 2015).

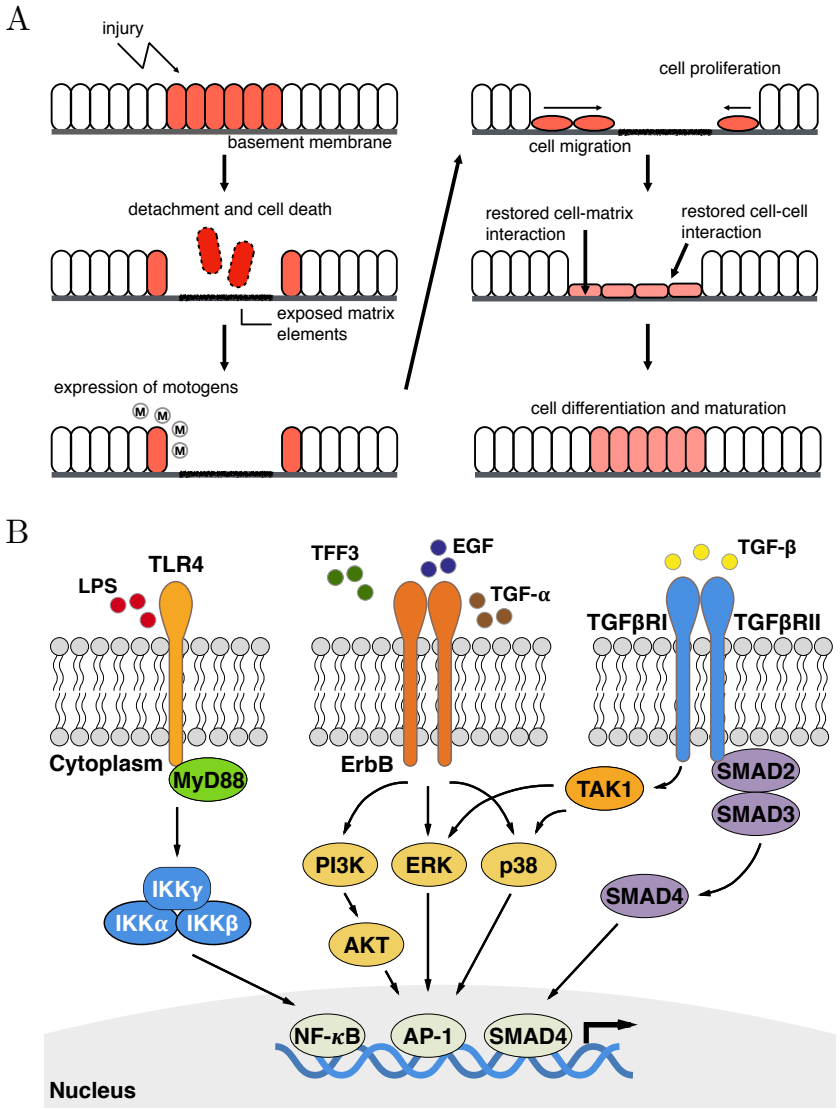


Figure 1.4: Tissue restitution and regeneration. (A) Schematic overview of tissue restitution and regeneration. Various injurious agents can cause epithelial cell death and detachment from the basement membrane, leaving the underlying matrix elements exposed to the environment. This results in a rapid release of migration-promoting agents (motogens; M) from adjacent epithelial and stromal cells, leading to the proliferation and migration of surviving epithelial cells. The process of tissue regeneration involves the restoration of epithelial continuity, i.e., cell–matrix and cell–cell interactions, supplemented by cell differentiation and maturation. (B) Signal pathways implicated in tissue restitution and regeneration.

Several evolutionarily conserved signalling pathways have been implicated in intestinal tissue regeneration. First and foremost is the MAPK–AP-1 (activator protein 1) pathway (Karin et al. 2016). In the mammalian intestine, epidermal growth factor receptor (EGFR) ligands regulate the proliferation and migration of ISCs through the activation of the MAPK cascade (Frey et al. 2004). Another signalling pathway that controls intestinal tissue integrity is the IKKβ (IκB kinase β)-dependent nuclear factor-κB (NF-κB) pathway (Ben-Neriah et al. 2011). NF-κB induces the expression of IL-6 by lamina propria immune cells, thereby promoting the survival and proliferation of intestinal epithelial cells (IECs) through the IL-6/STAT3 axis (Grivennikov et al. 2009).

The Hippo/YAP (yes-associated protein) signalling pathway is another pathway that is critical for intestinal tissue regeneration (Gregorieff et al. 2017; Figure 1.5). In response to tissue injuries, the Hippo/YAP pathway is activated by IL-6 and other cytokines produced by lamina propria macrophages and dendritic cells (Karin et al. 2016). Mechanistically, IL-6 and IL-11 activate glycoprotein 130 (gp130) signalling and thereby the tyrosine kinase activity of Src family kinases (SFKs). Activated SFKs then phosphorylate YAP and induce its nuclear translocation (Taniguchi et al. 2015). It is important to note that YAP/TAZ is dispensable for intestinal homeostasis under steady-state conditions, but is required for the regeneration of the Lgr5$^+$ stem cell population following chemical injury or gamma irradiation (Cai et al. 2010; Barry et al. 2014; Gregorieff et al. 2015). Interestingly, YAP activation in IECs leads to the activation of Notch signalling, further contributing to the maintenance of ISCs and TA cells in the crypt compartment (Taniguchi et al. 2015).

Lastly, as the most prominent regulator of ISCs, the Wnt/β-catenin signalling pathway plays a central role in intestinal tissue regeneration. *In vivo* studies have revealed that Wnt activity increases markedly during episodes of tissue damage and inflammation, leading to the hyperplasia of intestinal crypt cells, and increased numbers of stem cells and Paneth cells (Ashton et al. 2010). In fact, increases in the size and number of Paneth cells can be viewed as a special form of inflammation,

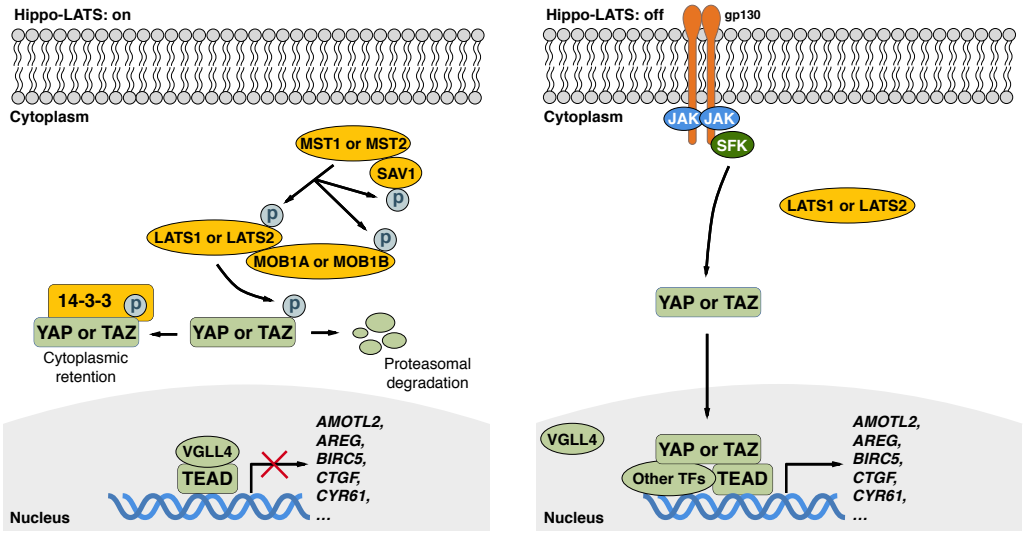


Figure 1.5: The Hippo/YAP pathway (adapted from Moroishi et al. 2015). In non-stimulated mammalian epithelial cells (Hippo-LATS: on), YAP and its orthologue TAZ (transcriptional coactivator with PDZ-binding motif) are phosphorylated by the large tumour suppressor 1 (LATS1) and LATS2. The inhibitory kinase module is composed of LATS1/2, the mammalian STE20-like protein kinase 1/2 (MST1/2), together with their activating adaptor proteins, salvador family WW domain containing protein 1 (SAV1), MOB kinase activator 1A (MOB1A) and MOB1B. Phosphorylated YAP/TAZ is retained in the cytoplasm by 14-3-3 and targeted for proteasomal degradation. In the absence of the kinase modules or their activators (Hippo-LATS: off), YAP and TAZ remain unphosphorylated and therefore stabilised, leading to their nuclear translocation. There, YAP/TAZ interacts with sequence specific transcription factors TEAD 1-4 (TEA domain family protein 1-4) and other transcription factors (such as SMAD, RUNX, and TBX5), activating the expression of downstream genes that are mostly associated with proliferation and cell survival. Hippo-independent SFK downstream of gp130 also activates the YAP signalling and thereby connects inflammatory signals to regenerative responses. AMOTL2, angiomotin like protein 2; AREG, amphiregulin; BIRC5, baculoviral IAP repeat containing protein 5; CTGF, connective tissue growth factor; CYR61, cysteine rich angiogenic inducer 61; SFK, Src family kinase; TF, transcription factor.

driving the formation of new stem cell niches and initiating tissue regeneration (Karin et al. 2016; Clevers et al. 2014).

1.2 Inflammation in the Intestine

1.2.1 The intestinal microenvironment

The intestinal epithelium constitutes the largest barrier surface that separates mammalian hosts from the external environment. It is a unique microenvironment where an elaborate balance between immune tolerance and response needs to be tightly regulated (Kayama et al. 2012). The intestinal epithelium, together with the

commensal microbiota and the intestinal immune system, constitutes an important tripartite functional relationship. It serves as a dynamic barrier that enables the absorption of dietary nutrients while excludes the potentially harmful compounds from entering the submucosal tissue (Barreau et al. 2014).

The intestinal mucosa provides the microbiota with a hospitable environment that is rich in nutrients and stable in temperature. In return, the microflora is implicated in several important intestinal functions, such as nutrient absorption and the maturation of the mucosal immune system (Hooper et al. 2001; Figure 1.6). In support of this, the intestinal immune systems of mice housed in germ-free conditions are largely underdeveloped, and deficiencies in various immune components including mucosal T cells and the immunoglobulin A (IgA) system are observed (Cebra 1999). The commensal microflora is also indispensable for the prevention of opportunistic infections. For instance, the microbiota confers colonisation resistance and facilitates pathogen clearance in a mouse model of *Salmonella typhimurium* infection (Endt et al. 2010).

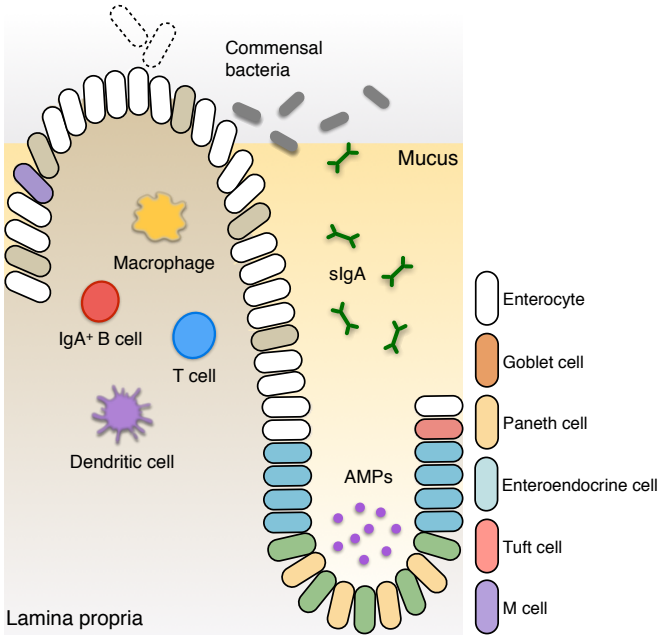


Figure 1.6: Schematic overview of intestinal homeostasis. The intestinal mucosal barrier is composed of a single layer of epithelial cells, the microbiota, and the underlying immune system. The epithelium is primarily protected by the mucosal layer populated with Paneth cell-secreted antimicrobial proteins (AMPs) and antigen-specific secretory IgA (sIgA).

The functionality of the intestinal epithelium as a frontline tissue barrier lies in its capacity to support selective permeability, only allowing specific luminal contents to pass into the lamina propria. This requires the formation of tight junctions, which connect adjacent IECs and integrate with their cytoplasmic actin and myosin networks (Peterson et al. 2014). Deletion of one of the transmembrane components of tight junctions, JAM-A (junctional adhesion molecule), results in increased mucosal permeability and colonic inflammation, suggesting the functional importance of tight junctions in the homeostatic control of the intestinal barrier (Laukoetter et al. 2007). In addition, the secretion of AMPs and mucins by Paneth cells and goblet cells, respectively, further strengthens the biochemical and physical aspects of the intestinal barrier (Peterson et al. 2014). Lastly, IECs are responsible for transporting secretory IgA produced by plasma cells in the lamina propria to the apical surface of the intestinal epithelium via transcytosis (Johansen et al. 2011).

Apart from the intestinal microbiota and the epithelium, the intestinal microenvironment also comprises the largest compartment of the immune system (Mowat et al. 2014). Specialised lymphoid structures such as isolated lymphoid follicles and Peyer's patches are involved in the sampling of luminal antigens and the stimulation of the mucosal immune system (Mowat et al. 2014). Under normal conditions, the intestinal immune system directs a largely tolerant response to the resident commensals. The tolerance is mainly achieved by a well-coordinated cytokine network rich in IL-33 and TGF-β, promoting the development of CD103$^+$ dendritic cells and regulatory T cells (Tregs) (Brown et al. 2013). When the host–microbe balance is disturbed, often caused by a breakdown of the intestinal barrier, the homeostatic immune response goes awry and leads to intestinal inflammation (Figure 1.7).

1.2.2 Innate and adaptive immunity of the intestine

Inflammation in the intestine arises when the intestinal barrier function is compromised or overwhelmed by luminal pathogenic stimuli. Microbe-associated molecular patterns, or MAMPs, are molecules shared by a variety of pathogenic microbes and are strong activators of innate immune responses (Didierlaurent et al. 2006).

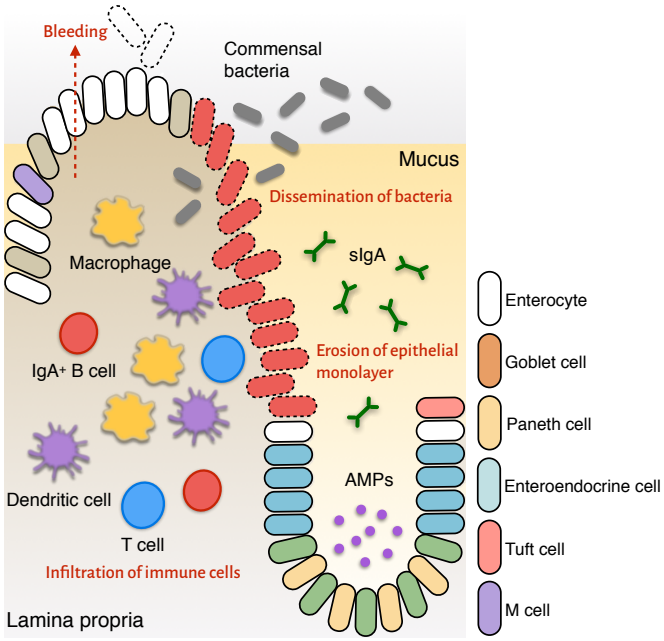


Figure 1.7: Breakdown of the intestinal barrier. Various chemical or biological insults lead to erosion of the epithelial monolayer, causing the dissemination of bacteria and their products into the underlying lamina propria. This will subsequently result in the infiltration and activation of immune cells, by which the secretion of proinflammatory cytokines further escalates the local inflammation. Because of the massive cell death occurring in this situation, haemorrhage and diarrhoea sometimes happen as a result.

Bacterial lipopolysaccharide (LPS) and endotoxins found on gram-negative bacteria are prototypical classes of MAMPs (Silhavy et al. 2010). MAMPs activate innate immune responses via the engagement of pattern recognition receptors (PRRs) such as toll-like receptors (TLRs) and nucleotide-binding oligomerization domain (NOD)-like receptors (NLRs) (Kayama et al. 2012). The intracellular domain of TLRs is homologous to the cytoplasmic region of IL-1 receptors, also known as the Toll/IL-1 receptor (TIR) domain (Kawai et al. 2007b). Once activated, the cytoplasmic domain of TLRs triggers the recruitment of a set of intracellular TIR-domain-containing adapters, including myeloid differentiation primary-response protein 88 (MyD88) (Medzhitov et al. 1998; Kawai et al. 2007b). Downstream events of this signalling cascade result in the activation of the NF-κB signalling pathway (Kawai et al. 2007a; Figure 1.8).

The NF-κB signalling cascade is a prototypical proinflammatory pathway, the activation of which leads to the expression of various proinflammatory cytokines,

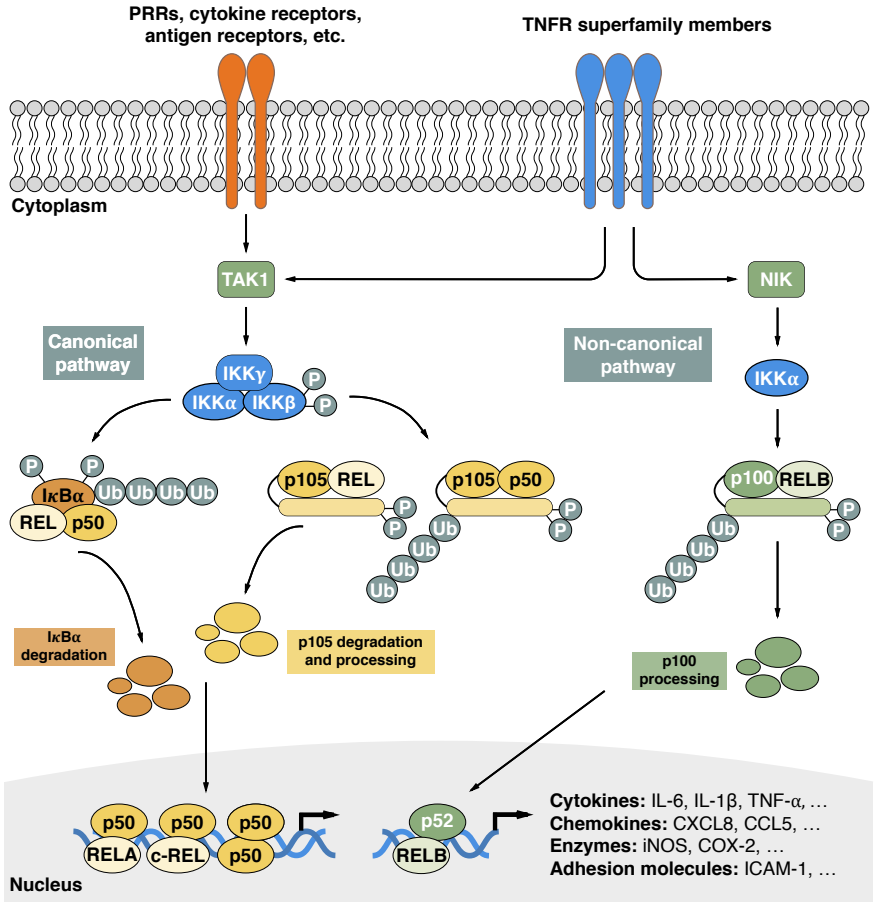


Figure 1.8: Canonical and non-canonical NF-κB pathways (adapted from Sun 2017). The canonical NF-κB pathway is triggered by engagement of various immune receptors, which activate the TGF-β activated kinase 1 (TAK1). The activity of NF-κB is tightly regulated by the inhibitory IκB proteins. Under normal conditions, a trimeric IκB kinase (IKK) complex composed of catalytic (IKKα and IKKβ) and regulatory (IKKγ) IKK proteins is activated by TAK1 via the phosphorylation of IKKβ. The IKK complex binds to NF-κB transcription factors and sequester them in the cytoplasm, thereby inhibiting their transcriptional activity. Once activated, IκB proteins are phosphorylated by IKK complexes and targeted for proteasomal degradation. NF-κB proteins are then free to translocate into the nucleus and activate target gene expression in the form of various dimeric complexes. By contrast, non-canonical NF-κB signalling is based on the processing of p100 downstream of a subset of tumour necrosis factor receptor (TNFR) superfamily members and the kinase NF-κB-inducing kinase (NIK). NIK phosphorylates and activates IKKα, which in turn phosphorylates p100, leading to the generation of p52 from p100 and the nuclear translocation of p52 and RELB. PRRs, pattern recognition receptors.

chemokines and adhesion molecules, including IL-1β, IL-6 and tumour necrosis factor (TNF)-α (Hiscott et al. 1993; Libermann et al. 1990; Shakhov et al. 1990). The mammalian NF-κB family of transcription factors is composed of five members, namely p65/RelA, c-Rel, RelB, p50, and p52 (Wullaert et al. 2010). The cascade of

signalling ultimately leads to the initiation of the adaptive immune response, characteristic of T cell activation and effector cytokine production (Bonizzi et al. 2004).

The compartmentalisation of the immune system into T and B cell immunity, namely the adaptive immune system, emerged early in evolution (Kato et al. 2014). In the intestinal tract, the adaptive immune response is mainly regulated by the balance between T helper cells and Tregs (Kayama et al. 2012). Classic helper T cells have been classified into T_H1 and T_H2 subgroups. They produce immunity effectors against intracellular bacteria and extracellular parasites, respectively (Zhu et al. 2008). The principal effector cytokine of T_H1 cells is interferon-γ (IFN-γ), which activates macrophages to increase their microbicidal activity (Suzuki et al. 1988). IL-4 triggers the differentiation of T_H2 cells that express IL-4 and other interleukins, including IL-5 and IL-13 (Nemoto et al. 2011). The IL-17-producing T_H17 cell is a distinct helper T cell population that mediates immune responses against extracellular pathogens (Weaver et al. 2007). It is interesting to note that the numbers of both T_H1 and T_H17 cells increase in the lamina propria of Crohn's disease (CD) patients, indicating crosstalk between these cell populations in the pathogenesis of inflammatory bowel disease (IBD) (Maloy et al. 2008). Lastly, Tregs, delineated by the expression of the transcription factor FoxP3, are able to suppress inflammatory responses through the production of anti-inflammatory cytokines such as IL-10 and transforming growth factor-β (TGF-β) (Zhu et al. 2008). In addition, Tregs can inhibit the function of antigen-presenting cells via the expression of CTLA-4 (cytotoxic T-lymphocyte associated protein 4), LAG-3 (lymphocyte-activation gene 3), CD39, and Neurophilin, indirectly blocking the activation of Foxp3-negative T Cells (Shevach 2009).

Notably, both the innate and adaptive immune systems are implicated in the regulation of reparative inflammation and the activation of tissue regeneration. The sensors and activators of regenerative inflammation are listed in Table 1.1, and the key cytokines and their effector proteins are listed in Table 1.2 (adapted from Karin et al. 2016).

Table 1.1: Sensors and Activators of Regenerative Inflammation

Sensor/Mediator	Activators	Products
TLR	PAMPs (Mogensen 2009) and DAMPs (Piccinini et al. 2010)	*Tnf*, *Il1β*, and *Mmp* mRNAs, IL-23, IL-6 and IL-22
NLR (NLRP3)	ATP, mtDNA, mtROS (Elliott et al. 2015) and uric acid (Martinon et al. 2006)	IL-1β and IL-18
MMP/ADAM	TLR, TNF and IL-1 through AP-1 and NF-κB (Scheller et al. 2011)	TNF, EGF, Areg and Ereg

Abbreviations: PAMPs, pathogen-associated molecular patterns; DAMPs, damage-associated molecular patterns; MMP, matrix metalloprotease; mtDNA, mitochondrial DNA; mtROS, mitochondrial reactive oxygen species; EGF, epidermal growth factor; Areg, amphiregulin; Ereg, epiregulin.

Table 1.2: Regeneration-inducing Cytokines and Their Effectors

Cytokine	Source	Direct effectors
IL-6	Epithelial cells, fibroblasts, lymphoid cells and myeloid cells	STAT3 (Grivennikov et al. 2009), MAPKs (Heinrich et al. 2003), SFKs, Notch and YAP (Taniguchi et al. 2015)
IL-17	T_H17 cells, $\gamma\delta$T cells and iLCs	NF-κB and MAPKs (Hata et al. 2002)
IL-22	T_H17 cells, iLCs and myeloid cells	STAT3 (Pickert et al. 2009), MAPKs (Nikoopour et al. 2015)
TNF	T cells, macrophages, epithelial cells and fibroblasts	MAPKs (Sabio et al. 2014), Notch (Ando et al. 2003), NF-κB and AP-1 (Grivennikov et al. 2011)

Abbreviation: iLCs, innate lymphoid cells.

1.2.3 Inflammatory bowel diseases

Various factors can compromise intestinal homeostasis and lead to chronic inflammatory conditions in the intestine. Such disorders include changes in the intestinal microflora, defects in the epithelial barrier function, and alterations in innate immune responses (Souza et al. 2016). Crohn's disease and ulcerative colitis are examples of chronic intestinal disorders that are commonly referred to as inflammatory bowel diseases, causing symptoms such as diarrhoea, anaemia, and fatigue (Podolsky 1991).

In IBD, the persistent inflammation is characterised by hyperactivation of effector immune cells, which leads to an excessive production of proinflammatory chemokines and cytokines such as TNF-α, IL-6, and IFN-γ (Atreya et al. 2008). In fact, epidemiological studies supported by genome-wide association study suggest that IBD is associated with polymorphisms in several genes of the immune system, including NOD2 (nucleotide-binding oligomerization domain protein 2) and ATG16L1 (autophagy related 16-like protein 1) (Hugot et al. 2001; Massey et al. 2007). Furthermore, activation of the NF-κB pathway has also been observed in IBD patients, which results in the transcription of TNF (Foxwell et al. 2000).

It is important to note that patients with chronic inflammation driven by IBD have an increased risk of developing colitis-associated colorectal cancer (CAC), as will be discussed in section 1.3.2 (Rubin et al. 2012).

1.3 Tumourigenesis in the Intestine

1.3.1 Genetics of colorectal cancer

Colorectal cancer (CRC), also known as colon or bowel cancer, is the third most commonly diagnosed cancer in both men and women (Siegel et al. 2017). Approximately 90% of CRC cases happen sporadically without family history or genetic predisposition, while less than 10% can be attributed to certain hereditary components (Bogaert et al. 2014).

CRC is a heterogeneous disease and generally arises from one or more of three aberrant pathways, i.e., chromosomal instability (CIN), CpG island methylator phenotype (CIMP), and microsatellite instability (MSI) (Tariq et al. 2016). More

specifically, CRCs can be robustly classified into four distinct consensus molecular subtypes (CMSs) as shown in Table 1.3, providing invaluable insights into clinical stratification and strategies for targeted therapies (Bijlsma et al. 2017).

Table 1.3: Consensus Molecular Subtypes of CRC

Subtype	Features	Percentage
CMS1	Hypermutated, dMMR, MSI, MLH1-sil, CIMP-high, BRAF-mut, immune infiltration	14%
CMS2	SCNA-high, WNT and MYC activation	37%
CMS3	SCNA-low, CIMP-low, KRAS-mut, metabolic deregulation, epithelial signature	13%
CMS4	SCNA-high, stromal infiltration, TGF-β activation, EMT, C', angiogenesis, matrix remodelling	23%
Mixed	Transition phenotype/intratumoural heterogeneity	13%

Adapted from Müller et al. 2016.
Abbreviations: CMS, consensus molecular subtypes; dMMR, defective mismatch repair; MSI, microsatellite instability; MLH1-sil, MLH1 silencing by promoter hypermethylation; CIMP, CpG Island methylator phenotype; SCNA, somatic copy number alteration; C', complement activation signature.

In this section, the four most frequently altered genes/signalling pathways underlying the initiation and progression of CRC, namely adenomatous polyposis coli (APC), KRAS, SMAD4 and TP53, will be discussed. In fact, the sequential alteration of these genes is clearly manifested in the adenoma–carcinoma sequence model for sporadic CRC (SCC) development (Vogelstein et al. 1988; Figure 1.9).

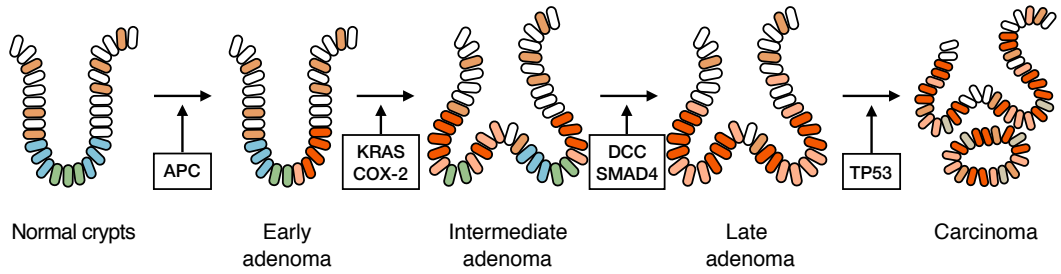


Figure 1.9: Common genetic alterations in SCC. The initial event in SCC development is the activation of Wnt signalling, caused by loss of APC or mutations in β-catenin. This will lead to the development of early adenoma. Subsequent accumulation of mutations in the small GTPase KRAS, the transcription factor SMAD4, and the tumour suppressor TP53 precedes the formation of larger adenomas and early carcinomas.

APC

As a key regulator of the Wnt signalling cascade and the most frequently mutated gene in CRC, APC is considered the gene for CRC (Cancer Genome Atlas Network 2012; Fodde et al. 2001). Mutations in APC can be inherited or arise sporadically (Segditsas et al. 2006). Germline mutations of APC is associated with hereditary colonic disorders such as familial adenomatous polyposis, which, if not identified and treated at an early stage, exhibits a 100% risk of progressing to CRC (Groden et al. 1991). Sporadic mutations of APC, on the other hand, represent the earliest genetic alteration in the process of colorectal tumourigenesis (S. M. Powell et al. 1992). This is believed to be associated with the onset of colorectal neoplasia and the initiation of the adenoma–carcinoma sequence (Fodde et al. 2001).

The tumour suppressive function of APC is implicated in its capacity to regulate the intracellular level of β-catenin and consequently the activity of Wnt signalling, as described in section 1.1.2. Not surprisingly, most APC mutations result in truncated proteins that are no longer capable of forming the destruction complex for β-catenin, leading to its accumulation and transactivation of Wnt target genes (Miyaki et al. 1994). This may confer growth advantages to APC-deficient crypts and initiate their clonal expansion (Fodde et al. 2001). It is worth noting that activating mutations of β-catenin have been found in SCC cases where the expression of APC is intact (Morin et al. 1997). The mutually exclusive pattern of APC and β-catenin mutations reinforces the notion that the regulation of β-catenin delineates the tumour suppressive roles of APC.

Importantly, it has been suggested that heterozygous APC mutations may result in an increase in stem cell number, possibly via an increase in the probability of symmetrical divisions of stem cells towards stem cell progeny (K.-M. Kim et al. 2004). The hypothesis was investigated computationally, which led to the revelation of the connection between heterozygous APC mutations and niche succession (Sasikumar et al. 2011). Niche succession is a phenomenon by which normal intestinal crypts get periodically taken over by descendants from a single stem cell lineage as a result of selective advantage, genetic drift, or hitchhiking (Leedham et al. 2008).

Taken together, these observations provide one possible explanation as to how heterozygous APC mutations contribute to observed changes in precancerous colonic crypts (Sasikumar et al. 2011).

KRAS

KRAS is mutated in approximately 50% of SCC cases (Forrester et al. 1987; Bos et al. 1987). Following the inactivation of APC, activating mutations of KRAS occur as the next step constituting the adenoma–carcinoma sequence (Vogelstein et al. 1988).

KRAS is an essential mediator of the MAPK signalling pathway, downstream of EGFR. As a member of the Ras GTPase family of proteins, KRAS acts as a molecular switch, with its activation status dependent on whether it is bound to guanosine triphosphate (GTP) or guanosine diphosphate (GDP) (Downward 2003). It is implicated in the regulation of a wide range of cellular processes, including cell cycle progression, cell growth, apoptosis, senescence, and more (Nussinov et al. 2016). Oncogenic mutations of KRAS lead to constitutive activation of its downstream signalling cascades, including the PI3K (phosphoinositide 3-kinase)/AKT/mTOR and the RAF/MEK/ERK pathway, promoting cell proliferation and survival independent of EGFR (Armaghany et al. 2012).

SMAD4

SMAD4 is a tumour suppressor and an important member of the TGF-β pathway. TGF-β signalling is naturally implicated in diverse developmental and homeostatic processes, such as cell proliferation, differentiation, and regulation of the extracellular microenvironment (Wrana 2013). In the development of CRC, the loss of SMAD4 is considered to be a relatively late event as rates of SMAD4 loss are 0, 8, 6, and 22% in CRC stages I–IV, respectively (Maitra et al. 2000). It is notable that SMAD4 has been used as a prognostic marker for CRC. Mutations or decreased SMAD4 expression portends a worse prognosis and poorer responses to 5-fluorouracil (5-FU)-based chemotherapy (Boulay et al. 2002). Interestingly, based on a next-generation sequencing analysis of primary and metastatic tumour pairs, mutations of SMAD4 have been associated with clonal divergence and are therefore implicated

in cancer evolution (Goswami et al. 2015). This observation partially justifies the role of SMAD4 as a prognostic marker for CRC.

Apart from SMAD4, the type II TGF-β receptor (TGFBR2) is also frequently mutated in CRC. The microsatellite sequences within the TGFBR2 gene render it susceptible to replication errors, especially in the context of MMR gene inactivation (Ilyas et al. 1999). In fact, the overall incidence of TGFBR2 mutations is around 30% in CRC, with frameshift mutations found in more than 80% of MSI-positive CRC cases (Xu et al. 2007). When challenged with the carcinogen Azoxymethane (AOM), followed by induction of chronic colitis with dextran sulfate sodium (DSS), mice depleted of TGFBR2 showed increased susceptibility to the development of colonic adenoma and adenocarcinoma (Biswas et al. 2004). These observations suggest that TGFBR2 functions as a tumour suppressor in CRC.

TP53

The p53 protein encoded by TP53 is one of the most important tumour suppressors identified to date. p53 is a master regulator of cell cycle and apoptosis. In response to cellular stresses such as DNA damage and chromosomal aberrations, p53 is activated to inhibit cell growth through the induction of apoptosis or cell cycle arrest, thereby preventing the development of tumours (Vousden et al. 2002).

The TP53 gene is reported to be mutated in approximately 40–50% of SCC cases (Li et al. 2015). According to the adenoma–carcinoma sequence model, such mutations are believed to occur late in the process of tumourigenesis and facilitate the transition from adenoma to carcinoma (Armaghany et al. 2012). Different types of p53 mutations delineate the pathological characteristics of CRC, including invasive depth, sites of metastasis, and prognosis (Li et al. 2015). For instance, CRC patients with mutant p53 exhibit a worse response to 5-FU-based chemotherapy and have poorer prognosis than those with wild-type p53 (Iacopetta 2003).

Most TP53 mutations are missense mutations that lead to p53 dysfunction. Therapeutic strategies to restore p53 functions include the inhibition of MDM2 (mouse double minute 2 homolog)-mediated p53 degradation and, more importantly,

the reactivation of mutant p53. In fact, several small molecules have been demonstrated to be able to rescue p53 with specific mutations, such as PRIMA-1 and its analogue PRIMA-1^{MET} (Bykov et al. 2002; Bykov et al. 2005). PRIMA-1^{MET} is currently being tested in a phase I/II clinical trial and promising preliminary results have been obtained (Bykov et al. 2014).

1.3.2 Colitis-associated colorectal cancer

As described in section 1.2.3, inflammatory bowel diseases are chronic inflammatory disorders of the intestinal tract that constitute a risk factor for CRC. In fact, CAC is responsible for the deaths of approximately 10–15% of all IBD patients (Van Der Kraak 2015).

CAC, as opposed to SCC discussed in section 1.3.1, exhibits a distinct sequence of events in the process of tumourigenesis. Instead of the adenoma–carcinoma sequence characteristic of SCC, an inflammation–dysplasia–carcinoma sequence is observed in IBD-driven CRC development (Harpaz et al. 2010; Figure 1.10). Moreover, SCC normally arises from a discrete focal dysplasia referred to as an adenomatous polyp, whereas CAC is frequently associated with dysplastic lesions that can be polypoid, flat, localised, or multifocal, implicating an increased risk for neoplasia (Ullman et al. 2011).

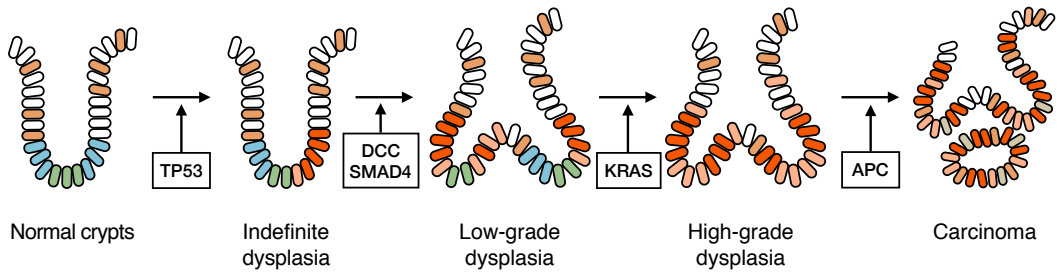


Figure 1.10: Common genetic alterations in CAC. CAC is characterised by the successive progress from dysplasia to the formation of carcinoma. Loss of p53 function is an early event of CAC, whereas APC mutations appear much later and are probably passengers in CAC.

Not surprisingly, an increased risk for CRC development is correlated with a longer duration of colitis (Ullman et al. 2011). It is therefore natural to speculate that

inflammation is a key mediator of CAC pathogenesis. In support of this hypothesis, *in vivo* studies have shown that chronic colitis predisposes mice to colorectal tumour formation even in the absence of known DNA mutagens (Grivennikov 2013). The mechanisms by which inflammation regulates the initiation and progression of CAC are not very well understood, but it has been suggested that inflammation promotes CpG island methylation and chromosomal and microsatellite instability (Ullman et al. 2011). In addition, reactive oxygen species and reactive nitrogen species produced by immune cells in the inflammatory microenvironment are also implicated in the induction of DNA damage, thereby contributing to the development of CAC (Hussain et al. 2003).

1.3.3 Inflammatory networks underlying colorectal cancer

In 2000, Douglas Hanahan and Robert A. Weinberg published a seminal review article named *The hallmarks of cancer*, identifying six common traits that govern the transformation of a normal cell into a malignant one. The hallmarks include self-sustained proliferation, evasion from growth suppression, resistance to cell death, acquisition of replicative immortality, induction of angiogenesis, and the activation of invasion and metastasis (Hanahan et al. 2000). In 2011, the authors updated the list with two emerging characteristics of cancer, metabolic reprogramming and evasion from immune destruction (Hanahan et al. 2011). It is not surprising that inflammation underpins these hallmarks and fosters the so called 'tumour microenvironment' (Colotta et al. 2009). The inflammatory spectrum underlying the development of CRC encompasses three major subgroups, namely chronic inflammation resulting from barrier dysfunction, focal inflammation mediated by ectopic lymphoid structures, and parainflammation caused by prolonged DNA damage (Lasry et al. 2016). Several transcription factors and proinflammatory cytokines have been recognised as important mediators of tumour-associated inflammation, including NF-κB, STAT3, IL-1β, IL-6 and TNF-α (Waldner et al. 2015).

As discussed in section 1.2.2, NF-κB is a central coordinator of inflammation and innate immunity. In fact, aberrant NF-κB activation is detected in more than

50% of CRC cases (Terzic et al. 2010). The functional relevance of NF-κB signalling was first demonstrated by Greten et al. using an IKKβ-deficient mouse model (Greten et al. 2004). Mice with deficiency of IKKβ in either intestinal epithelial or myeloid cells showed attenuated colorectal tumourigenesis compared with their wild-type counterparts (Greten et al. 2004). Consistently, mice with constitutively active IKKβ developed spontaneous CRC, further substantiating the roles of NF-κB in colorectal tumourigenesis (Shaked et al. 2012).

One of the major downstream effectors of the NF-κB pathway is IL-6, a multi-functional cytokine capable of promoting proliferation and inhibiting apoptosis (Colotta et al. 2009). Most of the effects of IL-6 in the initiation and progression of CRC are mediated by STAT3, which, like NF-κB, functions as another point of convergence for various oncogenic signalling pathways (Terzic et al. 2010; Figure 1.11). The IL-6–STAT3 signalling axis induces the expression of anti-apoptotic genes such as Bcl-2 (B-cell lymphoma 2) and Bcl-xL (B-cell lymphoma-extra large), proliferative genes such as Cyclin D1 and c-Myc, and VEGF (vascular endothelial growth factor) (Terzic et al. 2010). Taking advantage of the AOM/DSS challenge model, Bollrath et al. showed that conditional deletion of STAT3 in the intestinal epithelium led to reduced tumour growth, confirming the functional importance of STAT3 in the context of CRC development (Bollrath et al. 2009). Importantly, activated STAT3 is required for persistent NF-κB activation (H. Lee et al. 2009). The positive feedback loop between NF-κB and the IL-6–STAT3 signalling axis drives malignant transformation (Waldner et al. 2015).

Lastly, the composition of the intestinal microbiota also plays an important role in the modulation of colorectal tumourigenesis. This can be largely attributed to the homeostatic immune and metabolic functions of the microflora (Terzic et al. 2010). On the one hand, mice bred in a germ-free environment show decreased frequency of oncogenic mutations and colon tumour formation. For example, administration of AOM to IL-10-deficient mice leads to tumour development under normal conditions, but not under germ-free conditions (Uronis et al. 2009). On the other hand, intestinal inflammation and tumourigenesis can also result from

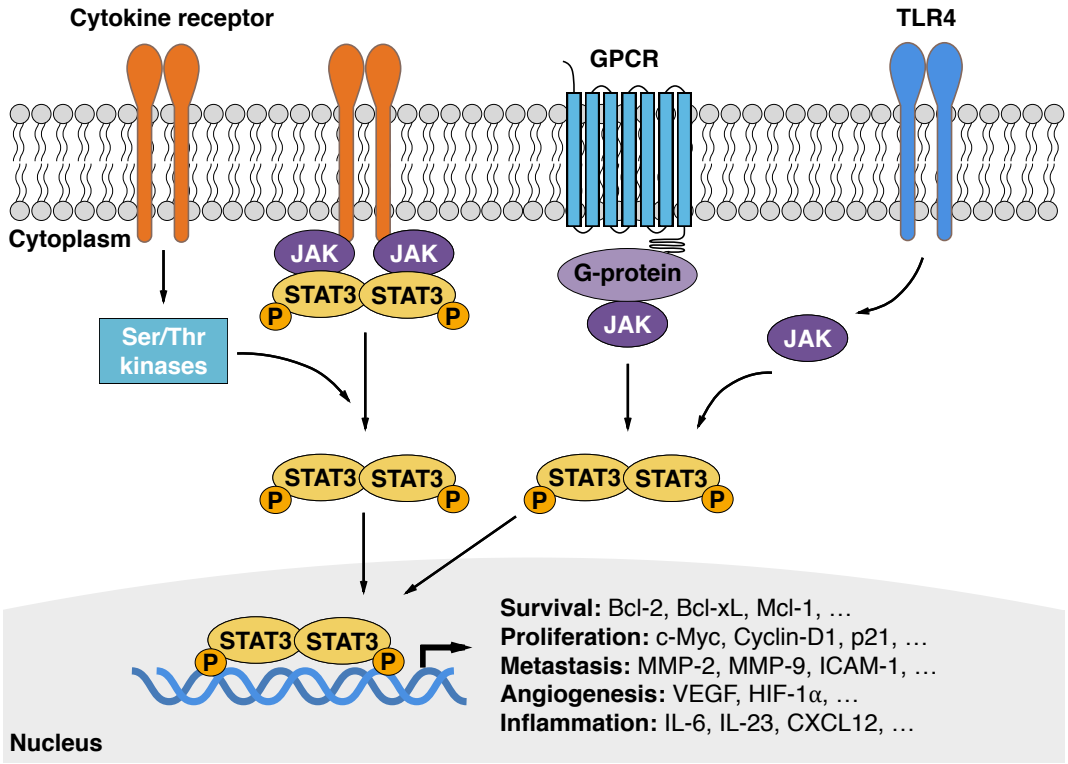


Figure 1.11: Pathways activating STAT3 signalling in cancer (adapted from Yu et al. 2014). The Janus kinase (JAK)–STAT3 pathway is activated by various receptors, including those for IL-6 and IL-6 family cytokines, as well as GPCRs and TLRs. Engagement of these receptors results in the activation of JAKs, which in turn phosphorylate STAT3 at Tyr705, leading to the translocation of activated STAT3 dimers to the nucleus. Phosphorylation of STAT3 at Ser727 mediated by Ser/Thr kinases further increases its transcriptional activity. In the nucleus, STAT3 is involved in the regulation of various biological processes required for cancer progression, including cell survival and proliferation, tumour metastasis, angiogenesis and inflammation.

aberrations of the balance between tolerogenic and proinflammatory microflora, i.e. dysbiosis (Terzic et al. 2010).

1.4 The Intestinal Organoid

1.4.1 Organoids: a brief history

Organoids are three-dimensional (3D) *ex vivo* culture systems derived from pluripotent or somatic stem cells. The essence of the organoid system lies in its capacity to capture the intrinsic propensity of stem cells to form a self-organised entity. It also recapitulates the 3D architecture that is physiologically relevant to the tissue type that the organoid originates from (Simian et al. 2017; Kretzschmar et al. 2016).

The conceptualisation of the term 'organoid' can be dated back to as early as the 1960s, when it first started to be used to refer to self-organised organotypic cultures by developmental biologists (Kretzschmar et al. 2016). Around 30 years later, Bissell et al. demonstrated the feasibility of using a laminin-rich matrix to support *ex vivo* hepatocellular functions (Bissell et al. 1987). Shortly after, a laminin-rich matrix-based assay was developed to study mammary morphogenesis in both healthy and malignant epithelial tissues (Petersen et al. 1992; Barcellos-Hoff et al. 1989). The term '3D culture models' came into being thereafter.

Despite the progress in 3D cell culture techniques as well as in stem cell biology, it has long been challenging to maintain long-term cultures of stem cells *in vitro*, as they become genetically unstable rather easily and thus lose their full differentiation potential (Kretzschmar et al. 2016). In 2009, Sato et al. reported a protocol to generate long-term 3D intestinal organoid culture from adult $Lgr5^+$ stem cells (Sato et al. 2009). In the presence of a defined cocktail of growth factors (EGF, the Wnt signal agonist R-spondin, and the BMP inhibitor Noggin), a single $Lgr5^+$ stem cell embedded in the extracellular matrix Matrigel is capable of giving rise to a fully differentiated cell aggregate reminiscent of the crypt–villus architecture *in vivo* (Sato et al. 2009; Figure 1.12). This has led to the renaissance of the organoid field.

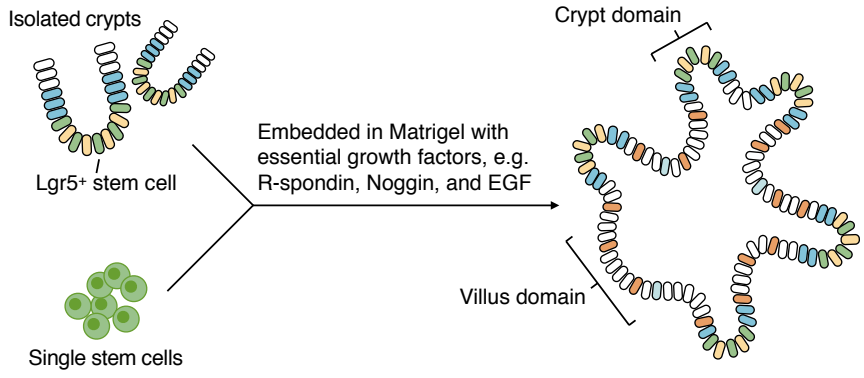


Figure 1.12: The intestinal organoid culture system. One of the most widely used protocols for intestinal organoid culture was established by Sato et al. in 2009, in which intact intestinal crypts or purified $Lgr5^+$ stem cells are embedded in Matrigel and cultured in the presence of a cocktail of growth factors, including EGF, Noggin, and R-spondin. This generates self-renewing organoids that are structurally reminiscent of the intestinal epithelium, with the villus-like region containing differentiated cell types and the crypt-like region enriched for Paneth and stem cells.

To date, the definition of organoids is still somewhat ambiguous, but it is generally accepted as an entity 'containing several cell types that develop from stem cells or organ progenitors and self-organise through cell sorting and spatially restricted lineage commitment, similar to the process *in vivo*' (Lancaster et al. 2014). Organoids can be derived from two types of stem cells, pluripotent stem cells and adult stem cells (ASCs). The former can be further classified into embryonic stem cells and induced pluripotent stem cells, capable of differentiating into different tissue types, whereas ASCs are organ-specific (Dutta et al. 2017). To better communicate the entity under investigation, special caution needs to be taken with the nomenclature for intestinal *in vitro* cultures. In this thesis, the term 'organoid' refers to epithelial cell-composed, multilobulated structures derived from the small intestine and the colon, also known as enteroids and colonoids, respectively (Stelzner et al. 2012).

1.4.2 Organoids in the study of intestinal physiology

As a primary cell-based tissue surrogate, the organoid system retains physiologically relevant tissue architecture and cell signalling, making it a model system that is applicable to the investigation of intestinal biology.

Developmental biology

Organoids represent an *ex vivo* model system that makes the study of developmental biology feasible. For instance, intestinal organoids have been used to interrogate signalling pathways implicated in cell lineage control. Notch inhibition in intestinal organoids predisposes progenitor cells to the secretory lineage, whereas exposure to Wnt3A directs secretory cells to dedifferentiate and regain stemness (VanDussen et al. 2012; Es et al. 2012). Along the same line, a whole-library screening has been performed to investigate the effects of epigenetic modulation on intestinal stem cell differentiation (Cao et al. 2015).

Furthermore, organoids have also been utilised to model organogenesis and tissue morphogenesis. In the initial stages of organoid development, a spheroid-like structure dominated by proliferative cells is formed, reminiscent of the early

development of the murine embryonic intestine (Shyer et al. 2015). The next step of intestinal tissue morphogenesis involves the crypt–villus compartmentalisation, restricting the stem cell population to the base of crypts while promoting cell differentiation along the villus (Kretzschmar et al. 2016). Such self-organisation is observed in the absence of mesenchymal niche factors (Sato et al. 2009). This is achieved, at least partially, via the control over the expression of EphB/ephrinB exerted by the Wnt signalling cascade (Batlle et al. 2002).

Stem cell biology

The growth and long-term maintenance of intestinal organoids relies on the perpetual self-renewal of ISCs. It is therefore a valuable model system to study stem cell biology. In agreement with the essential roles of Paneth cells in stem cell homeostasis *in vivo*, it has been reported that Paneth cells also support the crypt niche in intestinal organoids via the paracrine secretion of growth factors including EGF and Wnt3 (Sato, Es, et al. 2011). The efficiency of organoid formation is limited when single $Lgr5^+$ stem cells are seeded into Matrigel, whereas co-culturing $Lgr5^+$ stem cells with Paneth cells substantially increases the percentage of cells that develop into organoids (Sato, Es, et al. 2011). In fact, the physical interaction between stem cells and Paneth cells can be directly visualised in organoids (Farin et al. 2016). By integrating Wnt3-producing Paneth cells with Wnt3-deficient IECs, it is demonstrated that the contact between Paneth cells and stem cells enables the transfer of Wnt3 in a cell-bound manner rather than through free diffusion (Farin et al. 2016).

Organoids can also be used to study tissue plasticity. Treatment of intestinal organoids with CHIR99021 and valproic acid (VPA) promotes stem cell renewal, creating a homogenous population of $Lgr5^+$ stem cells (Yin et al. 2013). Organoids generated in this manner are suitable for further manipulations and thus facilitate the study of intestinal stem cell plasticity. For example, the enterocyte lineage is stimulated when intestinal organoids are treated with VPA and IWP-2 (inhibitor of Wnt production 2), but the differentiation is steered towards the secretory lineages when Notch signalling is inhibited with DAPT (Yin et al. 2013). Collectively, these

results suggest that organoid cultures can be applied to the study of stem cell lineage selection, especially when combined with other niche factors essential for the development of the intestinal epithelium (Kretzschmar et al. 2016).

Tissue microenvironment

Powerful as the organoid system is, one of its major limitations is the lack of associated mesenchyme, which is indispensable for the regulation of intestinal homeostasis *in vivo*. To that end, various organoid co-culture systems have been developed to investigate the crosstalk between epithelial cells and their microenvironment (Short et al. 2017). For example, Nozaki et al. recently established a protocol to incorporate intraepithelial lymphocytes (IELs) into the existing organoid culture system, allowing the study of immune–epithelial cell interaction (Nozaki et al. 2016). As a proof-of-concept study, their work demonstrates that immune cells are viable in organoid culture medium, and that their motility relative to epithelial cells is comparable to what is observed *in vivo* (Nozaki et al. 2016).

In addition to immune cells, the commensal microflora is another important component of the intestinal microenvironment. It has been reported that microbiota-derived metabolites, such as short-chain fatty acids, have a profound effect on the metabolism and gene expression of intestinal organoids (Lukovac et al. 2014). Moreover, studies of organoids cultured in the presence of various microbial antigens have led to the discovery of INF-γ-dependent mechanisms of Paneth cell degranulation (Farin et al. 2014). Lastly, organoids infected with *Salmonella* have been exploited to study bacterial–epithelial interactions. The model system turns out to faithfully recapitulate a number of *in vivo* observations post *Salmonella* infection, including activation of the NF-κB pathway and alterations in tight junctions (Zhang et al. 2014).

1.4.3 Organoids as a model for human diseases

While the organoid technology has been widely used to investigate the physiological functions of the intestine, it is also an invaluable tool to study intestinal dysfunctions and various human diseases, including CRC.

Infectious diseases

Since organoids are theoretically composed of all of the differentiated cell types of a given organ, they are well suited for the study of infectious diseases. This is particularly true for pathogens that are restricted to humans or that currently lack a suitable model system (Clevers 2016). As an illustrative example, intestinal organoids have been shown to support the growth of rotavirus and norovirus, which have previously been challenging to propagate *in vitro* (Finkbeiner et al. 2012; Ettayebi et al. 2016). These models hold promise for the study of enteric virus-related pathogenesis (Short et al. 2017).

However, it is worth noting that infection studies using organoids can be complicated by the fact that the apical/basal polarity of the epithelium is inverted in the system. As a result, the apical surface of the epithelial cell layer faces the lumen of the organoid, making it inaccessible to bacterial/viral attachment (Short et al. 2017). To overcome this, pathogenic bacteria can be inoculated into organoids via microinjection (Zhang et al. 2014). Alternatively, organoids can also be dissociated and grown as monolayers on the transwell system, allowing the exposure of the apical surface (Moon et al. 2014). Cells cultured in this manner preserve normal differentiation and polarisation, and are ready to be infected and monitored thereafter (In et al. 2016).

Hereditary diseases

In addition to the study of infectious diseases, organoids are also applicable to investigating monogenic hereditary diseases (Clevers 2016).

The most outstanding example in this respect is the translational research focused on cystic fibrosis (CF). CF is caused by a spectrum of mutations in the gene encoding the cystic fibrosis transmembrane conductance regulator (CFTR), which is normally expressed by epithelial cells and is responsible for chloride transport (Short et al. 2017). Dekkers et al. generated intestinal organoids derived from rectal biopsies of CF patients and used forskolin to evaluate CFTR's function (Dekkers et al. 2013). In this assay, forskolin activates wild-type CFTR and

induces ion uptake. This leads to robust swelling of wild-type organoids but not their CF counterparts (Dekkers et al. 2013). Importantly, the forskolin-induced swelling (FIS) phenotype can be restored in CFTR mutant organoids either by the addition of experimental CFTR corrector compounds or by correction of the mutation with the CRISPR (clustered regularly interspaced short palindromic repeats)/CAS9 (CRISPR-associated endonuclease) technology (Dekkers et al. 2013; Schwank et al. 2013). In fact, the FIS assay has already been applied to drug screening for real patients and has demonstrated promising predictive power over existing therapeutic strategies (Dekkers et al. 2016).

CRC

Given the success of culturing organoids derived from healthy ASCs, it is natural to envisage the application of the methodology to their malignant counterparts, i.e., the establishment of cancer organoids (tumouroids). These cancer organoids will provide unique possibilities for functional testing such as drug screening, and for a more refined understanding of the correlation between genetic mutations and cancer progression (Bartfeld et al. 2017; Clevers 2016).

Cancer organoids derived from human CRCs recapitulate the histopathological features of primary tumours, and those characteristics can be further maintained in patient-derived tumouroid xenografts (Fujii et al. 2016). It is not surprising to find that growth characteristics vary dramatically across different cancer organoid cultures, indicative of their individual mutational profiles (Fujii et al. 2016). To that end, a living biobank of CRC patient-derived organoids is being developed (Wetering et al. 2015). To date, as more tissue samples from cancer patients are being collected, a systematic screening platform is being established. This approach has already yielded some biological insight. For example, using a high-throughput workflow based on 19 cancer organoids and more than 5,000 measurements, the correlation between oncogenic mutations and a tumour's response to a set of targeted therapies has been determined (Wetering et al. 2015).

CRC can also be modelled with wild-type colonic organoids. In the so-called 'bottom-up' approach, oncogenic mutations are sequentially introduced into normal

organoids, simulating the multi-hit model of colorectal tumourigenesis (Short et al. 2017). Using CRISPR/CAS9 technologies, two research groups have independently demonstrated that sequential and/or combinatorial alterations in APC, TP53, KRAS/PIK3CA (phosphoinositide-3-kinase, catalytic, alpha polypeptide), and SMAD4 are sufficient to generate organoids capable of forming tumours in xenotransplant models (Drost et al. 2015; Matano et al. 2015). Intriguingly, the invasiveness of the organoid-derived tumours increases as new mutations are introduced, indicating that this is a suitable methodology to model novel oncogenic mutations and their effects on cell transformation and tumour progression. It is worth noting that the adenoma–carcinoma sequence is also recapitulated in an air–liquid interface organoid culture system (Li et al. 2014).

1.5 ASPP2 - A Key Regulator of Epithelial Cell Biology

1.5.1 The ASPP protein family

The ASPP (Apoptosis Stimulating Protein of p53) protein family is composed of three members: ASPP1, ASPP2, and inhibitory ASPP (iASPP). Their sequence similarity lies in their shared C-termini, which contain ankyrin repeats, an SH3 domain, and a proline-rich region. Therefore, their name also stands for 'Ankyrin repeats, SH3 domain and Proline-rich region-containing Protein' (Sullivan et al. 2007; Figure 1.13A). Moreover, the C-terminus also mediates the interaction between ASPP proteins and their binding partners, including the p53 family of proteins and Bcl-2 (Gorina et al. 1996; Naumovski et al. 1996).

Functionally, ASPP1 and ASPP2 bind to p53 and promote its proapoptotic activity, while p53-dependent cell cycle arrest is not affected (Samuels-Lev et al. 2001; Bergamaschi et al. 2004). iASPP, on the other hand, antagonises that effect and specifically inhibits p53-mediated apoptosis (Bergamaschi et al. 2003; Figure 1.13B). The precise mechanism by which this occurs is still not completely understood. Nevertheless, it has been shown that the C-termini of ASPP proteins interact with the DNA-binding domain of p53, which may induce conformational changes of p53 or recruit other transcription factors, conferring its target specificity

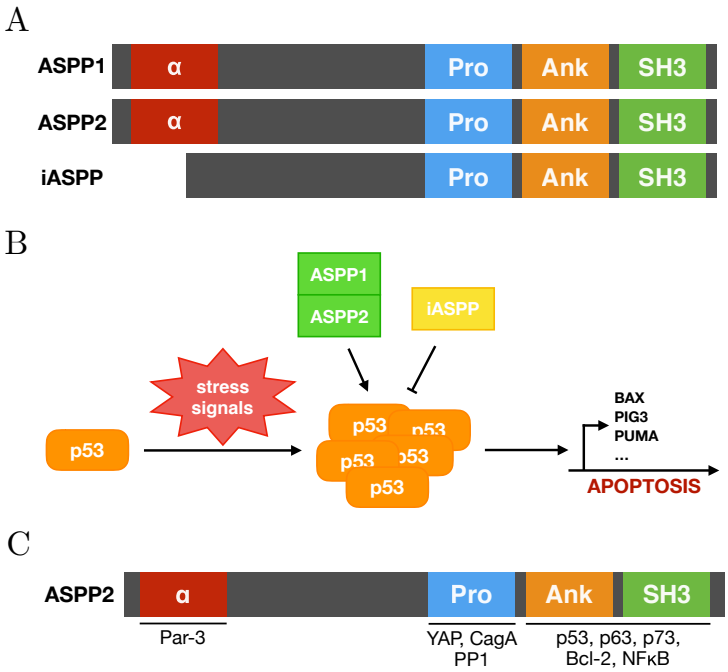


Figure 1.13: The ASPP family of proteins. (A) The ASPP protein family consists of three members: ASPP1, ASPP2, and iASPP. All three proteins share the signature structure of a proline-rich region (Pro), ankyrin repeats (Ank), and an SH3 domain (SH3) in their C-termini. The N-terminal α-helical domain (α) is conserved between ASPP1 and ASPP2. (B) The ASPP family of proteins regulate p53-mediated apoptosis. Cellular stresses result in the stabilisation and activation of p53, the proapoptotic function of which is either enhanced by ASPP1/2 or repressed by iASPP. (C) Important binding partners of ASPP2. Most of the protein–protein interactions reported to date are mediated by the C-terminus of ASPP2, whereas Par-3 binds to ASPP2 through its N-terminal domain.

(Gorina et al. 1996). In addition, a ubiquitin-like structure resides in the N-terminus of ASPP2, which may mediate its interaction with other components of the apoptotic response network and, thus, contribute to its selective pro-apoptotic activity (Tidow et al. 2007).

In addition to the p53 family proteins, several other ASPP-binding partners have also been identified, including protein phosphatase 1 (PP1), RelA/p65, YAP1, Par-3, *Helicobacter pylori* cytotoxin-associated gene A (CagA), IκB, and active RAS (Helps et al. 1995; Yang, Hori, Sanda, et al. 1999; Espanel et al. 2001; Sottocornola et al. 2010; Buti et al. 2011; Tordella et al. 2013; Y. Wang et al. 2013; Figure 1.13C). Not surprisingly, the ASPP family proteins have been shown to be involved in a variety of cellular functions beyond the regulation of apoptosis. It is worth

noting that most of these interactions are mediated by the shared C-termini of the proteins, indicating that the functions conveyed might be evolutionarily conserved.

1.5.2 ASPP2 in tumourigenesis

Given that the ASPP proteins interact with p53 and regulate apoptosis, it is reasonable to speculate that they are implicated in the process of tumourigenesis. In fact, four amino acids in p53 that are essential for the ASPP/p53 interaction (178His, 181Arg, 243Met, and 247Arg) have been found to be frequently mutated in human cancers, corroborating that hypothesis (Cho et al. 1994; Gorina et al. 1996). In addition, the two most frequently mutated amino acids of p53 residing in its DNA-binding domain, 248Arg and 273Arg, are also in contact with ASPP2 (Gorina et al. 1996). This suggests that ASPP2 may be involved in p53-mediated tumour suppression. Indeed, a mutation of the ASPP/p53 contact residue, 181Arg of p53, has been observed in human cervical and breast cancer, rendering p53 defective in mediating apoptosis while leaving cell cycle arrest unaffected (Trigiante et al. 2006). Moreover, ASPP2 has been shown to potentiate RAS signalling and enhance the proapoptotic function of p53 in cancer cells (Y. Wang et al. 2013). Taken together, it is logical to hypothesise that ASPP2 may mediate tumour suppression, at least partially through its interaction with p53.

One of the major lines of evidence indicating ASPP2 as a tumour suppressor came from the study of an ASPP2 knockout mouse model, in which exon 3 of the murine Tp53bp2 gene (encoding ASPP2) is deleted (hereafter referred to as ASPP2$^{\Delta exon3}$), leading to a frame shift within the open reading frame and depletion of the protein (Vives et al. 2006). ASPP2$^{\Delta exon3}$ mice generated on a mixed 129SvJ×C57BL/6 background exhibit postnatal lethality, while ASPP2 heterozygous mice are viable but more susceptible to tumour formation compared with their wild-type counterparts, both spontaneously and after ionising irradiation (Vives et al. 2006; Kampa et al. 2009).

In a systematic tumour study carried out using p53 heterozygous (p53$^{+/-}$) mice crossed with ASPP2 heterozygous (ASPP2$^{+/\Delta exon3}$) mice, it was demonstrated

that combined heterozygosity of these two genes accelerates the onset of tumour development (Vives et al. 2006). The tumour formation is not accompanied by the loss of heterozygosity of ASPP2, suggesting that ASPP2 is a haploinsufficient tumour suppressor (Vives et al. 2006). The spectrum of tumours formed encompasses lymphoma, sarcoma, and very rarely carcinoma. Importantly, the onset of spontaneous lymphoma is significantly earlier in ASPP2$^{+/\Delta exon3}$, p53$^{+/-}$ mice than in their ASPP2$^{+/+}$, p53$^{+/-}$ counterparts, indicating that reduced expression of ASPP2 compromises the tumour suppressive function of p53 (Vives et al. 2006). It is interesting to note that the frequency and kinetics of sarcoma formation are largely unaffected by p53 status in the background of ASPP2 heterozygosity (Vives et al. 2006). This suggests that, under certain circumstances, ASPP2 may mediate tumour suppression independently of p53. Lastly, the ASPP2$^{\Delta exon3}$ mouse colony was later backcrossed on a Balb/c background with the majority of the resulting ASPP2$^{\Delta exon3}$ mice surviving after weaning (Sottocornola et al. 2010). Using that colony, it has been demonstrated that ASPP2 suppresses the development of spontaneous squamous cell carcinoma via the repression of p63 in a RelA/p65-dependent manner, further supporting the role of ASPP2 as a tumour suppressor (Tordella et al. 2013).

Studies of human cancers have also led to important insights supporting the tumour suppressive functions of ASPP2. The expression of ASPP2 has been found to be frequently downregulated in a wide variety of cancer types, such as breast cancer, acute lymphoblastic leukaemia, and hepatitis B virus-positive hepatocellular carcinoma (Samuels-Lev et al. 2001; Agirre et al. 2006; J. Zhao et al. 2010). The molecular mechanisms underlying its downregulation are still poorly understood, but epigenetic modifications such as DNA methylation are very likely to be involved (Liu et al. 2005). Importantly, reduced ASPP2 expression is found more frequently in tumours harbouring wild-type p53 than those with p53 mutations, consistent with the notion that ASPP2 is an upstream regulator of p53 (Samuels-Lev et al. 2001). More recent studies have shed light on some novel mechanisms by which ASPP2 can be targeted for inactivation. For example, the cytotoxin CagA produced by *H.*

pylori can relocalise ASPP2 to the site of infection and interfere with its interaction with p53, leading to p53 degradation and cell transformation (Buti et al. 2011; Nesic et al. 2014). Lastly, the downregulation of ASPP2 expression has been linked to poor clinical prognosis in breast cancer and diffuse large B cell lymphomas, suggesting that ASPP2 is also implicated in tumour progression (Sgroi et al. 1999; Lossos et al. 2009; Cobleigh et al. 2005).

1.5.3 ASPP2 in cell polarity and development

Over the past few years, it has become increasingly clear that ASPP2 is involved in a wide range of biological processes in addition to the regulation of apoptosis. Indeed, studies performed with genetically modified mouse models have proven that ASPP2 plays a central role in the establishment and maintenance of epithelial cell polarity.

Characterisation of the ASPP2 knockout mouse model has identified ASPP2 as a key regulator of central nervous system (CNS) development (Sottocornola et al. 2010). As mentioned in the previous section, the vast majority of ASPP2 knockout mice bred on the mixed 129Sv×C57BL/6J background die around birth, which is mostly attributable to severe defects in the CNS, such as hydrocephalus and errors in neural tube closure (Vives et al. 2006; Sottocornola et al. 2010). Histological analysis has revealed that the ASPP2 knockout mice exhibit extensive loss of cell polarity in the neuroepithelium, as well as abnormal expansion of the neural progenitor pool (Sottocornola et al. 2010). The impairment of normal epithelial integrity is the cause of hydrocephalus, since it leads to increased epithelial barrier permeability and thus an outflux of cerebrospinal fluid into the brain cavity (Sottocornola et al. 2010). The loss of apical/basal cell polarity, on the other hand, may partially explain the expansion of the progenitor cells, since compromised cell polarity has been associated with hyperproliferation and a lack of differentiation (Royer et al. 2011). In agreement, the enlargement of the neural progenitor pool is not associated with reduced p53-mediated apoptosis, but rather the shortening of the cell cycle (Sottocornola et al. 2010). A recent study focusing on the 1q41q42 mircrodeletion syndrome in humans further confirmed ASPP2 as a causative gene for CNS defects (Zak et al. 2016).

Mechanistically, ASPP2 regulates the apical/basal cell polarity within the neuroepithelium by maintaining the integrity of tight/adherens junctions. Sottocornola et al. showed that ASPP2 directly binds to Par-3, a member of the polarity complex Par-3/aPKC (atypical protein kinase C)/Par6, and controls its apical/junctional localisation (Sottocornola et al. 2010). It is important to note that ASPP2 is promptly recruited to cell–cell junctions upon calcium switching together with Par-3 and ZO-1 (Zonula Occludens-1), indicating that ASPP2 is an early component of the Par complex that is required for the establishment of epithelial tight junctions (Sottocornola et al. 2010; Cong et al. 2010). Additionally, ASPP2 anchors β-catenin at cell–cell junctions together with E-cadherin, suggesting that it might also be implicated in the regulation of adherens junctions (Y. Wang et al. 2014). These observations, together with the fact that the homologue of ASPP2 in *Drosophila* is also involved in the establishment of epithelial cell–cell junctions, suggesting that ASPP2 is an evolutionarily conserved regulator of epithelial homeostasis (Royer et al. 2011).

Apart from the neuroepithelium, another tissue compartment that plays a critical role as a physical barrier is the intestinal epithelium. Previous work of our group has revealed that ASPP2 is localised at tight junctions in both the duodenum and the colon (Figure 1.14, A and B; S. Koch, unpublished data). It has also been demonstrated that a loss of ASPP2 results in disorganisation of the colonic epithelium (Figure 1.14C; S. Koch, unpublished data). Starting from here, this project was aimed to investigate the functional relevance of ASPP2 in the intestinal epithelium.

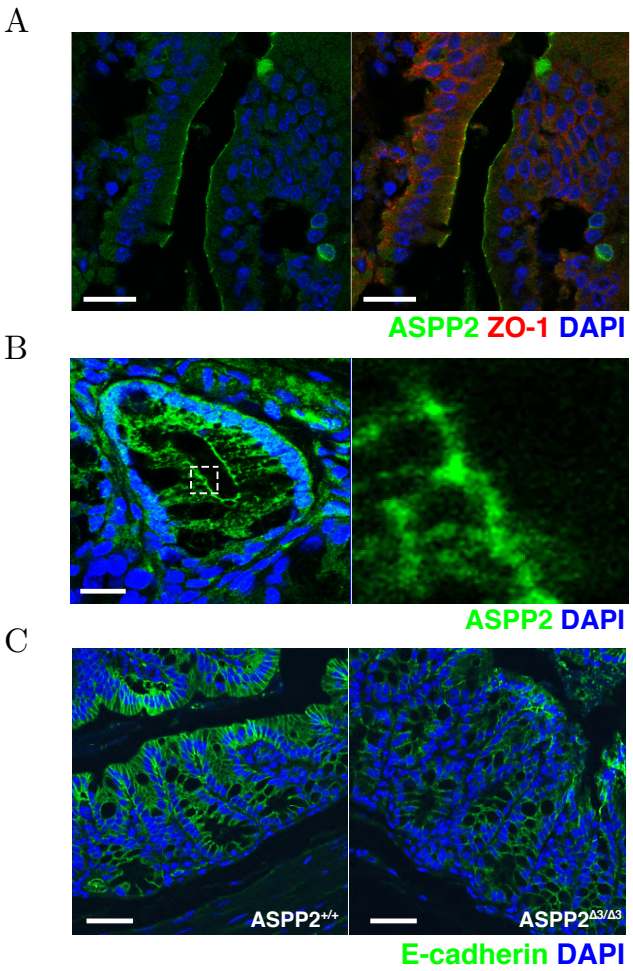


Figure 1.14: ASPP2 in the intestinal epithelium. (A) ASPP2 (green) is co-localised with ZO-1 (red) at epithelial tight junctions in the duodenum. Scale bars: 20 µm. (B) ASPP2 (green) is located at tight junctions in the colonic epithelium. Scale bar: 10 µm. (C) ASPP2 deficiency leads to disorganisation of the colonic epithelium, indicated by E-cadherin (green) staining. Scale bars: 50 µm. $ASPP2^{\Delta 3/\Delta 3}$, $ASPP2^{\Delta exon3/\Delta exon3}$.

1.6 Aims of the Study

This project originated from the observation that ASPP2 is localised at epithelial tight junctions in the intestine and is required for the maintenance of intestinal cell polarity (S. Koch, unpublished data). Therefore, the aim of the study is to better understand the role of ASPP2 in the intestinal epithelium, particularly in the context of intestinal pathologies such as inflammation and tumourigenesis.

Using transgenic mouse models and *ex vivo* organoid culture, the functional relevance of ASPP2 in the intestine is addressed in the following aspects:

1. The role of ASPP2 in chemically-induced colitis.
2. The role of ASPP2 in colitis-associated tumourigenesis.
3. The role of ASPP2 in cell autonomous regulation of intestinal homeostasis.

2 Materials and Methods

This chapter provides an overview of the materials and methods used in the described project. All reagents were purchased from Sigma-Aldrich if not otherwise stated.

2.1 Animal Work

2.1.1 Mouse colonies

All animal work carried out was approved by local ethical review and licensed by the UK Home Office (PIL: IDB1E2E61, PPL: 30/3451). Animals were bred and housed in individually ventilated cages at the Wellcome Trust Centre for Human Genetics, Oxford.

ASPP2$^{\Delta exon3}$ mutant mice were generated on a mixed C57BL/6J × 129SvJ background and backcrossed on a Balb/c background (Vives et al. 2006). Conditional ASPP2$^{exon3\text{-}fl/fl}$ mice, in which exon 3 of ASPP2 is flanked by two loxP sites, were crossed with Vil$^{cre/ERT2\ 23Syr}$, Gt(ROSA)26Sor$^{tm1(EYFP)Cos}$ mice to generate the Villin-CreER, EYFP (enhanced yellow fluorescent protein), ASPP2$^{exon3\text{-}fl/fl}$ mouse colony. Deletion of exon 3 of ASPP2 in intestinal epithelial cells (hereafter referred to as ASPP2$^{IEC\text{-}\Delta exon3}$) was induced by intraperitoneal injection of 4-hydroxytamoxifen (4-OHT). The mice were bred on the C57BL/6 background.

The conditional germline transgenic mouse model was generated by crossing ASPP2$^{exon3\text{-}fl/fl}$ mice with the Gt(ROSA)26Sor$^{tm1(cre/ERT)Brn}$ mouse colony. Deletion

of exon 3 of ASPP2 in the whole body (hereafter referred to as ASPP2$^{\Delta exon3}$) was induced by intraperitoneal injection of 4-OHT. The mice were bred on a mixed C57BL/6J × 129SvJ background (used in the DSS-induced colitis experiment), and later backcrossed to the pure C57BL/6 background (used in the AOM/DSS-induced tumourigenesis experiment).

2.1.2 Materials

4-OHT

4-OHT was dissolved in peanut oil at 20 mg/ml and stored at 4 °C for up to 1 week.

AOM

AOM was dissolved in double-distilled water (ddH_2O) at 10 mg/ml, aliquoted, and stored at −20 °C. The stock solution was diluted at a ratio of 1:10 in sterile isotonic saline immediately before use.

Base medium for lamina propria mononuclear cell (LPMC) stimulation

To prepare the base medium used to stimulate LPMCs, RPMI medium (Thermo Fisher Scientific) was supplemented with:
10% Foetal bovine serum (FBS)
2 mM L-Glutamine
200 units/ml Penicillin/Streptomycin
50 µM 2-Mercaptoethanol

DSS

2% (w/v) dextran sulfate sodium (DSS, Mw. 35,000 to 50,000, MP Biomedicals) was prepared in 1 L of filter-purified and sterilised water.

Ethylenediaminetetraacetic acid (EDTA) solution

A 0.5 M stock solution of EDTA was prepared by dissolving 18.6 g of EDTA in 100 ml ddH_2O. The pH was adjusted to 8.0 with concentrated NaOH.

GNT buffer

50 mM KCl

1.5 mM $MgCl_2$

10 mM Tris-HCl (pH 8.5)

0.01% (w/v) Gelatin

0.45% (v/v) NP-40

0.45% (v/v) Tween-20

The buffer was autoclaved and kept at 4 °C.

Percoll gradient

Percoll was purchased from GE Healthcare Life Sciences. It was mixed with 10× DPBS (Dulbecco's phosphate-buffered saline) at 9:1 to obtain the working solution (Percoll 100). To prepare 75% and 30% Percoll, Percoll 100 was diluted with 0.1% bovine serum albumin (BSA) in PBS, while 40% Percoll was prepared by diluting Percoll 100 with RPMI containing 10% FBS. The 75%/40% Percoll gradient was prepared by slowly pipetting 4 ml of 40% Percoll on top of a 3 ml 75% Percoll layer.

PBS

137 mM NaCl

2.7 mM KCl

1.8 mM KH_2PO_4

10 mM Na_2HPO_4

The pH was adjusted to 7.4 and the solution was kept at room temperature.

Tissue digestion buffer

0.05% (w/v) Collagenase D (Roche)

0.3% (w/v) Dispase II (Roche)

The buffer was prepared in phosphate-buffered saline (PBS) immediately before use.

2.1.3 Methods

AOM/DSS-induced colorectal tumourigenesis model

The AOM working solution was prepared at a concentration of 1 mg/ml on the day of the experiment. 6–8-week-old mice were intraperitoneally injected with AOM at 10 mg per 1 kg of body weight. On the same day, 2% (w/v) DSS was supplemented in the drinking water of the animals. DSS treatment lasted for 4 days before the DSS water was replaced with normal water, and the mice were then allowed to recover for 18 days. DSS treatment/recovery cycle was repeated three times. After the last round of recovery, the mice were sacrificed for analysis. The tumour load was determined by adding up the sizes of all tumours detected in each mouse (Neufert et al. 2007).

The mice were closely monitored for unwellness during the course of AOM/DSS treatment and sacrificed once one of the following endpoints was met: severe diarrhoea or greater than 25% loss of initial weight.

DNA extraction from ear biopsies

Mice were ear notched for identification and polymerase chain reaction (PCR) genotyping. The ear biopsies were digested in 100 µl of GNT buffer containing 7.8 mg/ml of proteinase K (QIAGEN) and incubated at 55 °C for 2 hours. The digested tissue was boiled for 10 minutes at 95 °C and 0.5 µl was used for PCR analysis.

DSS-induced colitis model: acute inflammation phase

Pilot experiments were performed with 2% or 4% (w/v) DSS to induce acute colitis, and the dosage of DSS was determined by the severity of the disease to best elicit the differences between wild-type and ASPP2-deficient mice.

For the project describe in this thesis, 2% (w/v) DSS was supplemented in the drinking water of 6–8-week-old mice for 5–8 consecutive days. The control group was treated with normal drinking water.

DSS-induced colitis model: recovery phase

Following the induction of acute colitis, the DSS water was replaced with normal water and the animals treated with DSS were allowed to recover for 2–6 days.

During the period of DSS treatment and recovery, the mice were closely monitored and their weight was recorded every day. Disease activity index (DAI) was determined by assigning scores for parameters including weight loss, stool consistency, and bleeding (J. J. Kim et al. 2012; Table 2.1).

Table 2.1: Disease Activity Index (DAI) Score

Score	Weight loss (%)	Stool consistency	Bleeding
0	None	Normal	None
1	0-5	–	Hemoccult positive
2	5-10	Loose stool	Visual pellet bleeding
3	10-20	–	–
4	>20	Diarrhoea	Gross bleeding

Animals were sacrificed once one of the following endpoints was met: severe diarrhoea or greater than 25% loss of the initial weight.

Flow cytometry analysis: LPMCs

The isolated colonic LPMCs were counted based on Trypan blue exclusion and 0.2 million live cells from each sample were seeded into a Corning® V-bottom 96-well plate. The cells were incubated in the base medium for LPMC restimulation in the presence of phorbol myristate acetate (PMA)/ionomycin cocktail (eBiosciences) and Brefeldin A (BioLegend) at 37 °C for 4 hours, washed with PBS, and stained with the LIVE/DEAD™ Fixable Aqua Dead Cell Stain Kit (Thermo Fisher Scientific) together with Fcblock (BioLegend) for 15 minutes on ice. After that, the cells were stained for surface markers and, where applicable, fixed and permeabilised using an eBioscience Fixation/Permeabilisation Kit. Intracellular cytokine staining was performed following the manufacturer's instructions, and staining for Foxp3 was performed using the Anti-Mouse/Rat Foxp3 Staining Set (eBioscience). Finally, the

stained LPMCs were analysed on an LSRFortessa™ cell analyser (BD Biosciences), and the data was processed using the FlowJo software (Tree Star, Inc.).

Histological scoring

Histological scores of colonic inflammation were determined in a blinded manner according to criteria described previously (Table 2.2; Horino et al. 2008).

Table 2.2: Histological Scoring System for Colitis

Feature scored	Score	Description
Inflammation severity	0	None
	1	Mild
	2	Moderate
	3	Severe
Inflammation extent	0	None
	1	Mucosa
	2	Mucosa and sub-mucosa
	3	Transmural
Crypt damage	0	None
	1	Basal 1/3 damaged
	2	Basal 2/3 damaged
	3	Crypts lost; surface epithelium present
	4	Crypts and surface epithelium lost
Percent involvement (%)	0	0
	1	1-25
	2	26-50
	3	51-75
	4	76-100

Adapted from Horino et al. 2008

Induction of transgene expression

4–6-week-old Villin-CreER, ASPP2$^{\text{exon3-fl/fl}}$ mice were intraperitoneally injected with 4-OHT dissolved in peanut oil for 4 consecutive days. All animal experiments were initiated at least one week after the last 4-OHT injection to allow complete washout of 4-OHT and successful induction of transgene expression.

Intestinal barrier permeability assay

To measure the permeability of the intestinal barrier, non-charged FITC (fluorescein isothiocyanate)-dextran (Mw. 4,000) was prepared at 50 mg/ml in PBS. The mice were gavaged with FITC-dextran at 50 mg per 100 g of body weight and fasted for 4 hours. Serum was collected via cardiac puncture and the signal of FITC-dextran was measured using a fluorometer (GloMax®-Multi Detection System) at 485 nm excitation and 510 nm emission.

Isolation of colonic LPMCs

LPMCs were isolated from the entire colon. In brief, the colon was harvested, opened longitudinally, and washed with 0.1% BSA in PBS. It was then cut into 0.5 cm segments and incubated at 37 °C for 20 minutes in RPMI medium containing 10% FBS and 5 mM EDTA, with shaking at 200 rpm. After the supernatant was aspirated, the colon segments were passed through a 100 µm cell strainer and the incubation was repeated. The tissue was incubated in RPMI containing 10% FBS for 10 minutes to neutralise the EDTA, and then incubated in tissue digestion buffer for 1 hour at 37 °C, with shaking at 200 rpm. Subsequently, the tissue was passed through a 70 µm cell strainer, centrifuged, and washed with ice-cold RPMI/FBS/EDTA. The wash step was repeated with PBS/BSA, while a 75%/40% Percoll gradient was prepared. The cells were resuspended in 3 ml of 30% Percoll and transferred onto the 40% Percoll layer. The 75%/45%/30% Percoll gradient was centrifuged at 1700 rpm for 20 minutes with the brake of the centrifuge off, and the LPMC-enriched population was recovered from the 75%/40% Percoll interface.

2.2 Tissue Culture and Cell-based Assays

2.2.1 Materials

Dulbecco's Modified Eagle's Medium (DMEM)

DMEM was purchased from Gibco-BRL, UK and stored at 4 °C.

FBS

FBS was purchased from PAA Laboratories. Heat-inactivation was performed at 55 °C for 30 minutes.

Freezing medium

90% (v/v) FBS
10% (v/v) Dimethyl sulfoxide (DMSO)
The medium was prepared and stored at 4 °C.

L-Glutamine

L-Glutamine was purchased from Gibco-BRL, UK and stored at −20 °C. The working concentration was 2 mM.

Penicillin/streptomycin

Penicillin/streptomycin was purchased from Gibco-BRL, UK and stored at −20 °C. The working concentration was 200 units/ml.

Trypsin-EDTA (0.05%)

Trypsin-EDTA (0.05%) was purchased from Gibco-BRL, UK and stored at 4 °C.

2.2.2 Methods

Cell transfection

Lipofectamine® 2000 (Thermo Fisher Scientific) was used for cell transfection according to the manufacturer's protocol. Downstream experiments were performed 24 hours after transfection.

Plasmids used in this study are listed in Table 2.3.

Table 2.3: List of Plasmids

Plasmid	Vector	Tag	Source
ASPP1-V5	pcDNA3.1	His, V5	Xin Lu's laboratory
ASPP2-V5	pcDNA3.1	His, V5	Xin Lu's laboratory

Continued on next page

Table 2.3 – continued from previous page

Plasmid	Vector	Tag	Source
iASPP-V5	pcDNA3.1	His, V5	Xin Lu's laboratory
hYAP-myc	pQCXIH	myc	Addgene

Freezing and thawing cells

Cells to be frozen down were collected by trypsinisation and centrifuged at 1,200 rpm for 5 minutes. After the supernatant was aspirated, the cells were resuspended in freezing medium and transferred to a labelled cryovial (1 ml/vial). The cryovials were kept in a Mr. Frosty™ freezing container at −80 °C for at least 24 hours, before being transferred to liquid nitrogen for long-term storage.

To thaw cells, cryovials taken from liquid nitrogen were incubated at 37 °C until the medium became liquid. The cells were transferred to a Corning® 15 ml centrifuge tube and centrifuged at 1,200 rpm for 5 minutes. The supernatant was discarded thereafter, and the cell pellet was resuspended in culture medium and seeded into new flasks/dishes at the desired density.

Maintenance and passage of cell lines

All immortalised cell lines were cultured in DMEM supplemented with 10% (v/v) FBS, L-glutamine, and penicillin/streptomycin. Cells were incubated at 37 °C in the presence of 10% CO_2. Depending on the density of the cells, medium was changed every 2–4 days. Once confluent, cells were washed with PBS once and incubated in Trypsin-EDTA at 37 °C until detachment. Trypsin was subsequently inactivated with culture medium containing FBS, and cells were seeded into new flasks/dishes at the desired density.

2.3 Primary Organoid Culture

2.3.1 Materials

Chelation buffer

2 mM EDTA

43.4 mM Sucrose

54.9 mM D-sorbitol

0.5 mM DL-dithiothreitol

The solution was prepared in PBS, filter sterilised and stored at 4 °C.

Reagents used in the establishment of intestinal organoids

Table 2.4: Reagents Used in the Establishment of Intestinal Organoids

Reagent name	Supplier	Solvent	Final conc.
Organoid culture base medium			
Advanced DMEM/F12	Invitrogen	–	–
HEPES, 1 M	Invitrogen	–	10 mM
GlutaMAX	Invitrogen	–	1×
Penicillin/Streptomycin	Invitrogen	–	1×
N2 Supplement	Invitrogen	–	1×
B27 Supplement	Invitrogen	–	1×
Growth factors and inhibitors			
Matrigel, growth factor reduced	BD Bioscience	–	–
Human recombinant EGF	Sigma-Aldrich	DPBS	50 ng/ml
Human recombinant Noggin	PeproTech	DPBS	100 ng/ml
Human recombinant R-spondin	PeproTech	DPBS	500 ng/ml
Mouse recombinant Wnt3a	PeproTech	DPBS	100 ng/ml

Noggin, R-spondin and Wnt3a can be replaced with conditioned medium, making up 5%, 10%, and 50% of the total volume, respectively.

2.3.2 Methods

5-ethynyl-2'-deoxyuridine (EdU) Incorporation

The Click-iT™ EdU Alexa Fluor™ 488 Flow Cytometry Assay Kit (Thermo Fisher Scientific) was used for the EdU incorporation experiment. Organoids were incubated in the presence of 10 µM EdU for 4.5 hours before being dissociated into

single cells. Fixable Viability Dye eFluor™ 780 (eBioscience) was used for live/dead discrimination. The staining procedure was performed following the manufacturer's protocol, and flow cytometry analysis was performed on an LSRFortessa™ cell analyser (BD Biosciences) using the FlowJo software (Tree Star Inc.).

Annexin V staining of organoids

Organoids were dissociated into single-cell suspensions and labelled by Annexin V/propidium iodide using the FITC Annexin V Apoptosis Detection Kit (BioLegend). The staining procedure was performed following the manufacturer's protocol, and flow cytometry analysis was performed on an LSRFortessa™ cell analyser (BD Biosciences) using the FlowJo software (Tree Star Inc.).

Assessment of organoid viability via MTT reduction

Organoids were retrieved from Matrigel using ice-cold PBS and seeded into a pre-warmed 96-well plate at 7 µl of Matrigel per well. The organoids were then incubated in normal culture medium containing 10 µg/ml of Resazurin for 2 hours at 37 °C. The supernatant was transferred to a black 96-well plate and fluorescence was measured with the GloMax®-Multi Detection System at 530 nm excitation and 590 nm emission.

The organoids were then subjected to various treatments. When a treatment was finished, stock MTT solution (10 mg/ml) was added to each well to a final concentration of 500 µg/ml. After incubation for 2 hours at 37 °C, the medium was removed and 20 µl of 2% SDS solution in ddH_2O was added to each well. The organoids were incubated for another 2 hours and the plate was agitated every 30 minutes. After the Matrigel was completely dissolved in the SDS solution, 75 µl of DMSO was added to each well to solubilise the reduced MTT. The OD value was measured at 562 nm using the Tecan's Sunrise Absorbance Microplate Reader. Finally, the organoid viability was calculated by normalising the MTT signal to the fluorescence value obtained from the Resazurin treatment.

Cell death induction in organoids

For the induction of apoptosis, organoids were treated with 40 ng/ml TNF-α or 5 µM Doxorubicin. Where applicable, 10 µM Z-VAD-fmk (Z-VAD) treatment was used to inhibit apoptosis.

For the induction of necroptosis, organoids were treated with 40 ng/ml TNF-α, 2 µM Compound A (a Smac mimetic), and 10 µM Z-VAD. Where applicable, 10 µM Necrostatin-1s treatment was used to inhibit necroptosis.

Cytokine preparation

IL-6, IL-22, and TNF-α were purchased from PeproTech and stock solutions were prepared following the manufacturer's protocol.

Freezing and thawing organoids

To freeze organoids, culture medium was removed and ice-cold PBS was added to each well. The Matrigel was broken up by pipetting and transferred to a Corning® 15 ml centrifuge tube. The organoid pellet was centrifuged at 150×g for 3 minutes, resuspended in freezing medium, and transferred to a labelled cryovial (1 ml/vial). The cryovials were kept in a Mr. Frosty™ freezing container at −80 °C for at least 24 hours, before being transferred to liquid nitrogen for long-term storage.

To thaw organoids, cryovials taken from liquid nitrogen were placed in a 37 °C water bath until the medium became liquid. The solution was then transferred to a Corning® 15 ml centrifuge tube and topped up with ice-cold PBS. After centrifugation at 150×g for 3 minutes, the organoids were resuspended in Matrigel and seeded into a prewarmed 48-well plate. The Matrigel was left to solidify for 10 minutes at 37 °C before the organoid culture medium was added.

Generation of colorectal tumour organoids

After the colon was collected and flushed with ice-cold PBS, colorectal tumours were isolated and dissected out with a scalpel, also washed with cold PBS. The tumours were then incubated in the chelation buffer for 60 minutes on ice. After that, the tumours were washed again with the chelation buffer and cold PBS to

get rid of the normal intestinal cells attached to them. The tumour fragments were then incubated in digestion buffer (as used for intestinal LPMC isolation) for 2 hours at 37 °C, and agitated briefly every 30 minutes. After the digestion, the tumour fragments were washed with cold PBS again and dissociated by vigorous pipetting. The cells were collected, centrifuged and embedded in Matrigel as for normal colonic crypts. Colorectal tumour organoids were maintained in organoid culture base medium supplemented with EGF, at 37 °C in the presence of 5% CO_2.

Generation of conditioned medium

Hek293T Rspo1-Fc cells (van den Brink lab), Hek293T Nog-Fc cells (van den Brink lab) and L Wnt3A cells (ATCC® CRL-2647™) were used to generate R-Spondin-, Noggin-, and Wnt3A-conditioned medium. The antibiotic selectable markers for each cell line are Zeocin (0.3 mg/ml), Puromycin (10 µg/ml) and G418 (0.4 mg/ml), respectively. The cells were cultured in advanced DMEM/F12 medium supplemented with GlutaMAX (1×), 10 µM HEPES, penicillin (100 units/ml), and streptomycin (100 µg/ml). For Rspo1-Fc and Nog-Fc cells, 5% FBS was also added to the medium.

Generation of intestinal organoids

The protocol for generating intestinal organoids was first described by Sato et al. In brief, small intestine or colon was dissected, opened longitudinally, and washed with cold PBS. The isolated tissue was then cut into 0.5 cm segments and vigorously washed with ice-cold PBS around five times until the supernatant was clear. Tissue fragments were then incubated in 2 µM EDTA/PBS and left rotating horizontally for 1 hour at 4 °C. The EDTA/PBS was removed after the incubation and the tissue segments were washed once with cold PBS. The tissue was then washed 4 times with Advanced DMEM/F12 (ADF) by vigorous pipetting. The supernatant obtained from these washes was collected and centrifuged for 5 minutes at 1,200 rpm. The cell pellet was resuspended in 15 ml ADF and passed through a 70 µm (for small intestine) or 100 µm (for colon) cell strainer. The cells were collected and centrifuged for 2 minutes at 600 rpm. At this point, the pellet was enriched with intestinal crypts, which were then resuspended in Matrigel, seeded into a prewarmed

48-well plate (Greiner Bio-One Ltd) at 20 µl Matrigel per well, and incubated for 10 minutes at 37 °C. 200 µl of organoid culture medium was added to each well and the plate was incubated at 37 °C in the presence of 5% CO_2 (Sato et al. 2009).

Lentiviral transduction of organoids

Lentiviruses expressing Venus or mCherry were kindly gifted by Dr. Rasmus Freter.

Organoids to be transduced were retrieved from Matrigel using ice-cold PBS and broken up mechanically by passing through a 23G, 5/8" syringe. The cells were centrifuged, resuspended in HBSS (Hank's Balanced Salt Solution, $+Ca^{2+}$) containing the lentivirus of interest, and transferred to a 6-well plate. The plate was centrifuged at $600\times g$ for 1 hour at room temperature and left at 37 °C for 4 hours. After that, the cells were collected and resuspended in Matrigel, and cultured at 37 °C in the presence of 5% CO_2 as normal organoids. The expression of transgenes could be detected 24 hours after the transduction.

Organoid-based regeneration model

Cell death induction was performed in a 48-well plate where organoids were routinely cultured. After the treatment, organoids were transferred to a 96-well plate and incubated with Resazurin, as described in the 'Assessment of organoid viability via MTT reduction' section. The organoids were left in culture for intended periods of time and the culture medium was changed every other day. MTT assays were performed at the end of the experiments as a readout for cell viability.

Organoid fusion

Organoids to be fused were retrieved from Matrigel using ice-cold PBS and washed once to get rid of cell debris. The organoids were then incubated in 100 µl of TrypLE Express Enzyme (Thermo Fisher Scientific) for 3 minutes at 37 °C, and broken up by pipetting. Next, 80 µl of organoid base medium was added to each tube, together with 20 µl of DNase I solution in PBS (2000 units/ml stock). The organoid fragments were incubated for 5 minutes at room temperature and mechanically broken up, again by pipetting. The aim was to split the organoids into small

fragments but not into single cells. The organoid fragments were then combined into one Eppendorf tube, centrifuged, and resuspended in 50 µl of complete culture medium containing 10% Matrigel, 1 µM CHIR99021, and 10 µM Y-27632. The cells were seeded into a V-bottom 96-well plate precoated with 5% FBS/PBS and kept at 37 °C in the presence of 5% CO_2. After 24 hours, the cell aggregates were collected, embedded in Matrigel, and cultured as normal organoids. Organoid fusion should be detected within 48 hours.

Organoid labelling with CellTracker™

CellTracker™Blue CMAC Dye was purchased from Invitrogen and the organoids were labelled following the manufacturer's protocol.

Passage of organoids

Organoids were retrieved from Matrigel using ice-cold PBS and broken up mechanically by passing through a 23G, 5/8" syringe. The organoid fragments were centrifuged and washed with ice-cold PBS, and then reseeded in fresh Matrigel. The passage was performed every 7–10 days at a ratio of 1:4.

Preparation of single cell suspension

Organoids were retrieved from Matrigel using ice-cold PBS and washed once to get rid of cell debris. The organoids were then incubated in 100 µl of TrypLE Express Enzyme (Thermo Fisher Scientific) for 5 minutes at 37 °C, and broken up by vigorous pipetting. Next, 80 µl of organoid base medium was added to each tube, together with 20 µl of DNase I solution in PBS (2000 units/ml stock). The organoid fragments were incubated for 10 minutes at room temperature and mechanically broken up again by pipetting.

Time-lapse imaging

Images were acquired using a Nikon TE 2000-E Eclipse inverted microscope, with a 10×/0.3 NA Plan Fluor Ph1 objective. The system was maintained at 37 °C in the presence of 5% CO_2. Z-stack images of 1 mm in depth were acquired at 100 µm intervals (11 steps per acquisition) approximately every 30 minutes.

Image analysis was performed using the MetaMorph software (Molecular Devices, LLC.) and ImageJ.

VPA/CHIR99021 treatment

VPA and CHIR99021 were purchased from Cambridge Bioscience Ltd and stock solutions were prepared following the manufacturer's protocols. The working concentrations of VPA and CHIR99021 were 1 mM and 3 µM, respectively.

Whole-mount immunofluorescent (IF) staining of organoids

Intestinal organoids to be stained were cultured in an 8-well μ-Slide (ibidi GmbH). The culture medium was removed and the wells were washed with ice-cold PBS. The organoids were then incubated with 4% paraformaldehyde (PFA) on a see-saw rocker for 30 minutes at 4 °C, with shaking at 30 rpm. After the incubation, the Matrigel was mostly dissolved and PFA was removed with care not to lose organoids. The wells were washed twice with PBS, and the organoids were then incubated in 50 mM NH_4Cl/PBS for 30 minutes at room temperature to minimise autofluorescence. The wash step was repeated, followed by immersing the organoids in 0.2% Triton/PBS for 30 minutes at room temperature. After another two washes, the organoids were incubated in 0.5% BSA/PBS for 45 minutes at room temperature to block unspecific binding of antibodies. Primary antibodies were diluted in 0.5% BSA/PBS, and the organoids were incubated at 4 °C overnight.

The next day, the organoids were washed 5 times with PBS, and secondary antibodies diluted in 0.5% BSA/PBS were prepared. The organoids were incubated in secondary antibodies together with 4',6-Diamidino-2-Phenylindole (DAPI)/Phalloidin (Thermo Fisher Scientific) for 2 hours at room temperature, away from light. After that, the organoids were washed 5 times with PBS and once with ddH_2O before mounting medium was applied. The stained samples were kept at 4 °C.

2.4 DNA and RNA Techniques

2.4.1 Materials

50× TAE Buffer

242 g Tris base

57.1 ml Glacial Acetic Acid

100 ml 0.5 M EDTA (pH 8.0)

ddH_2O was added up to 1 L and the pH was adjusted to 8.5.

Agarose gel for DNA electrophoresis

Agarose powder (Gibco BRL, UK) was weighed and dissolved in 1× Tris-Acetate-EDTA (TAE) buffer at an appropriate percentage (w/v). The solution was microwaved, supplemented with 20 µg/µl ethidium bromide, and poured into a gel-casting chamber to solidify.

DNA marker

DNA ladders (1 kb and 100 bp) were purchased from Bioline Reagents Ltd. and used as recommended by the manufacturer.

Ethidium bromide

A 10 mg/ml stock solution was prepared by dissolving 0.2 g of ethidium bromide in 20 ml of ddH_2O.

GoTaq® Green Master Mix

The GoTaq® Green Master Mix was purchased from Promega and used for genotyping PCR reactions.

SuperScript® First-Strand Synthesis System

The SuperScript® First-Strand Synthesis System Kit for complementary DNA (cDNA) synthesis was purchased from Invitrogen and stored at −20 °C.

2.4.2 Methods

Agarose gel electrophoresis

Agarose gel electrophoresis was performed with the Hoefer Nucleic Acid Electrophoresis System. Gels were run in 1× TAE Buffer at a constant voltage of 100 V, and signals were visualised using the UVP Bio Imaging System.

PCR programme for mouse genotyping

GoTaq® Green Master Mix (Promega) was used for genotyping PCR reactions. PCR reactions were performed on the ProFlex PCR System (Thermo Fisher Scientific). The PCR programme was as follows:

Table 2.5: PCR Programme for Mouse Genotyping

Step	Temperature	Duration
1	94 °C	3 min
2	94 °C	40 s
3	60 °C	40 s
4	72 °C	40 s
5	Repeat steps 2 to 4 for 29 times	
6	72 °C	3 min

PCR primers for genotyping

Table 2.6: PCR Primers for Genotyping

Gene	Primers	Expected bands
ASPP2	5'-CGGTTTGGAAGTCAAAGGAA-3' 5' -TCAATGTGTCCAGCACCCTA-3' 5'-TACCCGCTTCCATTGCTCAG-3'	WT: 650 bp Mutant: 800 bp
$ASPP2^{loxP}$	5'-TGGACAGGCTGAGCTGTTAG-3' 5'-ACACTTTCACCAACCCTAGGTC-3'	WT: < 200 bp Mutant: > 200 bp
EYFP	5'-AAGACCGCGAAGAGTTTGTC-3' 5'-AAAGTCGCTCTGAGTTGTTAT-3' 5'-GGAGCGGGAGAAATGGATATG-3'	WT: 600 bp Mutant: 320 bp
CreER	5'-CATTTGGGCCAGCTAAACAT-3' 5'-ATTCTCCCACCGTCAGTACG-3'	CreER: 308 bp

Continued on next page

Table 2.6 – continued from previous page

Gene	Primers	Expected bands
Actin	5'-GGTGTCATGGTAGGTATGGGT-3' 5'-CGCACAATCTCACGTTCAG-3'	Actin: 780 bp

Abbreviation: ASPP2^{loxP}, ASPP2$^{exon3\text{-}fl/fl}$.

Primers for real-time quantitative PCR (qPCR)

Primers were designed using the online platform Primer3Plus and synthesised by Eurofins Genomics if not otherwise stated. The lyophilised primers were dissolved in ddH_2O to a stock concentration of 100 µM.

Table 2.7: Primers for Real-time Quantitative PCR

Target Gene	Sequence
Cytokines	
IL-1β	F: 5'-TTGACGGACCCCAAAAGATG-3' R: 5'-AGAAGGTGCTCATGTCCTCA-3'
IL-6	F: 5'-CTGCAAGAGACTTCCATCCAG-3' R: 5'-AGTGGTATAGACAGGTCTGTTGG-3'
IL-22	F: 5'-GGAGAGATCAAGGCGATTGG-3' R: 5'-GAAGGCAGGAAGGAGCAGTT-3'
IL-23a	F: 5'-AATAATGTGCCCCGTATCCAGT-3' R: 5'-GCTCCCCTTTGAAGATGTCAG-3'
IFN-γ	F: 5'-ATGAACGCTACACACTGCATC-3' R: 5'-CCATCCTTTTGCCAGTTCCTC-3'
TNF-α	F: 5'-TCTCATCAGTTCTATGGCCC-3' R: 5'-GGGAGTAGACAAGGTACAAC-3'
Stem Cell Markers	
Bmi1	F: 5'-TCGCTTTGGGTGTGTCCT-3' R: 5'-CTTGCTGGTCTCCAAGTAACG-3'
Olfm4	F: 5'-GCACGATGAGTTACAGCCTTCT-3' R: 5'-GGTGATGTTGGAGGTGTGGT-3'
Lgr5	Sequence is intellectual property of Invitrogen
Intestinal Lineage Markers	
Mucin 2	F: 5'-ATGCCCACCTCCTCAAAGAC-3' R: 5'-GTAGTTTCCGTTGGAACAGTGAA-3'
Lysoyzme 1	F: 5'-GCTGTGCCTGTCCTGATCTT-3' R: 5'-TCCTGTGGTTATTGGCTGGT-3'

Continued on next page

Table 2.7 – continued from previous page

Target Gene	Sequence
Housekeeping Gene	
GAPDH	F: 5'-TGTCAGCAATGCATCCTGCA-3' R: 5'-TGTATGCAGGGATGATGTTC-3'

qPCR

qPCR was performed with the QuantiTect SyBr Green PCR Kit (QIAGEN) on the StepOnePlus Real-Time PCR System (Thermo Fisher Scientific). The reaction system and qPCR programme were as follows:

Table 2.8: Real-time qPCR Reaction System

Component	Volume
Sybr Green	5 µl
cDNA template	2.5 µl
Primer mix (10 µM)	1 µl
ddH_2O	1.5 µl

Table 2.9: Real-time qPCR Programme

Step	Temperature	Duration
1	95 °C	10 min
2	95 °C	15 s
3	60 °C	1 min
4	Repeat steps 2 and 3 for 39 times	
5	95 °C	15 s
6	60 °C	1 min
7	95 °C	15 s

Each qPCR reaction was performed in duplicate. The comparative Ct method ($\Delta\Delta C_T$ method) was used to compare the expression levels of target genes with GAPDH as the internal control.

RNA extraction and cDNA synthesis

RNA was extracted from cells according to the protocol of the QIAGEN RNeasy Mini Kit. Up to 250 ng of total RNA was used for cDNA synthesis following

the manufacturer's protocol. The cDNA generated was diluted at a 1:4 ratio for the qPCR experiment.

2.5 Histology Techniques

2.5.1 Materials

Acid alcohol

99% (v/v) 70% Alcohol
1% (v/v) Concentrated hydrochloric acid

Citric acid buffer

A 10× stock citric acid buffer (100 mM) was made by dissolving 29.4 g sodium citrate in 1 L ddH_2O. The pH was adjusted to 6.0 with NaOH.

DAPI staining solution

A 1,000× stock of DAPI solution (10 ml/mg) was prepared in ddH_2O and kept at −20 °C.

PFA fixing solution

4% (w/v) solution was prepared by dissolving PFA in ddH_2O in a fume-hood. 10× PBS was added until the final concentration of PBS was 1×. The pH was adjusted to 7.0 with concentrated HCl. The solution was aliquoted and stored at −20 °C.

Scott's tap water

2% (w/v) $NaHCO_3$
0.35% (w/v) $MgSO_4$

2.5.2 Methods

Haematoxylin and eosin (H&E) staining

Paraffin sections were deparaffinised in two changes of histoclear and rehydrated in a decreasing gradient of ethanol. Slides were then stained in haematoxylin for

3 minutes. After the excess stain was washed off with tap water, the slides were dipped in 1% acidic alcohol once, washed again in tap water, and immersed in Scott's tap water for 30 seconds. Slides were rinsed in tap water, stained in eosin for 4 minutes, washed again and dehydrated with an increasing gradient of ethanol solutions. Finally, the slides were cleared in two changes of histoclear and mounted with Vectamount mounting medium (Vector Labs).

Preparation of paraffin-embedded samples

Tissues collected from mice were kept in 10% formalin at 4 °C overnight and processed using an Excelsior™AS tissue processor (Thermo Fisher Scientific). For paraffin-embedded tissues, serial 4 mm sections were obtained.

TUNEL assay

Terminal deoxynucleotidyl transferase dUTP nick end labelling (TUNEL) analysis was performed using the ApopTag® Red In Situ Apoptosis Detection Kit (Millipore). Paraffin sections were labelled following the manufacturer's protocol.

Tissue IF staining

Paraffin sections were deparaffinised in two changes of histoclear and rehydrated in a decreasing gradient of ethanol. Heat-induced antigen retrieval was performed using the microwave oven method with citric acid buffer. In brief, slides were immersed in antigen retrieval buffer and boiled in a microwave oven at 1000 W for 10 minutes. The slides were then left in the buffer until they cooled down, followed by incubation with 5% NGS/PBS at room temperature for 30 minutes. After that, the slides were incubated with primary antibodies diluted in 5% NGS/PBS at 4 °C overnight in a humidified chamber.

The day after, the slides were washed three times for 5 minutes each with PBS, followed by incubation with secondary antibodies and DAPI for 45 minutes at room temperature. After another 3×5 min PBS washes, the slides were mounted with the Fluoromount-G™ mounting medium (Southern Biotech) and kept at 4 °C, away from light.

Tissue immunohistochemical (IHC) staining

Deparaffinised and rehydrated sections were incubated in 3% hydrogen peroxide in methanol for 10 minutes. Heat-induced antigen retrieval was performed using the pressure cooker method with citric acid buffer. In brief, antigen retrieval buffer was boiled in a pressure cooker, and slides were placed into it with the lid secured as per the manufacturer's instructions. The slides were then incubated at full pressure of the cooker for 3 minutes. Subsequently, the slides were transferred to an empty container and left in the antigen retrieval buffer until it was cold enough to handle. They were then blocked with 5% normal goat serum (NGS) diluted in PBS (NGS/PBS) for 30 minutes at room temperature. The slides were then incubated with primary antibodies diluted in 5% NGS/PBS at 4 °C overnight in a humidified chamber.

The day after, the slides were washed three times for 5 minutes each with PBS. Secondary antibodies were diluted in 5% NGS/PBS and applied to the slides for 1 hour at room temperature. After another 3×5 min PBS washes, the slides were incubated in the VECTASTAIN Elite ABC HRP Reagent (Vector Labs) for 15 minutes at room temperature. The slides were washed again, and the staining was developed with the DAB (3,3'-diaminobenzidine) Peroxidase (HRP) Substrate Kit (Vector Labs). Finally, the slides were counter-stained with haematoxylin, dehydrated, and mounted with Vectamount mounting medium (Vector Labs).

2.6 Biochemistry

2.6.1 Materials

4× SDS-polyacrylamide gel electrophoresisample (PAGE) buffer

0.2 M Tris-HCl (pH 6.8)

8% (w/v) SDS (sodium dodecyl sulfate)

40% (v/v) Glycerol

0.4% (w/v) Bromophenol blue

10% (v/v) β-Mercaptoethanol

10× SDS-PAGE running buffer

720 g Glycine

150 g Tris base

50 g SDS

ddH_2O was added up to 5 L.

1× SDS-PAGE transfer buffer

10% 10× Transfer buffer

20% Methanol

70% ddH_2O

10× Tris-buffered saline (TBS)

24 g Tris base

88 g NaCl

ddH_2O was added up to 1 L and the pH was adjusted to 7.6 with HCl.

1× TBS Tween (TBST)

10% (v/v) 10× TBS

0.1% (v/v) Tween-20

2× Tris-Tricine SDS-PAGE sample buffer

0.9 M Tris-HCl (pH 8.45)

8% (w/v) SDS

24% (v/v) Glycerol

0.015% Coomassie Blue G

0.2 M Dithiothreitol (DTT)

10× Tris-Tricine SDS-PAGE cathode buffer

1 M Tris-base

1 M Tricine

1% (w/v) SDS

Ammonium persulfate (APS)

APS powder was dissolved in ddH_2O at 10% (w/v).

Blocking buffer for western blotting

5% (w/v) fat-free milk or 5% (w/v) BSA was dissolved in TBS containing 0.1% Tween 20 (1× TBST).

COmplete™ protein inhibitor cocktail

One COmplete™ Protein Inhibitor Cocktail tablet (Roche Diagnostics) was dissolved in 2 ml of ddH_2O to make a 25× stock solution. This can be kept at −20 °C for up to 12 weeks.

NETN buffer

150 mM NaCl

1 mM EDTA

50 mM Tris (pH 8.0)

1% (v/v) NP40

The buffer was stored at 4 °C. Protease inhibitor and phosphatase inhibitor cocktails were added freshly for each experiment.

Phosphatase inhibitor cocktail

One PhosSTOP™ Phosphatase Inhibitor Cocktail tablet (Roche Diagnostics) was dissolved in 1 ml ddH_2O to make a 10× stock solution. This was kept at 4 °C.

Ponceau S solution

Ponceau S solution was purchased as a 0.1% (w/v) solution in 5% acetic acid.

Protein molecular weight markers

Prestained protein markers were purchased from New England Biolabs and used in SDS-PAGE.

Radioimmunoprecipitation assay (RIPA) buffer

150 mM NaCl

1% (v/v) NP-40

0.1% (w/v) SDS

50 mM Tris base

The buffer was stored at 4 °C. Protease and phosphatase inhibitor cocktails were added freshly for each experiment.

SDS-PAGE gels

SDS-PAGE was performed with homemade SDS-polyacrylamide gels prepared according to the recipes in Table 2.10.

Table 2.10: SDS-Polyacrylamide Gels

	Resolving gels				Stacking gel
	6%	8%	10%	12%	4%
30% Acryl/Bis	2 ml	2.7 ml	3.3 ml	4.0 ml	1.3 ml
1.5 M Tris-HCl pH 8.8	2.5 ml	2.5 ml	2.5 ml	2.5 ml	–
1.0 M Tris-HCl pH 6.8	–	–	–	–	2.5 ml
10% SDS	100 µl	100 µl	100 µl	100 µl	100 µl
10% APS	100 µl	100 µl	100 µl	100 µl	100 µl
TEMED	10 µl	8 µl	5 µl	5 µl	10 µl
ddH_2O	5.3 ml	4.6 ml	4.0 ml	3.3 ml	6.1 ml
Total Volume	10 ml	10 ml	10 ml	10 ml	10 ml

Abbreviations: Acry/Bis, acrylamide/bis-acrylamide; TEMED, tetramethylethylenediamine.

SDS solution

10% (w/v) solution of SDS was prepared in ddH_2O and stored at room temperature.

Tris-tricine gels

8% tris-tricine gels were made according to the following recipe (total volume 10 ml):

3 ml 30% Acrylamide/bis-acrylamide

33 µl APS

1.8 ml 50% Glycerol

12 µl TEMED

3.3 ml Tris-tricine SDS-PAGE gel buffer

ddH_2O was added up to 10 ml.

Tris-tricine SDS-PAGE gel buffer

3 M Tris-base

0.3% (w/v) SDS

The pH was adjusted to 8.5.

Urea buffer

8 M Urea

1 M Thiourea

0.5% (w/v) CHAPS

50 mM DTT

24 mM Spermine

The buffer was aliquoted and stored at −20 °C.

Water

15.0 MΩ water generated from the MilliQ water system was used for all procedures.

2.6.2 Methods

Immunoprecipitation (IP)

Protein lysates were prepared in RIPA or NETN buffer as described in the 'Protein lysate preparation' section. For each sample used for IP, up to 2 mg of protein was pre-cleared with 30 µl of 70% protein G agarose beads (Roche) at 4 °C for 1 hour, with rotation at 30 rpm. Simultaneously, another aliquot of 70% protein G agarose beads were blocked with DMEM containing 5% FBS. After the preclearing step, the protein lysate was centrifuged at 2,500 rpm for 30 seconds. The supernatant was transferred to a new Eppendorf tube, followed by 30 µl of blocked beads and IP antibodies at desired concentrations. The reaction was left rotating overnight at 4 °C. A separate tube containing non-specific IgG was used as a control.

On the next day, the beads were centrifuged at 3,000 rpm for 1 minute and washed three times with ice-cold lysis buffer. After the last wash, the supernatant was discarded and 30 µl of 2× SDS-PAGE sample buffer was added to the beads. The beads were incubated at 95 °C for 10 minutes and stored at −20 °C before SDS-PAGE/western blot analysis.

Protein lysate preparation

Cells or organoid cultures were washed with ice-cold PBS and lysed in chilled lysis buffer. The samples were kept on ice for 30 minutes and centrifuged at full speed for 15 minutes at 4 °C. The supernatant was transferred to a new tube and used for protein quantification. Finally, SDS-PAGE sample buffer was added to the protein samples and boiled at 95 °C for 5 minutes. The protein samples were stored at −20 °C.

Protein concentration determination

The concentration of protein lysates was determined using the Bradford protein assay. Measurements were taken in duplicate using a spectrophotometer (Anthus Labtech Instrument) at 595 nm, and the concentration was extrapolated from a standard curve generated with known concentrations of BSA.

SDS-PAGE

SDS-PAGE was performed using Mini-PROTEAN® Tetra Handcast Systems (Bio-Rad). Equal amounts of protein samples were loaded onto an SDS-PAGE gel along with prestained protein markers (New England Biolabs). Gels were run in 1× SDS-PAGE running buffer at a constant voltage of 100 V.

Western blotting

After the SDS-PAGE running process was complete, the proteins were blotted onto a nitrocellulose membrane (Whatman) using the Hoefer™ Standard Electrophoresis Blotting System. The transfer tank was filled with 1× SDS-PAGE transfer buffer complemented with 20% methanol. Protein transfers were performed at a constant voltage of 80 V for 3 hours at 4 °C.

When the transfer process was finished, the membrane was stained with Ponceau S solution to examine the quality of sample loading and protein transfer. The membranes were then washed with tap water and incubated in the blocking buffer for 1 hour at room temperature. Primary antibodies were diluted in 5% milk/TBST or BSA/TBST, depending on the recommendations of the manufacturers. The membranes were incubated in primary antibodies for 2 hours at room temperature or overnight at 4 °C. Subsequently, the membranes were washed three times for 10 minutes each with TBST and incubated with secondary antibodies diluted in 5% milk/TBST or BSA/TBST for 1 hour at room temperature. After another 3×10 min TBST washes, the membranes were incubated with Amersham ECL Prime Western Blotting Detection Reagent (GE Healthcare) followed by the visualisation of signals using a Fujifilm autoradiography-based system.

2.7 Antibodies

Primary antibodies

Table 2.11: Primary Antibodies

Antigen	Clone	Host/Type	Source	Catalog No.	Applications
ASPP2	S-32	Rabbit pAb	Lu lab	–	WB (1:750)
β-Actin	C-2	Mouse mAb	Santa Cruz	sc-803	WB (1:1500)
β-catenin	14	Mouse mAb	BD Pharmigen	610154	IF (1:200), WB (1:5000)
β-Tubulin	TUB2.1	Mouse mAb	abcam	ab11308	WB (1:1000)
CD3	17A2	Rat mAb	BioLegend	100227	FC (1:40)
CD4	RM4-4	Rat mAb	BioLegend	116011	FC (1:200)
CD45	30-F11	Rat mAb	BioLegend	103133	FC (1:40)
CD8a	53-6.7	Rat mAb	BioLegend	100721	FC (1:200)
Cleaved Caspase-3 (Asp175)	–	Rabbit pAb	Cell Signaling	9661	IF (1:300), WB (1:1000)
E-cadherin	36	Mouse mAb	BD Pharmigen	610181	IF (1:200)
EphB3	7E5	Mouse mAb	Santa Cruz	sc-100299	WB (1:200)
ERK1/2	137F5	Rabbit mAb	Cell Signaling	4695	WB (1:1000)
F4/80	BM8	Rat mAb	BioLegend	123117	FC (1:50)
FoxP3	FJK-16s	Rat mAb	eBioscience	11-5773-80	FC (1:100)
GFP/EYFP	D5.1	Rabbit mAb	Cell Signaling	2956	IHC/IF (1:100), WB (1:1000)
IL-1β	NJTEN3	Rat mAb	eBioscience	11-7114-80	FC (1:400)

Continued on next page

Table 2.11 – continued from previous page

Antigen	Clone	Host/Type	Source	Catalog No.	Applications
IL-6	MP5-20F3	Rat mAb	BioLegend	504503	FC (1:200)
Ki67	–	Rabbit pAb	abcam	ab15580	IF (1:2000)
Lysozyme	–	Rabbit pAb	Dako	A0099	IF (1:), WB (1:200)
Math1	–	Rabbit pAb	Santa Cruz	sc-98520	WB (1:1000)
MLKL	D6W1K	Rabbit mAb	Cell Signaling	37705	WB (1:1000)
Mucin 2	–	Rabbit pAb	Santa Cruz	sc-15334	IF (1:200)
Myc-tag	9E10	Mouse mAb	Lu lab	–	IP (1:200)
Phospho-ERK1/2 (Thr202/Tyr204)	–	Rabbit pAb	Cell Signaling	9101	IF (1:250), WB (1:1000)
Phospho-Histone H3 (Ser10)	–	Rabbit pAb	Millipore	06-570	IF (1:200), WB (1:500)
Phospho-MLKL (Ser345)	EPR9515(2)	Rabbit mAb	abcam	ab196436	WB (1:1000)
Phospho-STAT3 (Tyr705)	D3A7	Rabbit mAb	Cell Signaling	9145	WB (1:1000)
Phospho-YAP (Ser127)	–	Rabbit pAb	Cell Signaling	4911	WB (1:1000)
RIPK1	D94C12	Rabbit mAb	Cell Signaling	3493	WB (1:1000)
STAT3	124H6	Mouse mAb	Cell Signaling	9139	WB (1:1000)
TNF-α	MP6-XT22	Rat mAb	BioLegend	506349	FC (1:100)
V5-tag	–	Rabbit pAb	abcam	ab15828	WB (1:1000)
YAP	–	Rabbit pAb	Cell Signaling	4912	IHC (1:200), WB (1:1000)

Abbreviations: mAb - Monoclonal antibody; pAb - Polyclonal antibody; FC - Flow cytometry; IF - Immunofluorescence; IHC - Immunohistochemistry; IP - Immunoprecipitation; WB - Western blotting.

Secondary antibodies

Table 2.12: Secondary Antibodies

Type	Host	Supplier	Catalog No.	Application
Alexa Fluor®488 F(ab')$_2$ Anti-Rabbit IgG (H+L)	Goat	Invitrogen	A21246	IF (1:400)
Alexa Fluor®647 F(ab')$_2$ Anti-Mouse IgG (H+L)	Goat	Invitrogen	A21237	IF (1:400)
Alexa Fluor®488 Anti-Rabbit IgG (H+L)	Donkey	Invitrogen	A21206	IF (1:400)
Alexa Fluor®647 Anti-Mouse IgG (H+L)	Donkey	Invitrogen	A31571	IF (1:400)
Alexa Fluor®488 Anti-Rabbit IgG (H+L)	Goat	Invitrogen	A11008	IF (1:400)
Alexa Fluor®647 Anti-Mouse IgG (H+L)	Goat	Invitrogen	A21235	IF (1:400)
Anti-Rabbit Immunoglobulins/HRP	Pig	Dako	P0399	WB (1:2000)
Anti-Mouse Immunoglobulins/HRP	Rabbit	Dako	P0161	WB (1:2000)
Biotinylated Anti-Mouse IgG Antibody	Goat	Vector Labs	BA-9200	IHC (1:250)
Biotinylated Anti-Rabbit IgG Antibody	Goat	Vector Labs	BA-1000	IHC (1:250)

Abbreviations: HRP - Horseradish peroxidase; IF - Immunofluorescence; IHC - Immunohistochemistry; WB - Western blotting.

2.8 Data Analysis

Image analysis

Autoradiographs from western blotting experiments were scanned using the RICOH Aficio MP C5501 All-In-One (printer/scanner/copier). Adobe Photoshop (Adobe Systems Inc.) and ImageJ were used to manipulate images. The manipulations were limited to adjustment of image size, brightness, and/or contrast. For 3D reconstruction of z-stack images obtained from confocal microscopy, the standard deviation projection mode of ImageJ was used.

The quantification of Ki67-positive cells in colon tumour samples was performed on sections co-stained for Ki67 and E-cadherin by immunofluorescence. Confocal images were acquired using a Zeiss LSM 710 microscope, and at least three different fields of view were taken for each section. Positive staining for pH3 was quantified by an automated macro written for ImageJ by Mark Shipman. In brief, a mask for E-cadherin-positive epithelial cells was created, followed by a mask for DAPI-positive nuclei. This marked all nuclei of epithelial cells within the view. The mask was then used to measure the intensity of the nuclear Ki67 of epithelial cells. The cut-offs for Ki67 intensity and size of nucleus were set empirically, and the number of Ki67-positive cells were divided by the number of epithelial nuclei to calculate a tumour's proliferation index.

Statistical analysis

Statistical analysis was performed using Apple Numbers (Apple Inc.) and GraphPad Prism (GraphPad Software Inc.). The log-rank (Mantel–Cox) test was performed to determine the statistical significance of differences in cumulative survival of the AOM/DSS-treated mouse cohort. If not otherwise stated, two-tailed unpaired *t*-tests were used to calculate the statistical differences of other measurements. Differences were considered statistically significant at a p-value of 5% or lower.

3

Loss of ASPP2 Leads to Delayed Recovery from DSS-Induced Colitis

3.1 Introduction

In order to investigate the functional importance of ASPP2 *in vivo*, various ASPP2 transgenic mouse models have been generated. As for the ASPP2-deficient mouse colonies used for this study, the inactivation of ASPP2 was achieved by replacing exon 3 of the murine Tp53bp2 gene with a neomycin resistance gene cassette (Vives et al. 2006). The ASPP2$^{\Delta exon3}$ mouse model was first generated on the C57BL6/6J background, but homozygous pups were not viable (Vives et al. 2006). The colony was then crossed with the 129Sv mouse strain and further back-crossed to a pure Balb/c background, and the majority of the resultant ASPP2$^{\Delta exon3}$ mice were able to survive after weaning (Sottocornola et al. 2010).

Using the ASPP2$^{\Delta exon3}$ mouse model on the Balb/c background, it has been demonstrated that ASPP2 is an important regulator of a variety of biological processes, particularly the establishment and maintenance of the apical/basal polarity and tight junctions of the neuroepithelium (Sottocornola et al. 2010). Further to that, ASPP2 has also been shown to act as a haploinsufficient tumour suppressor, as well as an important regulator of the NF-κB pathway (Vives et al. 2006; Tordella et al. 2013). The importance of ASPP2 as a mediator of

inflammation is further supported by the observation that ASPP2 can be induced by LPS and IFN in a STAT1-dependent manner and mediates LPS-induced apoptosis (Turnquist et al. 2014). Taken together, it is reasonable to hypothesise that ASPP2 plays a key regulatory role at the crossroad of cell polarity, inflammation, and tumourigenesis.

With regard to this particular study, the intestine was used as a model system to investigate the functional relevance of ASPP2 in the epithelium. Previous work in our lab has shown that ASPP2 is localised at tight junctions of the intestinal epithelium, and that a loss of ASPP2 results in dysregulated intestinal cell polarity (S. Koch, unpublished data). Given that the polarisation of the intestinal epithelium is crucial for the maintenance of its homeostasis, and that the establishment of cell polarity is a determinant of tissue regeneration in the event of tissue damage (Roignot et al. 2013), the involvement of ASPP2 in both the acute phase and the recovery phase of DSS-induced colitis was investigated.

In the intestine, tissue regeneration is the result of a well-coordinated balance between proinflammatory and anti-inflammatory signals, accomplished by the constant crosstalk between epithelial cells and the immune system (Karin et al. 2016). Since the intestinal mucosa is the largest and most dynamic immunological compartment within the body, it is a suitable system to study epithelial cell autonomous and non-autonomous factors implicated in tissue regeneration. To that end, a germline ASPP2 mutant mouse model was employed in this study as a supplement to the intestinal epithelium-specific ASPP2-deficient mice. The aim was to better understand the functional implications of ASPP2 deficiency in the intestinal epithelium, particularly the distinction between epithelial cell autonomous and non-autonomous mechanisms.

3.2 Results

3.2.1 DSS-induced colitis was not affected by the loss of ASPP2 in the intestinal epithelium

In order to study the functional importance of ASPP2 in the intestinal epithelium, an IEC-specific ASPP2 conditional knockout mouse model was generated. The mice carried an ASPP2 transgene harbouring loxP-flanked exon 3 ($ASPP2^{exon3\text{-}fl/fl}$), together with a Villin promoter-driven CreER recombinase (Villin-CreER), which has been reported to be specifically induced by 4-hydroxytamoxifen (4-OHT) treatment in the gastrointestinal epithelium (El Marjou et al. 2004; Feil et al. 2009). In addition, the mice were crossed with the R26-stop-EYFP mouse line. As a result, the expression of EYFP can be used as an indicator of the activity of CreER, and EYFP-positive cells should be depleted of ASPP2. Immunohistochemical (IHC) staining of EYFP was performed on colon sections of 4-OHT-treated Villin-CreER, $ASPP2^{exon3\text{-}fl/fl}$ ($ASPP2^{IEC\text{-}\Delta exon3}$) mice to demonstrate that 4-OHT administration could indeed lead to the expression of the EYFP transgene (Figure 3.1A).

Since the ASPP2 antibody available for IHC and IF staining (clone S-32) was raised against amino acids 59–383 of murine ASPP2, which overlaps with its third exon (amino acids 97–123), it is not suitable for the distinction between wild-type and $ASPP2^{\Delta exon3}$ epithelial cells. As a result, in order to confirm the correlation between the positivity of EYFP and ASPP2 deficiency, intestinal epithelial cells from $ASPP2^{IEC\text{-}\Delta exon3}$ mice were sorted into EYFP-positive and -negative populations (Figure 3.1B). Western blot analysis was performed on the sorted cells, where the protein level of ASPP2 was significantly reduced in the EYFP-positive cell population, suggesting that the expression of EYFP was indicative of ASPP2 status (Figure 3.1C). It is worth noting that the recombination efficiency in the colon ranged from ∼50% to ∼80% across different batches of 4-OHT treated mice (data not shown), and the variability is important to be considered when interpreting data obtained from this mouse model. Taken together, the Villin-CreER, $ASPP2^{exon3\text{-}fl/fl}$ mouse model can be used to achieve IEC-specific depletion of ASPP2, and the expression of EYFP is a direct indicator of such transgenic modification.

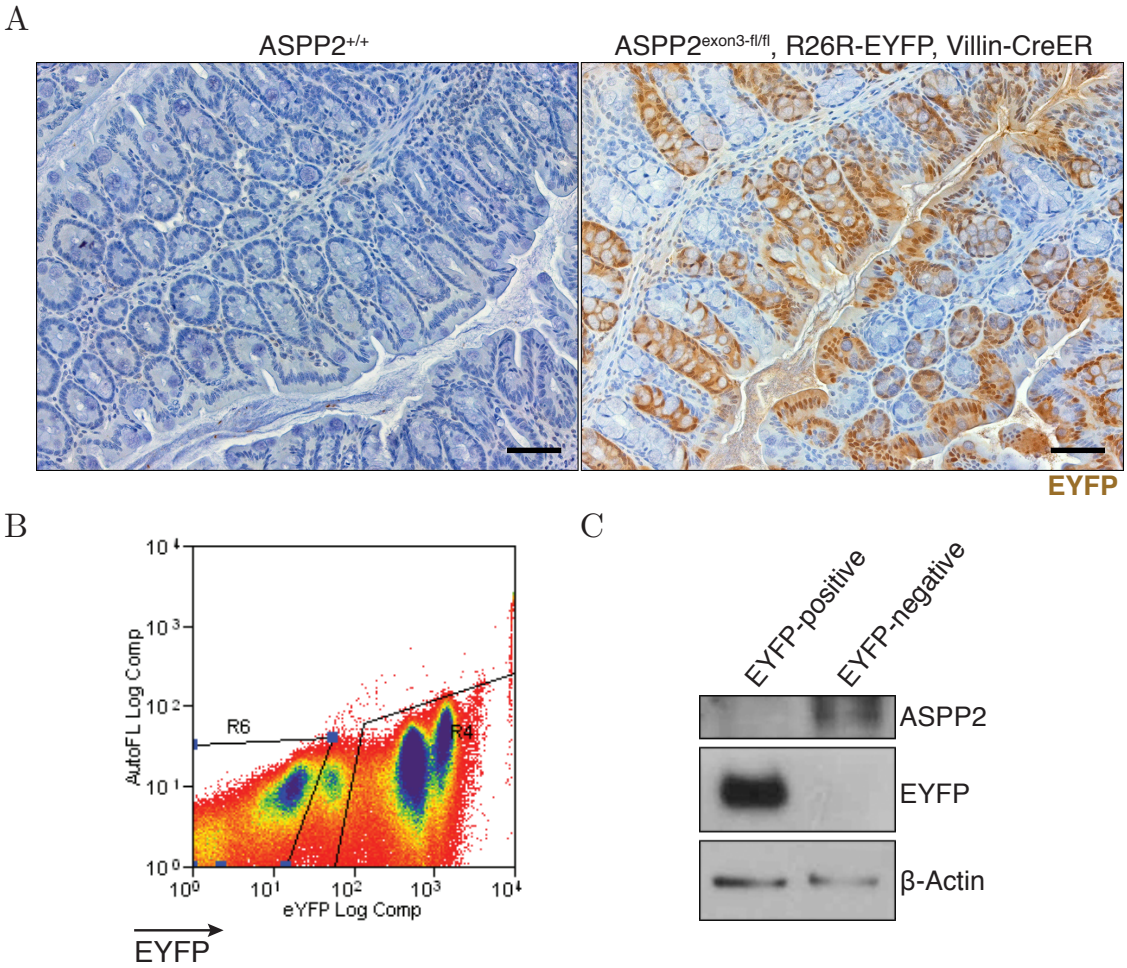


Figure 3.1: EYFP positivity is an indicator of ASPP2-depletion in the Villin-CreER, ASPP2$^{\text{exon3-fl/fl}}$ mouse model. (A) Representative IHC staining of EYFP on wild-type and 4-OHT-treated Villin-CreER, ASPP2$^{\text{exon3-fl/fl}}$ colons. The EYFP positivity is indicative of functional CreER. Scale bars: 25 µm. (B) Gating strategy for single-cell sorting of colonic epithelial cells isolated from ASPP2$^{\text{IEC-}\Delta\text{exon3}}$ mice. A pool of cells from 4 mice were sorted into EYFP-positive and -negative populations. (C) Western blot analysis of EYFP-positive and -negative epithelial cells obtained from the FACS sorting experiment described in (B), with β-Actin used as the loading control.

Since ASPP2 has been shown to localise at intestinal tight junctions and regulate the establishment and maintenance of intestinal cell polarity (S. Koch, unpublished data), whether or not the loss of ASPP2 in the intestinal epithelium would lead to a compromised intestinal barrier function was first investigated. ASPP2$^{\text{IEC-}\Delta\text{exon3}}$ mice did not develop spontaneous colitis, and their intestinal barrier permeability was comparable to that of their wild-type counterparts (Figure 3.2A). Based on these observations, the DSS-induced colitis model was employed to induce the

breakdown of the intestinal barrier to test whether wild-type and ASPP2-deficient animals would show different susceptibility. Mechanistically, DSS induces massive cell death in the intestinal epithelium, leading to predictable and reproducible localised colonic inflammation (Chassaing et al. 2001). Depending on the dosage and duration of the treatment, oral administration of DSS induces acute or chronic colitis in mice (Wirtz et al. 2007).

To perform this experiment, 4-OHT was intraperitoneally injected into Villin-CreER-negative and -positive animals to generate wild-type and ASPP2$^{\text{IEC-}\Delta\text{exon3}}$ mice, respectively. DSS treatment was initiated at least 7 days after the last 4-OHT injection, with the aim of minimising the effects of 4-OHT on the susceptibility of mice to DSS-induced colitis. The success of ASPP2 deletion was confirmed with IHC staining of EYFP.

In this experiment, 2% DSS was supplemented in the drinking water of wild-type and ASPP2$^{\text{IEC-}\Delta\text{exon3}}$ mice for 8 consecutive days. The control group was supplied with normal water without DSS. The physical conditions of the mice were monitored on a daily basis, and their body weight was measured every day during the course of the treatment. Although all mice treated with DSS showed signs of colitis, including anal bleeding and diarrhoea, they all survived to the end of the experiment. Progressive weight loss started to be noticeable on Day 3 of the treatment, but no difference in the loss of body weight was observed between ASPP2$^{\text{IEC-}\Delta\text{exon3}}$ mice and their wild-type counterparts (Figure 3.2B).

Given that DSS induces colitis via the breakdown of the intestinal barrier, intestinal permeability would serve as an indicator of susceptibility to this treatment. To that end, all mice treated with DSS or water were gavaged with FITC-dextran 4 hours before sacrifice, and the fluorescence intensity detected from their serum samples was used as a measurement for intestinal permeability. As expected, DSS treatment in both wild-type and ASPP2$^{\text{IEC-}\Delta\text{exon3}}$ mice led to an increase in the intestinal permeability when compared to the water-treated control group (Figure 3.2A). Although DSS-treated ASPP2$^{\text{IEC-}\Delta\text{exon3}}$ mice showed higher median intestinal permeability compared with wild-type animals, the difference was not statistically

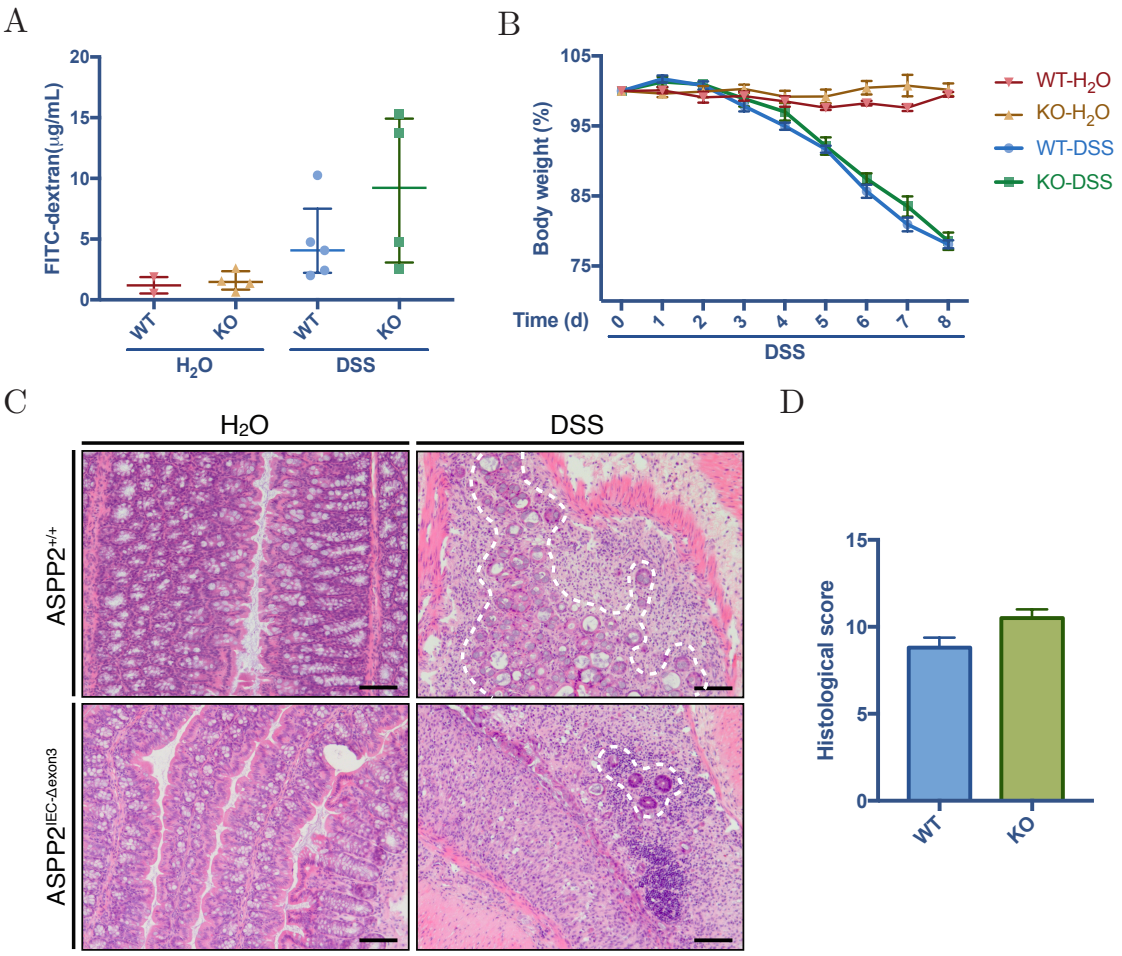


Figure 3.2: ASPP2$^{\text{IEC-}\Delta\text{exon3}}$ mice were equally susceptible to DSS-induced colitis as wild-type controls. (A) Time course of body weight loss. 6–8-week-old wild-type and ASPP2$^{\text{IEC-}\Delta\text{exon3}}$ mice were treated with water or 2% DSS for the indicated periods of time (n = 4 for each group), with their body weight measured on a daily basis. Relative body weight (%) compared to the initial value is plotted with the standard error of the mean (SEM). (B) Intestinal permeability of wild-type and ASPP2$^{\text{IEC-}\Delta\text{exon3}}$ mice after 8 days of water or 2% DSS treatment. Error bars represent median and interquartile range (IQR). (C) Representative H&E staining of colon sections from wild-type and ASPP2$^{\text{IEC-}\Delta\text{exon3}}$ mice treated with water or 2% DSS for 8 days. The white dashed lines delineate the areas of remaining crypts within the damaged tissue. Scale bars: 100 µm. (D) Histological scores of wild-type (n = 6) and ASPP2$^{\text{IEC-}\Delta\text{exon3}}$ (n = 5) mice after 8 days of DSS treatment. The scores were determined by inflammation severity and extent of crypt damage as described in Table 2.2. H_2O, water treatment; DSS, 2% DSS treatment; WT, ASPP2$^{+/+}$; KO, ASPP2$^{\text{IEC-}\Delta\text{exon3}}$.

significant (p = 0.1117). This result suggested that the loss of ASPP2 in the intestinal epithelium could only lead to a modest increase in the susceptibility of mice to DSS-induced intestinal barrier breakdown.

In order to further evaluate the severity of DSS-induced colitis in wild-type and

ASPP2$^{\text{IEC-}\Delta\text{exon3}}$ mice, histological analysis of DSS-treated animals was performed according to a scoring system described previously (Table 2.2). The scoring was performed in a blind manner, and the overall severity of colonic inflammation was represented by the average score for each experimental group. As expected, DSS treatment led to acute inflammation in the colonic epithelium, manifested by a loss of tissue architecture, massive immune cell infiltration, and crypt abscesses (Figure 3.2C). Consistent with the difference in intestinal permeability, ASPP2$^{\text{IEC-}\Delta\text{exon3}}$ mice showed a slightly higher histological score than wild-type animals, but the difference was not statistically significant ($p = 0.0529$, Figure 3.2D).

Taken together, these results suggested that the loss of ASPP2 in the intestinal epithelium led to a modestly compromised intestinal barrier function, but that defect was not sufficient to result in a significant increase in their susceptibility to DSS-induced intestinal barrier breakdown and acute colitis.

3.2.2 ASPP2$^{\text{IEC-}\Delta\text{exon3}}$ mice showed delayed recovery from DSS-induced colitis

Intestinal tissue regeneration is a highly dynamic process involving cell proliferation, migration, and polarisation (Roignot et al. 2013). Given the important roles of ASPP2 in the establishment and maintenance of intestinal cell polarity, it was hypothesised that a loss of ASPP2 in the intestinal epithelium would lead to delayed tissue regeneration from DSS-induced colonic inflammation.

To test this hypothesis, wild-type and ASPP2$^{\text{IEC-}\Delta\text{exon3}}$ mice were subjected to DSS-induced acute colitis as described in the previous section. After the treatment was terminated, the 2% DSS was replaced with normal water, and the animals were allowed to recover for indicated periods of time (Figure 3.3A). It is important to note that wild-type and ASPP2$^{\text{IEC-}\Delta\text{exon3}}$ mice showed similar levels of DSS-induced colitis; this mean that, where applicable, the differences observed during the recovery phase can be attributed to defects in tissue regeneration rather than differences in the initial tissue damage.

During the course of the experiment, the physical conditions of the mice were monitored on a daily basis and their body weight was measured every day. Of note,

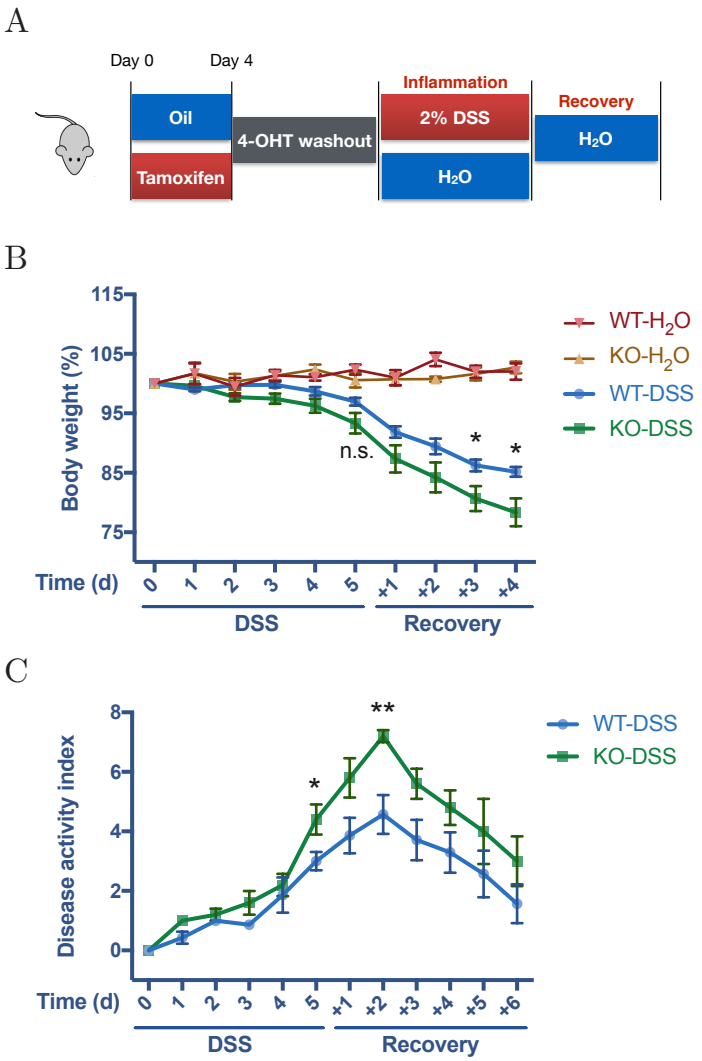


Figure 3.3: ASPP2$^{\text{IEC-}\Delta\text{exon3}}$ mice showed delayed recovery after DSS treatment. (A) Schematic timeline of the DSS treatment. (B) Time course of body weight loss. 6–8-week-old wild-type and ASPP2$^{\text{IEC-}\Delta\text{exon3}}$ mice were treated with water ($n \geq 3$ for each group) or 2% DSS for 5 days and allowed to recover for 4 days ($n \geq 10$ for each group). Relative body weight (%) compared to the initial value is plotted, with the error bars representing SEM. (C) Time course of disease activity index. The scores were determined on a daily basis during the course of DSS treatment and recovery, based on criteria including weight loss, stool consistency, and bleeding. Error bars represent SEM. +n, Day n of recovery; H_2O, water treatment; DSS, 2% DSS treatment; WT, ASPP2$^{+/+}$; KO, ASPP2$^{\text{IEC-}\Delta\text{exon3}}$; *, $p < 0.05$; **, $p < 0.01$; n.s., not significant.

the body weight of DSS-treated mice continued to decrease after the removal of the 2% DSS water for up to 3 days, and started to increase from approximately Day 4 of recovery, suggesting that the first three days of recovery were when the intestinal epithelium was undergoing active tissue repair. In this experiment, body

weight loss of ASPP2$^{\text{IEC-}\Delta\text{exon3}}$ mice was more dramatic than that of their wild-type littermates, indicating that intestinal tissue regeneration was less efficient in ASPP2 mutant animals (Figure 3.3B). The difference in weight loss was significant on Day 3 and Day 4 of recovery ($p = 0.0315$ and 0.0163, respectively; Figure 3.3B).

In order to characterise the physical conditions of the DSS-treated animals more accurately, various clinical parameters including weight loss, stool consistency, and bleeding were recorded every day. A disease activity index (DAI) can be scored accordingly, following the guidelines published previously (Table 2.1). Consistent with the sustained body weight loss after the removal of DSS, the DAI of the mice continued to increase for 2 days after the termination of the treatment (Figure 3.3C). However, when ASPP2$^{\text{IEC-}\Delta\text{exon3}}$ and wild-type mice were compared, the former group had a significantly higher DAI, particularly on Day 2 of recovery ($p = 0.0081$, Figure 3.3C). The difference was mainly due to the fact that ASPP2$^{\text{IEC-}\Delta\text{exon3}}$ mice suffered from a prolonged period of diarrhoea compared to wild-type animals, and the delayed body weight recovery also contributed to the observed difference.

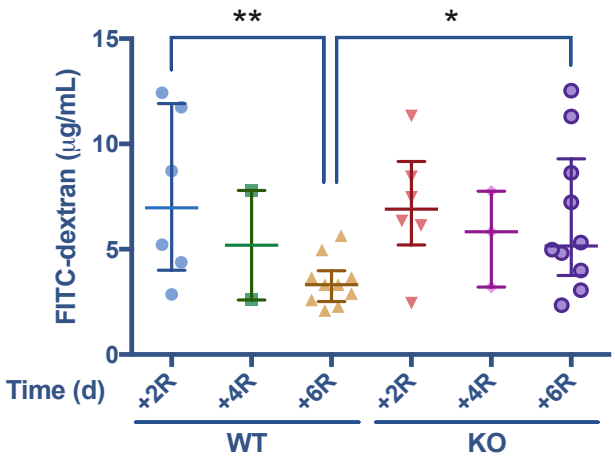


Figure 3.4: ASPP2$^{\text{IEC-}\Delta\text{exon3}}$ mice showed delayed restoration of intestinal permeability. Intestinal permeability test was performed on wild-type and ASPP2$^{\text{IEC-}\Delta\text{exon3}}$ mice. The mice were treated with 2% DSS for 5 days and left to recover for indicated periods of time. Error bars represent median and IQR. +nR, Day n of recovery; H_2O, water treatment; DSS, 2% DSS treatment; WT, ASPP2$^{+/+}$; KO, ASPP2$^{\text{IEC-}\Delta\text{exon3}}$; *, $p < 0.05$.

Similarly to the acute phase of DSS-induced colitis, intestinal permeability measurement was also performed on wild-type and ASPP2$^{\text{IEC-}\Delta\text{exon3}}$ animals at

different time points during the course of recovery (Figure 3.4). A trend of decreasing intestinal permeability was clearly seen in the group of wild-type mice treated with DSS, with a significant difference between Day 2 and Day 6 of recovery ($p = 0.0038$, Figure 3.4). A similar trend was also observed in ASPP2$^{\text{IEC-}\Delta\text{exon3}}$ animals, but this was not as significant. On Day 6 of recovery, the intestinal permeability of ASPP2$^{\text{IEC-}\Delta\text{exon3}}$ mice was significantly higher than that of wild-type animals ($p = 0.0168$, Figure 3.4). There was a certain level of variability observed within the ASPP2$^{\text{IEC-}\Delta\text{exon3}}$ group, which might be attributable to variable efficiencies of 4-OHT-induced ASPP2 deletion before the DSS treatment. In conclusion, these results suggested that the process of tissue repair was indeed delayed by the loss of ASPP2 in the intestinal epithelium.

Histological analysis was performed on colon samples collected on Days 2, 4, 6 of recovery from the 2% DSS treatment to evaluate the progression of colonic tissue repair. As expected, both wild-type and ASPP2$^{\text{IEC-}\Delta\text{exon3}}$ mice showed a certain level of tissue damage caused by the DSS-induced colitis, and regions of regenerative crypts were also observed (Figure 3.5A). Histological scores were evaluated according to the same criteria as in the previous section (Table 2.2). The score of wild-type mice decreased most dramatically from Day 2 to Day 4 of recovery, but was only seen later from Day 4 to Day 6 in ASPP2$^{\text{IEC-}\Delta\text{exon3}}$ animals (Figure 3.5B). As a result, the histological score of ASPP2$^{\text{IEC-}\Delta\text{exon3}}$ mice on Day 4 of recovery was significantly higher than that of their wild-type counterparts ($p = 0.0305$, Figure 3.5B). It is worth noting that wild-type and ASPP2$^{\text{IEC-}\Delta\text{exon3}}$ mice showed similar histological scores on Day 2 of recovery, again suggesting that the later difference was attributable to different rates of recovery rather differences in the initial levels of tissue damage.

3.2.3 ASPP2$^{\text{IEC-}\Delta\text{exon3}}$ mice showed reduced proliferation within regenerative crypts

Intestinal tissue regeneration relies on a fine-tuned balance between epithelial cell proliferation and cell death. On the one hand, cell proliferation and differentiation are required to compensate for the cell loss caused by tissue damage and to

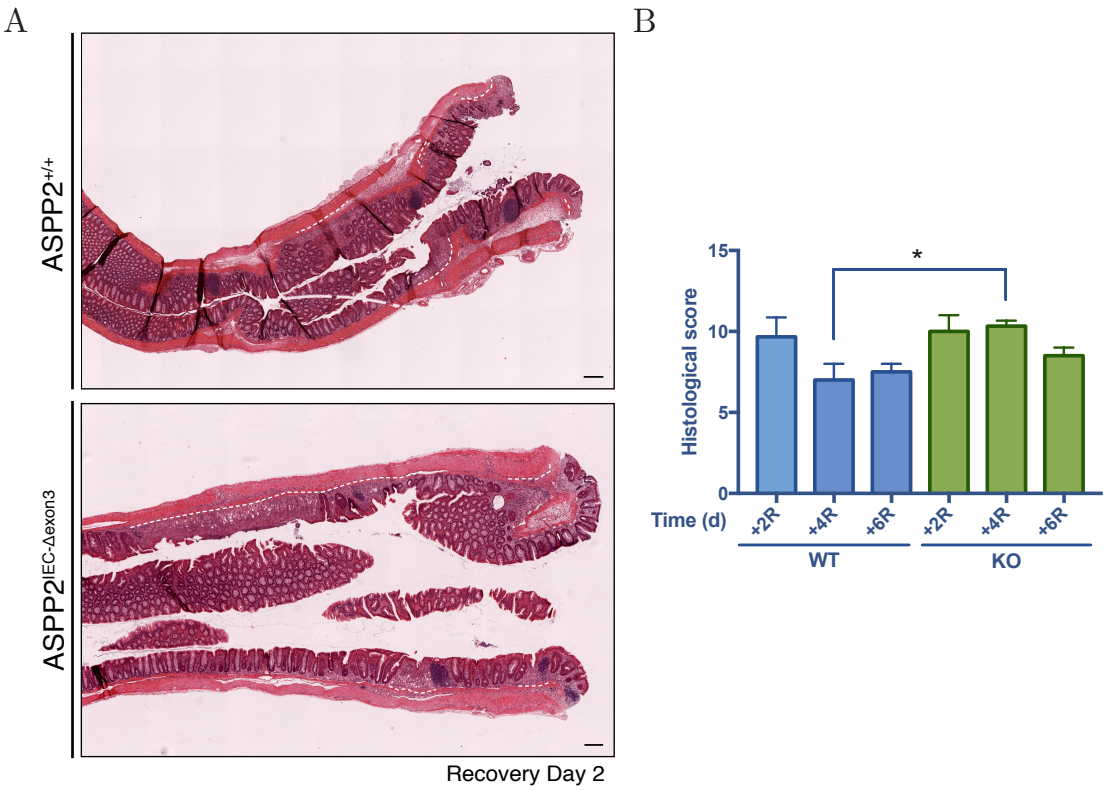


Figure 3.5: ASPP2$^{\text{IEC-}\Delta\text{exon3}}$ mice showed higher histological scores during recovery than wild-type animals. (A) Representative H&E staining of colon sections from wild-type and ASPP2$^{\text{IEC-}\Delta\text{exon3}}$ mice on recovery Day 2 after 7 days of 2% DSS treatment. The white dashed lines delineate regions of damaged colonic epithelium. The images are representative of three independent experiments. Scale bars: 1 µm. (B) Histological scores of wild-type and ASPP2$^{\text{IEC-}\Delta\text{exon3}}$ mice on recovery Days 2, 4, and 6 after 7 days of DSS treatment. The scores were determined by inflammation severity and extent of crypt damage as described in Table 2.2 ($n \geq 3$ for each group). +nR, Day n of recovery; WT, ASPP2$^{+/+}$; KO, ASPP2$^{\text{IEC-}\Delta\text{exon3}}$; *, $p < 0.05$.

restitute normal tissue architecture. On the other hand, unrestrained cell death will result in a prolonged proinflammatory microenvironment, impairing the process of tissue regeneration.

In order to investigate whether the delayed recovery observed in ASPP2$^{\text{IEC-}\Delta\text{exon3}}$ mice was due to defects in cell proliferation, IF staining of the proliferation marker Ki67 was performed on colon sections of both wild-type and ASPP2$^{\text{IEC-}\Delta\text{exon3}}$ animals sacrificed on Days 2 and 6 after the DSS water was removed. Although the overall pattern of cell proliferation was quite patchy across the colonic epithelium, regions of regenerative crypts indicated by stacking enterocytes and depletion

of goblet cells were observed in both groups (Figure 3.6A), and they were more proliferative than regions not affected by tissue damage (data not shown). Wild-type and ASPP2$^{\text{IEC-}\Delta\text{exon3}}$ mice showed similar levels of proliferation within areas undergoing active tissue regeneration (Figure 3.6A). However, western blot analysis performed on collective colonic crypts showed a higher level of pH3 in wild-type animals than in their ASPP2$^{\text{IEC-}\Delta\text{exon3}}$ littermates (Figure 3.6B). This observation suggested that a larger proportion of colonic tissue was undergoing regeneration in wild-type animals than in ASPP2-deficient mice. Furthermore, in line with the pro-proliferative functions believed to be exerted by the STAT3 signalling cascade, wild-type colonic crypts showed a higher level of STAT3 phosphorylation at tyrosine residue 705 (Figure 3.6B). Collectively, these results suggested that the delay in recovery from DSS-induced colitis can be partially attributed to a reduced level of epithelial cell proliferation in ASPP2$^{\text{IEC-}\Delta\text{exon3}}$ animals.

Cell death within the inflamed tissue on Day 6 of recovery was analysed by IF staining of cleaved Caspase-3. Since ASPP2 has been shown to promote apoptosis mediated by p53, it was hypothesised that a loss of ASPP2 in the intestinal epithelium would lead to reduced levels of apoptosis. However, apoptosis was barely detectable in damaged tissues of both wild-type and ASPP2$^{\text{IEC-}\Delta\text{exon3}}$ animals (Figure 3.7). This might be due to the fact that DSS-induced cell death is mostly necrotic, and even though apoptosis has also been shown to be induced (Araki et al. 2010), that effect might have been resolved by Day 6 of recovery. To summarise, a loss of ASPP2 in the intestinal epithelium did not seem to affect apoptosis in regenerative tissues.

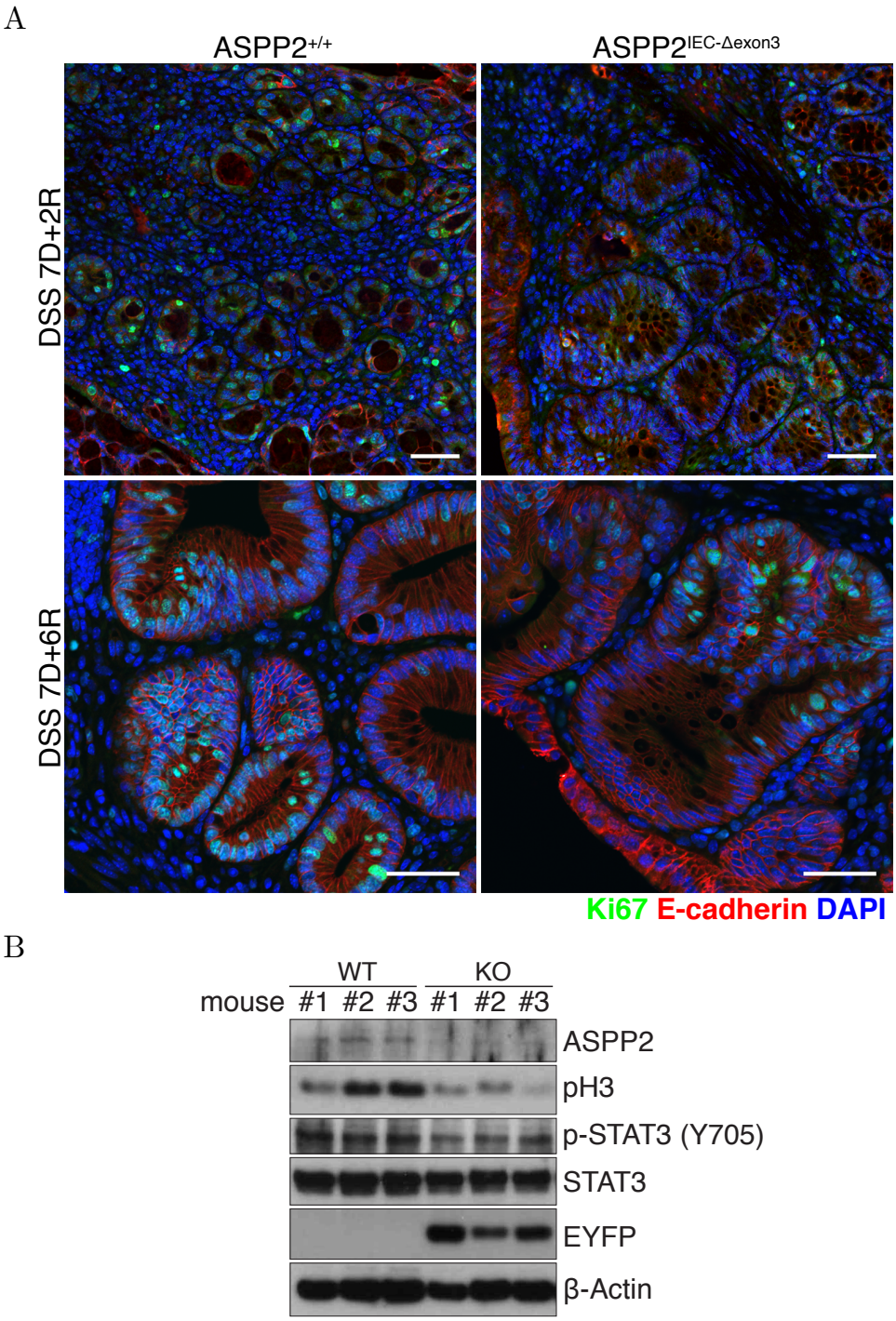


Figure 3.6: ASPP2$^{\text{IEC-}\Delta\text{exon3}}$ crypts were less proliferative than wild-type crypts. (A) Representative IF staining of Ki67 (green) and E-cadherin (red) on wild-type and ASPP2$^{\text{IEC-}\Delta\text{exon3}}$ colon sections. The mice were treated with 2% DSS for 7 days followed by indicated periods of recovery. +nR, Day n of recovery; scale bars: 50 µm. (B) Western blot analysis of colonic epithelial cells isolated from wild-type and ASPP2$^{\text{IEC-}\Delta\text{exon3}}$ mice, with β-Actin used as the loading control. The mice were treated with 2% DSS for 5 days followed by 6 days of recovery. WT, ASPP2$^{+/+}$; KO, ASPP2$^{\text{IEC-}\Delta\text{exon3}}$.

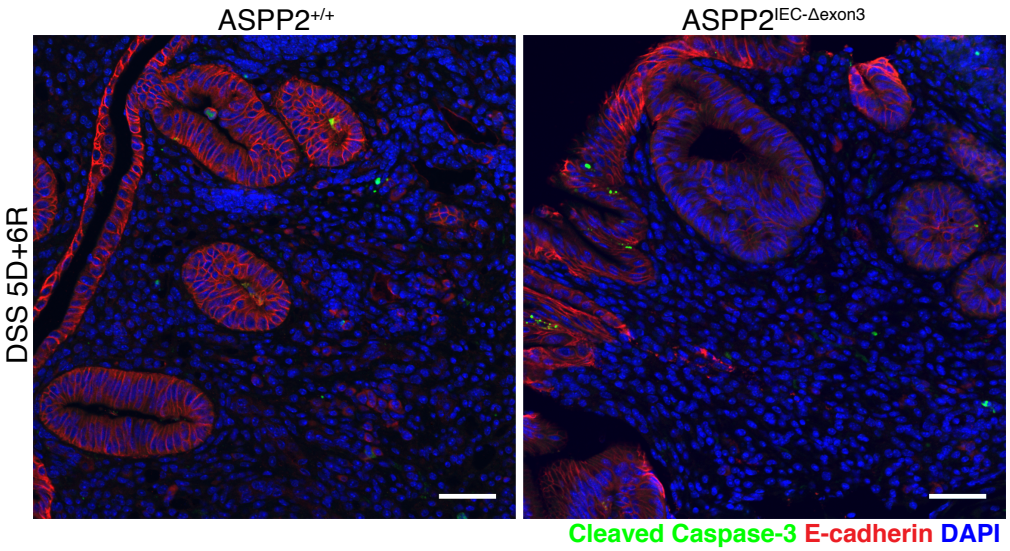


Figure 3.7: ASPP2$^{\text{IEC-}\Delta\text{exon3}}$ crypts showed a similar level of apoptosis as wild-type crypts. IF co-staining of cleaved Caspase-3 (green) and E-cadherin (red) was performed on colon sections of wild-type and ASPP2$^{\text{IEC-}\Delta\text{exon3}}$ mice, with nuclei counterstained with DAPI (blue). The mice were treated with 2% DSS for 5 days followed by 6 days of recovery. Scale bars: 50 µm. 5D+6R, Day 6 of recovery after 5-day DSS treatment.

3.2.4 Hippo/YAP signalling was not affected by the loss of ASPP2 in the intestinal epithelium

One of the best studied signalling pathways involved in intestinal tissue regeneration is the Hippo/YAP pathway. Activation of YAP promotes cell survival and drives ISC reprogramming (Gregorieff et al. 2015). Importantly, YAP is a binding partner of ASPP2, and it has been shown that ASPP2 could mediate the dephosphorylation of YAP at Ser127 by PP1 (Christophe Royer et al. 2014). The interaction was confirmed in an *in vitro* setting where both ASPP2 and YAP were overexpressed (Figure 3.8). Since overexpression of ASPP2 results in reduced phosphorylation of YAP at Ser127, thereby activating YAP activity, it was hypothesised that the loss of ASPP2 in the intestinal epithelium would lead to suppressed Hippo signalling.

To test this hypothesis, IHC staining of YAP and EYFP was performed on consecutive colon sections of ASPP2$^{\text{IEC-}\Delta\text{exon3}}$ mice that were treated with 2% DSS and left to recover for 2 days. Nuclear staining of YAP was observed in both normal crypts that were unaffected by the DSS treatment and crypts that were undergoing regeneration, indicative of the activation of YAP activity (Figure 3.9, A and B).

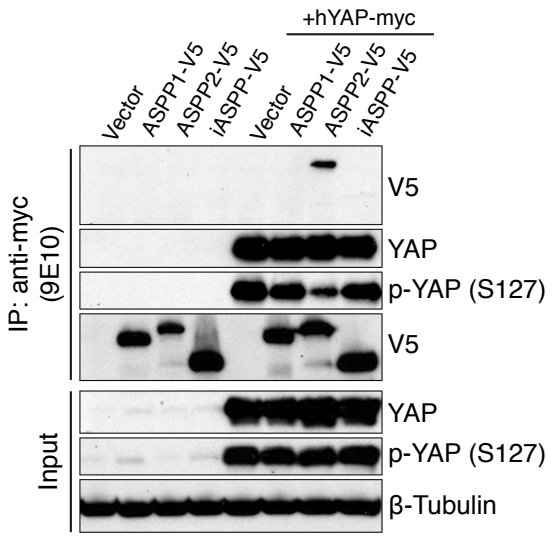


Figure 3.8: ASPP2 interacts with and dephosphorylates YAP. Co-IP experiment was performed using HEK293 cells overexpressing exogenous YAP and ASPP proteins. Following transfection with the indicated constructs, YAP was immunoprecipitated using an anti-myc monoclonal antibody (clone 9E10) and western blot analysis was performed using the indicated antibodies.

However, using EYFP-positive staining as an indicator of ASPP2 depletion, no correlation was observed between EYFP positivity and the localisation of YAP, suggesting that Hippo/YAP signalling was not affected by the loss of ASPP2 (Figure 3.9, A and B). Western blot analysis of colonic crypts further confirmed this result, where wild-type and ASPP2$^{\text{IEC-}\Delta\text{exon3}}$ mice showed similar levels of YAP phosphorylation at Ser127 (Figure 3.9C). These results suggested that ASPP2 deficiency in the intestinal epithelium did not affect the Hippo/YAP pathway, at least in the context of tissue regeneration following DSS-induced colitis. It is interesting to note the mosaic pattern of EYFP positivity within a single crypt in the mouse model (Figure 3.9A, B), which suggests its usability for the study of ASPP2's function in niche succession and stem cell drifting in the intestinal epithelium.

In addition to the Hippo/YAP pathway, several other signalling pathways are also implicated in the process of tissue regeneration, including Wnt/β-catenin and Notch. In order to investigate whether these pathways are affected by the loss of ASPP2, western blotting and IHC staining of β-catenin and NICD were performed, and similar expression levels and cellular localisation were observed in both wild-type

and ASPP2$^{\text{IEC-}\Delta\text{exon3}}$ animals (data not shown). Moreover, IHC staining of Trefoil Factor 3 (TFF3), an intestinal-specific mediator of epithelial restitution (Taupin et al. 2003), also revealed no difference between wild-type and ASPP2-deficient mice (data not shown). Taken together, the loss of ASPP2 in the intestinal epithelium did not seem to result in intrinsically dysregulated epithelial cell regeneration.

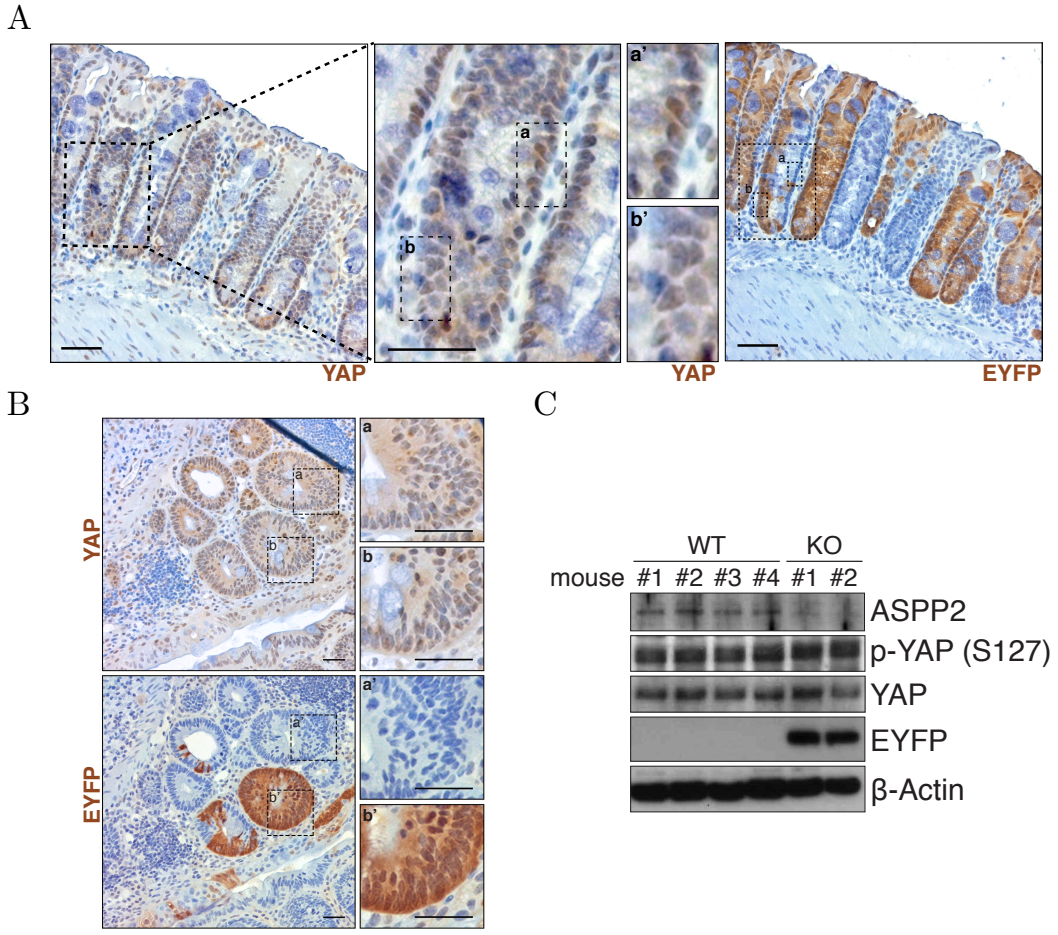


Figure 3.9: Hippo/YAP signalling was not affected by the loss of ASPP2. (A) IHC staining of EYFP and YAP performed on adjacent colon sections of ASPP2$^{\text{IEC-}\Delta\text{exon3}}$ mice, with the same region presented. Scale bars: 50 µm. Inserts (a) and (b) represent regenerative crypts that are negative and positive for EYFP, respectively, with (a') and (b') presenting the images at a higher magnification. (B) IHC staining of EYFP and YAP performed on adjacent colon sections of ASPP2$^{\text{IEC-}\Delta\text{exon3}}$ mice, with the same region presented. The mice were treated with 2% DSS for 7 days followed by 2 days of recovery. Scale bars: 25 µm. Inserts (a) and (b) represent regenerative crypts negative and positive for EYFP, respectively, with (a') and (b') presenting the images at a higher magnification. (C) Western blot analysis of colonic epithelial cells isolated from wild-type and ASPP2$^{\text{IEC-}\Delta\text{exon3}}$ mice, with β-Actin used as the loading control. The mice were treated with 2% DSS for 5 days followed by 6 days of recovery. WT, ASPP2$^{+/+}$; KO, ASPP2$^{\text{IEC-}\Delta\text{exon3}}$.

3.2.5 ASPP2 deficiency in the intestinal epithelium led to reduced expression of proinflammatory cytokines by LPMCs

Given that ASPP2 deficiency did not affect epithelial cell autonomous regulation of tissue regeneration, it was hypothesised that the delayed recovery observed in ASPP2$^{\text{IEC-}\Delta\text{exon3}}$ mice was due to extrinsic factors present in the inflammatory microenvironment, including epithelial–immune cell interaction. In fact, inflammation has long been believed to be a double-edged sword in the context of tissue regeneration. On the one hand, inflammation plays a protective role within injured tissues by mediating the elimination of its primary triggers, such as foreign organisms and dead cells. As a result, too little inflammation will lead to tissue damage caused by extended exposure to environmental insults, especially bacteria (Karin et al. 2016). On the other hand, chronic or uncontrolled inflammation will result in secondary tissue damage, potentially culminating in a variety of pathologies such as fibrosis and cancer (Karin et al. 2016).

To investigate whether the loss of ASPP2 would tip the balance of reparative inflammation from beneficial to detrimental, cell populations enriched for LPMCs were isolated from the lamina propria of wild-type and ASPP2$^{\text{IEC-}\Delta\text{exon3}}$ animals and subjected to qPCR analysis. The mice were treated with 2% DSS for a week and allowed to recover for 6 days. mRNA was extracted from the bulk cell population of LPMCs and transcribed into cDNA, so that an overall picture of the level of pro- and anti-inflammatory cytokine expression could be obtained (Figure 3.10). It is worth noting that the immune cells of both wild-type and ASPP2$^{\text{IEC-}\Delta\text{exon3}}$ mice should be genetically intact. Therefore, any differential expression of a particular cytokine, if observed, is likely to be due to dysregulated epithelial–immune cell crosstalk.

As expected, DSS treatment induced the expression of proinflammatory cytokines including IL-1β, IL-6, and TNF-α, in both wild-type and ASPP2$^{\text{IEC-}\Delta\text{exon3}}$ animals (Figure 3.10). As for anti-inflammatory cytokines, an increase in the expression of IFN-γ, IL-22, and IL-23a could also be seen, but to a much lesser extent (Figure 3.10). Intriguingly, despite no difference being observed in the expression of these cytokines between untreated animals, the mRNA levels of IL-1β and IL-6 were

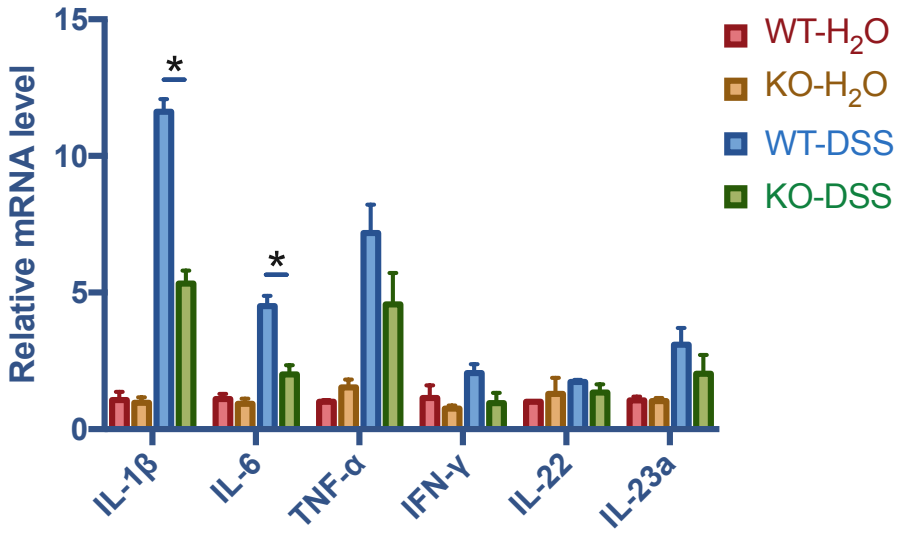


Figure 3.10: LPMCs of wild-type mice expressed higher levels of proinflammatory cytokines than those of ASPP2$^{\text{IEC-}\Delta\text{exon3}}$ mice. LPMCs were isolated from wild-type and ASPP2$^{\text{IEC-}\Delta\text{exon3}}$ mice treated with 2% DSS for 7 days followed by 6 days of recovery (n = 2 for each group). The control groups were treated with normal water (n = 3 for WT, n = 2 for KO). qPCR analysis of selected genes was performed on cDNA derived from the bulk population of LPMCs. This result is representative of two independent experiments. H_2O, water treatment; DSS, 2% DSS treatment; WT, ASPP2$^{+/+}$; KO, ASPP2$^{\text{IEC-}\Delta\text{exon3}}$; *, $p < 0.05$.

significantly higher in LPMCs isolated from wild-type animals than from their ASPP2-deficient counterparts after DSS treatment ($p = 0.0109$ and 0.0111 for IL-1β and IL-6, respectively; Figure 3.10). Notably, the downregulation of IL-6 was consistent with the observation that ASPP2$^{\text{IEC-}\Delta\text{exon3}}$ crypts showed a lower level of STAT3 phosphorylation than those of wild-type animals (Figure 3.6B). This result suggested that ASPP2-deficient mice may have reduced inflammatory responses in favour of tissue regeneration, which could partially explain their delayed recovery from DSS-induced colitis.

Taken together, these data suggested that a loss of ASPP2 resulted in decreased expression of proinflammatory cytokines by LPMCs, supporting the notion that epithelial cell non-autonomous factors can play a role in the regulation of tissue regeneration, particularly in the context of ASPP2 deficiency.

3.2.6 ASPP2$^{\Delta exon3}$ mice showed higher susceptibility to DSS-induced colitis than ASPP2$^{IEC\text{-}\Delta exon3}$ mice

In order to gain further insight into the contribution of epithelial cell non-autonomous factors in the pathogenesis of DSS-induced colitis, particularly in relation to ASPP2 deficiency, a germline ASPP2 transgenic mouse model was employed in this study. After the administration of 4-OHT, a mosaic pattern of ASPP2^{exon3} deletion would be achieved at the whole-body level by CreER-mediated recombination. The mice will be referred to as ASPP2$^{\Delta exon3}$ hereafter.

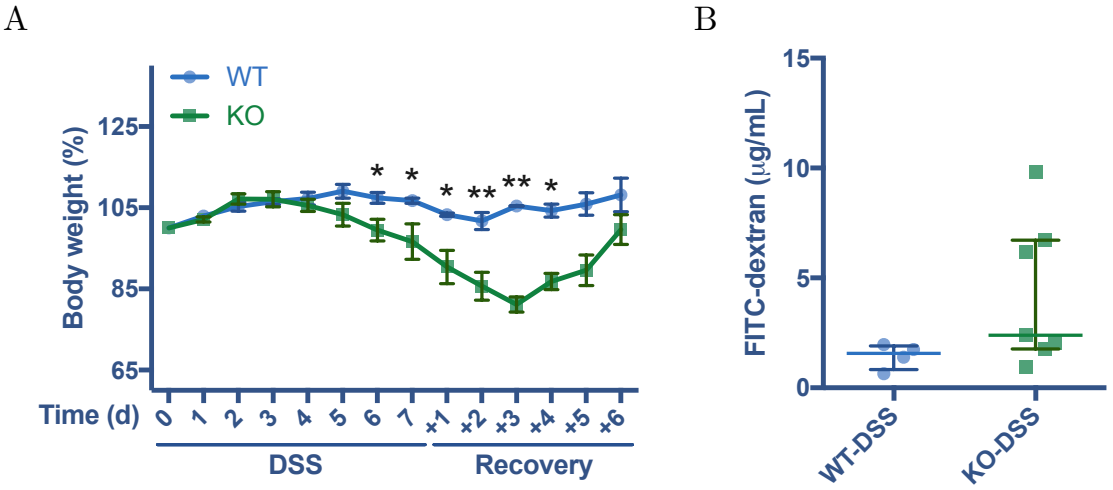


Figure 3.11: ASPP2$^{\Delta exon3}$ mice showed increased susceptibility to DSS-induced intestinal barrier breakdown. (A) Time course of body weight change. Wild-type (n = 4) and ASPP2$^{\Delta exon3}$ (n = 3) mice were treated with 2% DSS for 7 days and left to recover for 6 days. Relative body weight (%) compared to the initial value is plotted with SEM. *, $p < 0.05$; **, $p < 0.01$. (B) Intestinal permeability of wild-type and ASPP2$^{\Delta exon3}$ mice after 7 days of 2% DSS treatment. Error bars represent median and IQR. +nR, Day n of recovery; WT, ASPP2$^{+/+}$; KO, ASPP2$^{\Delta exon3}$.

Wild-type and ASPP2$^{\Delta exon3}$ mice were subjected to 2% DSS treatment for 7 days followed by 6 days of recovery. In contrast to ASPP2$^{IEC\text{-}\Delta exon3}$ mice, which were similarly susceptible to the DSS treatment as wild-type animals, ASPP2$^{\Delta exon3}$ mice showed increased susceptibility, as indicated by the time course of body weight loss (Figure 3.11A). On Days 6 and 7 of DSS treatment, as well as the first 4 days after the removal of the DSS water, the body weights of ASPP2$^{\Delta exon3}$ mice were significantly lower than those of their wild-type littermates ($p = 0.0338$, 0.0429, 0.0137, 0.0081, 0.0060, and 0.0210, respectively; Figure 3.11A). This observation recapitulated

the results obtained from an independent cohort of ASPP2$^{\Delta exon3}$ animals treated with 5% DSS (S. Koch, unpublished data). In spite of intragroup variability, ASPP2$^{\Delta exon3}$ mice still showed a trend of increasing intestinal permeability after 7 days of DSS treatment compared to their wild-type counterparts, suggesting more severely compromised intestinal barrier function ($p = 0.1332$, Figure 3.11B).

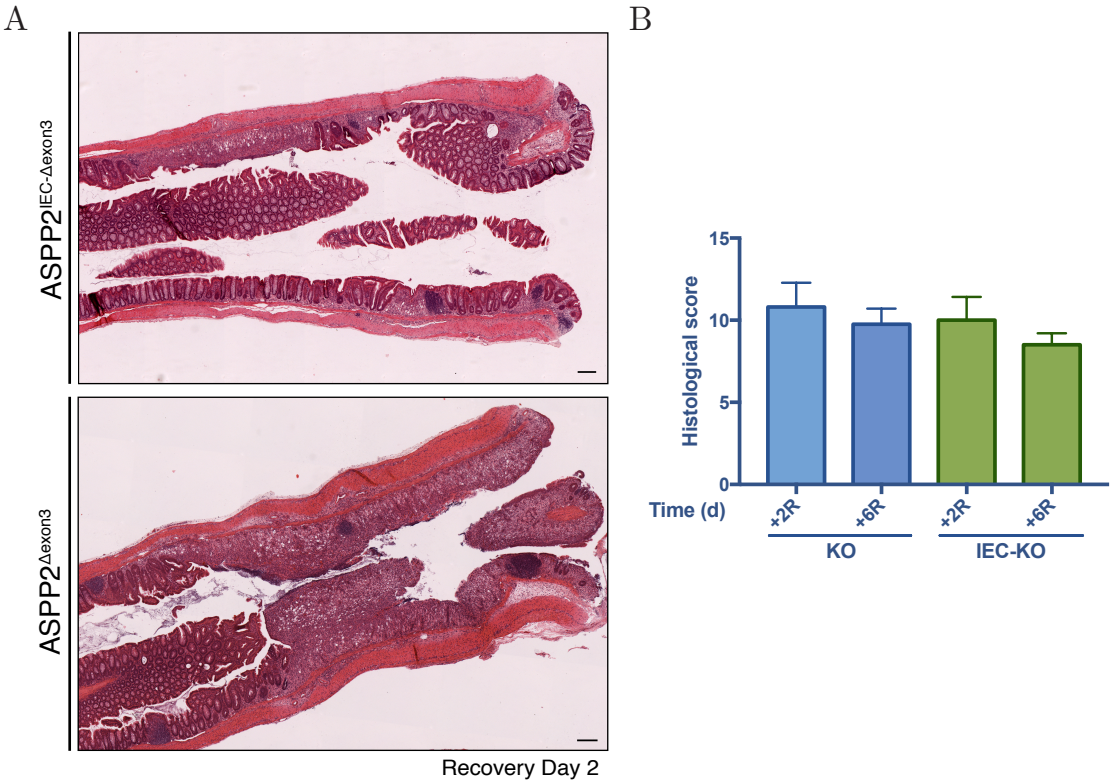


Figure 3.12: ASPP2$^{\Delta exon3}$ mice showed higher histological scores than ASPP2$^{IEC\text{-}\Delta exon3}$ animals. (A) Representative H&E staining of colon sections from ASPP2$^{IEC\text{-}\Delta exon3}$ and ASPP2$^{\Delta exon3}$ mice on recovery Day 2 after 7 days of 2% DSS treatment. The images are representative of three independent experiments. Scale bars: 1 µm. (B) Histological scores of ASPP2$^{IEC\text{-}\Delta exon3}$ and ASPP2$^{\Delta exon3}$ mice on recovery Day 2 and Day 6 after 7 days of DSS treatment. The scores were determined by inflammation severity and extent of crypt damage as described in Table 2.2 ($n \geq 3$ for each group). +nR, Day n of recovery; KO, ASPP2$^{\Delta exon3}$; IEC-KO, ASPP2$^{IEC\text{-}\Delta exon3}$.

To further confirm that ASPP2$^{\Delta exon3}$ mice were more susceptible to DSS-induced colitis than ASPP2$^{IEC\text{-}\Delta exon3}$ animals, histological analysis was performed based on the scoring system described previously (Table 2.2). Not surprisingly, germline ASPP2-deficient mice showed more severe colonic tissue damage than epithelium-specific knockout animals, particularly in the distal colon (Figure 3.12A).

The histological score of ASPP2$^{\Delta exon3}$ mice on recovery Day 6 was also slightly higher than that of ASPP2$^{IEC\text{-}\Delta exon3}$ animals (Figure 3.12B). In agreement with the observation that ASPP2$^{\Delta exon3}$ mice were more susceptible to DSS-induced colitis, and that the process of tissue regeneration in those mice was more delayed than that of the ASPP2$^{IEC\text{-}\Delta exon3}$ animals, reduced proliferation and increased apoptosis were also observed in ASPP2$^{\Delta exon3}$ animals (data not shown).

Although more than one factor involved in the intestinal microenvironment was altered in the germline transgenic mouse model compared with tissue-specific transgenic mice, making it difficult to identify a specific cell compartment that contributed to the observed phenotypes, the data presented support the hypothesis that epithelial cell non-autonomous factors are involved in the initiation and resolution of DSS-induced colitis.

3.3 Summary and Brief Discussion

In this chapter, the implications of ASPP2 deficiency in DSS-induced colitis were investigated using an IEC-specific ASPP2-deficient mouse model. ASPP2$^{IEC\text{-}\Delta exon3}$ mice showed a similar time course response to DSS treatment as wild-type animals, suggesting that the loss of ASPP2 at epithelial tight junctions does not render mice more susceptible to DSS-induced intestinal barrier breakdown. By contrast, loss of ASPP2 in the intestinal epithelium resulted in delayed recovery from DSS-induced colitis, as was reflected by the delayed restoration of body weight and intestinal barrier function.

Given the epithelium-specific nature of ASPP2 depletion in the ASPP2$^{IEC\text{-}\Delta exon3}$ mouse model, it was hypothesised that the observed phenotype was due to defects intrinsic to epithelial cells. If that is the case, it should be manifested by uncontrolled cell death, a failure to proliferate, and/or dysregulated suppression of signalling required for tissue regeneration. To that end, proliferation and apoptosis were examined in the inflamed tissue, as well as key pathways implicated in epithelial regeneration, including Hippo, Wnt, and Notch. Although ASPP2-deficient mice showed a modest decrease in regenerative proliferation, no significant difference was

observed in the above-mentioned aspects between wild-type and ASPP2-deficient animals. These results suggest that the delay in recovery of ASPP2-deficient mice might be due to epithelial cell non-autonomous factors.

Intestinal tissue regeneration is a highly dynamic and tightly regulated process, involving constant crosstalk between immune cells and the epithelium. The interaction is mediated by various pro- and anti-inflammatory cytokines, intricately implicated in the exacerbation or resolution of inflammation. In order to obtain an overall picture of the cytokines present in the intestinal microenvironment of wild-type and ASPP2-deficient mice, LPMCs were isolated and subjected to qPCR analysis as a bulk population. Loss of ASPP2 in the intestinal epithelium did not seem to alter the expression of proinflammatory cytokines under steady-state conditions, suggesting that ASPP2 deficiency alone is not sufficient to result in a proinflammatory microenvironment. However, after the mice were treated with DSS and left to recover, the induction of proinflammatory cytokine expression was less efficient in $ASPP2^{IEC\text{-}\Delta exon3}$ mice than in their wild-type counterparts, including cytokines required for reparative inflammation such as IL-6. This result partially explained the delayed recovery observed in ASPP-deficient animals. More importantly, it supported the hypothesis that a loss of ASPP2 in the intestinal epithelium would result in dysregulated epithelial–immune cell interactions. Intriguingly, a further increase in the susceptibility to DSS-induced colitis was observed in germline ASPP2 conditional knockout mice, again highlighting the importance of environmental factors in this context.

Taken together, the observation that depletion of ASPP2 in epithelial cells results in disrupted cytokine expression and delayed tissue repair suggests that epithelial–immune cell interaction is key to the restoration of intestinal homeostasis. In fact, these results are consistent with the observation that intestinal permeability is not affected by the loss of ASPP2, suggesting that defects other than defective tight junctions may be involved, e.g., alterations in the secretome. Considering that chronic inflammation is a risk factor for tumourigenesis, and that ASPP2 is a haploinsufficient tumour suppressor, it was next investigated whether a loss

of ASPP2 in the intestinal epithelium would result in an increased susceptibility of mice to colorectal tumourigenesis.

4

ASPP2 Deficiency Predisposes Mice to Colorectal Tumourigenesis

4.1 Introduction

Chronic inflammation is a risk factor for tumourigenesis. In the case of CRC, inflammatory bowel diseases such as CD and UC have been shown to predispose patients to colorectal tumourigenesis (Rubin et al. 2012). This is mainly due to DNA damage caused by persistent inflammation, as well as excessive production of reactive oxygen and nitrogen species perpetuated by infiltrating immune cells (Hussain et al. 2003). On the other side of the story, it has been shown that mucosal healing is one of the most important prognostic factors for long-term remission of IBD (Okamoto 2011). In fact, given the similarity between the mechanisms involved in tissue regeneration and tumourigenesis, cancer has been referred to as 'wounds that do not heal' (Waldner et al. 2015).

In order to investigate the sequence of events implicated in the transition from inflammation to cancer, various mouse models of CAC have been developed. Among all the chemically-induced CRC models established to date, the AOM and DSS-induced tumourigenesis model is one of the most widely used, mostly due to its reproducibility and relatively short latency (Thaker et al. 2012). Mechanistically, AOM is a colon-specific carcinogen that mainly causes mismatched base pairing

and G to A transitions (Van Der Kraak 2015). The combination of a single injection of AOM and three rounds of DSS treatment in mice has been proven to faithfully recapitulate the aberrant crypt foci–adenoma–carcinoma sequence that is characteristic of CAC in humans (De Robertis et al. 2011). More importantly, with sufficient duration, DSS treatment alone can also induce the formation of colorectal tumours, further supporting the notion that chronic inflammation is associated with an increased risk for tumourigenesis (Okayasu et al. 2002).

Previous work by our lab and others suggests that ASPP2 is a tumour suppressor, manifested by the fact that a loss of ASPP2 predisposes mice to tumour formation both spontaneously and after ionising irradiation (Vives et al. 2006; Kampa et al. 2009). The tumour suppressive functions of ASPP2 can be achieved in p53-dependent or -independent manners, depending on the type of tumour under investigation (Vives et al. 2006). Moreover, it has also been demonstrated *in vivo* that ASPP2 suppresses the development of spontaneous squamous cell carcinoma (Tordella et al. 2013).

Considering that ASPP2-deficient mice showed delayed recovery from DSS-induced colitis, which is intimately related to prolonged inflammation (Kinnebrew et al. 2012), and that ASPP2 is known to be a haploinsufficient tumour suppressor, it was hypothesised that a loss of ASPP2 would render mice more susceptible to AOM/DSS-induced colorectal tumourigenesis. To test this hypothesis, $ASPP2^{IEC\text{-}\Delta exon3}$ mice together with their wild-type littermates were subjected to the AOM/DSS treatment. Susceptibility was determined by the survival rate of mice under treatment and the evaluation of their tumour loads. Given our particular interest in the distinction between epithelial cell autonomous and non-autonomous factors implicated in this model, characterisation of the tumours was performed from the perspectives of both epithelial cells and the underlying microenvironment. Similarly to the DSS-induced colitis model, a small cohort of germline conditional ASPP2 transgenic mice were also characterised within the scheme of the AOM/DSS treatment.

4.2 Results

4.2.1 ASPP2$^{\text{IEC-}\Delta\text{exon3}}$ mice showed increased susceptibility to AOM/DSS-induced tumourigenesis

In order to investigate whether epithelium-specific deficiency of ASPP2 in mice would lead to an increase in their susceptibility to colorectal tumourigenesis, wild-type and ASPP2$^{\text{IEC-}\Delta\text{exon3}}$ mice were subjected to AOM/DSS treatment. The mice were first injected intraperitoneally with AOM, and then treated with 2% DSS for three rounds with 18 days of recovery in between (Figure 4.1A). Consistent with the observation that a loss of ASPP2 did not affect the susceptibility of mice to DSS-induced acute colitis, wild-type and ASPP2$^{\text{IEC-}\Delta\text{exon3}}$ mice showed similar level of body weight loss during the time course of each round of DSS treatment (Figure 4.1B). However, after the DSS water was removed, the body weight of ASPP2$^{\text{IEC-}\Delta\text{exon3}}$ mice recovered more slowly than that of wild-type animals. The difference was significant 1 week after the first and second rounds of DSS treatment ($p = 0.0127$ and 0.0297, respectively; Figure 4.1B). Given that the time course and extent of body weight loss in AOM/DSS-treated mice were comparable to those treated with DSS alone, the administration of AOM did not seem to substantially affect the susceptibility of mice to DSS. The correlation between AOM-induced mutations and DSS-induced colitis remains to be determined.

During the time course of the AOM/DSS experiment, the mice under treatment were monitored closely for symptoms such as diarrhoea and fatigue. Although most mice showed signs of acute colitis after each round of DSS treatment, and some needed to be sacrificed according to the predefined experimental endpoints (severe diarrhoea or greater than 25% loss of initial weight), more than 75% survived to the end of the experiment (Figure 4.1C). In line with the hypothesis that prolonged inflammation would render the mice more susceptible to colorectal tumourigenesis, ASPP2$^{\text{IEC-}\Delta\text{exon3}}$ mice showed a significantly lower cumulative survival rate than wild-type animals ($p = 0.0182$, Figure 4.1C). However, it is worth noting that the cause of death was mainly related to DSS-induced colitis rather than an excessive tumour load (see below).

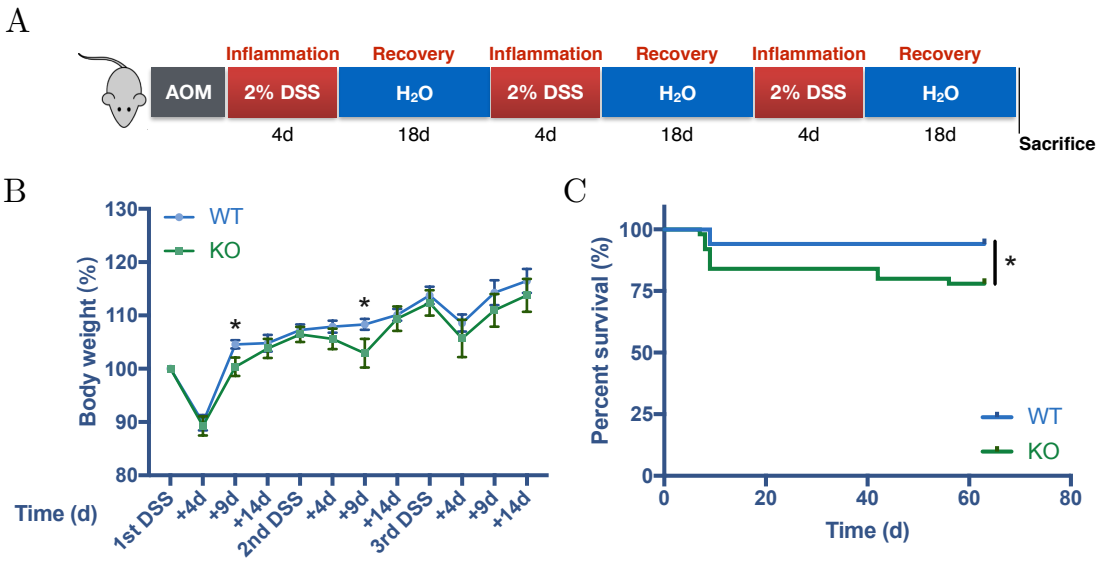


Figure 4.1: ASPP2$^{\text{IEC-}\Delta\text{exon3}}$ mice showed increased susceptibility to AOM/DSS treatment. (A) Schematic timeline of the AOM/DSS-induced tumourigenesis model. (B) Time course of body weight loss. Wild-type and ASPP2$^{\text{IEC-}\Delta\text{exon3}}$ mice were injected with AOM and subjected to three rounds of 4 day 2% DSS treatment ($n \geq 5$ for each time point). Body weight was measured at the indicated time points, and relative body weight (%) compared to the initial value is plotted with SEM. DSS, 2% DSS treatment; d, day. (C) Cumulative survival curves of wild-type ($n = 51$) and ASPP2$^{\text{IEC-}\Delta\text{exon3}}$ ($n = 50$) mice undergoing the AOM/DSS treatment in this study. d, day; WT, ASPP2$^{+/+}$; KO, ASPP2$^{\text{IEC-}\Delta\text{exon3}}$; *, $p < 0.05$.

After the third round of DSS administration followed by recovery, the mice were sacrificed and their tumour loads analysed. Both wild-type and ASPP2$^{\text{IEC-}\Delta\text{exon3}}$ mice under AOM/DSS treatment developed macroscopic tumours in the mid to distal colon, and the number of tumours ranged from 0–17 (Figure 4.2, A and B; Figure 4.3A). It has been reported that AOM-induced tumours can display aberrant crypt foci, adenomatous growth, and malignant degeneration, depending on the dose of AOM used and the susceptibility of the mouse strain being studied (Neufert et al. 2007). Of note, colorectal tumours developed in the experimental setting of this study were mostly tubular adenomas. Adenomatous polyps with low-grade dysplasia were frequently seen, but malignant growth invading the bowel wall was never observed (Dr. Robert Godin, pathology consult; Figure 4.2B; Boivin et al. 2003).

No difference in the localisation of tumours was observed between wild-type and ASPP2$^{\text{IEC-}\Delta\text{exon3}}$ mice (data not shown), but the latter showed a significant

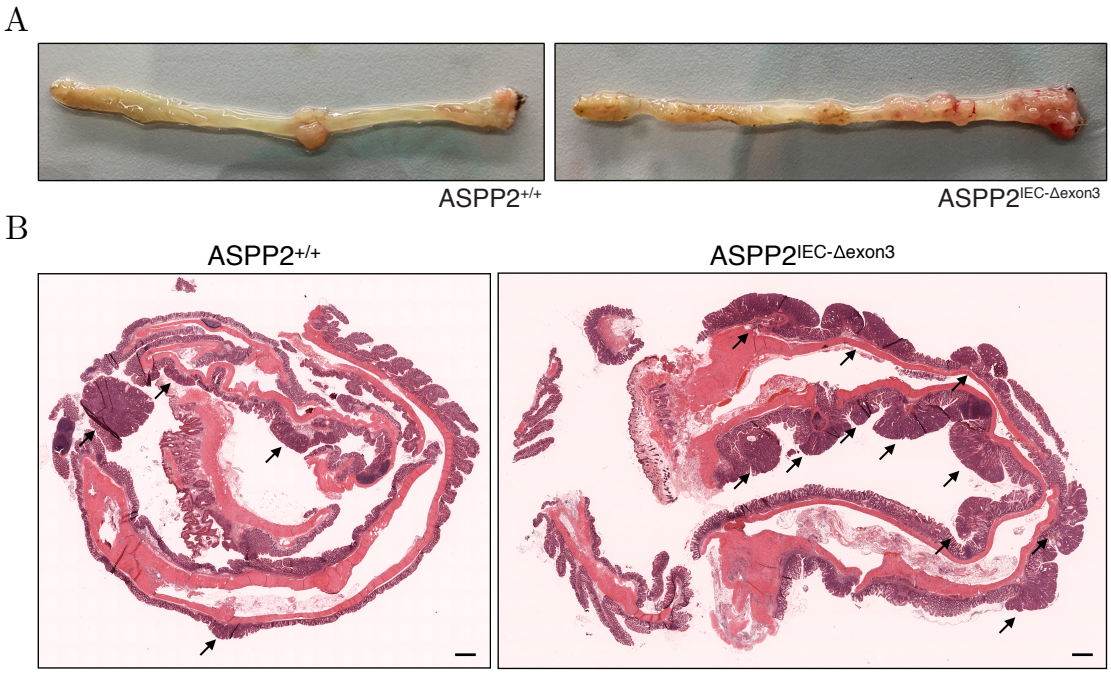


Figure 4.2: AOM/DSS treatment induced colorectal tumourigenesis. (A) Representative images of macroscopically visible colorectal tumours of wild-type and ASPP2$^{\text{IEC-}\Delta\text{exon3}}$ mice following AOM/DSS treatment. (B) Representative H&E staining of colon sections from wild-type and ASPP2$^{\text{IEC-}\Delta\text{exon3}}$ mice following AOM/DSS treatment. Black arrows point to established colonic polyps. Scale bars: 1 mm.

increase in the number of tumours developed ($p = 0.0019$, Figure 4.3A). Of the wild-type mice, 25% did not develop any macroscopically visible tumours, whereas the percentage was only 8% for ASPP2-deficient animals. It is interesting to note that tumours developed in wild-type mice showed a higher median tumour size compared with those developed in their ASPP2$^{\text{IEC-}\Delta\text{exon3}}$ counterparts ($p = 0.0111$, Figure 4.3B), suggesting that they might be more proliferative or less apoptotic than tumours developed in ASPP2-deficient animals. An alternative explanation would be that some of the smaller tumours observed in ASPP2$^{\text{IEC-}\Delta\text{exon3}}$ mice were developed at relatively late time points of the AOM/DSS treatment. To that end, the time course of tumour development needs to be further determined. Given the intragroup variability observed in the number and size of tumours developed, the tumour load of each mouse was calculated. By adding up the sizes of all tumours detected in each animal, the outlier effect was to some extent eliminated. Still, ASPP2$^{\text{IEC-}\Delta\text{exon3}}$ mice showed a significantly higher tumour load than that of the

wild-type animals (p = 0.0263, Figure 4.3C). Taken together, the results described in this section suggested that deficiency of ASPP2 in the intestinal epithelium resulted in an increased susceptibility to AOM/DSS-induced colorectal tumourigenesis.

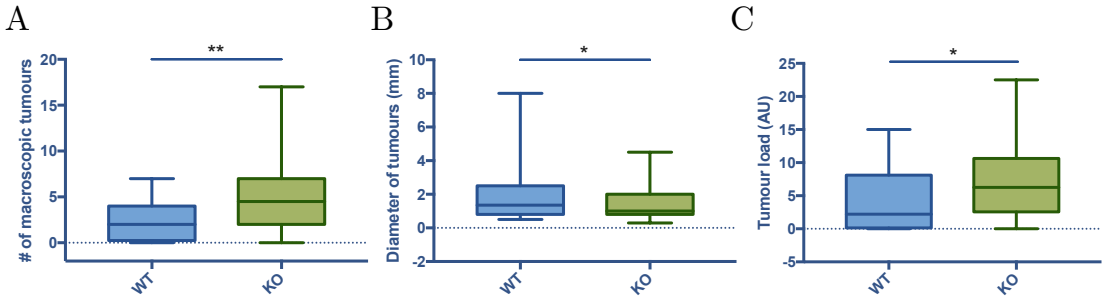


Figure 4.3: ASPP2$^{\text{IEC-}\Delta\text{exon3}}$ mice showed increased tumour loads. (A) Box-and-whisker plot of the number of macroscopic tumours developed in wild-type (n = 32) and ASPP2$^{\text{IEC-}\Delta\text{exon3}}$ (n = 24) mice following the AOM/DSS treatment. (B) Box-and-whisker plot of the size of macroscopic tumours developed in wild-type and ASPP2$^{\text{IEC-}\Delta\text{exon3}}$ mice following the AOM/DSS treatment. 74 tumours from wild-type mice and 104 tumours from ASPP2$^{\text{IEC-}\Delta\text{exon3}}$ mice were included in the analysis. (C) Box-and-whisker plot of the tumour loads of wild-type (n = 32) and ASPP2$^{\text{IEC-}\Delta\text{exon3}}$ (n = 24) mice following the AOM/DSS treatment. AU, arbitrary unit, defined as the sum of the sizes of all macroscopic tumours developed in each animal. The bottom and top of the box represent the first and third quartiles, and the whiskers represent the minimum and maximum of all the data within the group. WT, ASPP2$^{+/+}$; KO, ASPP2$^{\text{IEC-}\Delta\text{exon3}}$; *, $p < 0.05$; **, $p < 0.01$.

4.2.2 Wild-type and ASPP2$^{\text{IEC-}\Delta\text{exon3}}$ crypts showed similar incidence of colorectal tumour initiation

The multi-step process of tumour development comprises three canonical phases: initiation, promotion and progression. In the case of AOM/DSS-induced tumourigenesis, the initiation step is induced by the administration of AOM, and the recovery following DSS treatment promotes the proliferation of epithelial cells, eventually leading to tumour formation (De Robertis et al. 2011). Importantly, the AOM/DSS treatment constitutes a model system that closely mimics the early phase of colorectal tumourigenesis, orchestrating colitis with genetic/epigenetic alterations (De Robertis et al. 2011). Therefore, this protocol allows simultaneous examination of both the initiation and promotion phases of colorectal tumourigenesis, and possibly the distinction between the two stages.

The fact that ASPP2$^{\text{IEC-}\Delta\text{exon3}}$ mice showed an increased number of AOM/DSS-induced tumours suggested that a loss of ASPP2 rendered mice more susceptible to colorectal tumour initiation. Taking advantage of the mosaic pattern of ASPP2 depletion in the ASPP2$^{\text{IEC-}\Delta\text{exon3}}$ mouse model, and using EYFP positivity as a marker for ASPP2 deficiency, the numbers of EYFP-positive and -negative tumours can represent the incidence of colon tumour initiation from ASPP2-deficient and wild-type crypts, respectively. Given that all the crypts in ASPP2$^{\text{IEC-}\Delta\text{exon3}}$ mice were exposed to the same colonic microenvironment, the wild-type crypts can be used as an internal control to investigate whether the loss of ASPP2 would affect the intrinsic tendency of epithelial cells to tumourigenesis.

IF co-staining of EYFP and β-catenin was performed on tumour sections collected from ASPP2$^{\text{IEC-}\Delta\text{exon3}}$ mice. As expected, clusters of both EYFP-positive and -negative cells were observed in the colonic epithelium, in agreement with the mosaic pattern of 4-OHT-induced, CreER-mediated recombination (Figure 4.4A, EYFP). An increase in the protein level of β-catenin was observed in tumour tissues compared with adjacent normal crypts, regardless of the status of ASPP2 (Figure 4.4A, β-catenin). When EYFP-positive tumours were compared with EYFP-negative tumours, the expression and cellular localisation of β-catenin did not seem to be affected by the depletion of ASPP2 (Figure 4.4A, β-catenin). Interestingly, most of the tumours developed in ASPP2$^{\text{IEC-}\Delta\text{exon3}}$ mice were either positive or negative for EYFP, and only a very small fraction were found to consist of a mixture of EYFP-positive and -negative cells. This observation agrees with the theory that colorectal tumours can originate from a single crypt and evolve in a clonal manner (Humphries et al. 2008; Choi et al. 2017).

In order to quantify the frequency of colorectal tumour initiation from wild-type and ASPP2-deficient crypts, the number of ASPP2 wild-type and ASPP2-deficient tumours were counted based on the positivity of EYFP. Both genotypes constituted around 50% of all the tumours developed, suggesting that the loss of ASPP2 did not intrinsically alter the predisposition of epithelial cells to the initiation of tumourigenesis (Figure 4.4B). This analysis was based on the assumption that

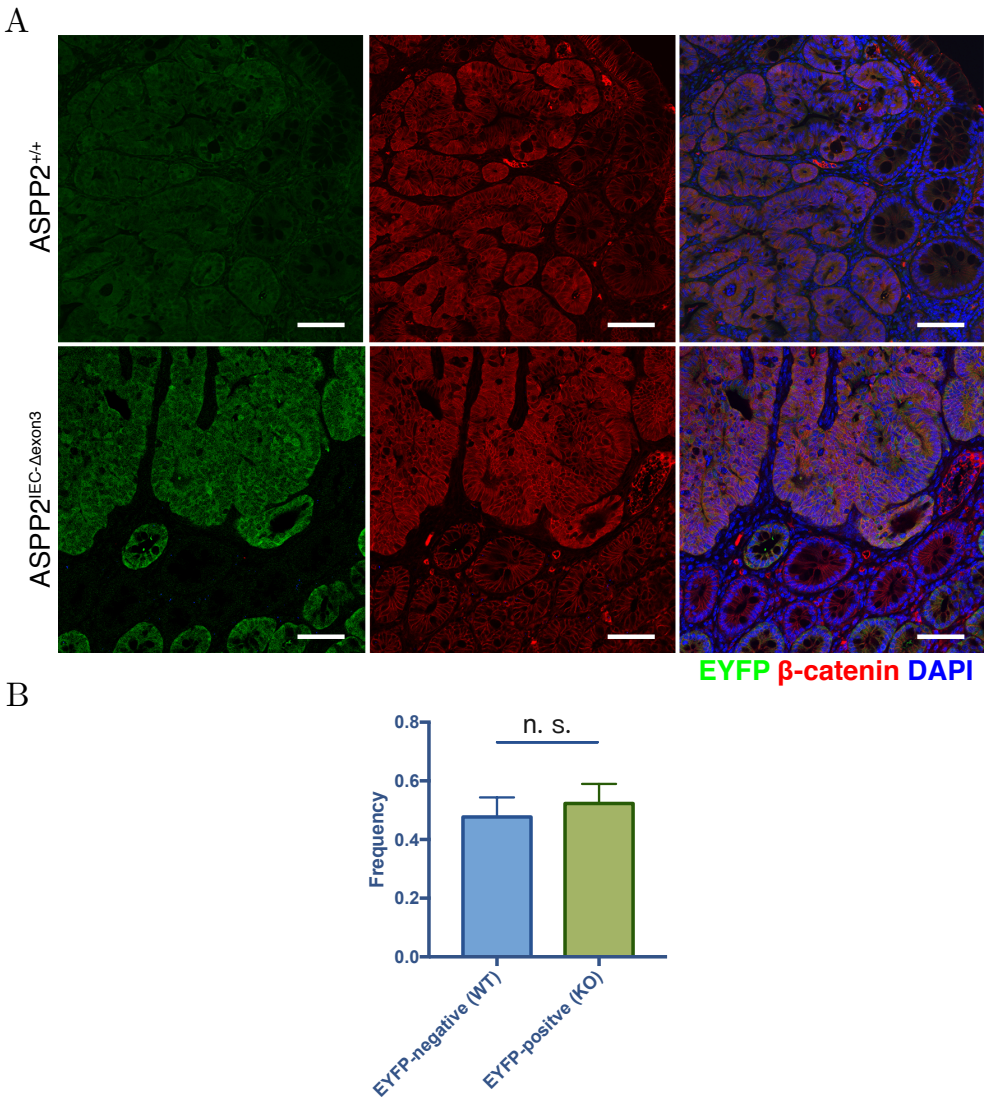


Figure 4.4: ASPP2$^{\text{IEC-}\Delta\text{exon3}}$ crypts showed similar incidence of colon tumour formation as wild-type crypts. (A) Representative IF co-staining of EYFP (green) and β-catenin (red) on colon tumour sections collected from ASPP2$^{\text{IEC-}\Delta\text{exon3}}$ mice, with nuclei counterstained with DAPI (blue). The images are representative of three independent experiments. Scale bars: 25 µm. (B) Quantification of the frequency of EYFP-negative and -positive tumours observed in ASPP2$^{\text{IEC-}\Delta\text{exon3}}$ mice (n = 7). WT, ASPP2$^{+/+}$; KO, ASPP2$^{\text{IEC-}\Delta\text{exon3}}$; n.s., not significant.

the efficiency of 4-OHT-induced, CreER-mediated recombination ranged around 50% in the first place, which was determined empirically. A more meticulous quantification of the baseline efficiency of ASPP2 depletion, ideally on an animal-by-animal basis, is required to corroborate this conclusion. This result seemed to contradict with the increased tumour numbers observed in ASPP2$^{\text{IEC-}\Delta\text{exon3}}$ mice.

One possible explanation for this discrepancy is that the depletion of ASPP2 in IECs may prime the colonic microenvironment to be more tumourigenic, so that the wild-type tumours formed in this context could be secondary to the dysregulated epithelial–stromal cell interactions, which will be investigated in section 4.2.7.

4.2.3 ASPP2$^{\text{IEC-}\Delta\text{exon3}}$ and wild-type tumours showed similar levels of proliferation and apoptosis

Uncontrolled crypt cell proliferation is a common characteristic of CRC (Tanaka 2009). Given that ASPP2$^{\text{IEC-}\Delta\text{exon3}}$ mice showed a higher tumour load but smaller average tumour size compared to their wild-type counterparts, whether or not the observed difference was due to different levels of tumour cell proliferation was investigated. IF co-staining of Ki67 and E-cadherin was performed on colon tumour sections of both wild-type and ASPP2$^{\text{IEC-}\Delta\text{exon3}}$ mice. Tumours developed in both genotypes were highly proliferative as expected, but no difference in the level or pattern of proliferation was observed (Figure 4.5A). In order to quantify the level of tumour cell proliferation, the percentage of Ki67-positive epithelial cells within a tumour was defined as its proliferation index. The quantification further confirmed that tumours developed in wild-type and ASPP2$^{\text{IEC-}\Delta\text{exon3}}$ mice were equally proliferative (Figure 4.5B).

It has been reported that abundant apoptotic cellular debris can be observed in neoplastic crypts (Boivin et al. 2003), but that was not seen in the mouse model used in this study. As indicated by the IF staining of cleaved Caspase-3, only a very small percentage of cells undergoing apoptosis were detectable in tumours developed in the AOM/DSS-treated mice, and no difference in the number or pattern of apoptotic cells was observed between wild-type and ASPP2$^{\text{IEC-}\Delta\text{exon3}}$ animals (Figure 4.6). Consistently, western blot analysis of colon tumour samples also showed negligible signals of cleaved Caspase-3 (data not shown). Taken together, the loss of ASPP2 in the intestinal epithelium did not seem to alter the proliferation or apoptosis of AOM/DSS-induced colorectal tumours.

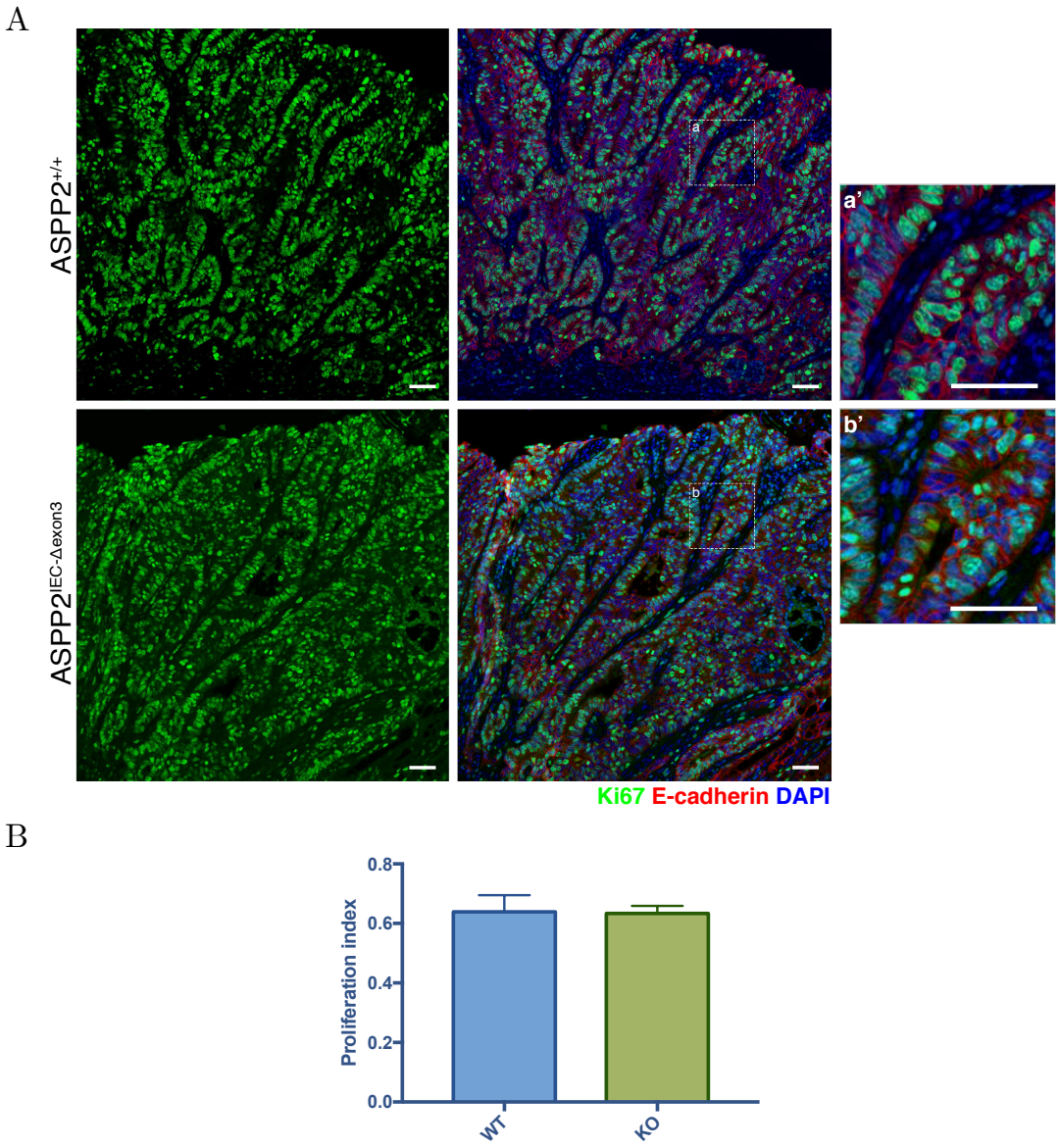


Figure 4.5: Tumours developed in ASPP2$^{\text{IEC-}\Delta\text{exon3}}$ mice showed similar levels of proliferation as those of wild-type animals. (A) Representative IF co-staining of Ki67 (green) and E-cadherin (red) on sections of colorectal tumours developed in wild-type and ASPP2$^{\text{IEC-}\Delta\text{exon3}}$ mice, with nuclei counterstained with DAPI (blue). Scale bars: 25 µm. (B) Proliferation indices of colorectal tumours developed in wild-type and ASPP2$^{\text{IEC-}\Delta\text{exon3}}$ mice based on the IF staining of Ki67. The proliferation index is defined as the percentage of Ki67-positive epithelial cells within a tumour. Tumours from 3 wild-type and 3 ASPP2$^{\text{IEC-}\Delta\text{exon3}}$ mice were included in the analysis.

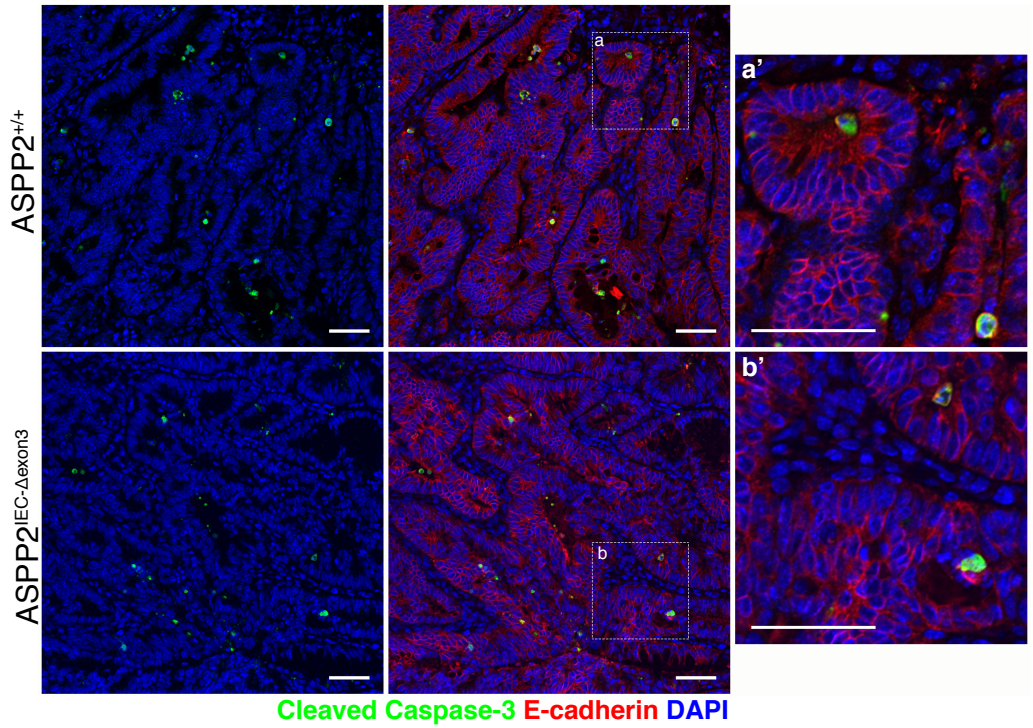


Figure 4.6: Tumours developed in ASPP2$^{\text{IEC-}\Delta\text{exon3}}$ mice showed similar levels of apoptosis as those of wild-type animals. IF co-staining of cleaved Caspase-3 (green) and E-cadherin (red) was performed on sections of colorectal tumours developed in wild-type and ASPP2$^{\text{IEC-}\Delta\text{exon3}}$ mice, with nuclei counterstained with DAPI (blue). Scale bars: 50 µm.

4.2.4 The Wnt/β-catenin pathway was not affected by the loss of ASPP2 in the intestinal epithelium

In order to characterise the molecular alterations of AOM/DSS-induced tumours in wild-type and ASPP2$^{\text{IEC-}\Delta\text{exon3}}$ animals, several signalling pathways implicated in colorectal tumourigenesis were examined.

Wnt signalling, a key regulator of stem cell turnover and homeostasis of the intestinal epithelium, is known to be involved in colorectal tumourigenesis when aberrantly activated (De Robertis et al. 2011). To that end, IHC staining of β-catenin, the effector protein of the canonical Wnt signalling cascade, was performed on tumour sections from both wild-type and ASPP2$^{\text{IEC-}\Delta\text{exon3}}$ animals. As expected, the expression of β-catenin was upregulated in tumour tissues compared with normal crypts. In contrast to the junctional localisation of β-catenin observed in normal tissue, both nuclear and cytoplasmic staining of β-catenin was detectable

in tumour samples. Tumours developed in ASPP2$^{\text{IEC-}\Delta\text{exon3}}$ mice showed similar expression levels and cellular localisation of β-catenin compared with those of wild-type animals (Figure 4.7A). This result suggested that canonical Wnt signalling was not affected in ASPP2-deficient colorectal tumours.

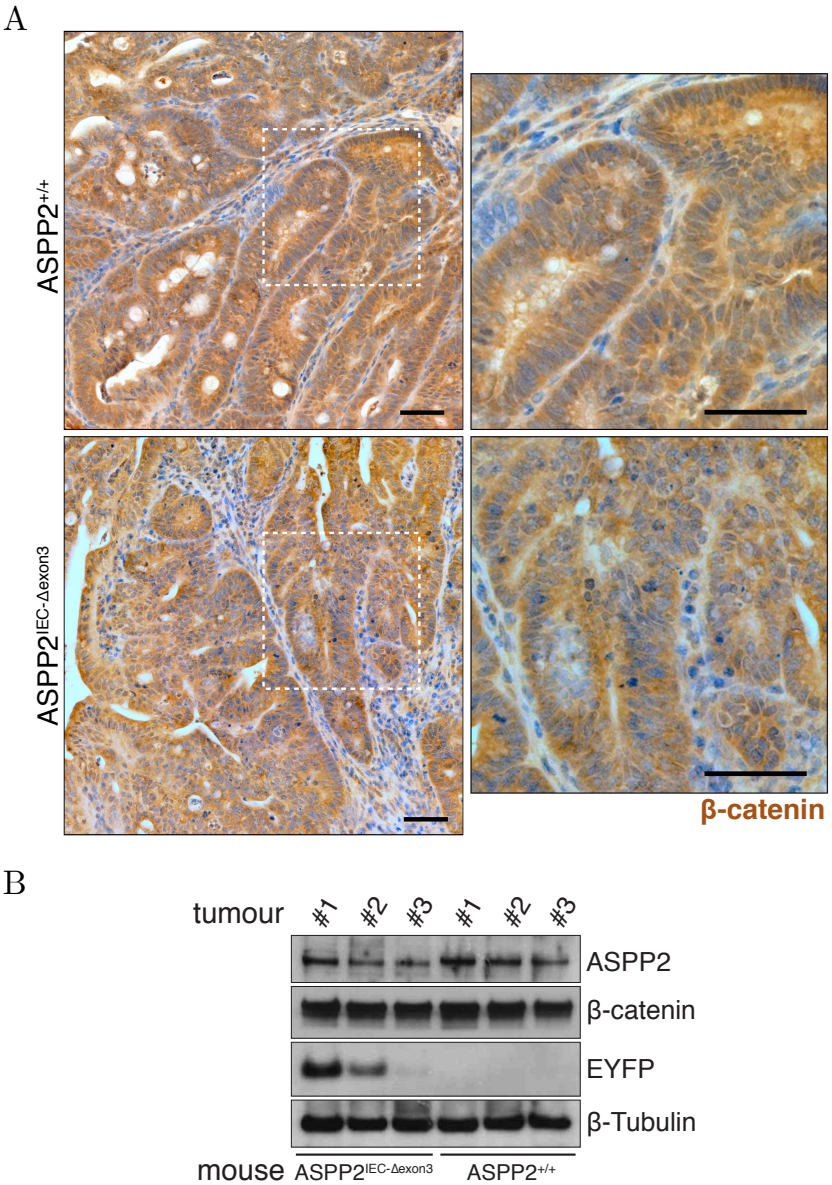


Figure 4.7: Loss of ASPP2 in the intestinal epithelium did not affect cellular localisation of β-catenin. (A) Representative IHC staining of β-catenin on colon tumour sections of wild-type and ASPP2$^{\text{IEC-}\Delta\text{exon3}}$ mice. Zoomed-in views of the areas delineated by white squares are shown on the right side of the panel. Scale bars: 25 µm. (B) Western blot analysis of colorectal tumours isolated from one ASPP2$^{\text{IEC-}\Delta\text{exon3}}$ mouse and one wild-type mouse, with β-Tubulin used as the loading control. Note that tumour #3 in the ASPP2$^{\text{IEC-}\Delta\text{exon3}}$ mouse represents a tumour derived from a wild-type crypt.

In order to investigate whether the stability of β-catenin was affected by the loss of ASPP2, western blot analysis was performed on tumour samples harvested from wild-type and ASPP2$^{\text{IEC-}\Delta\text{exon3}}$ animals. Notably, tumours isolated from ASPP2$^{\text{IEC-}\Delta\text{exon3}}$ mice can be either positive or negative for EYFP, depending on its crypt of origin (Figure 4.7B). Regardless of the heterogeneity, no difference was observed in the protein level of β-catenin between the two genotypes, suggesting that ASPP2 is not involved in the regulation of the stability of β-catenin (Figure 4.7B). Taken together, these results suggested that the Wnt/β-catenin pathway was not affected by the loss of ASPP2 in the intestinal epithelium.

4.2.5 ASPP2$^{\text{IEC-}\Delta\text{exon3}}$ mice showed decreased phosphorylation of YAP at Ser127 in AOM/DSS-induced colorectal tumours

Signal transduction through the Hippo/YAP pathway has been shown to be implicated in the control of organ size and regulation of tumourigenesis (B. Zhao et al. 2010). Activation of the Hippo pathway kinase cascade results in the phosphorylation and inhibition of the YAP/TAZ transcription coactivators, thereby repressing proliferation and promoting apoptosis (B. Zhao et al. 2010). Given the fact that phosphorylation of YAP at Ser127 results in its binding to 14-3-3 and cytoplasmic retention (B. Zhao et al. 2007), and that ASPP2 can mediate the dephosphorylation of Ser127 of YAP by PP1 (Christophe Royer et al. 2014), it was hypothesised that colorectal tumours that developed in ASPP2$^{\text{IEC-}\Delta\text{exon3}}$ mice may display hyperphosphorylation of YAP and suppressed YAP/TAZ activity.

To test this hypothesis, IHC staining of YAP was performed on tumour sections from wild-type and ASPP2$^{\text{IEC-}\Delta\text{exon3}}$ mice. A reduction in the nuclear localisation of YAP was observed in ASPP2-deficient animals (Figure 4.8A), and the sequestration of YAP in the cytoplasm might be partially achieved by the loss of ASPP2-mediated YAP dephosphorylation at Ser127. The upregulation of YAP phosphorylation was further confirmed with western blot analysis of tumour samples collected from wild-type and ASPP2$^{\text{IEC-}\Delta\text{exon3}}$ animals (Figure 4.8B).

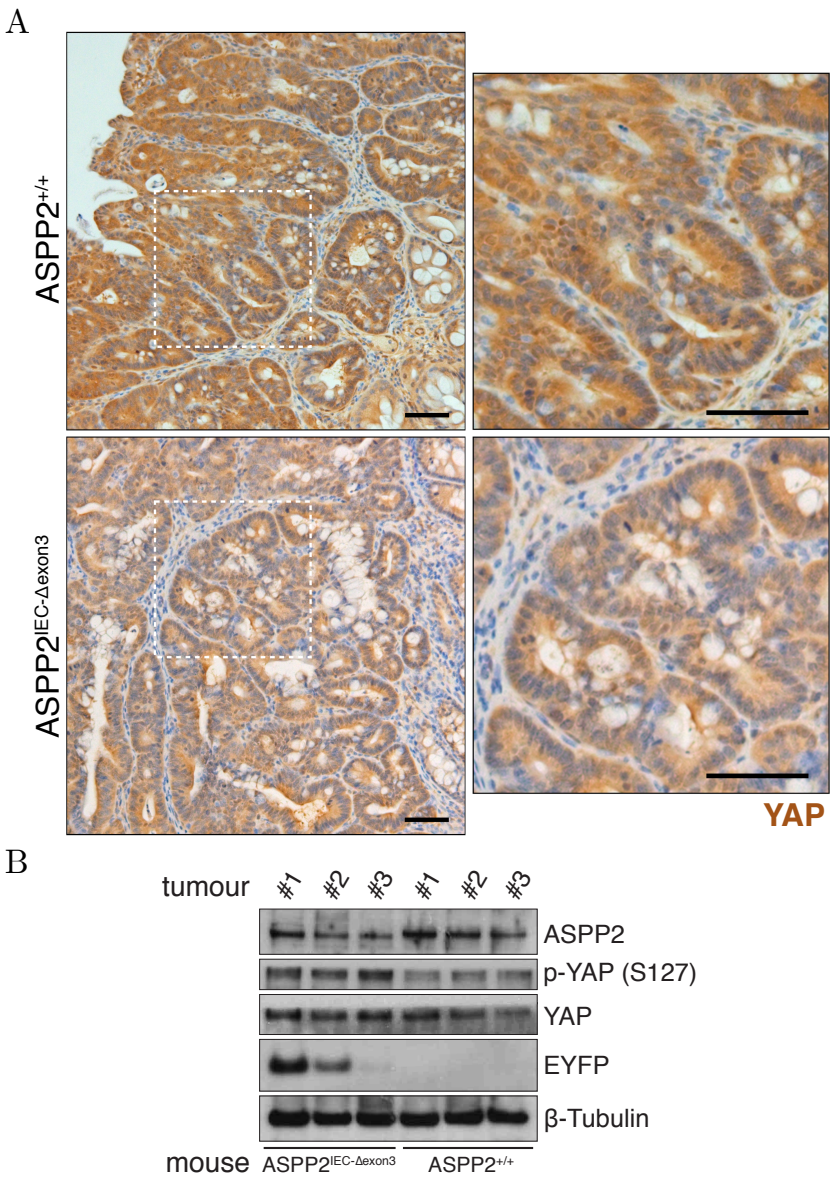


Figure 4.8: ASPP2$^{\text{IEC-}\Delta\text{exon3}}$ tumours showed reduced YAP activity. (A) Representative IHC staining of YAP on colon tumour sections of wild-type and ASPP2$^{\text{IEC-}\Delta\text{exon3}}$ mice. Zoomed-in views of the areas delineated by white squares are shown on the right side of the panel. Scale bars: 50 µm. (B) Western blot analysis of colorectal tumours isolated from one ASPP2$^{\text{IEC-}\Delta\text{exon3}}$ mouse and one wild-type mice, with β-Tubulin used as the loading control. The blots were obtained from the same batch of experiment as shown in Figure 4.7B, and therefore have shared ASPP2, EYFP, and β-Tubulin. Similarly, tumour #3 in the ASPP2$^{\text{IEC-}\Delta\text{exon3}}$ mouse represents a tumour derived from a wild-type crypt.

The reason for the detection of ASPP2 in tumours developed in ASPP2$^{\text{IEC-}\Delta\text{exon3}}$ mice can be attributed to the mosaic pattern of ASPP2 depletion and thus the heterogenous nature of the tumour cells. It may also be due to stromal cells that were harvested together with the tumours when the tissue samples were prepared.

Notably, the overall protein level of YAP stayed unchanged in ASPP2-deficient tumours, suggesting that the phosphorylation of YAP on Ser381, which is known to prime it for proteasomal degradation (Zhao et al. 2011), was not affected by the loss of ASPP2. Given the pro-survival function of the YAP signalling, this result may suggest a possible explanation for the increased tumour size observed in wild-type animals.

4.2.6 Tumours developed in ASPP2$^{\text{IEC-}\Delta\text{exon3}}$ mice showed increased ERK phosphorylation

Activation of EGFR is a common feature of CRC, with an estimation of 60–80% CRC cases being affected (Pabla 2015). Of note, the overexpression of EGFR correlates with tumour stage, and therefore has long been recognised as a prognostic marker for tumour progression and metastasis (Spano et al. 2005; Pabla 2015). The major signalling cascade downstream of EGFR is the RAS-RAF-ERK pathway (Markman et al. 2010). It has been reported that radiotherapy of CRC results in a reduction in ERK phosphorylation, suggesting its prognostic value (Corn et al. 2008). In order to better understand the role of ASPP2 in the progression of colorectal tumourigenesis, whether or not a loss of ASPP2 would lead to dysregulated ERK activation was investigated.

IF staining of phospho-ERK (p-ERK, Thr202/Tyr204) was performed on colon tumour sections from wild-type and ASPP2$^{\text{IEC-}\Delta\text{exon3}}$ mice. Clusters of cells positive for p-ERK were observed in both genotypes, but more frequently in ASPP2$^{\text{IEC-}\Delta\text{exon3}}$ mice than in their wild-type counterparts (Figure 4.9A). It is worth noting that not all cells positive for EYFP in ASPP2$^{\text{IEC-}\Delta\text{exon3}}$ animals were positive for p-ERK (Figure 4.9A), suggesting that a loss of ASPP2 alone was not sufficient to drive the activation of ERK. This observation indicated the involvement of external signals beyond deficiencies intrinsic to epithelial cells, supporting the hypothesis that defects caused by ASPP2 depletion could be achieved through alterations in epithelial–stromal cell interactions.

To further confirm the upregulation of ERK phosphorylation, western blot analysis of tumour samples collected from wild-type and ASPP2$^{\text{IEC-}\Delta\text{exon3}}$ mice

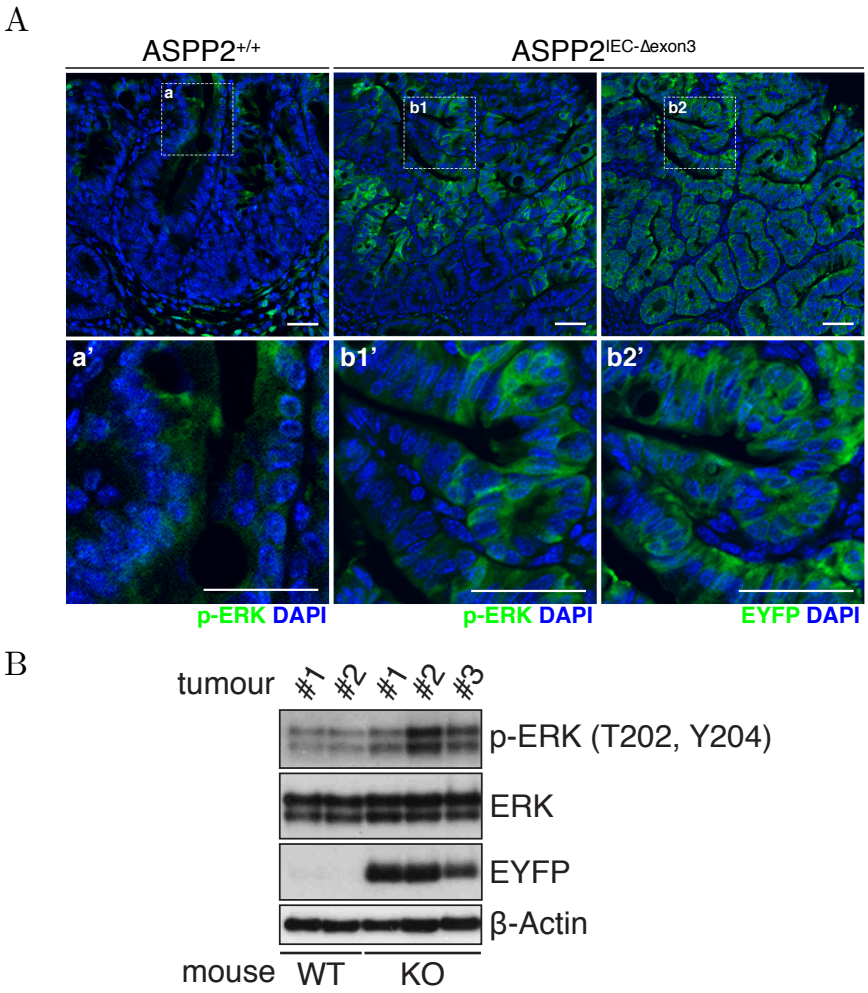


Figure 4.9: Loss of ASPP2 in IECs resulted in upregulated ERK phosphorylation in AOM/DSS-induced tumours. (A) Representative IF staining of p-ERK (Thr202/Tyr204) or EYFP (green) on sections of colorectal tumours collected from wild-type and ASPP2$^{\text{IEC-}\Delta\text{exon3}}$ mice, with nuclei counterstained with DAPI (blue). For the wild-type mouse, insert (a) and the enlarged image (a') highlight a region positive for p-ERK. For the ASPP2$^{\text{IEC-}\Delta\text{exon3}}$ animal, consecutive colon tumour sections were stained for p-ERK and EYFP, respectively. Insert (b1) and (b2) were taken as immediately adjacent areas within the tumour, with (b1') and (b2') presenting the images at a higher magnification. Scale bars: 50 µm. (B) Western blot analysis of colorectal tumours isolated from one wild-type mouse and one ASPP2$^{\text{IEC-}\Delta\text{exon3}}$ mouse, with β-Actin used as the loading control. WT, ASPP2$^{+/+}$; KO, ASPP2$^{\text{IEC-}\Delta\text{exon3}}$.

was performed (Figure 4.9B). The total protein level of ERK was not affected by the loss of ASPP2, but tumours isolated from ASPP2$^{\text{IEC-}\Delta\text{exon3}}$ mice did show upregulated ERK phosphorylation. Variable levels of EYFP were observed in ASPP2$^{\text{IEC-}\Delta\text{exon3}}$ tumours, consistent with the expected heterogeneity (Figure 4.9B). Taking the protein level of EYFP as an indicator of ASPP2 deficiency, the extent of

ASPP2 depletion was not correlated with the level of p-ERK within a tumour, again suggesting the involvement of epithelial cell non-autonomous factors (Figure 4.9B).

Importantly, the activation of MAPKs, a family of serine/threonine kinases of which ERK is a member, has long been associated with IBD (Broom et al. 2009). Moreover, it has been demonstrated in an $APC^{Min/+}$ mouse model that activation of ERK drives colorectal tumourigenesis (Lee et al. 2010). These observations suggest that activation of ERK could happen prior to the onset of tumourigenesis. Along that line, it was hypothesised that a loss of ASPP2 may result in the activation of ERK, thereby predisposing mice to colorectal tumourigenesis.

In order to investigate whether a loss of ASPP2 would affect the activation of ERK under the conditions of colonic inflammation, western blot analysis was performed on colonic crypts of wild-type and $ASPP2^{IEC\text{-}\Delta exon3}$ animals that were treated with 2% DSS for 5 days followed by 6 days of recovery. As expected, phosphorylation of ERK was observed in both genotypes, but to a significantly higher degree in ASPP2-deficient mice than in their wild-type counterparts (Figure 4.10A). This observation was consistent with the increased tumour loads observed in $ASPP2^{IEC\text{-}\Delta exon3}$ animals.

Further to that, the pattern of ERK phosphorylation in inflamed colonic tissue was examined by IF staining. Phosphorylation of ERK can be detected in regenerative crypts of both wild-type and $ASPP2^{IEC\text{-}\Delta exon3}$ animals, particularly in regions undergoing re-epithelialisation (Figure 4.10B). Despite the fact that the phosphorylation of ERK was not perfectly associated with ASPP2 deficiency as indicated by EYFP positivity, the pattern of ERK activation was more consistent in $ASPP2^{IEC\text{-}\Delta exon3}$ mice compared with wild-type animals (Figure 4.10B). Taken together, a loss of ASPP2 would lead to increased activation of ERK in the context of both colonic inflammation and tumourigenesis.

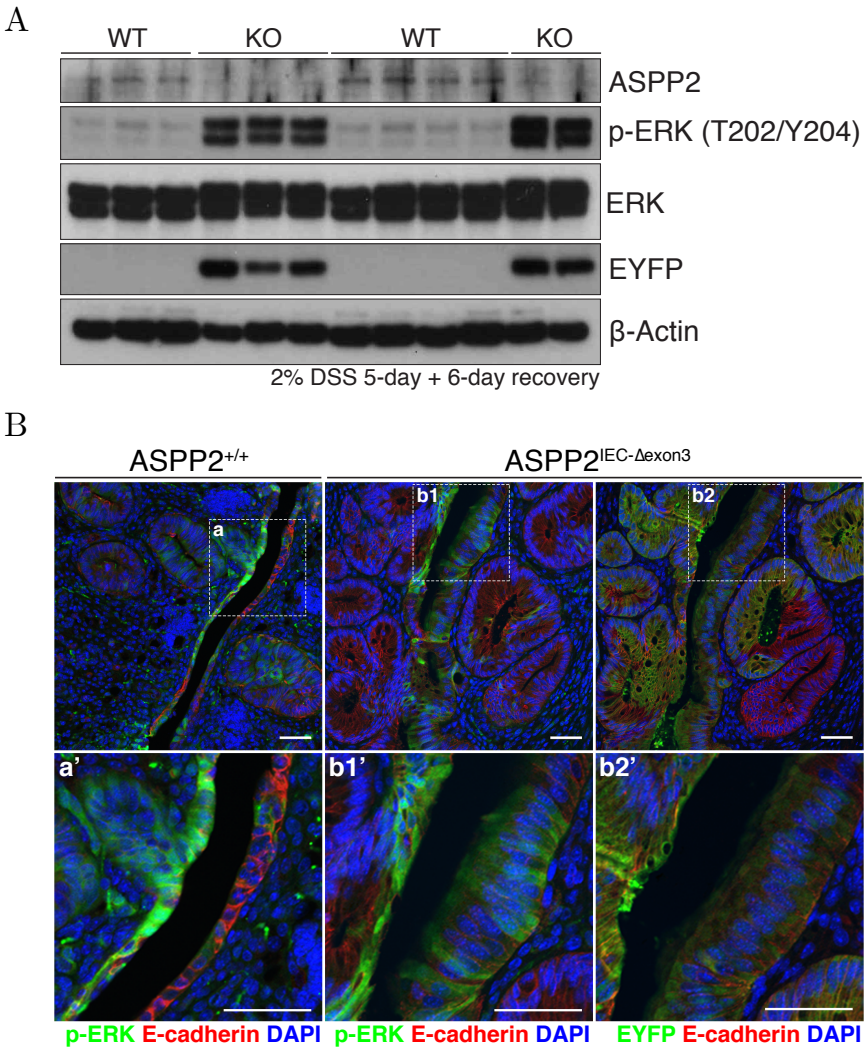


Figure 4.10: Loss of ASPP2 in IECs resulted in upregulated ERK phosphorylation in regenerative colonic epithelium. (A) Western blot analysis of colonic epithelial cells isolated from wild-type and ASPP2$^{\text{IEC-}\Delta\text{exon3}}$ mice, with β-Actin used as the loading control. The mice were treated with 2% DSS for 5 days followed by 6 days of recovery. The blots were obtained from the same batch of experiment as shown in Figure 3.6B and Figure 3.9C, and therefore have shared ASPP2, EYFP, and β-Actin. WT, ASPP2$^{+/+}$; KO, ASPP2$^{\text{IEC-}\Delta\text{exon3}}$. (B) Representative IF co-staining of p-ERK (Thr202/Tyr204) or EYFP (green) and E-cadherin (red) on wild-type and ASPP2$^{\text{IEC-}\Delta\text{exon3}}$ colon sections, with nuclei counterstained with DAPI (blue). For the wild-type mouse, insert (a) and the enlarged image (a') highlight a region positive for p-ERK. For the ASPP2$^{\text{IEC-}\Delta\text{exon3}}$ animal, consecutive colon tumour sections were stained for p-ERK and EYFP, respectively. Insert (b1) and (b2) were taken as immediately adjacent areas within the tumour, with (b1') and (b2') presenting the images at a higher magnification. Scale bars: 50 µm.

4.2.7 Loss of ASPP2 in the intestinal epithelium resulted in a local immune microenvironment favouring tumour progression

In the AOM/DSS model of colorectal tumourigenesis, the administration of AOM introduces genetic alterations to the intestinal epithelium and induces the initiation of tumourigenesis, whereas DSS treatment creates a chronic inflammatory microenvironment favouring the promotion of tumour growth (Neufert et al. 2007). The results presented in the previous section suggested that the loss of ASPP2 did not affect the intrinsic susceptibility of epithelial cells to AOM-induced tumour initiation. As a result, the increased susceptibility of ASPP2$^{\text{IEC-}\Delta\text{exon3}}$ mice to AOM/DSS-induced tumourigenesis might be largely due to their delayed recovery from DSS-induced colitis, i.e. the prolonged inflammation.

To test this hypothesis, LPMCs of wild-type and ASPP2$^{\text{IEC-}\Delta\text{exon3}}$ mice were examined during the recovery phase of DSS-induced colitis. Given that macrophages are the most abundant leukocytes in the colonic mucosa (Mowat et al. 2014), and that tumour associated macrophages have been reported to promote colorectal tumour progression (Miao et al. 2016; Kang et al. 2010), the infiltration of macrophages into the lamina propria was investigated in this context.

Colonic LPMCs were isolated from wild-type and ASPP2$^{\text{IEC-}\Delta\text{exon3}}$ mice and subjected to flow cytometry analysis. ASPP2-deficient mice showed a higher percentage of F4/80^{+} macrophages within the CD45^{+} immune cell population ($p = 0.0157$, Figure 4.11, A and B). Interestingly, after the LPMCs were stimulated with PMA/ionomycin, a higher percentage of macrophages derived from ASPP2$^{\text{IEC-}\Delta\text{exon3}}$ mice expressed proinflammatory cytokines including IL-1β, IL-6, and TNF-α ($p = 0.0217$, 0.0172, and 0.1390, respectively; Figure 4.11C). The increase in macrophage infiltration and proinflammatory cytokine production may partially explain the increased tumour loads observed in ASPP2$^{\text{IEC-}\Delta\text{exon3}}$ mice. More importantly, it supports the hypothesis that epithelial–immune cell interactions can be implicated in AOM/DSS-induced tumourigenesis.

In addition to macrophage infiltration, another pivotal factor that is implicated in tumour progression is the immunosuppressive effect exerted by Tregs (Facciabene

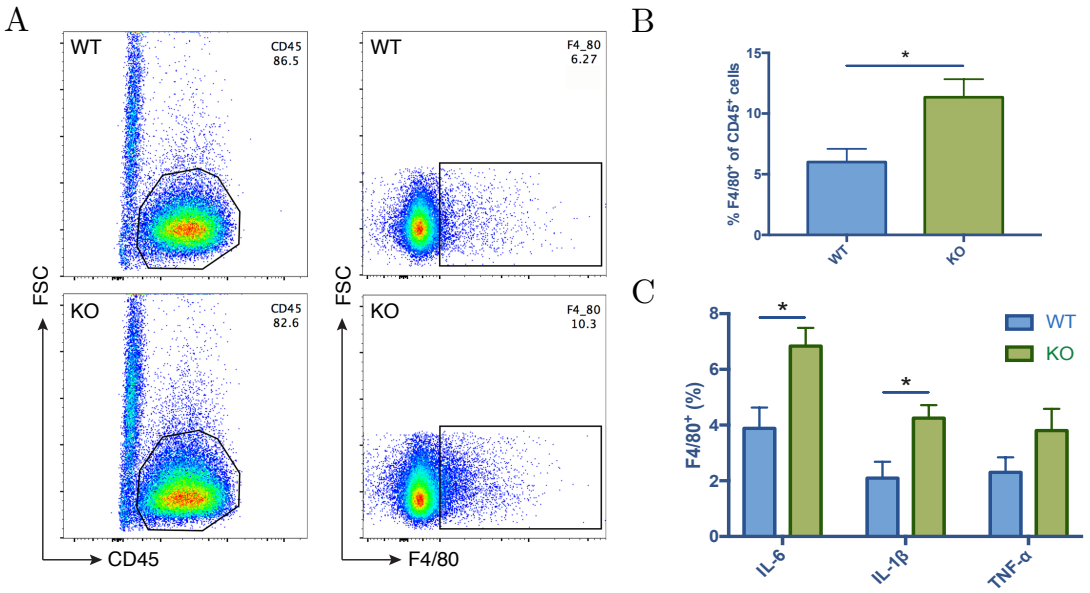


Figure 4.11: Loss of ASPP2 in IECs resulted in increased macrophage infiltration. (A) Representative results of flow cytometry analysis of $CD45^+$ leukocytes and $F4/80^+$ macrophages present in the lamina propria of wild-type and $ASPP2^{IEC\text{-}\Delta exon3}$ mice. The mice were treated with 2% DSS for 5 days followed by 6 days of recovery. (B) Percentage of $F4/80^+$ macrophages in $CD45^+$ leukocytes in the lamina propria of wild-type (n = 6) and $ASPP2^{IEC\text{-}\Delta exon3}$ (n = 5) mice. The mice were treated with 2% DSS for 5 days followed by 6 days of recovery. Error bars represent SEM. (C) Percentage of IL-6^+, TNF-α^+, and IL-$1\beta^+$ cells in $F4/80^+$ macrophages in the lamina propria of wild-type (n = 6) and $ASPP2^{IEC\text{-}\Delta exon3}$ (n = 5) mice. The mice were treated with 2% DSS for 5 days followed by 6 days of recovery. Error bars represent SEM. WT, $ASPP2^{+/+}$; KO, $ASPP2^{IEC\text{-}\Delta exon3}$; *, $p < 0.05$.

et al. 2012). Under homeostatic conditions, Tregs are considered to mediate peripheral tolerance and immune suppression (Smigiel et al. 2014). In the context of the tumour microenvironment, Tregs have been shown to promote the immunological ignorance of cancer cells, and therefore suppress anti-tumour immune responses (Facciabene et al. 2012).

In order to investigate whether a loss of ASPP2 would affect the induction of Treg responses in the context of AOM/DSS-induced tumourigenesis, LPMCs of wild-type and $ASPP2^{IEC\text{-}\Delta exon3}$ mice were isolated and analysed at the endpoint of the AOM/DSS treatment. It is worth noting that this time point represents a stage at which the colonic tissue already bears a certain number of established tumours, as opposed to the relatively early phase when the analysis of macrophage infiltration was performed. No difference in the percentage of $CD4^+$ T cells in the

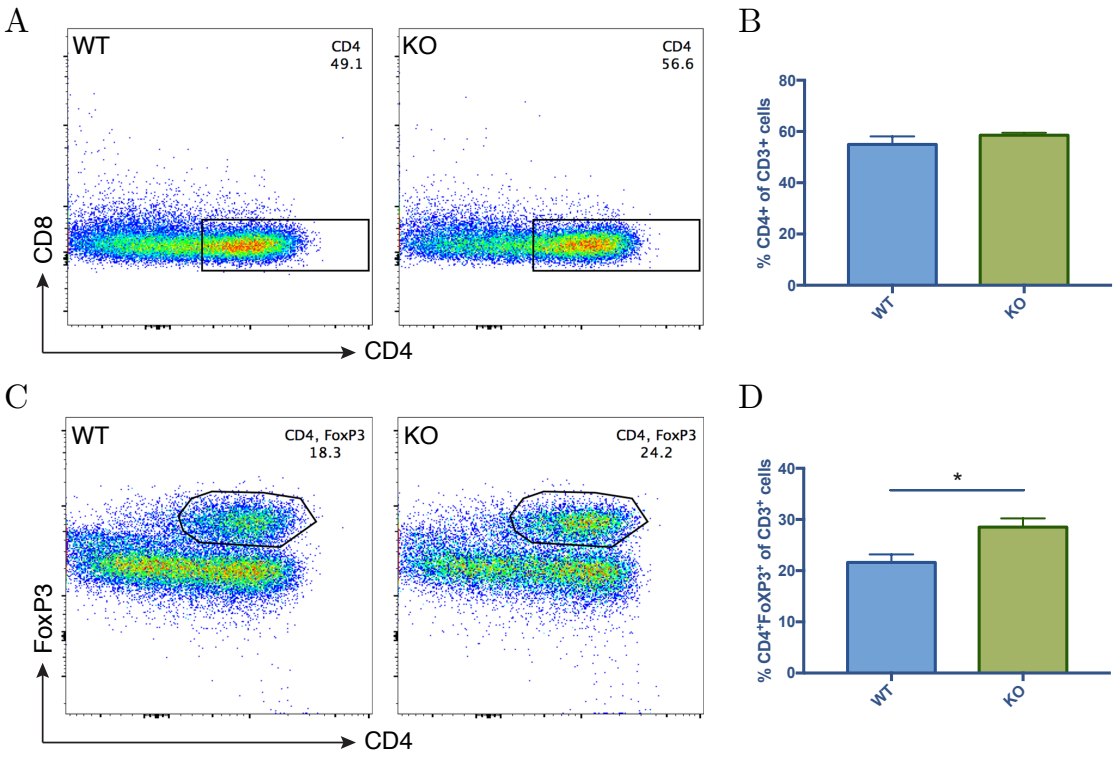


Figure 4.12: ASPP2$^{\text{IEC-}\Delta\text{exon3}}$ mice showed increased presence of Tregs in the lamina propria. LPMCs were isolated from wild-type and ASPP2$^{\text{IEC-}\Delta\text{exon3}}$ mice at the endpoint of the AOM/DSS treatment. (A) Representative results of flow cytometry analysis of CD4$^+$ T cells present in the lamina propria CD3$^+$ T cells of wild-type and ASPP2$^{\text{IEC-}\Delta\text{exon3}}$ mice. (B) Percentage of CD4$^+$ T cells in the CD3$^+$ T cell population present in the lamina propria of wild-type (n = 3) and ASPP2$^{\text{IEC-}\Delta\text{exon3}}$ (n = 3) mice. (C) Representative results of flow cytometry analysis of CD4$^+$, FoxP3$^+$ Tregs present in the lamina propria of wild-type and ASPP2$^{\text{IEC-}\Delta\text{exon3}}$ mice. (D) Percentage of CD4$^+$, FoxP3$^+$ Tregs in CD3$^+$ T cells in the lamina propria of wild-type (n = 5) and ASPP2$^{\text{IEC-}\Delta\text{exon3}}$ (n = 4) mice. WT, ASPP2$^{+/+}$; KO, ASPP2$^{\text{IEC-}\Delta\text{exon3}}$; *, $p < 0.05$.

CD3$^+$ T cell population was observed between wild-type and ASPP2$^{\text{IEC-}\Delta\text{exon3}}$ mice (Figure 4.12, A and B). However, a significant increase in the proportion of CD4$^+$, FoxP3$^+$ Tregs was observed in lamina propria CD3$^+$ T cells of ASPP2$^{\text{IEC-}\Delta\text{exon3}}$ animals compared with their wild-type counterparts ($p = 0.0213$, Figure 4.12; C and D). This observation suggested that ASPP2-deficient mice may exhibit a more tumour-permissive microenvironment.

Taken together, the data presented in this section supported the hypothesis that a loss of ASPP2 in the intestinal epithelium would result in a local immune microenvironment that favours tumour progression.

4.2.8 ASPP2$^{\Delta exon3}$ mice were not more susceptible to AOM/DSS-induced tumourigenesis than wild-type mice

In a similar way that the conditional germline ASPP2 transgenic mice were employed in the study of DSS-induced acute colitis, ASPP2$^{\Delta exon3}$ mice were also subjected to the AOM/DSS treatment to test their susceptibility to colorectal tumourigenesis. A cohort of 9 wild-type and 10 ASPP2$^{\Delta exon3}$ mice were used in this experiment.

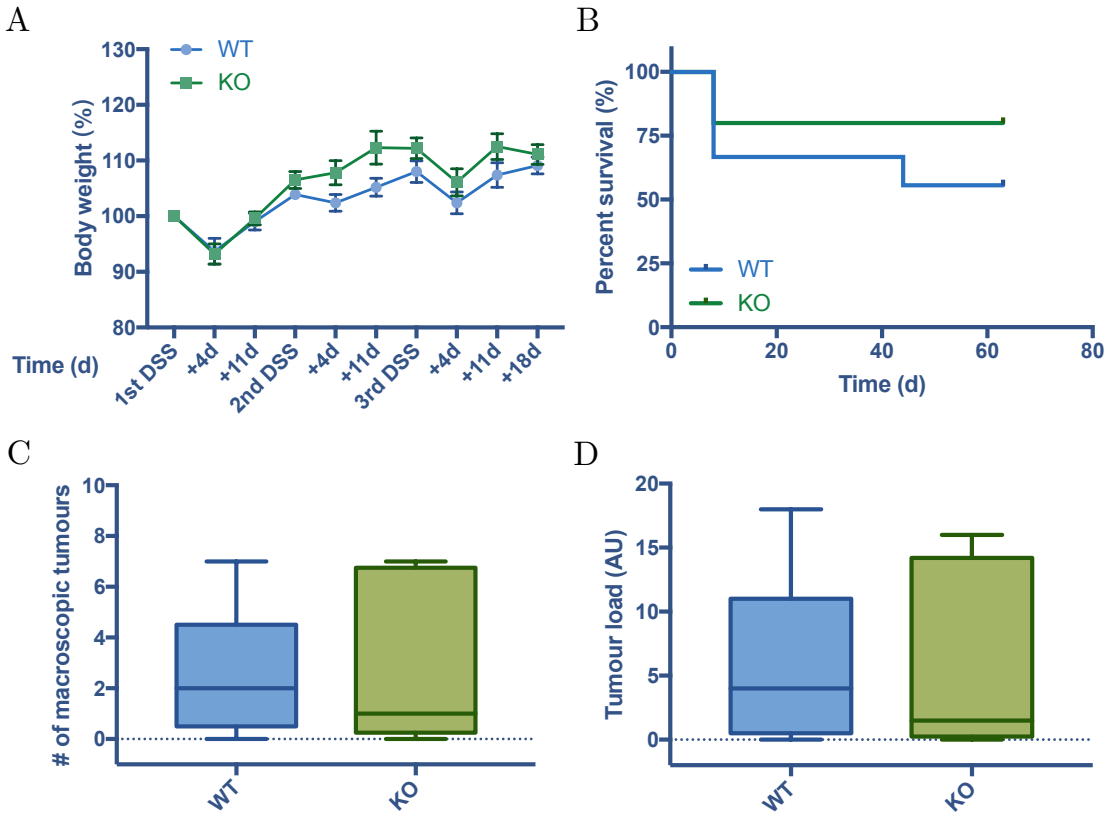


Figure 4.13: ASPP2$^{\Delta exon3}$ mice showed similar susceptibility to AOM/DSS-induced tumourigenesis as wild-type animals. (A) Time course of body weight loss. Wild-type (n = 4) and ASPP2$^{\Delta exon3}$ (n = 9) mice were injected with AOM and subjected to three rounds of 4 day 2% DSS treatment. The body weight was measured at the indicated time points, and relative body weight (%) compared to the initial value is plotted with SEM. DSS, 2% DSS treatment; d, day. (B) Cumulative survival curves of wild-type (n = 9) and ASPP2$^{\Delta exon3}$ (n = 10) mice undergoing AOM/DSS treatment in this study. (C) Box-and-whisker plot of the number of macroscopic tumours developed in wild-type (n = 5) and ASPP2$^{\Delta exon3}$ (n = 8) mice following the AOM/DSS treatment. (D) Box-and-whisker plot of the tumour loads of wild-type (n = 5) and ASPP2$^{\Delta exon3}$ (n = 8) mice following the AOM/DSS treatment. The bottom and top of the box represent the first and third quartiles, and the whiskers represent the minimum and maximum of all the data within the group. AU, arbitrary unit, defined as the sum of the sizes of all macroscopic tumours developed in each animal. WT, ASPP2$^{+/+}$; KO, ASPP2$^{\Delta exon3}$.

During the time course of the AOM/DSS experiment, the mice under treatment were closely monitored for illness and their body weight was recorded on a weekly basis. A trend of weight loss was found in all animals after each round of DSS administration, but no difference was found between ASPP2$^{\Delta exon3}$ mice and their wild-type counterparts (Figure 4.13A). Similarly to the scenario of the ASPP2$^{IEC\text{-}\Delta exon3}$ cohort, DSS-caused fatality mostly happened after the first round of DSS treatment (Figure 4.13B). This was probably due to the fact that the mice were still relatively young at this stage and were therefore more susceptible to DSS-induced colitis. In contrast to the results obtained from the ASPP2$^{IEC\text{-}\Delta exon3}$ mice, no difference was observed between the cumulative survival rates of wild-type and ASPP2$^{\Delta exon3}$ animals (Figure 4.13B). After the completion of the experiment, all mice that survived to the endpoint of the experiment were sacrificed for analysis. Wild-type and ASPP2$^{\Delta exon3}$ mice showed similar tumour numbers and tumour loads, as opposed to the difference observed between wild-type and ASPP2$^{IEC\text{-}\Delta exon3}$ animals (Figure 4.13, C and D).

It is worth noting that the numbers of tumours developed in this cohort of mice ranged from 0 to 7, identical to those of the wild-type animals from the ASPP2$^{IEC\text{-}\Delta exon3}$ cohort (Figure 4.3A, 4.13C). This observation suggested that the two batches of experiments were comparable to each other, and that the loss of ASPP2 in tissue compartments other than IECs could rescue mice from the increased susceptibility to AOM/DSS-induced tumourigenesis observed in ASPP2$^{IEC\text{-}\Delta exon3}$ animals.

4.3 Summary and Brief Discussion

In this chapter, the implications of ASPP2 deficiency in CAC were interrogated using the AOM/DSS-induced tumourigenesis model. After a single injection of the carcinogenic agent AOM, the mice were subjected to repeated cycles of epithelial cell injury and repair induced by DSS. As expected, ASPP2$^{IEC\text{-}\Delta exon3}$ mice showed decreased cumulative survival during the time course of the treatment, and exhibited higher tumour loads at the endpoint of the experiment. Interestingly, although

ASPP2-deficient mice developed a larger number of colorectal tumours, the average tumour size was significantly smaller than that of the wild-type animals. The discrepancy between the gross tumour load and the growth of each individual tumour suggested that the loss of ASPP2 might be more involved in tumour initiation rather than in tumour progression.

As with the DSS-induced colitis model, proliferation and apoptosis within established tumours were first examined. Unexpectedly, no difference was observed between wild-type and ASPP2-deficient animals, suggesting that the intrinsic regulation of tumour cell turnover was not affected by the loss of ASPP2. It is worth noting that the proliferation index used in this analysis has not been normalised to tumour size, the incorporation of which may confer more control over the development stage of the tumours under examination. As for the signalling pathways implicated in tumour progression, the activation status of Wnt, Hippo, and MAPK signalling was investigated. Tumours developed in wild-type and ASPP2$^{\text{IEC-}\Delta\text{exon3}}$ mice showed similar expression levels and cellular localisation of β-catenin, suggesting that the Wnt signalling pathway is not affected by the loss of epithelial ASPP2. However, tumours developed in ASPP2$^{\text{IEC-}\Delta\text{exon3}}$ mice showed decreased phosphorylation of YAP at Ser127. Moreover, an increase of ERK phosphorylation was observed in tumours developed in ASPP2$^{\text{IEC-}\Delta\text{exon3}}$ mice, which was even more significant in the context of colonic inflammation. Although the activation of ERK is believed to be more related to tumour progression, the early onset of ERK phosphorylation, possibly downstream of EGFR signalling, may provide an explanation for the increased tumour loads observed in ASPP2$^{\text{IEC-}\Delta\text{exon3}}$ animals.

One of the major confounding factors underlying the analysis described in this chapter is the mosaic pattern of ASPP2 depletion in the Villin-CreER mouse model. As a result, despite the fact that all the tumours developed in wild-type mice are known to originate from wild-type epithelial cells, tumours developed in ASPP2$^{\text{IEC-}\Delta\text{exon3}}$ mice can be derived from either wild-type or ASPP2-deficient crypts. In spite of the confusion that might arise from such heterogeneity, the wild-type crypts that remain in ASPP2-deficient mice can be used as an internal

control in this system. Regardless of genotype, all the epithelial cells within ASPP2$^{\text{IEC-}\Delta\text{exon3}}$ mice are exposed to the same local microenvironment, so any differences observed between wild-type and ASPP2-deficient tumours are likely to be due to mechanisms intrinsic to epithelial cells. Given that tumours induced by the AOM/DSS treatment mostly undergo clonal expansion, and that ASPP2-deficient cells in the mouse model are labelled with EYFP, the numbers of EYFP-negative and -positive tumours represent the frequency of tumour initiation from wild-type and ASPP2-deficient crypts, respectively. Surprisingly, no difference was observed in the frequency of wild-type and ASPP2-deficient tumours among all the ASPP2$^{\text{IEC-}\Delta\text{exon3}}$ mice examined, suggesting that ASPP2 deficiency did not intrinsically affect the predisposition of epithelial cells to tumour initiation. This led us to an examination of the immune microenvironment.

In order to characterise the immune cell compartment in the context of AOM/DSS-induced tumourigenesis, LPMCs were isolated from wild-type and ASPP2$^{\text{IEC-}\Delta\text{exon3}}$ mice and analysed by flow cytometry. Since our hypothesis was more focused on the environmental factors that predispose epithelial cells to tumour formation, immune cells that infiltrate into established tumours were not characterised in this study. As expected, the composition of the lamina propria in ASPP2$^{\text{IEC-}\Delta\text{exon3}}$ mice showed characteristics favouring tumour initiation and progression, including increased macrophage infiltration and Treg differentiation. These results suggested that the increased number of tumours formed in ASPP2$^{\text{IEC-}\Delta\text{exon3}}$ mice was a result of a dysregulated immune microenvironment. Admittedly, in order to obtain a more complete picture of the epithelial–immune cell crosstalk implicated in different stages of tumour development, immune cell profiling needs to be performed at different time points during the course of the experiment. It will also be critical to include a more detailed examination of tumour-infiltrated immune cells. All of these questions will be addressed in future experiments.

Taken together, the data obtained from both the DSS-induced colitis model and the AOM/DSS-induced tumourigenesis model suggested that a deficiency of ASPP2 in the intestinal epithelium would lead to alterations in epithelial–immune

cell interactions. To better distinguish epithelial cell non-autonomous factors from their intrinsic properties, we decided to employ an epithelium-specific model system, i.e. the intestinal organoid.

5

Organoids as a Model System to Study Intestinal Biology

5.1 Introduction

Over the last decade, the renaissance of the organoid culture technique has attracted tremendous interest in the field of developmental biology and human disease modelling. As a matter of fact, the organoid represents an *ex vivo* system that makes feasible the study of fundamental biological questions that have been difficult to answer using conventional methods.

As a tissue surrogate derived from primary cells, the intestinal organoid retains physiologically relevant tissue architecture and cell fate determination characteristics of its origin. It is therefore an indispensable model system for the study of basic intestinal biology, such as tissue morphogenesis and stem cell biology (Rookmaaker et al. 2015). Indeed, intestinal organoids derived from human pluripotent stem cells (hPSCs) have been shown to resemble human foetal intestine (Chin et al. 2017). When transplanted into the mouse kidney capsule, hPSC-derived organoids undergo morphological and functional changes reminiscent of the development of the foetal intestine (Watson et al. 2014). Moreover, small intestinal organoids have been used to demonstrate how Paneth cells constitute the niche required by stem cells for their self-renewal (Sato, Es, et al. 2011).

Another key advantage of the intestinal organoid is manifested by the fact that it is exclusively composed of epithelial cells, allowing the characterisation of their intrinsic properties. For example, the ability of intestinal organoids to develop from a single $Lgr5^+$ stem cell is evidence that intestinal crypt–villus units are capable of self-organising in the absence of a mesenchymal niche (Sato et al. 2009).

However, the simplicity of the organoid can also be a double-edged sword. In fact, one of the major limitations of the system is the lack of environmental factors. In order to study the interaction between epithelial cells and tissue elements present in their immediate environment, various co-culture systems have been established. A study of murine IELs co-cultured with intestinal organoids has shed light on the motility dynamics of $\alpha\beta$T and $\gamma\delta$T IELs and their spatiotemporal interactions with epithelial cells (Nozaki et al. 2016). It is important to note that epithelial cells have been shown to act as a source of cytokines and chemokines, adding to the complexity of the organoid–immune cell co-culture system (Stadnyk 2002).

With regard to translational studies, intestinal organoids have been widely applied to drug screening and disease modelling (Clevers 2016). Cell damage in the intestinal epithelium is frequently associated with inflammatory disorders as well as drug-mediated toxicity (Grabinger et al. 2014). To that end, the organoid system has offered new possibilities to assess different modes of cell death. For example, it has been demonstrated that the loss of Bim (Bcl-2 interacting mediator of cell death), a pro-apoptotic Bcl-2 homolog, will lead to an increase in the resistance of small intestinal organoids to cisplatin-induced, but not TNF-α-induced, cell death (Grabinger et al. 2014). When applied to a broader context, such an approach may enable a more refined understanding of the mechanisms underlying chemo- and radiotherapy-induced cytotoxicity and therefore holds promise for therapeutic applications. Indeed, there is an ongoing effort to derive a living organoid biobank from CRC patients, which, once established, will revolutionise the concept and implementation of bench-to-bedside translational research (Wetering et al. 2015).

In this chapter, small intestinal organoid cultures derived from wild-type and $ASPP2^{IEC\text{-}\Delta exon3}$ mice were used to develop a workflow for the analysis of

organoid growth dynamics. Given its ease of implementation, the small intestinal organoid was employed as a proof-of-concept system to demonstrate that organoids can recapitulate *in vivo* scenarios and are amenable to *in vitro* manipulations. The methods developed were then applied to colonic organoids with the aim of establishing a cell viability-based model of tissue regeneration. Where applicable, organoids derived from germline ASPP2$^{\Delta exon3}$ mice were used instead of those derived from the conditional ASPP2$^{IEC\text{-}\Delta exon3}$ animals, mainly due to the fact that the former represents a cleaner model system and should exhibit more definitive phenotypes. Finally, colorectal tumour organoids were derived from AOM/DSS-induced colorectal tumours as a supplement to the *in vivo* tumourigenesis study.

5.2 Results

5.2.1 ASPP2-deficient organoids recapitulated epithelial hyperproliferation observed *in vivo*

The maintenance of intestinal homeostasis relies on a fine-tuned regulation of proliferation, differentiation, and cell death. In order to demonstrate that organoids can be used as a model system to study these key biological events *in vitro*, a selected panel of processes implicated in the homeostatic control of the intestinal epithelium were examined in a mouse model/organoid-matched manner.

One phenotype observed in the small intestine of ASPP2$^{\Delta exon3}$ mice is an increase in the number of cells undergoing mitosis in crypts (S. Koch, unpublished data). In order to examine whether a similar phenotype can be seen in IEC-specific ASPP2-deficient mice, IHC staining of pH3 was performed on sections of wild-type and ASPP2$^{IEC\text{-}\Delta exon3}$ small intestines. As expected, pH3-positive cells were located in crypts, i.e. the proliferative compartment of the intestinal epithelium in both genotypes of mice (Figure 5.1A). The overall morphology of the intestinal epithelium was not affected by the loss of ASPP2, but an increase in the number of cells stained positive for pH3 was observed in ASPP2$^{IEC\text{-}\Delta exon3}$ mice (Figure 5.1, A and B). This observation agreed with the result obtained from an independent cohort of ASPP2$^{\Delta exon3}$ mice (S. Koch, unpublished data), and was further confirmed by

western blot analysis (Figure 5.1C). A significant increase in the protein level of pH3 was observed in ASPP2$^{\Delta exon3}$ crypts compared with their wild-type counterparts.

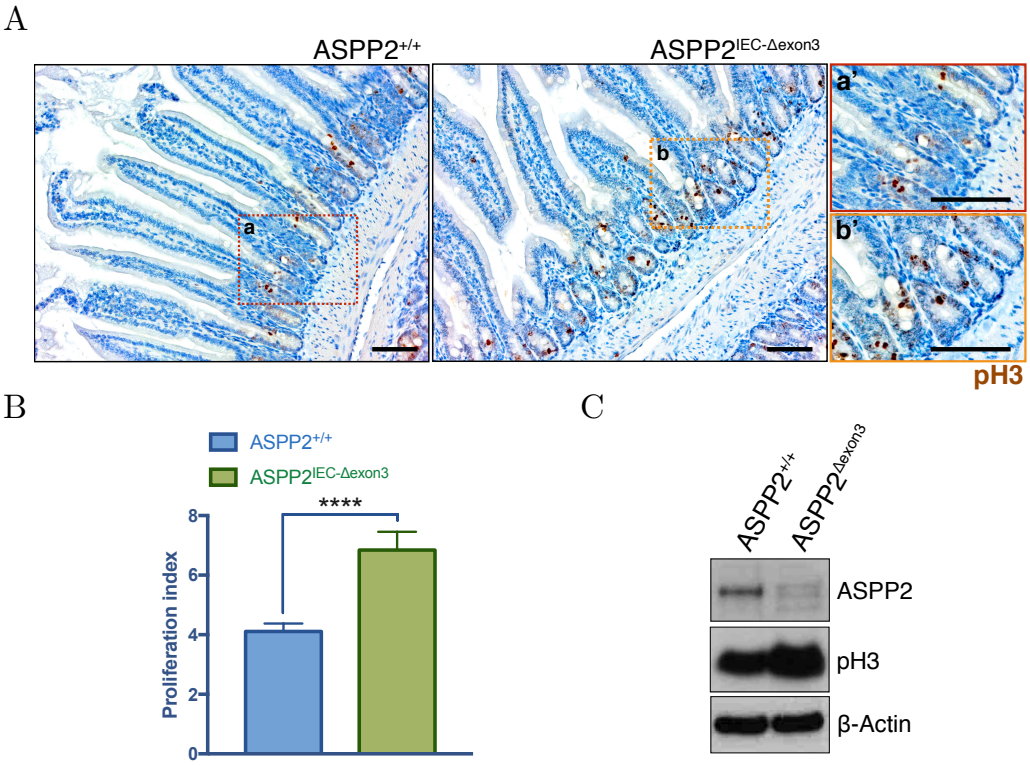


Figure 5.1: Loss of ASPP2 in duodenal epithelial cells resulted in hyperproliferation. (A) Representative IHC staining of pH3 on duodenal sections of wild-type and ASPP2$^{\text{IEC-}\Delta exon3}$ mice. Zoomed-in views of the areas delineated by inserts (a) and (b) are shown in (a') and (b'). Scale bars: 100 µm. (B) Quantification of the number of pH3-positive cells per crypt, defined as the proliferation index, in wild-type and ASPP2$^{\text{IEC-}\Delta exon3}$ duodenums (n = 2 for each group; 27 wild-type crypts and 20 crypts of ASPP2$^{\text{IEC-}\Delta exon3}$ mice were included in the analysis). ****, p<0.0001. (C) Western blot analysis of duodenal epithelial cells isolated from wild-type and ASPP2$^{\Delta exon3}$ mice, with β-Actin used as the loading control.

Following on from the *in vivo* observations outlined above, small intestinal organoids were generated from wild-type and ASPP2$^{\text{IEC-}\Delta exon3}$ mice to investigate whether the phenotype observed *in vivo* can be faithfully recapitulated *in vitro*. Organoids derived from both genotypes were viable in the standard ENR culture medium (advanced DMEM/F12 base medium supplemented with EGF, Noggin and R-spondin), exhibiting characteristics of small intestinal organoids with no perceptible differences. In order to visualise the growth dynamics of wild-type and ASPP2-deficient organoids, time-lapse images were acquired for 50 ASPP2-

deficient organoids and 25 wild-type organoids over a period of 120 hours. ASPP2-deficient organoids showed an increased rate of proliferation, manifested mainly by volume enlargement (Figure 5.2A). Intriguingly, 29 out of 50 ASPP2$^{\text{IEC-}\Delta\text{exon3}}$ organoids developed into an irregular shape lacking a well-defined central lumen, the frequency of which was 10 out of 25 for their wild-type counterparts, suggesting that ASPP2-deficient organoids may exhibit an imbalance between proliferation and differentiation. Taken together, these results suggested that a loss of ASPP2 may intrinsically increase the proliferative potential of IECs.

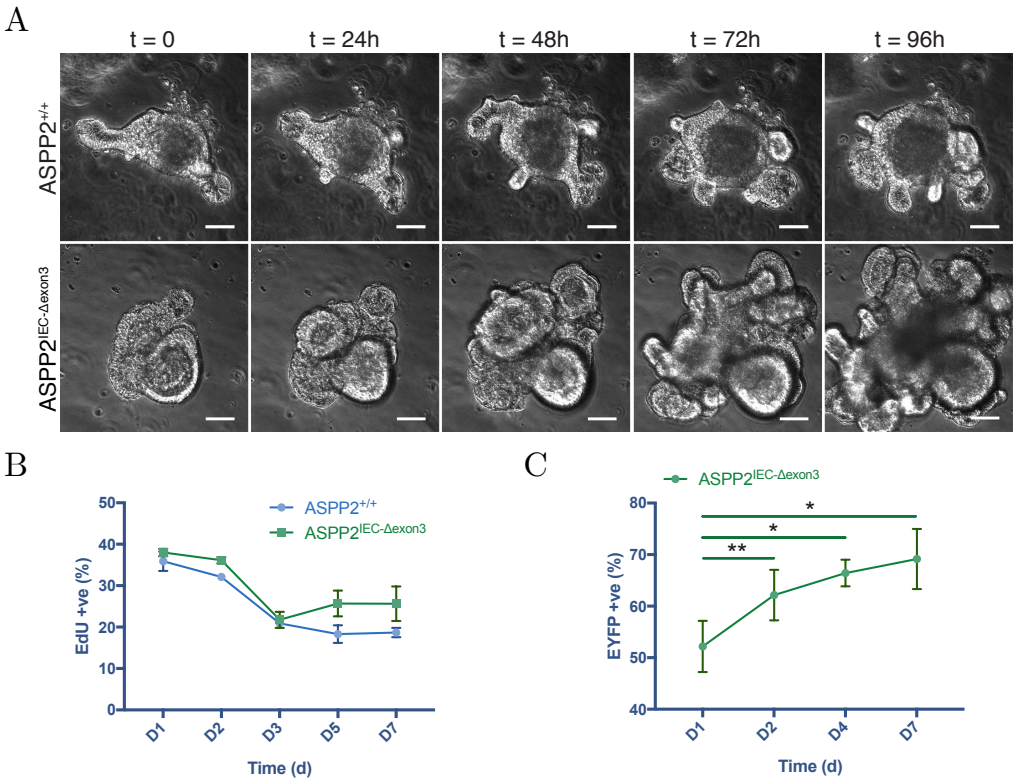


Figure 5.2: ASPP2-deficient small intestinal organoids showed increased proliferation. (A) Representative time-lapse DIC imaging of wild-type and ASPP2$^{\text{IEC-}\Delta\text{exon3}}$ small intestinal organoids over 96 hours. Scale bars: 100 µm. (B) EdU incorporation (4.5 hours) in wild-type (n = 2) and ASPP2$^{\text{IEC-}\Delta\text{exon3}}$ (n = 2) small intestinal organoids. The experiments were performed on Days 1, 2, 3, 5, and 7 after the organoid culture was established from primary tissue. Error bars represent SEM. (C) The percentage of EYFP-positive cells within newly established small intestinal organoids. Organoids derived from ASPP2$^{\text{IEC-}\Delta\text{exon3}}$ mice (n = 6) were analysed on Days 1, 2, 4, and 7 of culture by flow cytometry. Error bars represent SEM. D, day; *, $p < 0.05$; **, $p < 0.01$; +ve, positive.

One of the key features standing out from the time-lapse videos is that the

organoid culture represents a highly heterogeneous population of entities displaying considerable inter- and intragroup variability. One way to balance out the variability is to take a large enough number of organoids and treat them as a whole, rather than carry out the analysis on an organoid-by-organoid basis. To that end, EdU incorporation analysis was performed on wild-type and ASPP2$^{\text{IEC-}\Delta\text{exon3}}$ organoids to characterise proliferation at a population level. On Days 1, 2, 3, 5, and 7 after the organoid culture was established from primary tissue, the organoids were incubated with EdU for 4.5 hours and the percentage of cells incorporated with EdU was determine by flow cytometry. In agreement with the hypothesis that a loss of ASPP2 would lead to hyperproliferation of epithelial cells, ASPP2$^{\text{IEC-}\Delta\text{exon3}}$ organoids showed a modest increase in the rate of EdU incorporation (Figure 5.2B). This phenotype was further confirmed by the fact that the percentage of EYFP-positive cells within ASPP2$^{\text{IEC-}\Delta\text{exon3}}$ organoids increased over the first 7 days after they were put into culture (Figure 5.2C). The difference was significant between Days 1 and 2, Days 1 and 4, and Days 1 and 7 ($p = 0.0089$, 0.0422, and 0.0337, respectively; paired *t*-test). This result suggested that ASPP2-deficient epithelial cells overtook their wild-type counterparts in the early stage of organoid development. Taken together, ASPP2-deficient small intestinal organoids recapitulated epithelial hyperproliferation observed *in vivo*.

5.2.2 Loss of ASPP2 predisposed IECs to the secretory lineage

As a primary cell-based culture system, the intestinal organoid retains physiologically relevant tissue architecture and cell fate determination, making it a suitable model to study cell differentiation (Sato et al. 2009). However, it is worth noting that the organoid is an extremely heterogeneous system. The heterogeneity is reflected in at least two aspects. On the one hand, each organoid is composed of different cell types, encompassing all the cell lineages present in the intestinal epithelium (hereafter referred to as intra-organoid heterogeneity). On the other hand, depending on the initial state of the crypt, organoids cultured under the same conditions may still grow at different rates and end up in different developmental stages

(hereafter referred to as interorganoid heterogeneity). As a result, the challenge of organoid characterisation lies in the possibility that the signature of a specific cell lineage could be largely masked by background noise, particularly in the case of relatively small cell populations.

One way to cope with the heterogeneity outlined above is to expand the $Lgr5^+$ stem cell population within the organoids, which can be achieved by treating the organoids with VPA and CHIR99021 (Yin et al. 2013). The hypothesis is that, if VPA/CHIR99021-treated, stem cell-enriched organoids are allowed to differentiate for a sufficient period of time, any difference in the predisposition to a particular cell lineage, possibly caused by intrinsic defects in the differentiation programme, should be recognisable.

In order to confirm that the combined treatment of organoids with VPA and CHIR99021 could synergistically expand the $Lgr5^+$ stem cell population and result in a nearly homogeneous culture, small intestinal organoids derived from Lgr5-EGFP-IRES-CreERT2 mice were cultured in standard ENR culture medium, as described in the previous section. As expected, $Lgr5^+$ stem cells were enriched in the bottom of crypts, recapitulating their localisation *in vivo* (Figure 5.3A, Control). After the organoids were treated with VPA/CHIR99021 for 72 hours, the percentage of $Lgr5^+$ stem cells within the organoids increased dramatically, as indicated by the GFP positivity (Figure 5.3A). It is worth noting that the morphology of the organoids was also altered by the treatment. The spherical shape of the organoids indicated a reduction of intra-organoid heterogeneity (Figure 5.3A), whereas organoids with elongated crypts suggested a phenotype of hyperproliferation (Figure 5.3D).

Western blot analysis was performed on untreated organoids and organoids treated with VPA/CHIR99021 for 5 days. Consistent with the role of VPA as an activator of Notch signalling (Greenblatt et al. 2007; Stockhausen et al. 2005), the expression of Math1, a transcription factor downstream of Notch that directs the differentiation of secretory cell lineages, was downregulated by VPA/CHIR99021 treatment (Figure 5.3B). Interestingly, the phosphorylation of ERK was also induced by the VPA/CHIR99021 treatment (Figure 5.3B). This observation may partially

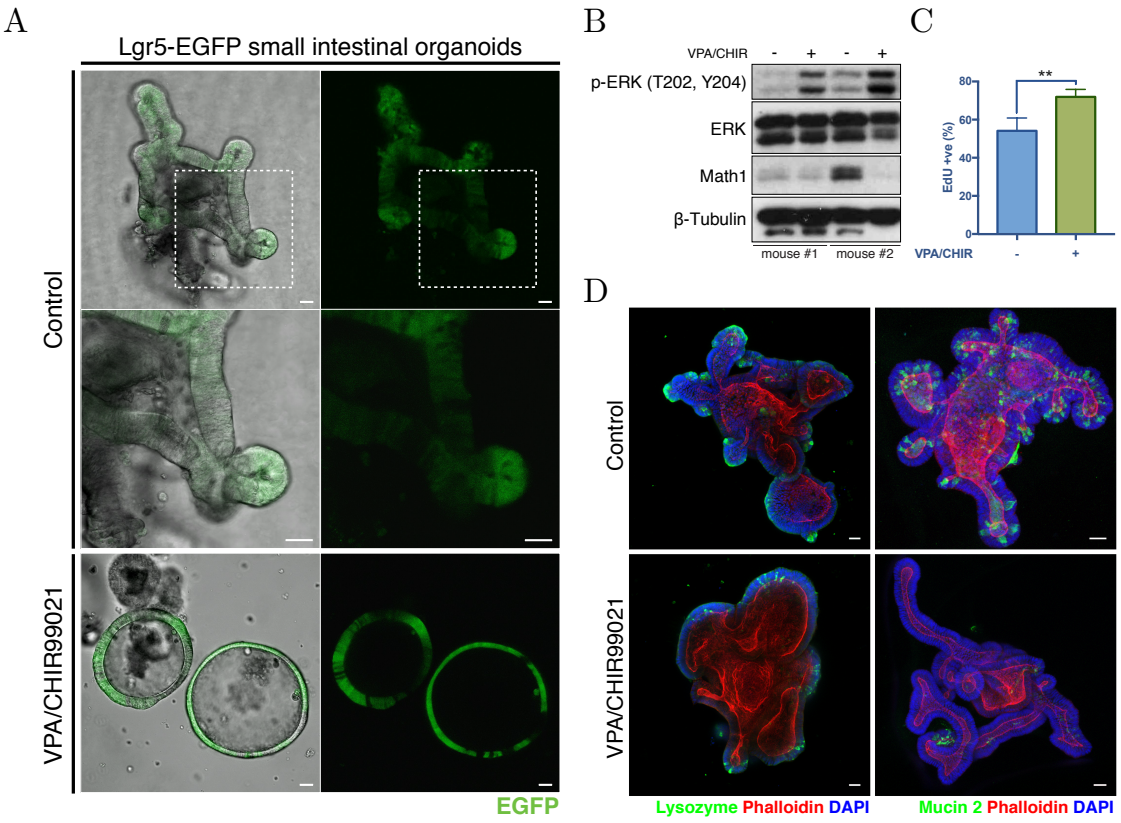


Figure 5.3: VPA/CHIR99021 treatment led to the expansion of the Lgr5$^+$ stem cell population. (A) Live imaging of untreated and VPA/CHIR99021-treated Lgr5-EGFP small intestinal organoids, showing EGFP (green) and DIC images. For the control group, zoomed-in views of the areas delineated by white squares are shown in the lower panel. Scale bars: 25 µm. (B) Western blot analysis of untreated small intestinal organoids and organoids treated with VPA/CHIR99021 for 5 days. β-Tubulin was used as the loading control. CHIR, CHIR99021. (C) EdU incorporation (4.5 hours) in untreated organoids (n = 4) and organoids treated with VPA/CHIR99021 (n = 4) for 4 days. **, $p < 0.01$; +ve, positive; Error bars represent SEM. (D) Representative IF co-staining of Lysozyme or Mucin 2 (green) and Phalloidin (red), with nuclei counterstained with DAPI (blue). The organoids were untreated (Control) or treated with VPA/CHIR99021 for 5 days. Scale bars: 25 µm.

explain the increased proliferation observed in VPA/CHIR99021-treated organoids as indicated by EdU incorporation ($p = 0.0090$, Figure 5.3C). The suppressed cell differentiation was further confirmed with IF staining, where fewer cells stained positive for the Paneth cell marker Lysozyme or the goblet cell marker Mucin 2 were observed in VPA/CHIR99021-treated organoids (Figure 5.3D).

Previous work in our lab has shown that a loss of ASPP2 will lead to an increase in the number of Paneth cells and their mislocalisation beyond the bottom of crypts

in the small intestine (S. Koch, unpublished data). This result was recapitulated in an independent cohort of ASPP2$^{\Delta exon3}$ mice, in which mislocalised Paneth cells at the crypt–villus junction was observed, as well as an increase in the protein level of Lysozyme (Figure 5.4A). Intriguingly, the loss of ASPP2 led to increased expression of EphB3 in small intestinal crypts (Figure 5.4B). This result suggested that the misregulation of Paneth cell positioning along the crypt–villus axis may be attributed to compromised ephrin-EphB interactions (Batlle et al. 2002; Holmberg et al. 2006).

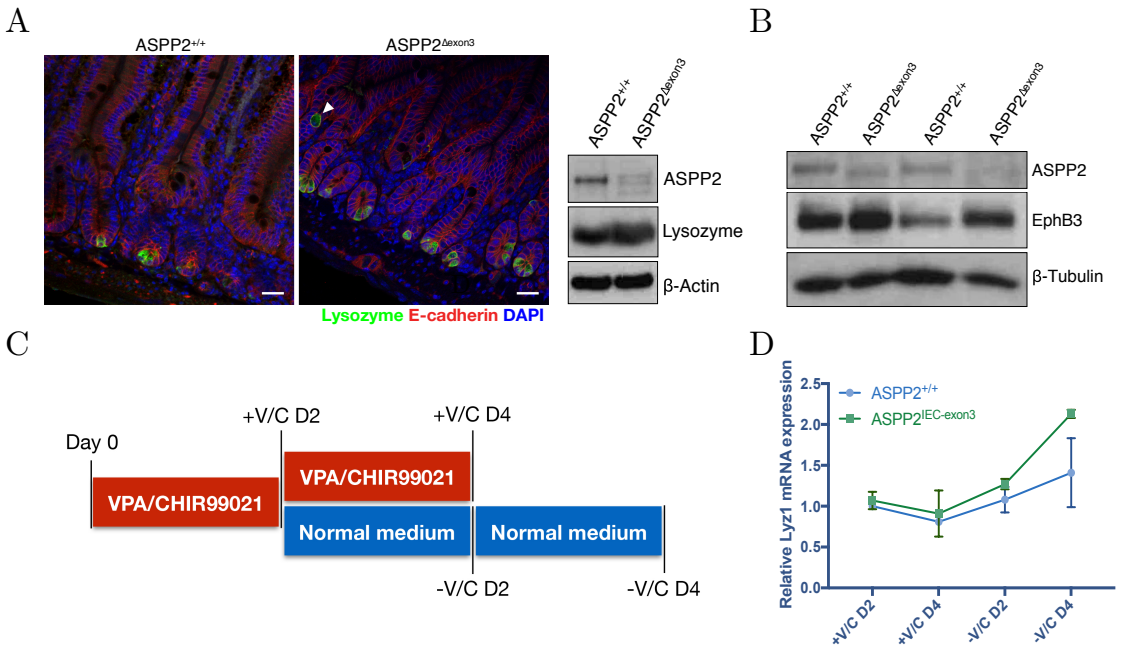


Figure 5.4: Loss of ASPP2 predisposed intestinal epithelial cells to the secretory lineage. (A) Left panel: representative IF co-staining of Lysozyme (green) and E-cadherin (red) on wild-type and ASPP2$^{\Delta exon3}$ duodenal sections, with nuclei counterstained with DAPI (blue). The white arrowhead points to a mislocalised Paneth cell. Scale bars: 25 µm. Right panel: western blot analysis of small intestinal crypts isolated from wild-type and ASPP2$^{\Delta exon3}$ mice, with β-Actin used as the loading control. (B) Western blot analysis of small intestinal crypts isolated from wild-type and ASPP2$^{\Delta exon3}$ mice, with β-Tubulin used as the loading control. (C) Schematic representation of the VPA/CHIR99021 treatment-based experimental system to study cell differentiation in organoids. (D) qPCR analysis of Lysozyme 1 expression in wild-type (n = 3) and ASPP2$^{\text{IEC-}\Delta exon3}$ (n = 2) small intestinal organoids following the VPA/CHIR99021 treatment. Error bars represent SEM, and the result is representative of two independent experiments. Lyz1, Lysozyme 1; V/C, VPA/CHIR99021; Dn, Day n.

In order to investigate whether the increased differentiation of Paneth cells in ASPP2-deficient animals can be recapitulated in organoids, a VPA/CHIR99021

treatment-based experimental system was established. Organoids were collected for analysis on Days 2 and 4 of VPA/CHIR99021 treatment, as well as Days 2 and 4 after the removal of the two compounds (Figure 5.4C). qPCR analysis was performed on organoids collected at each time point. As expected, the mRNA levels of Lysozyme 1 decreased over the course of VPA/CHIR99021 treatment (Figure 5.4D). When the treatment was terminated and the organoids were left to differentiate, a recovery of Lysozyme 1 expression was observed, to a greater extent in the ASPP2-deficient organoids than in their wild-type counterparts (Figure 5.4D). The same trend was also observed for the goblet cell marker Mucin 2 (data not shown). These results suggested that a loss of ASPP2 may intrinsically predispose IECs to the secretory cell lineage, independent of other niche factors. Moreover, this experiment is a proof-of-concept demonstration that the organoid system is amenable to *ex vivo* manipulations and is therefore suitable for mechanistic studies.

5.2.3 Organoids as an *ex vivo* system to study cell death

In addition to proliferation and differentiation, cell death is also tightly regulated in the intestinal epithelium to maintain tissue homeostasis (Delgado et al. 2015). It has long been accepted that apoptosis is essential for epithelial turnover, and the importance of necroptosis *in vivo* has also started to be appreciated in the last few years (Günther et al. 2013). Along that line, intestinal organoids have been proven to be a physiologically relevant model system for the study of cell death *in vitro* (Grabinger et al. 2014).

Previous work in our lab has shown that a loss of ASPP2 leads to increased apoptosis in the small intestinal epithelium (S. Koch, unpublished data). This observation was confirmed in an independent cohort of ASPP2$^{\Delta exon3}$ mice, as an increased number of epithelial cells positive for TUNEL staining were observed at the tips of villi in ASPP2-deficient animals (Figure 5.5A). Cells in organoids also undergo apoptosis, as indicated by the IF staining of cleaved Caspase-3 (Figure 5.5B). Considering that the whole-mount IF staining was a snapshot of the organoids at a relatively well-established stage, quantification of the cleaved Caspase-3 signal

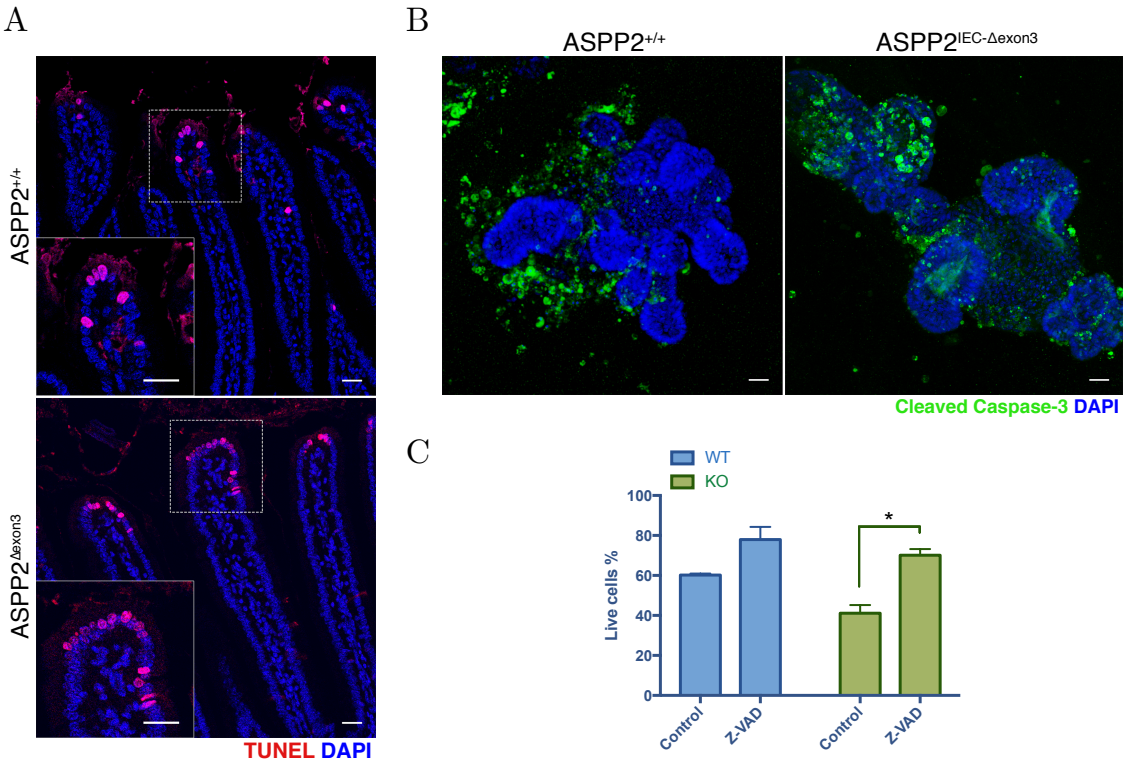


Figure 5.5: Loss of ASPP2 in duodenal epithelial cells led to increased apoptosis. (A) Representative TUNEL staining (red) on duodenal sections of wild-type and ASPP2$^{\Delta exon3}$ mice, with nuclei counterstained with DAPI (blue). Zoomed-in views of the areas delineated by white squares are shown in the lower left corners of each image. Scale bars: 25 µm. (B) Representative IF staining of cleaved Caspase-3 (green) on wild-type and ASPP2$^{IEC\text{-}\Delta exon3}$ small intestinal organoids, with nuclei counterstained with DAPI (blue). Scale bars: 25 µm. (C) Flow cytometry analysis of live cell populations in wild-type and ASPP2$^{IEC\text{-}\Delta exon3}$ small intestinal organoids (n = 2 per group). The organoids were cultured in normal medium (Control) or medium containing 10 µM of Z-VAD for 5 days. Error bars represent SEM, and the result is representative of two independent experiments. WT, ASPP2$^{+/+}$; KO, ASPP2$^{IEC\text{-}\Delta exon3}$; *, $p < 0.05$.

was confounded by the surrounding cell debris. An alternative route to determine the contribution of apoptotic cell death in organoids is to examine cell viability while blocking spontaneous apoptosis, which can be achieved by treating organoids with Z-VAD (Slee et al. 1996). Wild-type and ASPP2$^{IEC\text{-}\Delta exon3}$ organoids were dissociated into single crypts, cultured in ENR medium supplemented with Z-VAD, and analysed by flow cytometry 5 days later. As expected, the Z-VAD treatment resulted in an increased percentage of live cells within the organoids, to a greater extent in ASPP2$^{IEC\text{-}\Delta exon3}$ organoids than in their wild-type counterparts ($p = 0.0300$, Figure 5.5C). This result suggested that ASPP2-deficient organoids were

more dependent on apoptotic cell death.

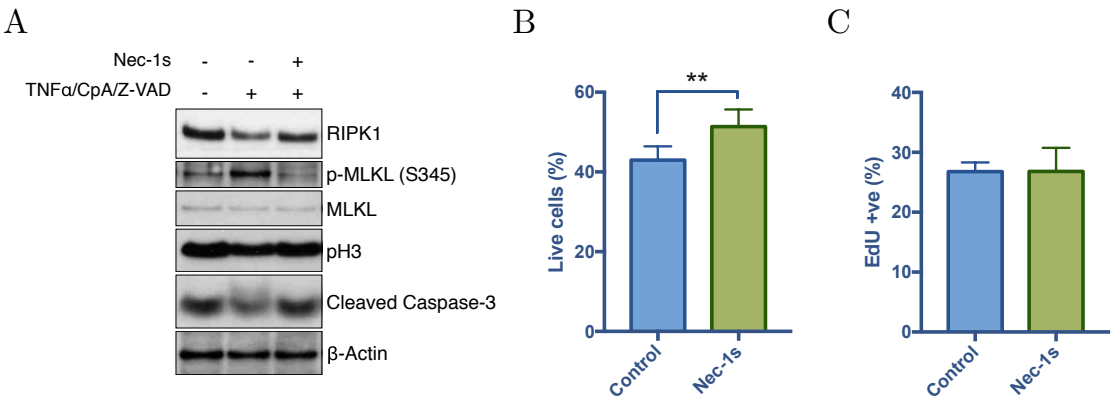


Figure 5.6: Necroptosis occurs in intestinal organoids. (A) Western blot analysis of small intestinal organoids treated with TNF-α, Compound A and Z-VAD, in the presence or absence of Nec-1s for 2 hours, with β-Actin used as the loading control. (B) Flow cytometry analysis of the percentage of live cells in untreated small intestinal organoids (Control) or organoids treated with Nec-1s for 5 days (n = 5 for each group). Error bars represent SEM. (C) EdU incorporation (4.5 hours) in untreated small intestinal organoids (Control) or organoids treated with Nec-1s for 5 days (n = 3 for each group). Error bars represent SEM. Nec-1s, Necrostatin-1s; CpA, compound A; Z-VAD, Z-VAD-fmk; +ve, positive; **, $p < 0.01$.

In order to investigate whether necroptotic cell death occurs in intestinal organoids, Necrostatin-1s (Nec-1s), a necroptosis inhibitor, was used to treat organoids in a similar manner to the treatment of organoids with Z-VAD. It has been reported that a cocktail of TNF-α, Compound A (CpA, a Smac mimetic), and Z-VAD is a potent inducer of necroptosis (Damgaard et al. 2013). Western blot analysis was performed on organoids treated with TNF-α/CpA/Z-VAD, in the presence or absence of Nec-1s. The induction of necroptosis was indicated by the phosphorylation of MLKL (mixed lineage kinase domain-like protein), an effector protein of the necroptosis pathway (Wang et al. 2014) (Figure 5.6A). On the other hand, the specificity of Nec-1s was confirmed by its ability to reverse the phosphorylation of MLKL at Ser345 (Figure 5.6A). Treatment of wild-type organoids with Nec-1s resulted in an expansion of the live cell population, suggesting that necroptosis does occur in intestinal organoids ($p = 0.0032$, Figure 5.6B). Of note, proliferation was not affected by Nec-1s treatment, as was indicated by the protein level of pH3 and EdU incorporation analysis (Figure 5.6, B and C). This

observation ruled out the possibility that the increased live cell population was due to decelerated organoid growth (which may also lead to delayed cell death) rather than the inhibition of necroptosis.

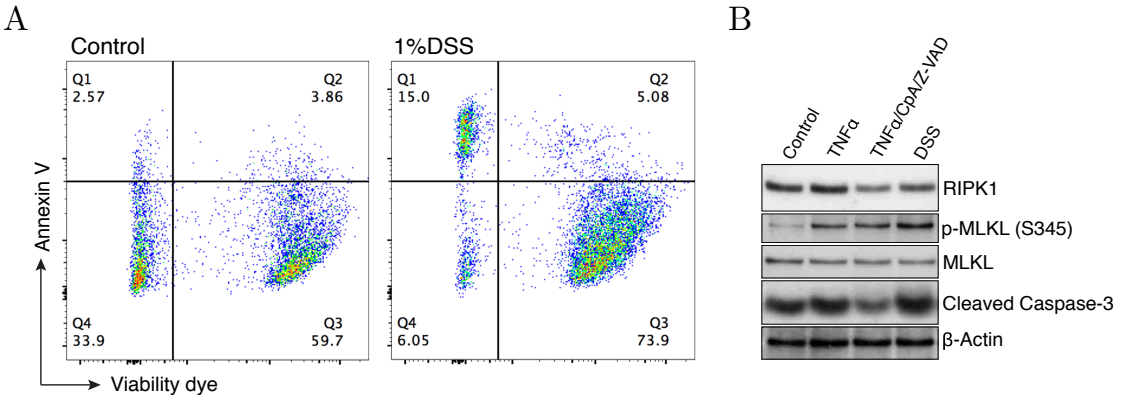


Figure 5.7: DSS induces apoptosis and necroptosis in organoids. (A) Representative results from Annexin V binding experiments performed on untreated small intestinal organoids (Control) and organoids treated with 1% DSS for 1 hour. Q1 to Q4 represent early apoptotic, late apoptotic, dead, and live cell populations, respectively. (B) Western blot analysis of small intestinal organoids treated with TNF-α, TNF-α/Compound A/Z-VAD, or 1% DSS for 2 hours. β-Actin was used as the loading control. CpA, compound A; Z-VAD, Z-VAD-fmk.

Given that both apoptosis and necroptosis can be monitored in organoid cultures, it can serve as a suitable system for the study of more sophisticated modes of cell death. As a proof-of-concept example and a supplement to the *in vivo* animal work, Annexin V binding analysis was performed on untreated small intestinal organoids and organoids cultured in the presence of 1% DSS. Not surprisingly, DSS was a potent inducer of cell death for the intestinal organoid, and apoptosis was induced by DSS treatment (Figure 5.7A). In order to investigate whether DSS can also induce necroptosis, western blot analysis was performed on organoids treated with DSS, in parallel with those treated with TNF-α (to induce apoptosis and necroptosis) or a cocktail of TNF-α/CpA/Z-VAD (to induce necroptosis) (Han et al. 2011; Damgaard et al. 2013). As expected, TNF-α induced the phosphorylation of MLKL and the cleavage of Caspase-3, whereas TNF-α/CpA/Z-VAD only led to MLKL phosphorylation (Figure 5.7B). Interestingly, DSS-treated organoids showed signatures of both apoptosis and necroptosis, and this result provided the first

experimental evidence that necroptotic cell death can be induced by DSS treatment (Figure 5.7B). Taken together, the organoid system has the potential to be used as an *ex vivo* platform to study cell death in the intestinal epithelium.

5.2.4 ASPP2-deficient colonic organoids showed increased expression of stem cell markers

The long-term maintenance and propagation of organoids is highly dependent on the self-renewal ability of ISCs. In parallel, the process of tissue regeneration *in vivo* is also driven by the stem cell population (Barker 2013).

As demonstrated in Chapter 3, a loss of ASPP2 in the intestinal epithelium would result in delayed recovery from DSS-induced colitis. In order to understand whether the phenotype is caused by intrinsic defects in the turnover of ISCs, qPCR analysis of a panel of stem cell markers was performed on colonic crypts and organoids derived from wild-type and ASPP2$^{\Delta exon3}$ animals. There was a significant increase in the mRNA levels of Lgr5 in ASPP2$^{\Delta exon3}$ crypts compared with their wild-type counterparts ($p = 0.0140$), which was recapitulated to a lesser extent in ASPP2$^{\Delta exon3}$ organoids (Figure 5.8). Consistently, the expression of Olfm4 (Olfactomedin-4), another marker for Lgr5-type stem cells (Muñoz et al. 2012), was also upregulated in ASPP2-deficient crypts ($p = 0.0422$) as well as organoids (Figure 5.8). Interestingly, the expression of Olfm4 has been shown to be directly dependent on Notch signalling (VanDussen et al. 2012). Therefore, the upregulation of Olfm4 agrees with the observation that the Notch pathway is activated in ASPP2-deficient colonic epithelium (S. Koch, unpublished data). Along the same line, a significant increase in the expression of Bmi1 was observed in ASPP2-deficient crypts ($p = 0.0162$, Figure 5.8). Notably, the expression of Bmi1 is also regulated by Notch signalling and represents a stem cell population distinct from Lgr5^{+} ISCs (López-Arribillaga et al. 2015; K. Yan et al. 2012). Collectively, these results suggested that a loss of ASPP2 would result in the upregulated expression of various stem cell markers.

To some extent, the observation outlined above contradicted with the delayed recovery of ASPP2$^{\text{IEC-}\Delta exon3}$ mice observed in the DSS model. In order to investigate whether ASPP2-deficient stem cells were indeed more capable of giving rise to

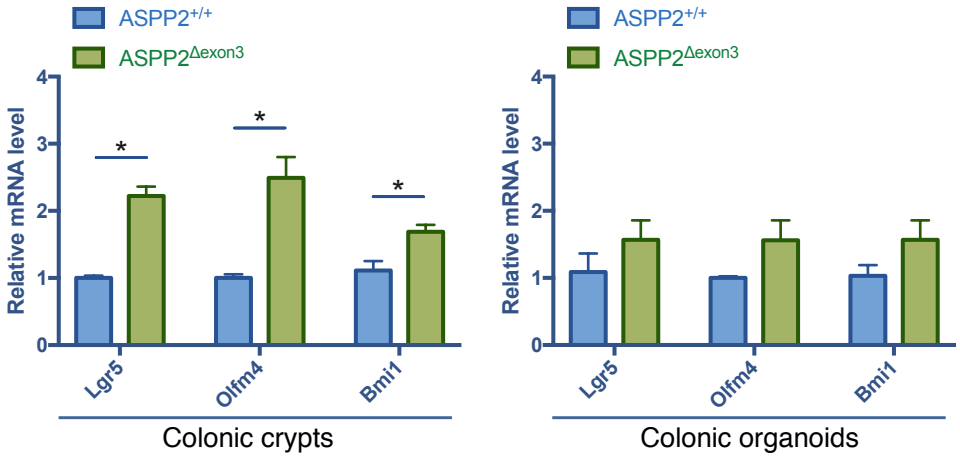


Figure 5.8: Stem cell markers were upregulated in ASPP2-deficient colonic crypts and organoids. qPCR analysis of selected stem cell markers was performed on colonic epithelial cells (left panel, n $\geq$ 2 for each group) and colonic organoids (right panel, n $\geq$ 3 for each group). Error bars represent SEM; *, p $<$ 0.05.

differentiated cells, an experimental model in a similar idea to the lineage tracing strategy used *in vivo* was established. Given that Villin is expressed in all IECs, Villin-CreER mediated recombination would occur in ISCs (El Marjou et al. 2004). Taking advantage of the mosaic pattern of EYFP positivity in ASPP2$^{\text{IEC-}\Delta\text{exon3}}$ organoids, the percentage of EYFP-positive cells within the organoids can be monitored in real time.

In contrast to small intestinal organoids, ASPP2$^{\text{IEC-}\Delta\text{exon3}}$ colonic organoids showed a decrease in the percentage of EYFP-positive cells during the first 5 days of culture, with a significant difference between Day 1 and Day 5 (p = 0.0054, Figure 5.9A). This result suggested that ASPP2$^{\Delta\text{exon3}}$ cells were overtaken by the progeny of wild-type stem cells. Importantly, the decrease in the percentage of EYFP-positive cells was not due to a reduction in their proliferation rate, which was confirmed with EdU incorporation experiments. Similar to small intestinal organoids, ASPP2$^{\Delta\text{exon3}}$ colonic organoids showed a significantly higher rate of EdU incorporation than their wild-type counterparts (p = 0.0381, Figure 5.9B). Taken together, these results suggested that although the loss of ASPP2 would lead to an increase in the expression of ISC markers, the upregulation was not correlated with an increased regenerative potential of ASPP2-deficient ISCs.

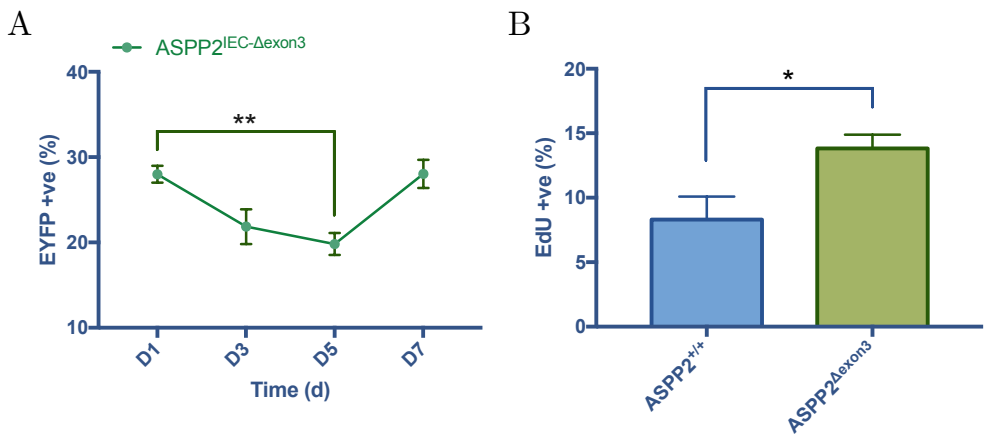


Figure 5.9: ASPP2-deficient epithelial cells were overtaken by wild-type cells in colonic organoids. (A) The percentage of EYFP-positive cells within newly established colonic organoids. Organoids derived from ASPP2$^{\text{IEC-}\Delta\text{exon3}}$ mice (n = 2) were analysed on Days 1, 3, 5, and 7 of culture by flow cytometry. Error bars represent SEM. D, day; **, $p < 0.01$. (B) EdU incorporation (4.5 hours) in wild-type (n = 4) and ASPP2$^{\Delta\text{exon3}}$ (n = 4) colonic organoids. Error bars represent SEM, and the result is representative of three independent experiments. *, $p < 0.05$; +ve, positive.

5.2.5 Development of a colonic organoid-based tissue regeneration model

Given that the organoid is able to recapitulate *in vivo* observations and is robust enough to be manipulated *in vitro*, it constitutes a potentially useful system to supplement animal-based studies. On the one hand, the organoid retains physiologically relevant properties reminiscent of its tissue of origin, offering insight into *in vivo* scenarios. On the other hand, the simplicity of the system allows the incorporation of environmental factors such as cytotoxic agents and cytokines, and therefore the responses of epithelial cells to such external stimuli can be examined in a better controlled manner. With that in mind, a colonic organoid-based tissue regeneration model was established.

The implementation of the model is composed of two phases: induction and recovery. Induction of cell damage is preferably performed in a relatively large-scale (24- or 48-well) format, so that after the treatment is finished and the organoids are transferred to a 96-well plate, a density of ∼15 organoids per condition can be achieved. The transfer step is essential for the removal of the leftover cell death inducers, thereby minimising any long-term adverse effects that they may have on

cell viability. As for cell density, it is optimised for the sensitivity range of the MTT viability assay. Resazurin, an oxidation reduction-based indicator of cell viability (O'Brien et al. 2000), was used to determine the viability of organoids prior to the treatment. Finally, qPCR or MTT assays were performed on the organoids to test their cellular responses and viability (Figure 5.10A).

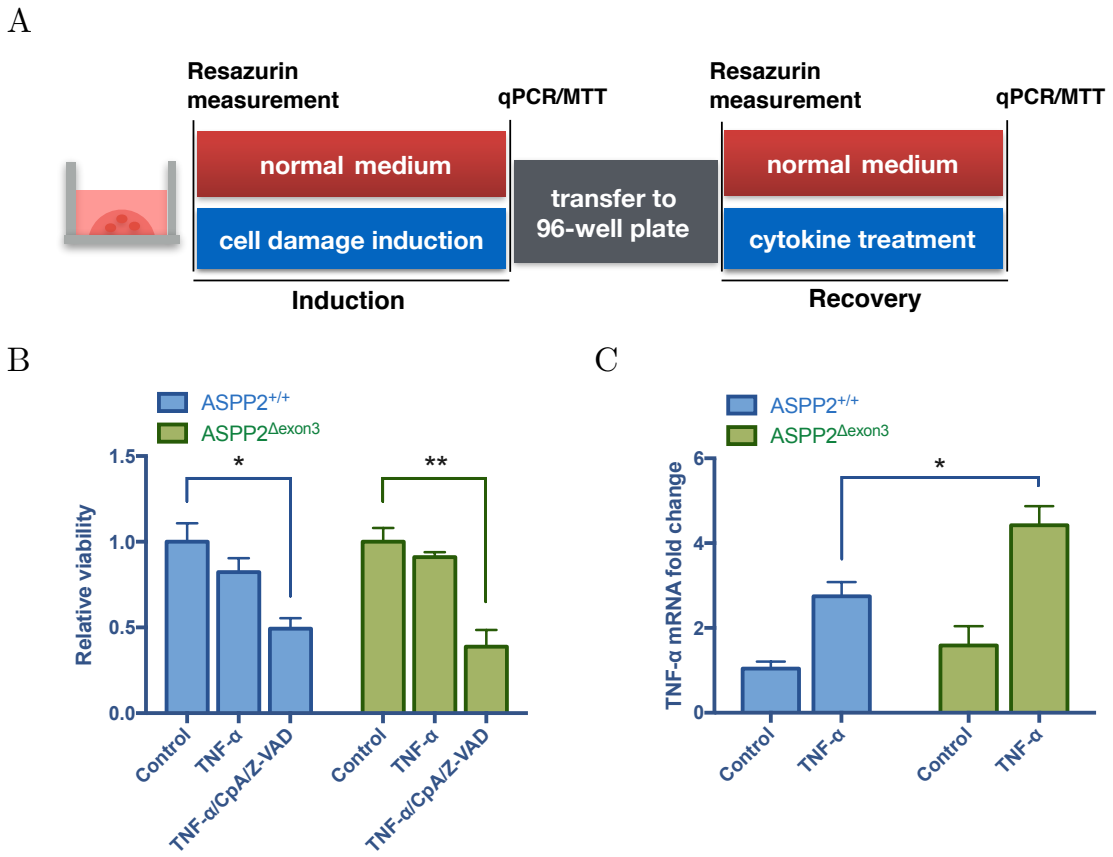


Figure 5.10: Establishment of a colonic organoid-based tissue regeneration model. (A) Schematic representation of the proposed colonic organoid-based tissue regeneration model. Organoids are subjected to the induction of cell damage, transferred to a 96-well plate, and left to recover in the presence or absence of external stimuli such as cytokine treatment. qPCR and MTT assay are used as the readout of cellular responses and cell viability, respectively. (B) MTT assay performed on wild-type (n = 3) and ASPP2$^{\Delta exon3}$ (n = 4) colonic organoids. The organoids were cultured in normal medium (Control), medium containing 20 ng/ml TNF-α for 48 hours, or medium containing 40 ng/ml TNF-α, 2 µM Compound A, and 10 µM Z-VAD for 2 hours. CpA, Compound A; Z-VAD, Z-VAD-fmk. (C) qPCR analysis of TNF-α expression in wild-type and ASPP2$^{IEC\text{-}\Delta exon3}$ colonic organoids (n = 4 per group). The organoids were cultured in normal medium (Control) or treated with 20 ng/ml TNF-α for 2 hours. Error bars represent SEM, and the results are representative of at least two independent experiments. *, $p < 0.05$; **, $p < 0.01$.

In order to test the feasibility and sensitivity of the proposed system, wild-type

and ASPP2$^{\Delta exon3}$ colonic organoids were subjected to TNF-α-induced apoptosis or TNF-α/CpA/Z-VAD-induced necroptosis followed by MTT viability assays. As expected, both treatments led to a reduction in cell viability ($p = 0.0151$ and 0.0029 for wild-type and ASPP2$^{\Delta exon3}$ organoids in the case of necroptosis, Figure 5.10B). In addition, organoids of both genotypes showed higher sensitivity to TNF-α/CpA/Z-VAD treatment than to TNF-α treatment alone (Figure 5.10B). Interestingly, qPCR analysis revealed that when treated with TNF-α, IECs can also act as a source of pro- and anti-inflammatory cytokines, such as TGF-β and TNF-α. In particular, ASPP2-deficient organoids showed a higher induction of TNF-α transcription than their wild-type counterparts ($p = 0.0240$, Figure 5.10C). These results suggested that the established model is suitable for the testing of organoid viability in response to various treatments, and has the potential to be applied to the study of epithelial–immune cell interactions.

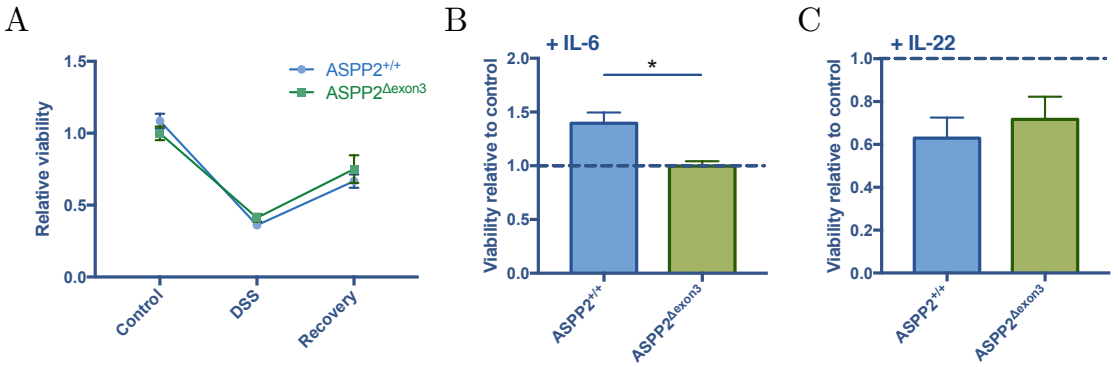


Figure 5.11: DSS-induced cell death and recovery in colonic organoids. (A) MTT assay performed on wild-type and ASPP2$^{\Delta exon3}$ colonic organoids (n = 3 per group). The organoids were cultured in normal medium (Control), treated with 0.1% DSS for 16 hours (DSS), or treated with DSS and left to recover for 4 days (Recovery). (B) MTT assay performed on wild-type (n = 5) and ASPP2$^{\Delta exon3}$ (n = 3) colonic organoids. The organoids were treated with 0.2% DSS for 2 hours, transferred to a 96-well plate, and cultured for 3 days in the absence (Control) or presence of 50 ng/ml IL-6. The dashed line represents the viability of organoids recovered in the absence of IL-6. (C) MTT assay performed on wild-type (n = 4) and ASPP2$^{\Delta exon3}$ (n = 2) colonic organoids. The organoids were treated with 0.2% DSS for 2 hours, transferred to a 96-well plate, and cultured for 5 days in the absence (Control) or presence of 5 ng/ml IL-22. The dashed line represents the viability of organoids recovered in the absence of IL-22. Error bars represent SEM, and the results are representative of at least two independent experiments. *, $p < 0.05$.

The experimental system was then applied to the scenario of DSS treatment. MTT assays were performed on untreated wild-type and ASPP2-deficient organoids, organoids incubated with 0.1% DSS for 16 hours, and organoids recovered for 4 days after the DSS treatment. No difference was observed in the relative viability between wild-type and ASPP2$^{\Delta exon3}$ organoids, at either the induction or recovery phase (Figure 5.11A). This result suggested that a loss of ASPP2 did not intrinsically affect the sensitivity of colonic epithelial cells to DSS-induced cell death or the process of epithelial regeneration.

When organoids were treated with DSS and then allowed to recover in the presence of IL-6, wild-type organoids showed significantly higher viability compared with their ASPP2-deficient counterparts ($p = 0.0271$, Figure 5.11B). Of note, IL-6 is one of the proinflammatory cytokines that was differentially expressed by LPMCs of wild-type and ASPP2$^{\text{IEC-}\Delta exon3}$ animals after DSS treatment (Figure 3.10). The observation may therefore partially explain the delayed recovery of ASPP2-deficient animals from DSS-induced acute colitis. Along the same line, the effects of IL-22 on the viability of organoids following DSS treatment was examined. Surprisingly, both wild-type and ASPP2$^{\Delta exon3}$ organoids incubated with IL-22 showed a ∼40% reduction in viability compared to organoids recovered in the absence of IL-22 (Figure 5.11C). This was unexpected since IL-22 has been shown to promote wound healing and regeneration of the intestinal epithelium (Pickert et al. 2009; Lindemans et al. 2015).

In order to further characterise the effects of IL-22 on organoid growth, MTT assays were performed on wild-type and ASPP2$^{\Delta exon3}$ organoids. In the absence of IL-22, wild-type and ASPP2-deficient organoids showed comparable viability after 48 hours in culture (Figure 5.12A). When the organoids were incubated in culture medium supplemented with IL-22, ASPP2$^{\Delta exon3}$ organoids showed significantly higher viability compared with their wild-type counterparts ($p = 0.0100$, Figure 5.12A). This result partially confirmed the pro-proliferative effect of IL-22, to which ASPP2-deficient organoids might be more sensitive than wild-type organoids.

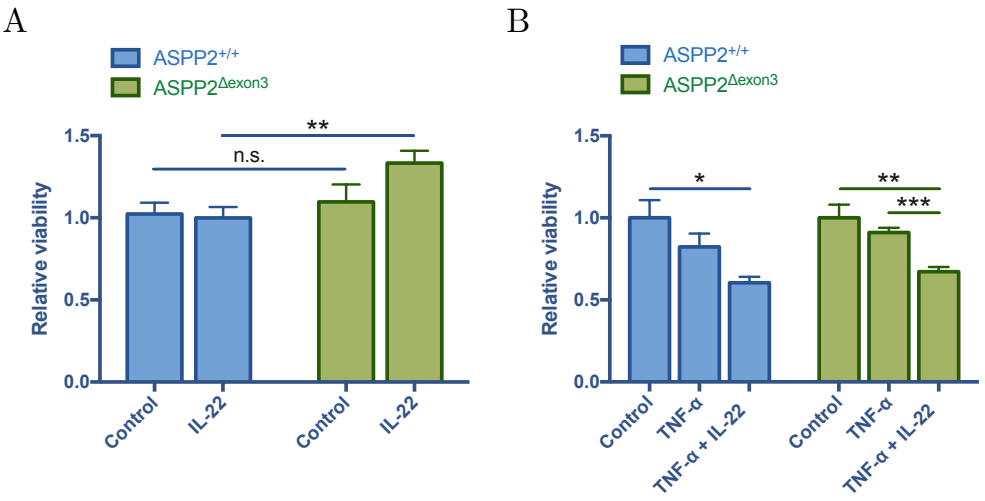


Figure 5.12: Effects of IL-22 treatment on organoid growth. (A) MTT assay performed on wild-type (n = 5) and ASPP2$^{\Delta exon3}$ (n = 5) colonic organoids. The organoids were cultured in normal medium (Control) or medium containing 5 ng/ml IL-22 for 48 hours. (B) MTT assay performed on wild-type (n = 3) and ASPP2$^{\Delta exon3}$ (n = 4) colonic organoids. The organoids were cultured in normal medium (Control), medium containing 20 ng/ml TNF-α, or medium containing 20 ng/ml TNF-α and 5 ng/ml IL-22 for 48 hours. Error bars represent SEM, and the results are representative of at least two independent experiments. *, $p < 0.05$; **, $p < 0.01$; ***, $p < 0.001$; n.s., not significant.

Considering that incubating organoids with IL-22 would lead to a further reduction of cell viability following DSS treatment, it was hypothesised that IL-22 sensitised organoids to induced-cell death. To test this hypothesis, wild-type and ASPP2$^{\Delta exon3}$ colonic organoids were treated with TNF-α with or without IL-22. Although TNF-α alone was not a very potent inducer of cell death in organoids, a synergistic effect was observed in the presence of IL-22 ($p = 0.0110$ and 0.0087 for wild-type and ASPP2$^{\Delta exon3}$ organoids, respectively; Figure 5.12B). Interestingly, the synergistic effect was only significant for ASPP2-deficient organoids, again suggesting that a loss of ASPP2 may sensitise organoids to IL-22 treatment ($p = 0.0009$, Figure 5.12B). Taken together, the results described in this section suggested that epithelial cell non-autonomous factors such as exogenous cytokines may play a role in the regulation of epithelial regeneration.

5.2.6 Colorectal tumour organoids as a supplement to *in vivo* tumour characterisation

In a similar manner to the application of organoids in the study of normal intestinal physiology, the system has also been applied to the modelling of CRC (Young et al. 2016). Derived from primary tissue, colorectal tumour organoids retain physiologically relevant characteristics such as apical/basal polarity, ability to differentiate, and anoikis (Xue et al. 2013). Given the advantages of organoids over cancer-derived cell lines, the system has the potential to supplement *in vivo* tumour characterisation. More importantly, it offers a relatively simple system to study cancer biology from a tumour cell autonomous perspective.

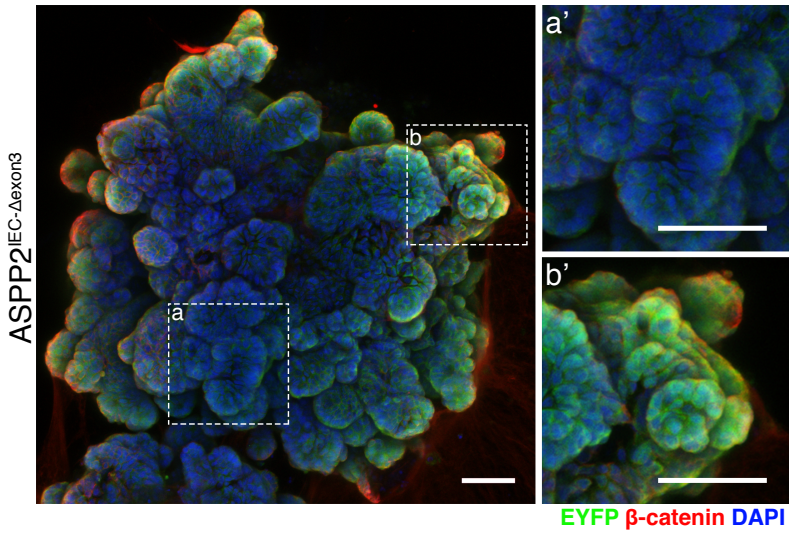


Figure 5.13: Colorectal tumour organoids retained physiologically relevant morphology. Representative IF co-staining of EYFP (Green) and β-catenin (red) on a colorectal tumour organoid, with nuclei counterstained with DAPI (blue). The morphology of the organoid is reminiscent of the crypt-like structure of adenomas. Inserts (a) and (b) represent crypts negative and positive for EYFP, respectively, with (a') and (b') presenting the images at higher magnification. Scale bars: 50 µm.

Tumour organoids were generated from AOM/DSS-induced colonic adenomas of both wild-type and ASPP2$^{\text{IEC-}\Delta\text{exon3}}$ animals (Figure 5.13). In contrast to the culture conditions for normal colonic organoids where the growth factors EGF, Noggin, R-spondin and Wnt3a are all indispensable, basal culture medium supplemented with EGF alone is sufficient for the maintenance of colorectal tumour organoids (Sato, Stange, et al. 2011). Despite intra-genotype variability, a certain percentage

of tumours formed in wild-type and ASPP2$^{\text{IEC-}\Delta\text{exon3}}$ mice can be isolated and developed into organoids. Morphologically, the organoids can be classified into two subtypes, the crypt-like group and the cyst-like group, with the former easier to propagate. The differences in organoid morphology and organoid-forming efficiency echoed the heterogeneity observed in the tumours they originated from.

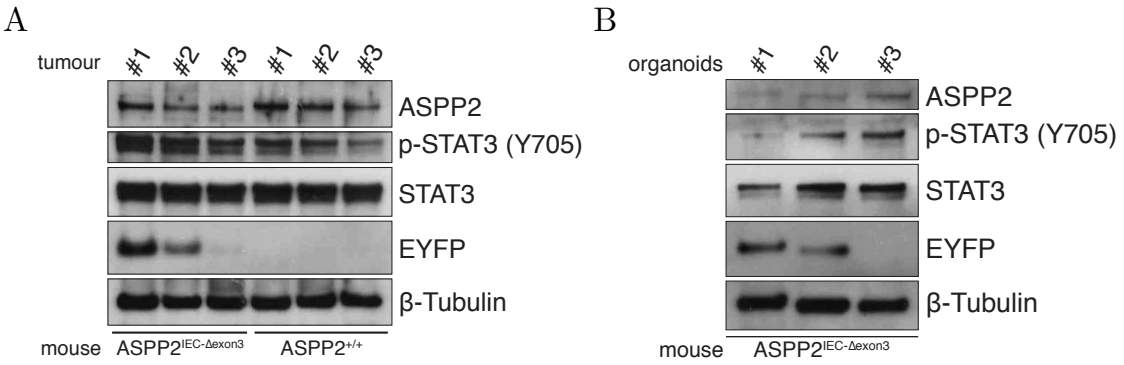


Figure 5.14: Characterisation of STAT3 phosphorylation in colorectal tumours and tumour organoids. (A) Western blot analysis of colorectal tumours isolated from one ASPP2$^{\text{IEC-}\Delta\text{exon3}}$ mouse and one wild-type mouse, with β-Tubulin used as the loading control. The blots were obtained from the same batch of experiment as shown in Figures 4.7B and 4.8B, and therefore have shared ASPP2, EYFP, and β-Tubulin. Similarly, tumour #3 in the ASPP2$^{\text{IEC-}\Delta\text{exon3}}$ mouse represents a tumour derived from a wild-type crypt. (B) Western blot analysis of colorectal tumour organoids derived from one ASPP2$^{\text{IEC-}\Delta\text{exon3}}$ mouse, with β-Tubulin used as the loading control. Organoids #1 and #2 were derived from ASPP2-deficient (EYFP-positive) tumours whereas organoids #3 were derived from a wild-type (EYFP-negative) tumour.

As an epithelium-only system, the tumour organoid is a suitable platform to study epithelial cell intrinsic and extrinsic pathways underlying tumour development. One of the key factors that could be implicated in colorectal tumourigenesis by both routes is STAT3 signalling. On the one hand, STAT3 is frequently activated in malignant cells through genetic or epigenetic alterations, exerting pro-proliferative and -survival effects (Yu et al. 2009). On the other hand, STAT3 can also be activated by external signals such as IL-6 secreted by myeloid cells present in the tumour microenvironment (Grivennikov et al. 2009). In order to examine the activation status of STAT3 in AOM/DSS-induced colorectal tumours, western blot analysis was performed on tumour samples isolated from wild-type and ASPP2$^{\text{IEC-}\Delta\text{exon3}}$ mice. Intriguingly, tumours developed in ASPP2-deficient mice showed a higher level of

STAT3 phosphorylation, particularly the ones with ASPP2 deficiency (Figure 5.14A, tumour #1 and 2 compared with tumour #3 of the ASPP2$^{\text{IEC-}\Delta\text{exon3}}$ mouse and all the other tumours developed in wild-type animals). However, the upregulation of STAT3 activation was not recapitulated by colorectal tumour organoids, in which the level of STAT3 phosphorylation positively correlated with the level of ASPP2 expression (Figure 5.14B, organoids #1 and 2 versus organoid #3). Notably, the depletion of ASPP2 was more clear in tumour organoids than in tumour samples directly collected from mice, further supporting the notion that the organoid is a relatively clean system to study intrinsic properties of tumour cells (Figure 5.14). Taken together, the discrepancy between the tumour samples and the organoids suggested that a loss of ASPP2 in the epithelium alone was not sufficient to activate STAT3, and that epithelial–stromal cell crosstalk may be involved. A more detailed examination of the underlying signalling networks, including but not limited to the NF-κB pathway, remains to be carried out.

5.3 Summary and Brief Discussion

In this chapter, intestinal organoids were derived from wild-type and ASPP2-deficient mice to complement the animal experiments outlined in previous chapters. As an *ex vivo* culture system, the organoid has the potential to bridge the gap between conventional cell culture and mouse models. The prerequisite is that the organoid can meet the following criteria: physiological relevance and amenability to manipulation. To that end, small intestinal organoids were cultured and characterised as a proof of concept.

One of the key phenotypes observed in the small intestine of ASPP2-deficient mice is the hyperproliferation of crypt cells (S. Koch, unpublished data). As demonstrated via time-lapse imaging and EdU incorporation analysis, the phenotype was recapitulated in ASPP2-deficient small intestinal organoids. It is interesting to note that the percentage of EYFP-positive cells in ASPP2$^{\text{IEC-}\Delta\text{exon3}}$ organoids can be used as an indicator of cell proliferation, as it directly reflects the competition

between wild-type and ASPP2-deficient epithelial cells. This is one example of taking advantage of the heterogeneity of organoids to understand their complexity.

Next, small intestinal organoids were applied to the study of Paneth cell differentiation. Characterisation of the ASPP2$^{\Delta exon3}$ mouse model revealed that ASPP2-deficient small intestine showed an increased presence of Paneth cells (S. Koch, unpublished data). Since Paneth cells only constitute a small population within the intestinal organoid, in order to model cell differentiation, intra-organoid heterogeneity first needs to be minimised. This was achieved by treating the organoids with VPA and CHIR99021, which has been proven to expand the Lgr5^{+} stem cell population. As expected, after the organoids were treated with VPA/CHIR99021 and left to differentiate, higher expression levels of the Paneth cell marker Lysozyme 1 was observed in ASPP2-deficient organoids than in their wild-type counterparts. The key message conveyed by this experiment is that the predisposition of ASPP2-deficient progenitor cells to differentiate into the Paneth cell lineage is intrinsic to the epithelium and independent of other niche factors.

The feasibility of organoids as a tissue surrogate was then interrogated in the context of cell death analysis. Reassuringly, the organoid is reasonably sensitive to the blockage of spontaneous cell death as well as the induction of apoptosis and necroptosis. It was also demonstrated, for the first time, that DSS will induce apoptotic and necroptotic epithelial cell death. Taken together, the data suggested that organoids retain physiologically relevant biological properties and are robust enough for *ex vivo* manipulations. As a result, we decided to apply the techniques developed and optimised with small intestinal organoids, including but not limited to qPCR, EdU incorporation, flow cytometry analysis, and MTT assay, to the characterisation of colonic organoids.

To begin with, the expression of stem cell markers was examined in colonic organoids. Given that ASPP2$^{\text{IEC-}\Delta exon3}$ mice showed delayed recovery from DSS-induced colitis, it was hypothesised that the homeostatic control of the stem cell pool could be affected by the loss of ASPP2. Unexpectedly, both ASPP2-deficient colonic crypts and organoids showed higher expression of Lgr5, Olfm4

and Bmi1, suggesting that a loss of ASPP2 may result in an expansion of colonic stem cells. Intriguingly, despite the fact that ASPP2-deficient colonic organoids showed a higher proliferation rate than their wild-type counterparts, the percentage of EYFP-positive cells dropped within newly-derived ASPP2$^{\text{IEC-}\Delta\text{exon3}}$ organoids. This result suggested that the upregulated expression of stem cell markers did not necessarily correlate with the potential of stem cells to repopulate the epithelium upon tissue damage. Admittedly, the 'lineage tracing'-like experiment would be more accurate if ASPP2 was specifically depleted in stem cells. It is also worth noting that one of the caveats of using organoids to study stem cell biology is that organoid culture conditions are designed for the long-term propagation of stem cells, so the dynamics might have been distorted. As a result, comparisons between different genotypes are more biologically relevant than extrapolation of *ex vivo* observations back to *in vivo* scenarios.

The development of the organoid-based tissue regeneration model was an attempt to link the organoid technique with animal-based studies. The aim was to simulate a simplistic model of tissue regeneration, where the contribution of epithelial cell autonomous and non-autonomous factors can be readily distinguished. Relying on qPCR and the MTT assay, the established model exhibited acceptable sensitivity. Notably, although only a limited number of cytokines were tested on the system, alone or in combination, the differential response of wild-type and ASPP2-deficient organoids has already shed some light on the *in vivo* observations. It was clear that epithelial cells were in constant interaction with immune cells and their secreted factors present in the microenvironment. The observation that ASPP2-deficient organoids were less responsive to the pro-survival effect exerted by IL-6 might provide a mechanistic explanation for their delayed recovery from DSS-induced colitis *in vivo*. Moreover, the synergistic effect of TNF-α and IL-22 in the induction of cell death highlighted the complexity underlying the epithelial–stromal cell crosstalk. Future experiments would benefit from information obtained from animal studies, such as the involvement of specific types of immune cells and/or cytokines.

6

Discussion and Future Perspectives

In this study, the role of ASPP2 in intestinal homeostasis and tumourigenesis was investigated. It began with animal work, followed by characterisation of the organoid system, and finished with the establishment of an organoid-based tissue regeneration model. Taking advantage of the tissue specificity of ASPP2 depletion in the ASPP2$^{\Delta exon3}$ mouse model, and the epithelium-only composition of intestinal organoids, this study reveals, for the first time, that ASPP2 can be implicated in the pathological conditions of the intestine in an epithelial cell non-autonomous manner. In this chapter, the implications and limitations of the project, as well as suggestions for future experiments, will be outlined and discussed.

6.1 ASPP2: A Putative Role in the Restoration of Intestinal Barrier Function

Originating from the observations that ASPP2 is localised at intestinal tight junctions and that a loss of ASPP2 will result in compromised epithelial cell polarity, the primary aim of this study was to understand whether ASPP2 is implicated in the regulation of intestinal barrier integrity. To that end, an intestinal-specific ASPP2-deficient mouse model was generated and subjected to DSS-induced acute colitis. The observation that ASPP2$^{\text{IEC-}\Delta exon3}$ mice do not exhibit increased susceptibility to DSS-induced colitis but rather display delayed recovery from the

treatment suggests that ASPP2 may be more involved in the restoration, rather than maintenance, of the intestinal barrier function. To better interpret the data, the following aspects should be taken into consideration.

First, when using DSS-induced colitis to model the breakdown and restitution of intestinal barrier function, the timing of the onset of tissue damage and tissue regeneration deserves particular attention. On the one hand, during the time course of the DSS treatment, especially at relatively late stages, tissue damage and tissue repair occur simultaneously. That is why special emphasis has been put on the fact that ASPP2-deficient mice are not more susceptible to DSS-induced intestinal barrier dysfunction in the first place (Figure 3.2). As a result, the delayed recovery of body weight and intestinal permeability observed in ASPP2$^{\text{IEC-}\Delta\text{exon3}}$ mice can be mainly attributed to defects in the regulation of tissue regeneration. On the other hand, it is important to note the temporal differences in the pathological manifestations induced by DSS treatment (Y. Yan et al. 2009). For example, during the recovery phase of DSS-induced colitis, ASPP2$^{\text{IEC-}\Delta\text{exon3}}$ mice showed higher histological scores on Day 4, but the difference in intestinal permeability was more significant on Day 6 (Figures 3.4 and 3.5). This discrepancy could be due to limitations of the sensitivity of the assays performed, but may also shed light on the dynamic involvement of ASPP2 in a particular process, such as the restitution of epithelial continuity.

Secondly, in the intestinal mucosa, intestinal epithelial cells are in constant dialogue with the underlying mesenchyme and immune system (Powell et al. 2011). Of note, ASPP2 has been reported to be expressed by peripheral leukocytes (Yang, Hori, Takahashi, et al. 1999). This notion justifies our approach to using an intestinal epithelial-specific ASPP2-deficient mouse model to profile the cytokines expressed by lamina propria immune cells. Intriguingly, despite the fact that ASPP2$^{\text{IEC-}\Delta\text{exon3}}$ mice did not show compromise of pathways intrinsic to epithelial cells, such as Hippo, Wnt, and Notch signalling (Figure 3.9 and data not shown), the immune cell compartment did express lower levels of proinflammatory cytokines including IL-1β, IL-6, and TNF-α (Figure 3.10). Given that defective epithelial barrier function and dysregulated immune activity would operate in a self-amplifying cycle, an important

question that needs to be answered is whether the observed alterations in cytokine expression are the cause or consequence of the delayed restitution of intestinal integrity in ASPP2$^{\text{IEC-}\Delta\text{exon3}}$ mice. Moreover, considering that inflammation can both promote and retard the progress of tissue repair, it remains to be elucidated whether the proinflammatory signalling conveyed by the cytokines listed above is indeed playing a proreparatory role in wild-type animals (Karin et al. 2016).

In order to get a more complete picture of the reciprocal regulation between ASPP2-deficient epithelial cells and the mucosal immune system, more systematic profiling of the types of immune cells present in the inflammatory microenvironment and their activation status needs to be carried out. To that end, flow cytometry analysis of infiltrated T cells and myeloid cells will be performed, as well as ELISAs (enzyme-linked immunosorbent assays) on serum samples, as both have been widely used to characterise the cytokine landscape of DSS-treated animals (J. J. Kim et al. 2012). The focus of the profiling will be put on the regeneration-inducing cytokines and their producers listed in Table 1.2. In addition, it has been demonstrated that multiplex cytokine profiling can be especially powerful in the quantitative analysis of the disease activity and severity induced by DSS (Alex et al. 2009). With the information obtained from these experiments, educated guesses can be made and neutralisation of a particular signalling pathway may be performed to yield more mechanistic insight into the regulation of tissue regeneration, as has been demonstrated in the case of the IL-33/ST2 signalling (Sedhom et al. 2013).

Thirdly, one of the key observations emerging from the DSS-induced colitis model was the dysregulation of the IL-6/STAT3 signalling axis in ASPP2$^{\text{IEC-}\Delta\text{exon3}}$ mice (Figure 6.1). Western blot analysis revealed that wild-type colonic crypts showed a higher level of STAT3 phosphorylation on the tyrosine 705 residue (Figure 3.6). Consistently, the expression of IL-6 by LPMCs was also significantly higher in wild-type animals (Figure 3.10). This result supported the hypothesis that epithelial cell non-autonomous factors can be implicated in the restoration of intestinal homeostasis in the context of ASPP2 deficiency. Considering that other stromal cells such as fibroblasts and endothelial cells may also be involved in the process (Owens

et al. 2013), it is worthwhile to perform further characterisation along that line. On the other hand, from the perspective of epithelial cell autonomous activation of STAT3, it is worth noting that ASPP2 is a binding partner of the protein phosphatase PP1 (Helps et al. 1995), for which STAT3 has been shown to be a substrate (Zgheib et al. 2012). Interestingly, the downregulation of STAT3 phosphorylation was recapitulated in a mouse model where ASPP2 harbours a mutation in the ASPP2-PP1 binding site, suggesting that the ASPP2/PP1 interaction is not involved in the regulation of STAT3 activation, at least for STAT3 Y705 in the context of DSS-induced colitis (data not shown). However, given that a number of ASPP2 binding partners such as Par-3 and YAP have been shown to be regulated by phosphorylation reactions (Nakayama et al. 2008; Christophe Royer et al. 2014), the potential role of ASPP2/PP1 as a hub for dephosphorylation may still have functional implications in a broader biological context (Figure 6.1).

Lastly, considering the possibility that the delayed recovery observed in ASPP2-deficient mice was due to excessive cell death, the specific types of cell death that occur in inflamed and regenerating colonic tissue remain to be characterised. Apoptosis was not affected by the loss of ASPP2 in the intestinal epithelium (Figures 3.7 and 4.6), suggesting that p53 may not be involved in the experimental setting of this study. *In vivo* characterisation of necroptosis was not performed due to limited antibody availability, but the intestinal organoid may serve as an alternative system to interrogate the involvement of ASPP2 in necroptotic cell death (Figure 5.6). Pyroptosis is a third type of programmed cell death that is highly inflammatory and mostly occurs upon infection with intracellular pathogens (Fink et al. 2005). Notably, in a Caspase-11-deficient mouse model, it has been demonstrated that pyroptosis is activated in colonic epithelial cells in response to DSS treatment (Demon et al. 2014). Therefore, it is worth investigating whether ASPP2 is implicated in the regulation of pyroptosis.

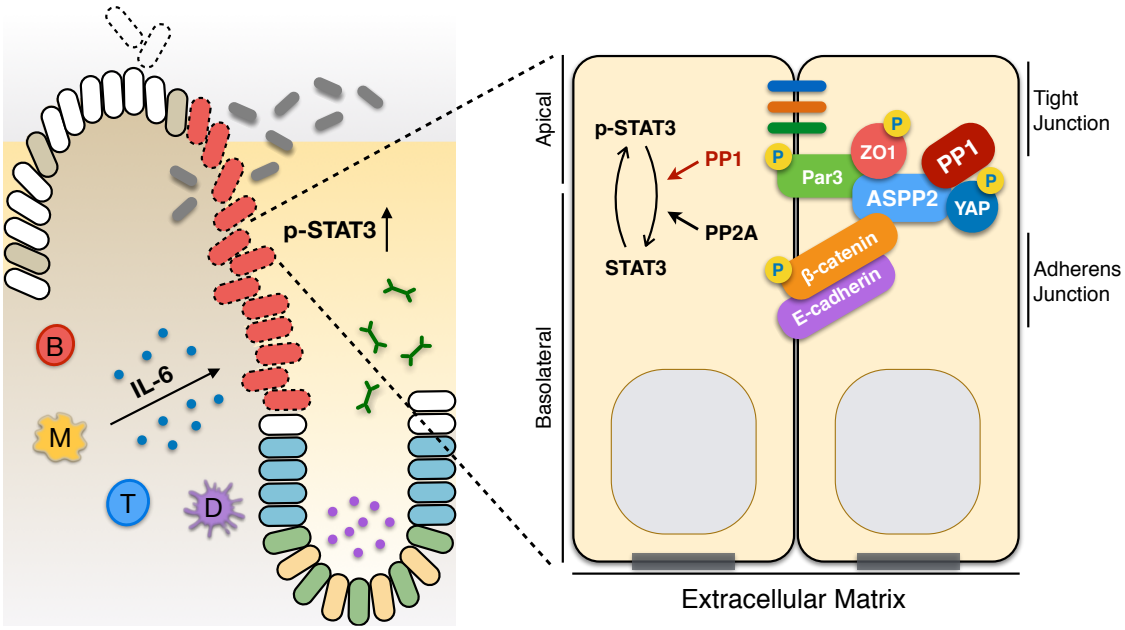


Figure 6.1: Epithelial cell autonomous and non-autonomous regulation of STAT3 signalling. In the event of intestinal inflammation, IL-6 secreted by stromal cells and lamina propria immune cells induces the phosphorylation of STAT3 in epithelial cells. The zoomed-in image shows the co-localisation of ASPP2 and Par3 at intestinal tight junctions. Binding partners of ASPP2 that can be regulated by phosphorylation are highlighted, suggesting the potentially important role of the ASPP2/PP1 complex in mediating dephosphorylation reactions. Importantly, STAT3 has been reported to be a substrate of PP1. B, B cell; M, Macrophage; T, T cell; D, Dendritic cell; PP1, protein phosphatase 1; PP2A, protein phosphatase 2A; p, phosphate group.

6.2 ASPP2: At the Crossroad of Tumour Initiation and Progression

Inflammation plays critical roles at different stages of tumour development, including initiation, promotion, malignant transformation, and metastasis (Grivennikov et al. 2010). In addition, it is generally accepted that chronic inflammation is a risk factor for tumourigenesis (Landskron et al. 2014). Given the intricate link between chronic inflammation, tissue regeneration, and tumourigenesis (Okayasu et al. 2002; Waldner et al. 2015), it was hypothesised that the delayed recovery from DSS-induced colitis would render ASPP2-deficient mice more susceptible to colorectal tumourigenesis. To test this hypothesis, the AOM/DSS-induced tumourigenesis model was employed in this study. The observation that ASPP2$^{\text{IEC-}\Delta\text{exon3}}$ mice exhibited higher tumour loads agreed with our hypothesis. However, peculiar

patterns of tumour initiation and progression were observed in wild-type and ASPP2-deficient mice, some of which seemingly counterintuitive and therefore deserves further discussion.

To better interpret the data obtained from this experiment, it is important to take the internal controls embedded in the system into consideration. On the one hand, as an epithelium-specific transgenic mouse model, ASPP2$^{\text{IEC-}\Delta\text{exon3}}$ mice enabled the distinction between epithelial cell autonomous and non-autonomous factors implicated in colorectal tumourigenesis. Based on the assumption that immune cells in these mice are functionally intact, any alteration in their infiltration or cytokine expression can be attributed to disturbed epithelial–immune cell interactions. On the other hand, and more importantly, the mosaic pattern of Villin-CreER-mediated ASPP2 depletion resulted in the exposure of wild-type and ASPP2-deficient crypts and tumours to a shared microenvironment, and thus identical inflammatory and tumourigenic stresses (Figure 4.4). Therefore, comparison of wild-type epithelial cells within wild-type and ASPP2-deficient animals may yield additional information regarding alterations of the intestinal microenvironment caused by the loss of epithelial ASPP2.

The next point to be put forward is the distinction between tumour initiation and progression, with the former reflected in the number of tumours developed and the latter in the characteristics of established tumours (Weinberg 2013). By the end of the AOM/DSS treatment, more colonic tumours were observed in ASPP2-deficient mice than in their wild-type counterparts, suggesting that the loss of ASPP2 is associated with an increased likelihood of tumour initiation (Figure 4.3). If the predisposition is intrinsic to epithelial cells, more tumours are expected to be derived from ASPP2-deficient than wild-type crypts in ASPP2$^{\text{IEC-}\Delta\text{exon3}}$ mice, which, surprisingly, was not the case (Figure 4.4). This led us to the hypothesis that the increased tumour count was not merely due to epithelial cell autonomous defects, but rather a more tumourigenic immune microenvironment caused by the loss of epithelial ASPP2. From the perspective of tumour progression, tumours

developed in wild-type animals showed higher YAP activity than those of ASPP2-deficient animals, suggesting that they may have reached a more advanced stage of tumour development (Figure 4.8). In addition, the average sizes of tumours were also significantly larger in wild-type mice than in ASPP2$^{\text{IEC-}\Delta\text{exon3}}$ animals (Figure 4.3). Taken together, these results suggested that the loss of ASPP2 in the intestinal epithelium may promote tumour initiation, while simultaneously suppressing tumour progression.

In order to better understand how epithelial–immune cell interaction is implicated in the process of colorectal tumourigenesis, LPMCs of wild-type and ASPP2$^{\text{IEC-}\Delta\text{exon3}}$ mice were isolated and analysed by flow cytometry. During the recovery phase of DSS-induced colitis, i.e. the early stage of inflammation-driven tumourigenesis, an increase in the infiltration of F4/80^{+} macrophages was observed in ASPP2$^{\text{IEC-}\Delta\text{exon3}}$ mice (Figure 4.11). Moreover, ASPP2-deficient mice also showed an increased presence of regulatory T cells at a relatively late time point when colonic adenomas were fully established (Figure 4.12). Collectively, these results suggested that a deficiency of ASPP2 in the intestinal epithelium may result in an inflammatory microenvironment that favours tumour development, as depicted in Figure 6.2, regardless of the genotype of epithelial cells being affected.

Admittedly, the model described above is far from complete, as it does not explain why tumours that develop in wild-type animals seemed to progress at a higher rate than those formed in ASPP2-deficient mice. To further refine the proposed model, more systematic characterisation of lamina propria immune cells needs to be performed at different stages of AOM/DSS-induced tumourigenesis. In particular, if the depletion of epithelial ASPP2 does result in a more tumourigenic intestinal microenvironment, the question is whether such a predisposition would also lead to an early onset of tumour formation. To that end, the development of colonic tumours should ideally be monitored in real time, possibly via colonoscopy. In regard to tumour progression, given that all tumours developed within the current time frame of AOM/DSS treatment were benign adenomas, it would be worth extending the duration of the experiment and examining whether the tumours

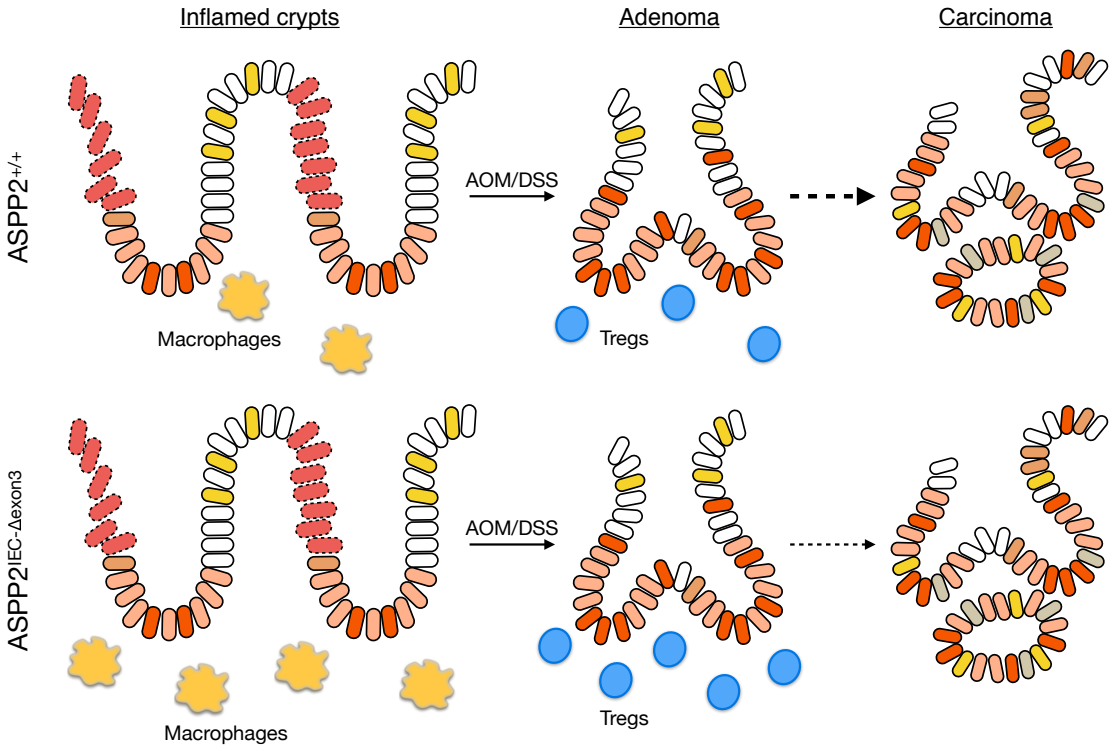


Figure 6.2: Proposed model for the involvement of epithelial ASPP2 in colorectal tumourigenesis. Under inflammatory conditions, loss of ASPP2 in the colonic epithelium results in increased infiltration of macrophages into the inflamed tissue. When tumours are fully established, more Tregs are observed in the lamina propria of ASPP2$^{\text{IEC-}\Delta\text{exon3}}$ animals. Adenomas developed in wild-type animals are generally found to have reached a more advanced stage compared with those developed in ASPP2$^{\text{IEC-}\Delta\text{exon3}}$ mice, but their potential to progress to invasive carcinomas remains to be investigated. Epithelial cells with dashed borders represent inflamed crypts.

would become invasive at a later time point. If that is the case, the extended AOM/DSS-induced tumourigenesis model will serve as a more suitable system to investigate the involvement of ASPP2 in tumour progression.

Lastly, the work presented in this thesis did not address the contribution of genetic background to the observed phenotypes. The interpretation of the data was complicated by the fact that the germline ASPP2-deficient mice used in this study were bred on a C57BL/6J × 129SvJ background, whereas the tissue-specific ASPP2 transgenic mice were bred on the C57BL/6 background. In spite of that, the observation that the mixed-background ASPP2$^{\Delta\text{exon3}}$ mice showed higher susceptibility to DSS-induced colitis but were more resistant to AOM/DSS-induced tumourigenesis has shed light on the complexity of the underlying epithelial–stromal

and epithelial–immune cell interactions. This issue is worth investigating in the future using better controlled mouse cohorts.

6.3 Organoids: A Potential Tissue Surrogate

In this study, intestinal organoids were generated from normal tissue as well as colonic tumours to supplement *in vivo* animal work. As a primary cell-based model system, the organoid has the potential to recapitulate physiologically relevant processes such as proliferation and cell fate determination. Nevertheless, the organoid technique is still in its infancy and exhibits various problems, hence it is not yet accepted as a complete tissue surrogate. The study described in this thesis has provided several strategies to cope with the limitations of the organoid technology.

As mentioned in section 5.2.2, one of the major challenges of the organoid culture technique lies in its heterogeneity, which may confound the interpretation of data obtained from it. In order to deal with inter-organoid heterogeneity, organoids can be tracked individually, as demonstrated in this study by time-lapse imaging (Figure 5.2). In addition to single-organoid resolution, this approach also provides time course information about the development of organoids, including volume enlargement and crypt branching. Admittedly, it remains quite challenging to extract comprehensive information from this system, as most existing analytical methodology fails to accommodate its 3D complexity. To that end, an automated motion analysis algorithm is under development, which, when complete, would be suitable for combination with the current paradigm of viability-based screening strategies (F. Zhou, unpublished data).

As for intra-organoid heterogeneity, the single-cell resolution guaranteed by flow cytometry offers the possibility of treating organoids as a bulk population while retaining the capability to dissect their internal complexity. In addition, by expanding the Lgr5-positive stem cell population, the VPA/CHIR99021 treatment provides an alternative method to reduce intra-organoid heterogeneity (Figure 5.3). However, a caveat of this approach is that such an effect may only be achieved at the expense of the physiological relevance of the system. Caution needs to be

taken in interpreting data derived from this experiment, and comparisons made between different genotypes will be better grounded than those made between *in vitro* and *in vivo* systems.

Apart from heterogeneity, another major drawback of the organoid culture system is the lack of niche factors. As an epithelium-only system, the organoid offers a relatively simple model to study epithelial cell-intrinsic properties. However, its simplicity is also a limiting factor as the system does not incorporate the contribution of environmental cues. Starting from here, the next step will be to incrementally build up the system by means of organoid co-culture (Figure 6.3, A and B). Depending on the biological questions of interest, the proposed model could be applied to the study of either physical interactions between epithelial cells and other cell types or the effects of secreted factors on different components within the system. Downstream analysis could be performed using flow cytometry or multiplex analysis enabled by the recently developed next-generation mass cytometry technology (Tape 2017). It is worth noting that monolayered epithelial cell cultures derived from intestinal organoids could be used to further simplify the implementation of the co-culture system (Moon et al. 2014).

To further explore the potential of the organoid as a building block for more sophisticated systems, we have proposed a workflow composed of organoid derivation, *in vitro* manipulation, and orthotopic transplantation (Figure 6.3C). It has been demonstrated that organoids can be stably labelled with fluorescent proteins via lentiviral transduction *in vitro*, which offers a powerful tracking tool to follow the growth dynamics of organoids after they are injected back *in vivo* (Figure 6.3D). More intriguingly, the organoid labelling technique lays the foundation for an organoid fusion protocol, where intestinal epithelial cells derived from mice of different genotypes are allowed to grow in close proximity with each other (Figure 6.3D). One potentially interesting question that could be answered with this system is whether cancer cells bearing certain oncogenic mutations tend to be more tumourigenic when they are physically in contact with cells containing a different spectrum of

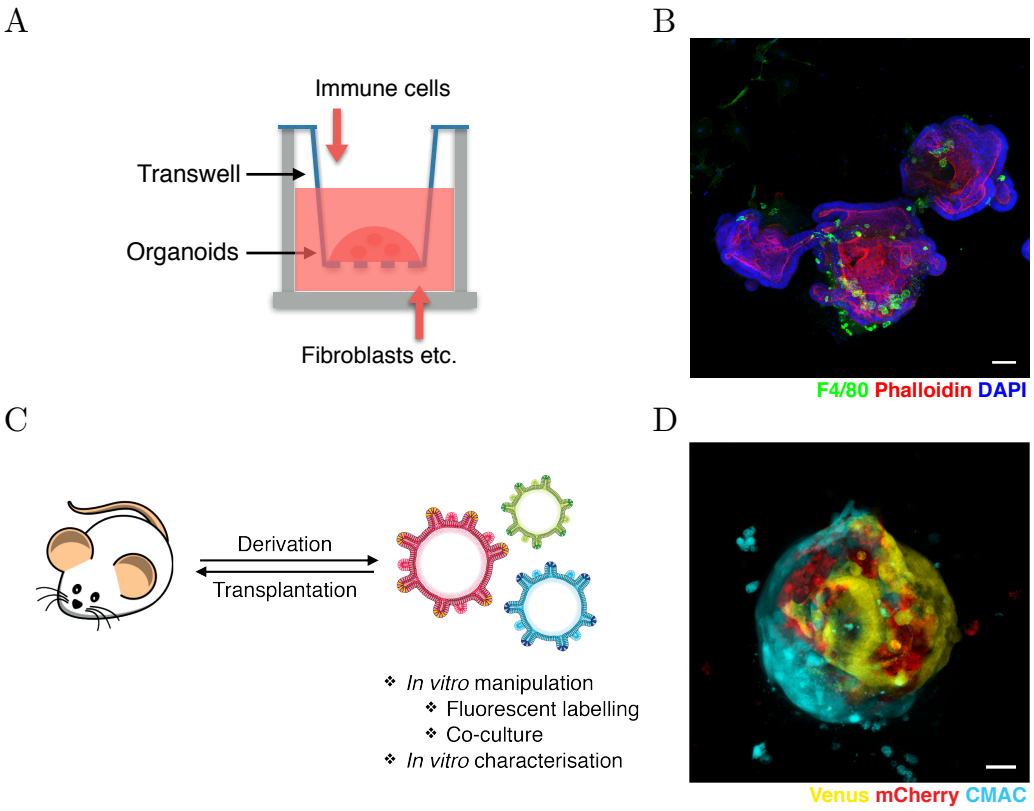


Figure 6.3: Establishment of organoid-based co-culture systems. (A) Schematic representation of the proposed organoid co-culture system. When combined with the transwell system, organoids can be co-cultured with other cell types such as immune cells and/or fibroblasts. Their interaction can be achieved either through physical interaction or via the exchange of secreted factors. (B) Representative IF co-staining of F4/80 (green) and Phalloidin (red) on a wild-type small intestinal organoid co-cultured with wild-type bone marrow-derived macrophages, with nuclei counterstained with DAPI (blue). Scale bar: 50 µm. (C) Proposed workflow for the derivation and transplantation of intestinal organoids. Organoids derived from primary tissue can be characterised and manipulated *in vitro*, followed by orthotopic transplantation, which enables the examination of their interaction with a physiologically relevant microenvironment. (D) Representative live imaging of a fused colonic organoid integrating three different populations, labelled with Venus (yellow), mCherry (red), and CMAC (cyan), respectively. The image was taken 72 hr after the fusion experiment. Scale bar: 25 µm.

mutations. To that end, the combination of organoid fusion and transplantation has the potential to take our understanding of tumour heterogeneity to the next level.

As part of the effort to apply the culture of organoids to the study of cancer biology, tumour organoids originating from AOM/DSS-induced adenomas were generated and characterised. The simplicity of the tumour organoid makes it an attractive model system to examine characteristics intrinsic to tumour cells.

However, it has been reported that tumours induced by AOM/DSS treatment exhibit a distinct pattern of mutations compared with those that naturally occur in human CRC, and thus the biological implications derived from this model should be carefully evaluated (Pan et al. 2017). Moreover, manifestations of intra-tumour heterogeneity may become even more pronounced in tumour organoids due to their mode of clonal propagation. As a result, in the interests of biological relevance, future applications of the tumour organoid should be more focused on spontaneously developed tumours or tumours derived from human patients. This, when combined with orthotopic transplantation, will be a promising strategy to yield insight into the crosstalk between tumour cells and their physiological microenvironment. Lastly, it is worth pointing out that the analytical methodology described in this thesis is very likely to be transferrable to other organoid-based studies.

In conclusion, this study has demonstrated that a loss of ASPP2 in the intestinal epithelium of mice will result in their delayed recovery from DSS-induced acute colitis and increased susceptibility to AOM/DSS-induced colorectal tumourigenesis. The defects can be partially attributed to alterations in the epithelial–immune cell interaction, the mechanistic details of which deserve further investigation using the organoid culture system.

References

Agirre, X, J Roman-Gomez, A Jimenez-Velasco, L Garate, C Montiel-Duarte, G Navarro, I Vázquez, et al. 2006. "ASPP1, a common activator of TP53, is inactivated by aberrant methylation of its promoter in acute lymphoblastic leukemia." *Oncogene* 25, no. 13 (March): 1862–1870.

Alex, Philip, Nicholas C Zachos, Thuan Nguyen, Liberty Gonzales, Tian-E Chen, Laurie S Conklin, Michael Centola, and Xuhang Li. 2009. "Distinct Cytokine Patterns Identified from Multiplex Profiles of Murine DSS and TNBS-Induced Colitis." *Inflammatory Bowel Diseases* 15, no. 3 (March): 341–352.

Andersson-Rolf, Amanda, Matthias Zilbauer, Bon-Kyoung Koo, and H Clevers. 2017. "Stem Cells in Repair of Gastrointestinal Epithelia." *Physiology (Bethesda, Md.)* 32, no. 4 (July): 278–289.

Ando, K, S Kanazawa, T Tetsuka, S Ohta, X Jiang, T Tada, M Kobayashi, N Matsui, and T Okamoto. 2003. "Induction of Notch signaling by tumor necrosis factor in rheumatoid synovial fibroblasts." *Oncogene* 22 (49): 7796–7803.

Araki, Yoshio, Ken-ichi Mukaisyo, Hiroyuki Sugihara, Yoshihide Fujiyama, and Takanori Hattori. 2010. "Increased apoptosis and decreased proliferation of colonic epithelium in dextran sulfate sodium-induced colitis in mice." *Oncology reports* 24, no. 4 (October): 869–874.

Armaghany, Tannaz, Jon D Wilson, Quyen Chu, and Glenn Mills. 2012. "Genetic alterations in colorectal cancer." *Gastrointestinal cancer research : GCR* 5, no. 1 (January): 19–27.

Artavanis-Tsakonas, Spyros, Matthew D Rand, and Robert J Lake. 1999. "Notch Signaling: Cell Fate Control and Signal Integration in Development." *Science* 284, no. 5415 (April): 770–776.

Ashton, Gabrielle H, Jennifer P Morton, Kevin Myant, Toby J Phesse, Rachel A Ridgway, Victoria Marsh, Julie A Wilkins, et al. 2010. "Focal Adhesion Kinase Is Required for Intestinal Regeneration and Tumorigenesis Downstream of Wnt/c-Myc Signaling." *Developmental cell* 19, no. 2 (August): 259–269.

Atreya, I, R Atreya, and M F Neurath. 2008. "NF-kappaB in inflammatory bowel disease." *Journal of internal medicine* 263, no. 6 (June): 591–596.

Barcellos-Hoff, M H, J Aggeler, T G Ram, and M J Bissell. 1989. "Functional differentiation and alveolar morphogenesis of primary mammary cultures on reconstituted basement membrane." *Development (Cambridge, England)* 105, no. 2 (February): 223–235.

Barker, Nick. 2013. "Adult intestinal stem cells: critical drivers of epithelial homeostasis and regeneration." *Nature Reviews Molecular Cell Biology* 15, no. 1 (December): 19–33.

Barker, Nick, Johan H van Es, Jeroen Kuipers, Pekka Kujala, Maaike van den Born, Miranda Cozijnsen, Andrea Haegebarth, et al. 2007. "Identification of stem cells in small intestine and colon by marker gene Lgr5." *Nature* 449, no. 7165 (October): 1003–1007.

Barreau, F, and J P Hugot. 2014. "Intestinal barrier dysfunction triggered by invasive bacteria." *Current opinion in microbiology* 17 (February): 91–98.

Barry, Evan R, Teppei Morikawa, Brian L Butler, Kriti Shrestha, Rosemarie de la Rosa, Kelly Yan, Charles S Fuchs, et al. 2014. "Restriction of intestinal stem cell expansion and the regenerative response by YAP." *Nature* 493, no. 7430 (April): 106–110.

Bartfeld, Sina, and H Clevers. 2017. "Stem cell-derived organoids and their application for medical research and patient treatment." *Journal of Molecular Medicine* 95, no. 7 (April): 1–10.

Batlle, Eduard, Jeffrey T Henderson, Harry Beghtel, Maaike M W van den Born, Elena Sancho, Gerwin Huls, Jan Meeldijk, et al. 2002. "Beta-catenin and TCF mediate cell positioning in the intestinal epithelium by controlling the expression of EphB/ephrinB." *Cell* 111, no. 2 (October): 251–263.

Ben-Neriah, Yinon, and Michael Karin. 2011. "Inflammation meets cancer, with NF-κB as the matchmaker." *Nature Immunology* 12, no. 8 (July): 715–723.

Bergamaschi, Daniele, Yardena Samuels, Boquan Jin, Sai Duraisingham, Tim Crook, and Xin Lu. 2004. "ASPP1 and ASPP2: Common Activators of p53 Family Members." *Molecular and Cellular Biology* 24, no. 3 (January): 1341–1350.

Bergamaschi, Daniele, Yardena Samuels, Nigel J O'Neil, Giuseppe Trigiante, Tim Crook, Jung-Kuang Hsieh, Daniel J O'Connor, et al. 2003. "iASPP oncoprotein is a key inhibitor of p53 conserved from worm to human." *Nature Genetics* 33, no. 2 (January): 162–167.

Bevins, Charles L, and Nita H Salzman. 2011. "Paneth cells, antimicrobial peptides and maintenance of intestinal homeostasis." *Nature reviews. Microbiology* 9, no. 5 (May): 356–368.

Bijlsma, Maarten F, Anguraj Sadanandam, Patrick Tan, and Louis Vermeulen. 2017. "Molecular subtypes in cancers of the gastrointestinal tract." *Nature reviews. Gastroenterology & hepatology* 14, no. 6 (June): 333–342.

Bissell, D M, D M Arenson, J J Maher, and F J Roll. 1987. "Support of cultured hepatocytes by a laminin-rich gel. Evidence for a functionally significant subendothelial matrix in normal rat liver." *Journal of Clinical Investigation* 79, no. 3 (March): 801–812.

Biswas, Swati, Anna Chytil, Kay Washington, Judith Romero-Gallo, Agnieszka E Gorska, Pamela S Wirth, Shiva Gautam, Harold L Moses, and William M Grady. 2004. "Transforming growth factor beta receptor type II inactivation promotes the establishment and progression of colon cancer." *Cancer Research* 64, no. 14 (July): 4687–4692.

Bogaert, Julie, and Hans Prenen. 2014. "Molecular genetics of colorectal cancer." *Annals of gastroenterology* 27 (1): 9–14.

Boivin, Gregory P, Kay Washington, Kan Yang, Jerrold M Ward, Theresa P Pretlow, Robert Russell, David G Besselsen, et al. 2003. "Pathology of mouse models of intestinal cancer: Consensus report and recommendations." *Gastroenterology* 124, no. 3 (March): 762–777.

Bollrath, Julia, Toby J Phesse, Vivian A von Burstin, Tracy Putoczki, Moritz Bennecke, Trudie Bateman, Tim Nebelsiek, et al. 2009. "gp130-Mediated Stat3 Activation in Enterocytes Regulates Cell Survival and Cell-Cycle Progression during Colitis-Associated Tumorigenesis." *Cancer Cell* 15, no. 2 (February): 91–102.

Bonizzi, Giuseppina, and Michael Karin. 2004. "The two NF-kappaB activation pathways and their role in innate and adaptive immunity." *Trends in Immunology* 25, no. 6 (June): 280–288.

Bos, J L, E R Fearon, S R Hamilton, M Verlaan-de Vries, J H van Boom, A J van der Eb, and B Vogelstein. 1987. "Prevalence of ras gene mutations in human colorectal cancers." *Nature* 327, no. 6120 (June): 293–297.

Boulay, J L, G Mild, A Lowy, J Reuter, M Lagrange, L Terracciano, U Laffer, R Herrmann, and C Rochlitz. 2002. "SMAD4 is a predictive marker for 5-fluorouracil-based chemotherapy in patients with colorectal cancer." *British journal of cancer* 87, no. 6 (September): 630–634.

Brink, Gijs R van den. 2007. "Hedgehog Signaling in Development and Homeostasis of the Gastrointestinal Tract." *Physiological Reviews* 87, no. 4 (October): 1343–1375.

Broom, O J, B Widjaya, J Troelsen, J Olsen, and O H Nielsen. 2009. "Mitogen activated protein kinases: a role in inflammatory bowel disease?" *Clinical & Experimental Immunology* 158, no. 3 (December): 272–280.

Brown, Eric M, Manish Sadarangani, and B Brett Finlay. 2013. "The role of the immune system in governing host-microbe interactions in the intestine." *Nature Immunology* 14, no. 7 (June): 660–667.

Buczacki, Simon J A, Heather Ireland Zecchini, Anna M Nicholson, Roslin Russell, Louis Vermeulen, Richard Kemp, and Douglas J Winton. 2013. "Intestinal label-retaining cells are secretory precursors expressing Lgr5." *Nature* 495, no. 7439 (February): 65–69.

Buti, Ludovico, Eric Spooner, Annemarthe G Van der Veen, Rino Rappuoli, Antonello Covacci, and Hidde L Ploegh. 2011. "Helicobacter pylori cytotoxin-associated gene A (CagA) subverts the apoptosis-stimulating protein of p53 (ASPP2) tumor suppressor pathway of the host." *Proceedings of the National Academy of Sciences* 108, no. 22 (May): 9238–9243.

Bykov, Vladimir J N, Natalia Issaeva, Alexandre Shilov, Monica Hultcrantz, Elena Pugacheva, Peter Chumakov, Jan Bergman, Klas G Wiman, and Galina Selivanova. 2002. "Restoration of the tumor suppressor function to mutant p53 by a low-molecular-weight compound." *Nature Medicine* 8, no. 3 (March): 282–288.

Bykov, Vladimir J N, and Klas G Wiman. 2014. "Mutant p53 reactivation by small molecules makes its way to the clinic." *FEBS letters* 588, no. 16 (August): 2622–2627.

Bykov, Vladimir J N, Nicole Zache, Helene Stridh, Jacob Westman, Jan Bergman, Galina Selivanova, and Klas G Wiman. 2005. "PRIMA-1MET synergizes with cisplatin to induce tumor cell apoptosis." *Oncogene* 24, no. 21 (February): 3484–3491.

Cai, Jing, Nailing Zhang, Yonggang Zheng, Roeland F de Wilde, Anirban Maitra, and Duojia Pan. 2010. "The Hippo signaling pathway restricts the oncogenic potential of an intestinal regeneration program." *Genes & development* 24, no. 21 (November): 2383–2388.

Cancer Genome Atlas Network. 2012. "Comprehensive molecular characterization of human colon and rectal cancer." *Nature* 487, no. 7407 (July): 330–337.

Cao, Li, Anton Kuratnik, Wanli Xu, Jason D Gibson, Frederick Kolling, Eric R Falcone, Mohammed Ammar, et al. 2015. "Development of intestinal organoids as tissue surrogates: cell composition and the epigenetic control of differentiation." *Molecular Carcinogenesis* 54, no. 3 (March): 189–202.

Cebra, J J. 1999. "Influences of microbiota on intestinal immune system development." *The American journal of clinical nutrition* 69, no. 5 (May): 1046S–1051S.

Chassaing, Benoit, Jesse D Aitken, Madhu Malleshappa, and Matam Vijay-Kumar. 2001. *Dextran Sulfate Sodium (DSS)-Induced Colitis in Mice.* DSS-Induced Colitis in Mice. Hoboken, NJ, USA: John Wiley & Sons, Inc., May.

Chin, Alana M, David R Hill, Megan Aurora, and Jason R Spence. 2017. "Morphogenesis and maturation of the embryonic and postnatal intestine." *Seminars in Cell and Developmental Biology* 66 (June): 81–93.

Cho, Y, S Gorina, P D Jeffrey, and N P Pavletich. 1994. "Crystal structure of a p53 tumor suppressor-DNA complex: understanding tumorigenic mutations." *Science* 265, no. 5170 (July): 346–355.

Choi, Chang-Ho R, Ibrahim Al Bakir, Ailsa L Hart, and Trevor A Graham. 2017. "Clonal evolution of colorectal cancer in IBD." *Nature reviews. Gastroenterology & hepatology* 14, no. 4 (April): 218–229.

Clevers, H. 2016. "Modeling Development and Disease with Organoids." *Cell* 165, no. 7 (June): 1586–1597.

Clevers, H, Kyle M Loh, and Roel Nusse. 2014. "Stem cell signaling. An integral program for tissue renewal and regeneration: Wnt signaling and stem cell control." *Science* 346, no. 6205 (October): 1248012.

Cobleigh, Melody A, Bita Tabesh, Pincas Bitterman, Joffre Baker, Maureen Cronin, Mei-Lan Liu, Russell Borchik, Juan-Miguel Mosquera, Michael G Walker, and Steven Shak. 2005. "Tumor Gene Expression and Prognosis in Breast Cancer Patients with 10 or More Positive Lymph Nodes." *Clinical cancer research : an official journal of the American Association for Cancer Research* 11, no. 24 (December): 8623–8631.

Colotta, Francesco, Paola Allavena, Antonio Sica, Cecilia Garlanda, and Alberto Mantovani. 2009. "Cancer-related inflammation, the seventh hallmark of cancer: links to genetic instability." *Carcinogenesis* 30, no. 7 (July): 1073–1081.

Cong, Weili, Tomonori Hirose, Yutaka Harita, Akio Yamashita, Keiko Mizuno, Hisashi Hirano, and Shigeo Ohno. 2010. "ASPP2 Regulates Epithelial Cell Polarity through the PAR Complex." *Current Biology* 20, no. 15 (August): 1408–1414.

Corn, Benjamin W, Felix Kovner, Stella Bek, Isaiah Wexler, Beatrice Lifschits, and Rony Seger. 2008. "ERK Signaling in Colorectal Cancer: A Preliminary Report on the Expression of Phosphorylated ERK and the Effects of Radiation Therapy." *American Journal of Clinical Oncology* 31, no. 3 (June): 255–258.

Damgaard, Rune Busk, Berthe Katrine Fiil, Carsten Speckmann, Monica Yabal, Udo zur Stadt, Simon Bekker-Jensen, Philipp J Jost, Stephan Ehl, Niels Mailand, and Mads Gyrd-Hansen. 2013. "Disease-causing mutations in the XIAP BIR2 domain impair NOD2-dependent immune signalling." *EMBO Molecular Medicine* 5, no. 8 (August): 1278–1295.

Daniels, Danette L, and William I Weis. 2005. "Beta-catenin directly displaces Groucho/TLE repressors from Tcf/Lef in Wnt-mediated transcription activation." *Nature structural & molecular biology* 12, no. 4 (April): 364–371.

Davis, Hayley, Shazia Irshad, Mukesh Bansal, Hannah Rafferty, Tatjana Boitsova, Chiara Bardella, Emma Jaeger, et al. 2014. "Aberrant epithelial GREM1 expression initiates colonic tumorigenesis from cells outside the stem cell niche." *Nature Medicine* 21, no. 1 (December): 1–12.

De Robertis, Mariangela, Emanuela Massi, Maria Luana Poeta, Simone Carotti, Sergio Morini, Loredana Cecchetelli, Emanuela Signori, and Vito Michele Fazio. 2011. "The AOM/DSS murine model for the study of colon carcinogenesis: From pathways to diagnosis and therapy studies." *Journal of Carcinogenesis* 10 (1): 9.

Dekkers, Johanna F, Gitte Berkers, Evelien Kruisselbrink, Annelotte Vonk, Hugo R de Jonge, Hettie M Janssens, Inez Bronsveld, et al. 2016. "Characterizing responses to CFTR-modulating drugs using rectal organoids derived from subjects with cystic fibrosis." *Science Translational Medicine* 8, no. 344 (June): 344ra84–344ra84.

Dekkers, Johanna F, Caroline L Wiegerinck, Hugo R de Jonge, Inez Bronsveld, Hettie M Janssens, Karin M de Winter-de Groot, Arianne M Brandsma, et al. 2013. "A functional CFTR assay using primary cystic fibrosis intestinal organoids." *Nature Medicine* 19, no. 7 (June): 939–945.

Delgado, Maria Eugenia, Thomas Grabinger, and Thomas Brunner. 2015. "Cell death at the intestinal epithelial front line." *The FEBS Journal* 283, no. 14 (November): 2701–2719.

Demon, D, A Kuchmiy, A Fossoul, Q Zhu, T-D Kanneganti, and M Lamkanfi. 2014. "Caspase-11 is expressed in the colonic mucosa and protects against dextran sodium sulfate-induced colitis." *Mucosal Immunology* 7, no. 6 (November): 1480–1491.

Didierlaurent, Arnaud, Michel Simonet, and Jean-Claude Sirard. 2006. "Innate and acquired plasticity of the intestinal immune system." *Cellular and Molecular Life Sciences* 62, no. 12 (June): 1285–1287.

Downward, Julian. 2003. "Targeting RAS signalling pathways in cancer therapy." *Nature reviews. Cancer* 3, no. 1 (January): 11–22.

Drost, Jarno, Richard H van Jaarsveld, Bas Ponsioen, Cheryl Zimberlin, Ruben van Boxtel, Arjan Buijs, Norman Sachs, et al. 2015. "Sequential cancer mutations in cultured human intestinal stem cells." *Nature* 521, no. 7550 (April): 43–47.

Dutta, Devanjali, Inha Heo, and H Clevers. 2017. "Disease Modeling in Stem Cell-Derived 3D Organoid Systems." *Trends in Molecular Medicine* (March): 1–18.

El Marjou, Fatima, Klaus-Peter Janssen, Benny Hung-Junn Chang, Mei Li, Valérie Hindie, Lawrence Chan, Daniel Louvard, Pierre Chambon, Daniel Metzger, and Sylvie Robine. 2004. "Tissue-specific and inducible Cre-mediated recombination in the gut epithelium." *Genesis (New York, N.Y. : 2000)* 39, no. 3 (July): 186–193.

Elliott, Eric I, and Fayyaz S Sutterwala. 2015. "Initiation and perpetuation of NLRP3 inflammasome activation and assembly." *Immunological reviews* 265, no. 1 (May): 35–52.

Endt, Kathrin, Bärbel Stecher, Samuel Chaffron, Emma Slack, Nicolas Tchitchek, Arndt Benecke, Laurye Van Maele, et al. 2010. "The microbiota mediates pathogen clearance from the gut lumen after non-typhoidal Salmonella diarrhea." *PLoS pathogens* 6, no. 9 (September): e1001097.

Es, Johan H van, Toshiro Sato, Marc van de Wetering, Anna Lyubimova, Annie Ng Yee Nee, Alex Gregorieff, Nobuo Sasaki, et al. 2012. "Dll1+ secretory progenitor cells revert to stem cells upon crypt damage." *Nature Cell Biology* 14, no. 10 (September): 1099–1104.

Espanel, X, and M Sudol. 2001. "Yes-associated protein and p53-binding protein-2 interact through their WW and SH3 domains." *Journal of Biological Chemistry* 276, no. 17 (April): 14514–14523.

Ettayebi, Khalil, Sue E Crawford, Kosuke Murakami, James R Broughman, Umesh Karandikar, Victoria R Tenge, Frederick H Neill, et al. 2016. "Replication of human noroviruses in stem cell–derived human enteroids." *Science* 353, no. 6306 (September): 1387–1393.

Facciabene, Andrea, Gregory T Motz, and George Coukos. 2012. "T-regulatory cells: key players in tumor immune escape and angiogenesis." *Cancer Research* 72, no. 9 (May): 2162–2171.

Farin, Henner F, Ingrid Jordens, Mohammed H Mosa, Onur Basak, Jeroen Korving, Daniele V F Tauriello, Karin de Punder, et al. 2016. "Visualization of a short-range Wnt gradient in the intestinal stem-cell niche." *Nature* 530, no. 7590 (February): 340–343.

Farin, Henner F, Wouter R Karthaus, Pekka Kujala, Maryam Rakhshandehroo, Gerald Schwank, Robert G J Vries, Eric Kalkhoven, Edward E S Nieuwenhuis, and H Clevers. 2014. "Paneth cell extrusion and release of antimicrobial products is directly controlled by immune cell–derived IFN-γ." *Journal of Experimental Medicine* 211, no. 7 (June): 1393–1405.

Feil, Susanne, Nadejda Valtcheva, and Robert Feil. 2009. "Inducible Cre Mice." In *Gene Knockout Protocols,* 343–363. Totowa, NJ: Humana Press, February.

Fink, Susan L, and Brad T Cookson. 2005. "Apoptosis, pyroptosis, and necrosis: mechanistic description of dead and dying eukaryotic cells." *Infection and immunity* 73, no. 4 (April): 1907–1916.

Finkbeiner, Stacy R, Xi-Lei Zeng, Budi Utama, Robert L Atmar, Noah F Shroyer, and Mary K Estes. 2012. "Stem cell-derived human intestinal organoids as an infection model for rotaviruses." *MBio* 3 (4): e00159–12.

Flier, Laurens van der, and H Clevers. 2009. "Stem Cells, Self-Renewal, and Differentiation in the Intestinal Epithelium." *Annual Review of Physiology* 71, no. 1 (March): 241–260.

Fodde, Riccardo, Ron Smits, and H Clevers. 2001. "APC, Signal transduction and genetic instability in colorectal cancer." *Nature reviews. Cancer* 1, no. 1 (October): 55–67.

Forrester, K, C Almoguera, K Han, W E Grizzle, and M Perucho. 1987. "Detection of high incidence of K-ras oncogenes during human colon tumorigenesis." *Nature* 327, no. 6120 (June): 298–303.

Foxwell, Brian M J, Jan Bondeson, Fionula Brennan, and Marc Feldmann. 2000. "Adenoviral transgene delivery provides an approach to identifying important molecular processes in inflammation: evidence for heterogenecity in the requirement for NFκB in tumour necrosis factor production." *Annals of the Rheumatic Diseases* 59, no. suppl 1 (November): i54–i59.

Frey, Mark R, Anastasia Golovin, and D Brent Polk. 2004. "Epidermal growth factor-stimulated intestinal epithelial cell migration requires Src family kinase-dependent p38 MAPK signaling." *Journal of Biological Chemistry* 279, no. 43 (October): 44513–44521.

Frisch, S M, and H Francis. 1994. "Disruption of epithelial cell-matrix interactions induces apoptosis." *The Journal of Cell Biology* 124, no. 4 (February): 619–626.

Fujii, Masayuki, Mariko Shimokawa, Shoichi Date, Ai Takano, Mami Matano, Kosaku Nanki, Yuki Ohta, et al. 2016. "A Colorectal Tumor Organoid Library Demonstrates Progressive Loss of Niche Factor Requirements during Tumorigenesis." *Stem Cell* 18, no. 6 (June): 827–838.

Gerbe, François, Emmanuelle Sidot, Danielle J Smyth, Makoto Ohmoto, Ichiro Matsumoto, Valérie Dardalhon, Pierre Cesses, et al. 2016. "Intestinal epithelial tuft cells initiate type 2 mucosal immunity to helminth parasites." *Nature* 529, no. 7585 (January): 226–230.

Gorina, S, and N P Pavletich. 1996. "Structure of the p53 tumor suppressor bound to the ankyrin and SH3 domains of 53BP2." *Science* 274, no. 5289 (November): 1001–1005.

Goswami, Rashmi S, Keyur P Patel, Rajesh R Singh, Funda Meric-Bernstam, E Scott Kopetz, Vivek Subbiah, Ricardo H Alvarez, et al. 2015. "Hotspot Mutation Panel Testing Reveals Clonal Evolution in a Study of 265 Paired Primary and Metastatic Tumors." *Clinical cancer research : an official journal of the American Association for Cancer Research* 21, no. 11 (February): 2644–2651.

Grabinger, T, L Luks, F Kostadinova, C Zimberlin, J P Medema, M Leist, and T Brunner. 2014. "Ex vivo culture of intestinal crypt organoids as a model system for assessing cell death induction in intestinal epithelial cells and enteropathy." *Cell Death and Disease* 5, no. 5 (May): e1228.

Greenblatt, David Yu, Abram M Vaccaro, Renata Jaskula-Sztul, Li Ning, Megan Haymart, Muthusamy Kunnimalaiyaan, and Herbert Chen. 2007. "Valproic acid activates notch-1 signaling and regulates the neuroendocrine phenotype in carcinoid cancer cells." *The Oncologist* 12, no. 8 (August): 942–951.

Gregorieff, Alex, Yu Liu, Mohammad R Inanlou, Yuliya Khomchuk, and Jeffrey L Wrana. 2015. "Yap-dependent reprogramming of Lgr5+ stem cells drives intestinal regeneration and cancer." *Nature* 526, no. 7575 (October): 715–718.

Gregorieff, Alex, and Jeffrey L Wrana. 2017. "Hippo signalling in intestinal regeneration and cancer." *Current opinion in cell biology* 48 (May): 17–25.

Greten, Florian R, Lars Eckmann, Tim F Greten, Jin Mo Park, Zhi-Wei Li, Laurence J Egan, Martin F Kagnoff, and Michael Karin. 2004. "IKKβ Links Inflammation and Tumorigenesis in a Mouse Model of Colitis-Associated Cancer." *Cell* 118, no. 3 (August): 285–296.

Grivennikov. 2013. "Inflammation and colorectal cancer: colitis-associated neoplasia." *Seminars in immunopathology* 35 (2): 229–244.

Grivennikov, Florian R Greten, and Michael Karin. 2010. "Immunity, inflammation, and cancer." *Cell* 140, no. 6 (March): 883–899.

Grivennikov, Eliad Karin, Janos Terzic, Daniel Mucida, Guann-Yi Yu, Sivakumar Vallabhapurapu, JUrgen Scheller, et al. 2009. "IL-6 and Stat3 are required for survival of intestinal epithelial cells and development of colitis-associated cancer." *Cancer Cell* 15, no. 2 (February): 103–113.

Grivennikov and Michael Karin. 2011. "Inflammatory cytokines in cancer: tumour necrosis factor and interleukin 6 take the stage." *Annals of the Rheumatic Diseases* 70 Suppl 1, no. Suppl 1 (March): i104–8.

Groden, Joanna, Andrew Thliveris, Wade Samowitz, Mary Carlson, Lawrence Gelbert, Hans Albertsen, Geoff Joslyn, et al. 1991. "Identification and characterization of the familial adenomatous polyposis coli gene." *Cell* 66, no. 3 (August): 589–600.

Günther, Claudia, Helmut Neumann, Markus F Neurath, and Christoph Becker. 2013. "Apoptosis, necrosis and necroptosis: cell death regulation in the intestinal epithelium." *Gut* 62, no. 7 (July): 1062–1071.

Han, Jiahuai, Chuan-Qi Zhong, and Duan-Wu Zhang. 2011. "Programmed necrosis: backup to and competitor with apoptosis in the immune system." *Nature Immunology* 12, no. 12 (December): 1143–1149.

Hanahan, D, and R A Weinberg. 2000. "The hallmarks of cancer." *Cell* 100 (1): 57–70.

———. 2011. "Hallmarks of cancer: the next generation." *Cell* 144, no. 5 (March): 646–674.

Harpaz, Noam, and Alexandros D Polydorides. 2010. "Colorectal dysplasia in chronic inflammatory bowel disease: pathology, clinical implications, and pathogenesis." *Archives of pathology & laboratory medicine* 134, no. 6 (June): 876–895.

Hata, Kazunori, Akira Andoh, Mitsue Shimada, Sanae Fujino, Shigeki Bamba, Yoshio Araki, Takafumi Okuno, Yoshihide Fujiyama, and Tadao Bamba. 2002. "IL-17 stimulates inflammatory responses via NF-kappaB and MAP kinase pathways in human colonic myofibroblasts." *AJP: Gastrointestinal and Liver Physiology* 282, no. 6 (June): G1035–44.

Heinrich, Peter C, Iris Behrmann, Serge Haan, Heike M Hermanns, Gerhard Müller-Newen, and Fred Schaper. 2003. "Principles of interleukin (IL)-6-type cytokine signalling and its regulation." *Biochemical Journal* 374, no. Pt 1 (August): 1–20.

Helps, N R, H M Barker, S J Elledge, and P T Cohen. 1995. "Protein phosphatase 1 interacts with p53BP2, a protein which binds to the tumour suppressor p53." *FEBS letters* 377, no. 3 (December): 295–300.

Hiscott, J, J Marois, J Garoufalis, M D'Addario, A Roulston, I Kwan, N Pepin, J Lacoste, H Nguyen, and G Bensi. 1993. "Characterization of a functional NF-kappa B site in the human interleukin 1 beta promoter: evidence for a positive autoregulatory loop." *Molecular and Cellular Biology* 13, no. 10 (October): 6231–6240.

Holmberg, Johan, Maria Genander, Michael M Halford, Cecilia Annerén, Mariann Sondell, Michael J Chumley, Robert E Silvany, Mark Henkemeyer, and Jonas Frisén. 2006. "EphB receptors coordinate migration and proliferation in the intestinal stem cell niche." *Cell* 125, no. 6 (June): 1151–1163.

Hooper, Lora V, Melissa H Wong, Anders Thelin, Lennart Hansson, Per G Falk, and Jeffrey I Gordon. 2001. "Molecular Analysis of Commensal Host-Microbial Relationships in the Intestine." *Science* 291, no. 5505 (February): 881–884.

Hori, Kazuya, Anindya Sen, and Spyros Artavanis-Tsakonas. 2013. "Notch signaling at a glance." *Journal of Cell Science* 126, no. Pt 10 (May): 2135–2140.

Horino, J, M Fujimoto, F Terabe, S Serada, T Takahashi, Y Soma, K Tanaka, et al. 2008. "Suppressor of cytokine signaling-1 ameliorates dextran sulfate sodium-induced colitis in mice." *International Immunology* 20, no. 6 (June): 753–762.

Hugot, J P, M Chamaillard, H Zouali, S Lesage, J P Cézard, J Belaiche, S Almer, et al. 2001. "Association of NOD2 leucine-rich repeat variants with susceptibility to Crohn's disease." *Nature* 411, no. 6837 (May): 599–603.

Humphries, Adam, and Nicholas A Wright. 2008. "Colonic crypt organization and tumorigenesis." *Nature reviews. Cancer* 8, no. 6 (May): 415–424.

Hussain, S Perwez, Lorne J Hofseth, and Curtis C Harris. 2003. "Radical causes of cancer." *Nature reviews. Cancer* 3, no. 4 (April): 276–285.

Iacopetta, Barry. 2003. "TP53 mutation in colorectal cancer." *Human mutation* 21, no. 3 (March): 271–276.

Ilyas, M, J A Efstathiou, J Straub, H C Kim, and W F Bodmer. 1999. "Transforming growth factor beta stimulation of colorectal cancer cell lines: type II receptor bypass and changes in adhesion molecule expression." *Proceedings of the National Academy of Sciences of the United States of America* 96, no. 6 (March): 3087–3091.

In, Julie, Jennifer Foulke-Abel, Nicholas C Zachos, Anne-Marie Hansen, James B Kaper, Harris D Bernstein, Marc Halushka, et al. 2016. "Enterohemorrhagic Escherichia coli Reduces Mucus and Intermicrovillar Bridges in Human Stem Cell-Derived Colonoids." *Cellular and Molecular Gastroenterology and Hepatology* 2, no. 1 (January): 48–62.e3.

Ireland, Heather, Richard Kemp, Carol Houghton, Louise Howard, Alan R Clarke, Owen J Sansom, and Douglas J Winton. 2004. "Inducible cre-mediated control of gene expression in the murine gastrointestinal tract: effect of loss of β-catenin." *Gastroenterology* 126, no. 5 (May): 1236–1246.

Jensen, J, E E Pedersen, P Galante, J Hald, R S Heller, M Ishibashi, R Kageyama, F Guillemot, P Serup, and O D Madsen. 2000. "Control of endodermal endocrine development by Hes-1." *Nature Genetics* 24, no. 1 (January): 36–44.

Jessen, Kristjan R, Rhona Mirsky, and Peter Arthur-Farraj. 2015. "The Role of Cell Plasticity in Tissue Repair: Adaptive Cellular Reprogramming." *Developmental cell* 34, no. 6 (September): 613–620.

Johansen, F E, and C S Kaetzel. 2011. "Regulation of the polymeric immunoglobulin receptor and IgA transport: new advances in environmental factors that stimulate pIgR expression and its role in mucosal immunity." *Mucosal Immunology* 4, no. 6 (November): 598–602.

Kampa, Kerstin M, Jared D Acoba, Dexi Chen, Joel Gay, Hunjoo Lee, Kelly Beemer, Emerson Padiernos, et al. 2009. "Apoptosis-stimulating protein of p53 (ASPP2) heterozygous mice are tumor-prone and have attenuated cellular damage-response thresholds." *Proceedings of the National Academy of Sciences* 106, no. 11 (March): 4390–4395.

Kang, Jung Cheng, Jin Shuen Chen, Chien Hsing Lee, Jao Jen Chang, and Yi Shing Shieh. 2010. "Intratumoral macrophage counts correlate with tumor progression in colorectal cancer." *Journal of Surgical Oncology* 102, no. 3 (September): 242–248.

Karin, Michael, and H Clevers. 2016. "Reparative inflammation takes charge of tissue regeneration." *Nature* 529, no. 7586 (January): 307–315.

Kato, Lucia M, Shimpei Kawamoto, Mikako Maruya, and Sidonia Fagarasan. 2014. "The role of the adaptive immune system in regulation of gut microbiota." *Immunological reviews* 260, no. 1 (July): 67–75.

Kawai, Taro, and Shizuo Akira. 2007a. "Signaling to NF-κB by Toll-like receptors." *Trends in Molecular Medicine* 13, no. 11 (November): 460–469.

———. 2007b. "TLR signaling." *Seminars in immunology* 19, no. 1 (February): 24–32.

Kayama, Hisako, and Kiyoshi Takeda. 2012. "Regulation of intestinal homeostasis by innate and adaptive immunity." *International Immunology* 24, no. 11 (November): 673–680.

Kim, Janice J, Md Sharif Shajib, Marcus M Manocha, and Waliul I Khan. 2012. "Investigating Intestinal Inflammation in DSS-induced Model of IBD." *Journal of Visualized Experiments,* no. 60: 1–6.

Kim, Kyoung-Mee, Peter Calabrese, Simon Tavaré, and Darryl Shibata. 2004. "Enhanced stem cell survival in familial adenomatous polyposis." *The American journal of pathology* 164, no. 4 (April): 1369–1377.

Kinnebrew, Melissa A, and Eric G Pamer. 2012. "Innate immune signaling in defense against intestinal microbes." *Immunological reviews* 245, no. 1 (January): 113–131.

Kretzschmar, Kai, and H Clevers. 2016. "Organoids: Modeling Development and the Stem Cell Niche in a Dish." *Developmental cell* 38, no. 6 (September): 590–600.

Kuhnert, Frank, Corrine R Davis, Hsiao-Ting Wang, Pauline Chu, Mark Lee, Jenny Yuan, Roel Nusse, and Calvin J Kuo. 2004. "Essential requirement for Wnt signaling in proliferation of adult small intestine and colon revealed by adenoviral expression of Dickkopf-1." *Proceedings of the National Academy of Sciences of the United States of America* 101, no. 1 (January): 266–271.

Lancaster, Madeline A, and Juergen A Knoblich. 2014. "Organogenesis in a dish: modeling development and disease using organoid technologies." *Science* 345, no. 6194 (July): 1247125.

Landskron, Glauben, Marjorie De la Fuente, Peti Thuwajit, Chanitra Thuwajit, and Marcela A Hermoso. 2014. "Chronic inflammation and cytokines in the tumor microenvironment." *Journal of Immunology Research* 2014 (2): 149185–19.

Lasry, Audrey, Adar Zinger, and Yinon Ben-Neriah. 2016. "Inflammatory networks underlying colorectal cancer." *Nature Immunology* 17, no. 3 (February): 230–240.

Lau, W de, W C Peng, P Gros, and Hans Clevers. 2014. "The R-spondin/Lgr5/Rnf43 module: regulator of Wnt signal strength." *Genes & development* 28, no. 4 (February): 305–316.

Laukoetter, Mike G, Porfirio Nava, Winston Y Lee, Eric A Severson, Christopher T Capaldo, Brian A Babbin, Ifor R Williams, et al. 2007. "JAM-A regulates permeability and inflammation in the intestine in vivo." *The Journal of experimental medicine* 204, no. 13 (December): 3067–3076.

Lee, Heehyoung, Andreas Herrmann, Jie-Hui Deng, Maciej Kujawski, Guilian Niu, Zhiwei Li, Steve Forman, Richard Jove, Drew M Pardoll, and Hua Yu. 2009. "Persistently Activated Stat3 Maintains Constitutive NF-κB Activity in Tumors." *Cancer Cell* 15, no. 4 (April): 283–293.

Lee, Li-Li Hu, Jose Gonzalez-Navajas, Geom Seog Seo, Carol Shen, Jonathan Brick, Scott Herdman, et al. 2010. "ERK activation drives intestinal tumorigenesis in Apcmin/+ mice." *Nature Medicine* 16, no. 6 (May): 665–670.

Leedham, S J, and N A Wright. 2008. "Expansion of a mutated clone: from stem cell to tumour." *Journal of clinical pathology* 61, no. 2 (February): 164–171.

Li, Lincoln Nadauld, Akifumi Ootani, David C Corney, Reetesh K Pai, Olivier Gevaert, Michael A Cantrell, et al. 2014. "Oncogenic transformation of diverse gastrointestinal tissues in primary organoid culture." *Nature Medicine* (May): 1–11.

Li, Jianbiao Zhou, Zhi-Rong Chen, and Wee Joo Chng. 2015. "p53 mutations in colorectal cancer- molecular pathogenesis and pharmacological reactivation." *World Journal of Gastroenterology : WJG* 21, no. 1 (January): 84–93.

Libermann, T A, and D Baltimore. 1990. "Activation of interleukin-6 gene expression through the NF-kappa B transcription factor." *Molecular and Cellular Biology* 10, no. 5 (May): 2327–2334.

Lindemans, Caroline A, Marco Calafiore, Anna M Mertelsmann, Margaret H O'Connor, Jarrod A Dudakov, Robert R Jenq, Enrico Velardi, et al. 2015. "Interleukin-22 promotes intestinal-stem-cell- mediated epithelial regeneration." *Nature* (December): 1–18.

Liu, Ze-Jun, Xin Lu, Yun Zhang, Shan Zhong, Shou-Zhi Gu, Xiao-Bing Zhang, Xin Yang, and Hai-Ming Xin. 2005. "Downregulated mRNA expression of ASPP and the hypermethylation of the 5'-untranslated region in cancer cell lines retaining wild-type p53." *FEBS letters* 579, no. 7 (March): 1587–1590.

López-Arribillaga, Erika, Verónica Rodilla, Luca Pellegrinet, Jordi Guiu, Mar Iglesias, Angel Carlos Roman, Susana Gutarra, et al. 2015. "Bmi1 regulates murine intestinal stem cell proliferation and self-renewal downstream of Notch." *Development (Cambridge, England)* 142, no. 1 (January): 41–50.

Lossos, Izidore S, Yasodha Natkunam, Ronald Levy, and Charles D Lopez. 2009. "Apoptosis Stimulating Protein of p53 (ASPP2) Expression Differs in Diffuse Large B-cell and Follicular Center Lymphoma: Correlation with Clinical Outcome." *Leukemia & lymphoma* 43, no. 12 (July): 2309–2317.

Lukovac, Sabina, Clara Belzer, Linette Pellis, Bart J Keijser, Willem M de Vos, Roy C Montijn, and Guus Roeselers. 2014. "Differential Modulation by Akkermansia muciniphila and Faecalibacterium prausnitzii of Host Peripheral Lipid Metabolism and Histone Acetylation in Mouse Gut Organoids." *MBio* 5, no. 4 (August): e01438–14–e01438–14.

Madison, Blair B, Katherine Braunstein, Erlene Kuizon, Kathleen Portman, Xiaotan T Qiao, and Deborah L Gumucio. 2005. "Epithelial hedgehog signals pattern the intestinal crypt-villus axis." *Development (Cambridge, England)* 132, no. 2 (January): 279–289.

Mah, Amanda T, Kelly Yan, and Calvin J Kuo. 2016. "Wnt pathway regulation of intestinal stem cells." *The Journal of physiology* 594, no. 17 (September): 4837–4847.

Maitra, Anirban, Kyle Molberg, Jorge Albores-Saavedra, and Guy Lindberg. 2000. "Loss of Dpc4 Expression in Colonic Adenocarcinomas Correlates with the Presence of Metastatic Disease." *The American journal of pathology* 157, no. 4 (October): 1105–1111.

Maloy, K J, and M C Kullberg. 2008. "IL-23 and Th17 cytokines in intestinal homeostasis." *Mucosal Immunology* 1, no. 5 (September): 339–349.

Markman, Ben, Francisco Javier Ramos, Jaume Capdevila, and Josep Tabernero. 2010. "Egfr and Kras in Colorectal Cancer." *Advances in Clinical Chemistry, Vol 51* 51:71–119.

Martinon, Fabio, Virginie Pétrilli, Annick Mayor, Aubry Tardivel, and Jürg Tschopp. 2006. "Gout-associated uric acid crystals activate the NALP3 inflammasome." *Nature* 440, no. 7081 (March): 237–241.

Massey, Dunecan C O, and Miles Parkes. 2007. "Genome-wide Association Scanning Highlights Two Autophagy Genes, ATG16L1 and IRGM, as Being Significantly Associated with Crohn's Disease." *Autophagy* 3, no. 6 (October): 649–651.

Matano, Mami, Shoichi Date, Mariko Shimokawa, Ai Takano, Masayuki Fujii, Yuki Ohta, Toshiaki Watanabe, Takanori Kanai, and Toshiro Sato. 2015. "Modeling colorectal cancer using CRISPR-Cas9-mediated engineering of human intestinal organoids." *Nature Medicine* 21, no. 3 (March): 256–262.

Medzhitov, Ruslan, Paula Preston-Hurlburt, Elizabeth Kopp, Andrew Stadlen, Chaoqun Chen, Sankar Ghosh, and Charles A Janeway Jr. 1998. "MyD88 Is an Adaptor Protein in the hToll/IL-1 Receptor Family Signaling Pathways." *Molecular Cell* 2, no. 2 (August): 253–258.

Miao, Hongming, Juanjuan Ou, Yuan Peng, Xuan Zhang, Yujuan Chen, Lijun Hao, Ganfeng Xie, et al. 2016. "Macrophage ABHD5 promotes colorectal cancer growth by suppressing spermidine production by SRM." *Nature Communications* 7:11716.

Miyaki, M, M Konishi, R Kikuchi-Yanoshita, M Enomoto, T Igari, K Tanaka, M Muraoka, H Takahashi, Y Amada, and M Fukayama. 1994. "Characteristics of somatic mutation of the adenomatous polyposis coli gene in colorectal tumors." *Cancer Research* 54, no. 11 (June): 3011–3020.

Mogensen, Trine H. 2009. "Pathogen recognition and inflammatory signaling in innate immune defenses." *Clinical Microbiology Reviews* 22, no. 2 (April): 240–273.

Moon, C, K L VanDussen, H Miyoshi, and T S Stappenbeck. 2014. "Development of a primary mouse intestinal epithelial cell monolayer culture system to evaluate factors that modulate IgA transcytosis." *Mucosal Immunology* 7, no. 4 (July): 818–828.

Morin, Patrice J, Andrew B Sparks, Vladimir Korinek, Nick Barker, H Clevers, Bert Vogelstein, and Kenneth W Kinzler. 1997. "Activation of β-Catenin-Tcf Signaling in Colon Cancer by Mutations in β-Catenin or APC." *Science* 275, no. 5307 (March): 1787–1790.

Moroishi, Toshiro, Carsten Gram Hansen, and Kun-Liang Guan. 2015. "The emerging roles of YAP and TAZ in cancer." *Nature reviews. Cancer* 15, no. 2 (February): 73–79.

Morrison, Sean J, and Allan C Spradling. 2008. "Stem Cells and Niches: Mechanisms That Promote Stem Cell Maintenance throughout Life." *Cell* 132, no. 4 (February): 598–611.

Mowat, Allan M, and William W Agace. 2014. "Regional specialization within the intestinal immune system." *Nature Reviews Immunology* 14, no. 10 (September): 667–685.

Müller, Mike F, Ashraf E K Ibrahim, and Mark J Arends. 2016. "Molecular pathological classification of colorectal cancer." *Virchows Archiv* (August): 1–10.

Mumm, J S, and R Kopan. 2000. "Notch signaling: from the outside in." *Developmental Biology* 228, no. 2 (December): 151–165.

Muñoz, Javier, Daniel E Stange, Arnout G Schepers, Marc van de Wetering, Bon-Kyoung Koo, Shalev Itzkovitz, Richard Volckmann, et al. 2012. "The Lgr5 intestinal stem cell signature: robust expression of proposed quiescent '+4' cell markers." *The EMBO journal* 31, no. 14 (July): 3079–3091.

Murillo-Garzón, Virginia, and Robert Kypta. 2017. "WNT signalling in prostate cancer." *Nature Publishing Group* 14, no. 11 (November): 683–696.

Nakamura, Tetsuya, Kiichiro Tsuchiya, and Mamoru Watanabe. 2007. "Crosstalk between Wnt and Notch signaling in intestinal epithelial cell fate decision." *Journal of Gastroenterology* 42, no. 9 (September): 705–710.

Nakayama, Masanori, Takaaki M Goto, Masayuki Sugimoto, Takashi Nishimura, Takafumi Shinagawa, Sigeo Ohno, Mutsuki Amano, and Kozo Kaibuchi. 2008. "Rho-Kinase Phosphorylates PAR-3 and Disrupts PAR Complex Formation." *Developmental cell* 14, no. 2 (February): 205–215.

Naumovski, Louie, and M L Cleary. 1996. "The p53-binding protein 53BP2 also interacts with Bc12 and impedes cell cycle progression at G2/M." *Molecular and Cellular Biology* 16, no. 7 (July): 3884–3892.

Nemoto, Yasuhiro, and Mamoru Watanabe. 2011. "The Th1, Th2, and Th17 Paradigm in Inflammatory Bowel Disease." In *Crohn's Disease and Ulcerative Colitis,* 183–194. Boston, MA: Springer US, November.

Nesic, D, L Buti, Xin Lu, and C E Stebbins. 2014. "Structure of the Helicobacter pylori CagA oncoprotein bound to the human tumor suppressor ASPP2." *Proceedings of the National Academy of Sciences of the United States of America* 111, no. 4 (January): 1562–1567.

Neufert, Clemens, Christoph Becker, and Markus F Neurath. 2007. "An inducible mouse model of colon carcinogenesis for the analysis of sporadic and inflammation-driven tumor progression." *Nature Protocols* 2, no. 8 (August): 1998–2004.

Nikoopour, Enayat, Stacey M Bellemore, and Bhagirath Singh. 2015. "IL-22, cell regeneration and autoimmunity." *Cytokine* 74, no. 1 (July): 35–42.

Nozaki, Kengo, Wakana Mochizuki, Yuka Matsumoto, Taichi Matsumoto, Masayoshi Fukuda, Tomohiro Mizutani, Mamoru Watanabe, and Tetsuya Nakamura. 2016. "Co-culture with intestinal epithelial organoids allows efficient expansion and motility analysis of intraepithelial lymphocytes." *Journal of Gastroenterology* (January): 1–8.

Nussinov, Ruth, Chung-Jung Tsai, Hyunbum Jang, Ruth Nussinov, Chung-Jung Tsai, and Hyunbum Jang. 2016. "Independent and core pathways in oncogenic KRAS signaling." *Expert Review of Proteomics* 13, no. 8 (July): 711–716.

O'Brien, J, I Wilson, T Orton, and F Pognan. 2000. "Investigation of the Alamar Blue (resazurin) fluorescent dye for the assessment of mammalian cell cytotoxicity." *European journal of biochemistry* 267, no. 17 (September): 5421–5426.

Okamoto, Ryuichi. 2011. "Epithelial regeneration in inflammatory bowel diseases." *Inflammation and Regeneration* 31 (3): 275–281.

Okayasu, Isao, Masahiro Yamada, Tetuo Mikami, Tsutomu Yoshida, Jun Kanno, and Toshifumi Ohkusa. 2002. "Dysplasia and carcinoma development in a repeated dextran sulfate sodium-induced colitis model." *Journal of Gastroenterology and Hepatology* 17, no. 10 (October): 1078–1083.

Owens, B M J, and A Simmons. 2013. "Intestinal stromal cells in mucosal immunity and homeostasis." *Mucosal Immunology* 6, no. 2 (March): 224–234.

Pabla, Baldeep. 2015. "Colon cancer and the epidermal growth factor receptor: Current treatment paradigms, the importance of diet, and the role of chemoprevention." *World Journal of Clinical Oncology* 6 (5): 133–10.

Pan, Qingfei, Xiaomin Lou, Ju Zhang, Yinghui Zhu, Fuqiang Li, Qiang Shan, Xianwei Chen, et al. 2017. "Genomic variants in mouse model induced by azoxymethane and dextran sodium sulfate improperly mimic human colorectal cancer." *Scientific Reports* 7, no. 1 (February): 950–12.

Petersen, O W, L Rønnov-Jessen, A R Howlett, and M J Bissell. 1992. "Interaction with basement membrane serves to rapidly distinguish growth and differentiation pattern of normal and malignant human breast epithelial cells." *Proceedings of the National Academy of Sciences of the United States of America* 89, no. 19 (October): 9064–9068.

Peterson, Lance W, and David Artis. 2014. "Intestinal epithelial cells: regulators of barrier function and immune homeostasis." *Nature Reviews Immunology* 14, no. 3 (March): 141–153.

Piccinini, A M, and K S Midwood. 2010. "DAMPening inflammation by modulating TLR signalling." *Mediators of Inflammation* 2010 (2): 1–21.

Pickert, Geethanjali, Clemens Neufert, Moritz Leppkes, Yan Zheng, Nadine Wittkopf, Moritz Warntjen, Hans-Anton Lehr, et al. 2009. "STAT3 links IL-22 signaling in intestinal epithelial cells to mucosal wound healing." *Journal of Experimental Medicine* 206, no. 7 (July): 1465–1472.

Pinto, Daniel, Alex Gregorieff, Harry Begthel, and H Clevers. 2003. "Canonical Wnt signals are essential for homeostasis of the intestinal epithelium." *Genes & development* 17, no. 14 (July): 1709–1713.

Podolsky. 1991. "Inflammatory bowel disease." *New England Journal of Medicine* 325 (14): 1008–1016.

———. 1999. "Mucosal Immunity and Inflammation V. Innate mechanisms of mucosal defense and repair: the best offense is a good defense." *AJP: Gastrointestinal and Liver Physiology* 277, no. 3 (September): G495–G499.

Powell, Anne E, Yang Wang, Yina Li, Emily J Poulin, Anna L Means, Mary K Washington, James N Higginbotham, et al. 2012. "The Pan-ErbB Negative Regulator Lrig1 Is an Intestinal Stem Cell Marker that Functions as a Tumor Suppressor." *Cell* 149, no. 1 (March): 146–158.

Powell, S M, N Zilz, Y Beazer-Barclay, T M Bryan, S R Hamilton, S N Thibodeau, B Vogelstein, and K W Kinzler. 1992. "APC mutations occur early during colorectal tumorigenesis." *Nature* 359, no. 6392 (September): 235–237.

Powell, I V Pinchuk, J I Saada, Xin Chen, and R C Mifflin. 2011. "Mesenchymal cells of the intestinal lamina propria." *Annual Review of Physiology* 73:213–237.

Qi, Zhen, Yehua Li, Bing Zhao, Chi Xu, Yuan Liu, Haonan Li, Bingjie Zhang, et al. 2017. "BMP restricts stemness of intestinal Lgr5(+) stem cells by directly suppressing their signature genes." *Nature Communications* 8 (January): 13824.

Rehfeld, J F. 1998. "The new biology of gastrointestinal hormones." *Physiological Reviews* 78, no. 4 (October): 1087–1108.

Roignot, Julie, Xiao Peng, and Keith Mostov. 2013. "Polarity in mammalian epithelial morphogenesis." *Cold Spring Harbor Perspectives in Biology* 5, no. 2 (February).

Rookmaaker, Maarten B, Frans Schutgens, Marianne C Verhaar, and H Clevers. 2015. "Development and application of human adult stem or progenitor cell organoids." *Nature Publishing Group* (July): 1–9.

Royer, C, and Xin Lu. 2011. "Epithelial cell polarity: a major gatekeeper against cancer?" *Cell death and differentiation* 18, no. 9 (September): 1470–1477.

Royer, Christophe, Sofia Koch, Xiao Qin, Jaroslav Zak, Ludovico Buti, Ewa Dudziec, Shan Zhong, Indrika Ratnayaka, Shankar Srinivas, and Xin Lu. 2014. "ASPP2 links the apical lateral polarity complex to the regulation of YAP activity in epithelial cells." *PLoS ONE* 9 (10): e111384.

Rubin, Deborah C, Anisa Shaker, and Marc S Levin. 2012. "Chronic intestinal inflammation: inflammatory bowel disease and colitis-associated colon cancer." *Frontiers in immunology* 3:107.

Sabio, Guadalupe, and Roger J Davis. 2014. "TNF and MAP kinase signalling pathways." *Seminars in immunology* 26, no. 3 (June): 237–245.

Sailaja, Badi Sri, Xi C He, and Linheng Li. 2016. "The regulatory niche of intestinal stem cells." *The Journal of physiology* 594, no. 17 (July): 4827–4836.

Samuels-Lev, Yardena, Daniel J O'Connor, Daniele Bergamaschi, Giuseppe Trigiante, Jung Kuang Hsieh, Shan Zhong, Isabelle Campargue, Louie Naumovski, Tim Crook, and Xin Lu. 2001. "ASPP proteins specifically stimulate the apoptotic function of p53." *Molecular Cell* 8, no. 4 (October): 781–794.

Sancho, Elena, Eduard Batlle, and H Clevers. 2004. "SIGNALING PATHWAYS IN INTESTINAL DEVELOPMENT AND CANCER." *Annual review of cell and developmental biology* 20, no. 1 (November): 695–723.

Sangiorgi, Eugenio, and Mario R Capecchi. 2008. "Bmi1 is expressed in vivo in intestinal stem cells." *Nature Genetics* 40, no. 7 (June): 915–920.

Sasaki, Nobuo, Norman Sachs, Kay Wiebrands, Saskia I J Ellenbroek, Arianna Fumagalli, Anna Lyubimova, Harry Begthel, et al. 2016. "Reg4 +deep crypt secretory cells function as epithelial niche for Lgr5 +stem cells in colon." *Proceedings of the National Academy of Sciences of the United States of America* 113, no. 37 (September): E5399–E5407.

Sasikumar, Roschen, John Raji Rejitha, Ponthananiyil Kumaran Binumon, and Muraleedharan Manoj. 2011. "Role of Heterozygous APC Mutation in Niche Succession and Initiation of Colorectal Cancer – A Computational Study." *PLoS ONE* 6, no. 8 (August): e22720–8.

Sato, Toshiro, Johan H van Es, Hugo J Snippert, Daniel E Stange, Robert G Vries, Maaike van den Born, Nick Barker, Noah F Shroyer, Marc van de Wetering, and H Clevers. 2011. "Paneth cells constitute the niche for Lgr5 stem cells in intestinal crypts." *Nature* 469, no. 7330 (January): 415–418.

Sato, Toshiro, D E Stange, M Ferrante, R G J Vries, J H van Es, S van den Brink, W J van Houdt, et al. 2011. "Long-term Expansion of Epithelial Organoids From Human Colon, Adenoma, Adenocarcinoma, and Barrett's Epithelium." *YGAST* 141, no. 5 (November): 1762–1772.

Sato, Toshiro, Robert G Vries, Hugo J Snippert, Marc van de Wetering, Nick Barker, Daniel E Stange, Johan H van Es, et al. 2009. "Single Lgr5 stem cells build crypt-villus structures in vitro without a mesenchymal niche." *Nature* 459, no. 7244 (May): 262–265.

Scheller, JUrgen, Athena Chalaris, Christoph Garbers, and Stefan Rose-John. 2011. "ADAM17: a molecular switch to control inflammation and tissue regeneration." *Trends in Immunology* 32, no. 8 (August): 380–387.

Schwank, Gerald, Bon-Kyoung Koo, Valentina Sasselli, Johanna F Dekkers, Inha Heo, Turan Demircan, Nobuo Sasaki, et al. 2013. "Functional Repair of CFTR by CRISPR/Cas9 in Intestinal Stem Cell Organoids of Cystic Fibrosis Patients." *Stem Cell* 13, no. 6 (December): 653–658.

Sedhom, Mamdouh A K, Mélanie Pichery, Jenna R Murdoch, Benoit Foligné, Nathalie Ortega, Sylvain Normand, Kirsten Mertz, et al. 2013. "Neutralisation of the interleukin-33/ST2 pathway ameliorates experimental colitis through enhancement of mucosal healing in mice." *Gut* 62, no. 12 (December): 1714–1723.

Segditsas, S, and I Tomlinson. 2006. "Colorectal cancer and genetic alterations in the Wnt pathway." *Oncogene* 25, no. 57 (December): 7531–7537.

Sgroi, D C, S Teng, G Robinson, R LeVangie, J R Hudson, and A G Elkahloun. 1999. "In vivo gene expression profile analysis of human breast cancer progression." *Cancer Research* 59, no. 22 (November): 5656–5661.

Shaked, Helena, Lorne J Hofseth, Alena Chumanevich, Alexander A Chumanevich, Jin Wang, Yinsheng Wang, Koji Taniguchi, et al. 2012. "Chronic epithelial NF-κB activation accelerates APC loss and intestinal tumor initiation through iNOS up-regulation." *Proceedings of the National Academy of Sciences* 109, no. 35 (August): 14007–14012.

Shakhov, A N, M A Collart, P Vassalli, S A Nedospasov, and C V Jongeneel. 1990. "Kappa B-type enhancers are involved in lipopolysaccharide-mediated transcriptional activation of the tumor necrosis factor alpha gene in primary macrophages." *Journal of Experimental Medicine* 171, no. 1 (January): 35–47.

Shevach, Ethan M. 2009. "Mechanisms of Foxp3+ T Regulatory Cell-Mediated Suppression." *Immunity* 30, no. 5 (May): 636–645.

Short, Sarah P, Patricia W Costacurta, and Christopher S Williams. 2017. "Using 3D Organoid Cultures to Model Intestinal Physiology and Colorectal Cancer." *Current Colorectal Cancer Reports* 13, no. 3 (June): 1–9.

Shyer, Amy E, Tyler R Huycke, ChangHee Lee, L Mahadevan, and Clifford J Tabin. 2015. "Bending Gradients: How the Intestinal Stem Cell Gets Its Home." *Cell* 161, no. 3 (April): 569–580.

Siegel, Rebecca L, Kimberly D Miller, Stacey A Fedewa, Dennis J Ahnen, Reinier G S Meester, Afsaneh Barzi, and Ahmedin Jemal. 2017. "Colorectal cancer statistics, 2017." *CA: A Cancer Journal for Clinicians* 67, no. 3 (May): 177–193.

Silhavy, Thomas J, Daniel Kahne, and Suzanne Walker. 2010. "The Bacterial Cell Envelope." *Cold Spring Harbor Perspectives in Biology* 2, no. 5 (May): a000414–a000414.

Simian, Marina, and Mina J Bissell. 2017. "Organoids: A historical perspective of thinking in three dimensions." *The Journal of Cell Biology* 216, no. 1 (January): 31–40.

Singer, A J, and R A Clark. 1999. "Cutaneous wound healing." *New England Journal of Medicine* 341, no. 10 (September): 738–746.

Slee, Elizabeth A, Huijun Zhu, Sek C Chow, Marion MacFarlane, Donald W Nicholson, and Gerald M Cohen. 1996. "Benzyloxycarbonyl-Val-Ala-Asp (OMe) fluoromethylketone (Z-VAD.FMK) inhibits apoptosis by blocking the processing of CPP32." *Biochemical Journal* 315, no. 1 (April): 21–24.

Smigiel, Kate S, Shivani Srivastava, J Michael Stolley, and Daniel J Campbell. 2014. "Regulatory T-cell homeostasis: steady-state maintenance and modulation during inflammation." *Immunological reviews* 259, no. 1 (April): 40–59.

Sottocornola, Roberta, Christophe Royer, Virginie Vives, Luca Tordella, Shan Zhong, Yihua Wang, Indrika Ratnayaka, et al. 2010. "ASPP2 Binds Par-3 and Controls the Polarity and Proliferation of Neural Progenitors during CNS Development." *Developmental cell* 19, no. 1 (July): 126–137.

Souza, Heitor S P de, and Claudio Fiocchi. 2016. "Immunopathogenesis of IBD: current state of the art." *Nature reviews. Gastroenterology & hepatology* 13, no. 1 (January): 13–27.

Spano, J P, C Lagorce, D Atlan, G Milano, J Domont, R Benamouzig, A Attar, et al. 2005. "Impact of EGFR expression on colorectal cancer patient prognosis and survival." *Annals of oncology : official journal of the European Society for Medical Oncology* 16, no. 1 (January): 102–108.

Specian, R D, and M G Oliver. 1991. "Functional biology of intestinal goblet cells." *The American journal of physiology* 260, no. 2 Pt 1 (February): C183–93.

Stadnyk, Andrew W. 2002. "Intestinal epithelial cells as a source of inflammatory cytokines and chemokines." *Canadian journal of gastroenterology = Journal canadien de gastroenterologie* 16, no. 4 (April): 241–246.

Stelzner, M, M Helmrath, J C Y Dunn, S J Henning, C W Houchen, C Kuo, J Lynch, et al. 2012. "A nomenclature for intestinal in vitro cultures." *AJP: Gastrointestinal and Liver Physiology* 302, no. 12 (June): G1359–G1363.

Stockhausen, M T, J Sjölund, C Manetopoulos, and H Axelson. 2005. "Effects of the histone deacetylase inhibitor valproic acid on Notch signalling in human neuroblastoma cells." *British journal of cancer* 92, no. 4 (February): 751–759.

Sullivan, A, and Xin Lu. 2007. "ASPP: a new family of oncogenes and tumour suppressor genes." *British journal of cancer* 96, no. 2 (January): 196–200.

Sun, Shao-Cong. 2017. "The non-canonical NF-κB pathway in immunity and inflammation." *Nature Reviews Immunology* 17, no. 9 (June): 545–558.

Suzuki, Y, M A Orellana, R D Schreiber, and J S Remington. 1988. "Interferon-gamma: the major mediator of resistance against Toxoplasma gondii." *Science* 240, no. 4851 (April): 516–518.

Tanaka, Takuji. 2009. "Colorectal carcinogenesis: Review of human and experimental animal studies." *Journal of Carcinogenesis* 8 (1): 5–20.

Taniguchi, Koji, Li-Wha Wu, Grivennikov, Petrus R de Jong, Ian Lian, Fa-Xing Yu, Kepeng Wang, et al. 2015. "A gp130-Src-YAP module links inflammation to epithelial regeneration." *Nature* (February): 1–19.

Tape, Christopher J. 2017. "The Heterocellular Emergence of Colorectal Cancer." *TRENDS in CANCER* 3, no. 2 (February): 79–88.

Tariq, Kanwal, and Kulsoom Ghias. 2016. "Colorectal cancer carcinogenesis: a review of mechanisms." *Cancer biology & medicine* 13, no. 1 (March): 120–135.

Taupin, Douglas, and Daniel K Podolsky. 2003. "Trefoil factors: initiators of mucosal healing." *Nature Reviews Molecular Cell Biology* 4, no. 9 (September): 721–732.

Terzic, Janos, Grivennikov, Eliad Karin, and Michael Karin. 2010. "Inflammation and colon cancer." *Gastroenterology* 138, no. 6 (June): 2101–2114.e5.

Thaker, Ameet I, Anisa Shaker, M Suprada Rao, and Matthew A Ciorba. 2012. "Modeling colitis-associated cancer with azoxymethane (AOM) and dextran sulfate sodium (DSS)." *Journal of Visualized Experiments,* no. 67 (September): e4100.

Tian, Aiguo, and Jin Jiang. 2014. "Intestinal epithelium-derived BMP controls stem cell self-renewal in Drosophila adult midgut." *eLife* 3 (March): 695–23.

Tian, Hua, Brian Biehs, Søren Warming, Kevin G Leong, Linda Rangell, Ophir D Klein, and Frederic J de Sauvage. 2011. "A reserve stem cell population in small intestine renders Lgr5-positive cells dispensable." *Nature* 478, no. 7368 (October): 255–259.

Tidow, Henning, Antonina Andreeva, Trevor J Rutherford, and Alan R Fersht. 2007. "Solution Structure of ASPP2 N-terminal Domain (N-ASPP2) Reveals a Ubiquitin-like Fold." *Journal of Molecular Biology* 371, no. 4 (August): 948–958.

Tordella, Luca, Sofia Koch, Victoria Salter, Anna Pagotto, Jessica B Doondeea, Stephan M Feller, Indrika Ratnayaka, et al. 2013. "ASPP2 suppresses squamous cell carcinoma via RelA/p65-mediated repression of p63." *Proceedings of the National Academy of Sciences of the United States of America* 110 (44): 17969–17974.

Trigiante, Giuseppe, and Xin Lu. 2006. "ASPPs and cancer." *Nature reviews. Cancer* 6, no. 3 (March): 217–226.

Turnquist, Casmir, Yihua Wang, David T Severson, Shan Zhong, Bin Sun, Jingyi Ma, Stefan N Constaninescu, et al. 2014. "STAT1-induced ASPP2 transcription identifies a link between neuroinflammation, cell polarity, and tumor suppression." *Proceedings of the National Academy of Sciences* 111, no. 27 (July): 9834–9839.

Ullman, Thomas A, and Steven H Itzkowitz. 2011. "Intestinal inflammation and cancer." *Gastroenterology* 140, no. 6 (May): 1807–1816.

Uronis, Joshua M, Marcus Mühlbauer, Hans H Herfarth, Tara C Rubinas, Gieira S Jones, and Christian Jobin. 2009. "Modulation of the Intestinal Microbiota Alters Colitis-Associated Colorectal Cancer Susceptibility." *PLoS ONE* 4, no. 6 (June): e6026.

Van Der Kraak, Lauren. 2015. "Colitis-associated colon cancer: Is it in your genes?" *World Journal of Gastroenterology* 21 (41): 11688–13.

VanDussen, Kelli L, Alexis J Carulli, Theresa M Keeley, Sanjeevkumar R Patel, Brent J Puthoff, Scott T Magness, Ivy T Tran, et al. 2012. "Notch signaling modulates proliferation and differentiation of intestinal crypt base columnar stem cells." *Development (Cambridge, England)* 139, no. 3 (February): 488–497.

Vanuytsel, Tim, Stefania Senger, Alessio Fasano, and Terez Shea-Donohue. 2013. "Major signaling pathways in intestinal stem cells." *Biochimica et biophysica acta* 1830, no. 2 (February): 2410–2426.

Vermeulen, Louis, and Hugo J Snippert. 2014. "Stem cell dynamics in homeostasis and cancer of the intestine." *Nature reviews. Cancer* 14, no. 7 (June): 468–480.

Vives, Virginie, Jian Su, Shan Zhong, Indrika Ratnayaka, Elizabeth Slee, Robert Goldin, and Xin Lu. 2006. "ASPP2 is a haploinsufficient tumor suppressor that cooperates with p53 to suppress tumor growth." *Genes & development* 20, no. 10 (May): 1262–1267.

Vogelstein, B, E R Fearon, S R Hamilton, S E Kern, A C Preisinger, M Leppert, Y Nakamura, R White, A M Smits, and J L Bos. 1988. "Genetic alterations during colorectal-tumor development." *New England Journal of Medicine* 319, no. 9 (September): 525–532.

Vousden, Karen H, and Xin Lu. 2002. "Live or let die: the cell's response to p53." *Nature reviews. Cancer* 2, no. 8 (August): 594–604.

Waldner, Maximilian J, and Markus F Neurath. 2015. "Mechanisms of Immune Signaling in Colitis-Associated Cancer." *Cellular and Molecular Gastroenterology and Hepatology* 1, no. 1 (January): 6–16.

Wang, Richard N, Jordan Green, Zhongliang Wang, Youlin Deng, Min Qiao, Michael Peabody, Qian Zhang, et al. 2014. "Bone Morphogenetic Protein (BMP) signaling in development and human diseases." *Genes & Diseases* 1, no. 1 (September): 87–105.

Wang, Yihua, Fangfang Bu, Christophe Royer, Sebastien Serres, James R Larkin, Manuel Sarmiento Soto, Nicola R Sibson, et al. 2014. "ASPP2 controls epithelial plasticity and inhibits metastasis through β-catenin-dependent regulation of ZEB1." *Nature Cell Biology* 16, no. 11 (November): 1092–1104.

Wang, Yihua, N Godin-Heymann, X Dan Wang, Daniele Bergamaschi, S Llanos, and Xin Lu. 2013. "ASPP1 and ASPP2 bind active RAS, potentiate RAS signalling and enhance p53 activity in cancer cells." *Cell death and differentiation* 20, no. 4 (April): 525–534.

Wang, Liming Sun, Lijing Su, Josep Rizo, Lei Liu, Li-Feng Wang, Fu-Sheng Wang, and Xiaodong Wang. 2014. "Mixed Lineage Kinase Domain-like Protein MLKL Causes Necrotic Membrane Disruption upon Phosphorylation by RIP3." *Molecular Cell* 54, no. 1 (April): 133–146.

Watson, Carey L, Maxime M Mahe, Jorge Múnera, Jonathan C Howell, Nambirajan Sundaram, Holly M Poling, Jamie I Schweitzer, et al. 2014. "An in vivo model of human small intestine using pluripotent stem cells." *Nature Medicine* 20, no. 11 (October): 1310–1314.

Weaver, Casey T, Robin D Hatton, Paul R Mangan, and Laurie E Harrington. 2007. "IL-17 family cytokines and the expanding diversity of effector T cell lineages." *Annual review of immunology* 25 (1): 821–852.

Weinberg, Robert. 2013. *The Biology of Cancer, Second Edition.* Garland Science, May.

Weiner, Leslie P. 2008. "Definitions and Criteria for Stem Cells." In *Neural Stem Cells,* 3–8. Totowa, NJ: Humana Press.

Wetering, Marc van de, Hayley E Francies, Joshua M Francis, Gergana Bounova, Francesco Iorio, Apollo Pronk, Winan van Houdt, et al. 2015. "Prospective Derivation of a Living Organoid Biobank of Colorectal Cancer Patients." *Cell* 161, no. 4 (May): 933–945.

Wirtz, Stefan, Clemens Neufert, Benno Weigmann, and Markus F Neurath. 2007. "Chemically induced mouse models of intestinal inflammation." *Nature Protocols* 2 (3): 541–546.

Wrana, J L. 2013. "Signaling by the TGF Superfamily." *Cold Spring Harbor Perspectives in Biology* 5, no. 10 (October): a011197–a011197.

Wullaert, Andy, Marion C Bonnet, and Manolis Pasparakis. 2010. "NF-κB in the regulation of epithelial homeostasis and inflammation." *Cell Research* 21, no. 1 (December): 146–158.

Xu, Yanfei, and Boris Pasche. 2007. "TGF-β signaling alterations and susceptibility to colorectal cancer." *Human Molecular Genetics* 16, no. R1 (April): R14–R20.

Xue, Xiang, and Yatrik M Shah. 2013. "In vitro organoid culture of primary mouse colon tumors." *Journal of Visualized Experiments,* no. 75: e50210.

Yan, Kelly, Luis A Chia, Li, Akifumi Ootani, James Su, Josephine Y Lee, Nan Su, et al. 2012. "The intestinal stem cell markers Bmi1 and Lgr5 identify two functionally distinct populations." *Proceedings of the National Academy of Sciences of the United States of America* 109 (2): 466–471.

Yan, Yutao, Vasantha Kolachala, Guillaume Dalmasso, Hang Nguyen, Hamed Laroui, Shanthi V Sitaraman, and Didier Merlin. 2009. "Temporal and Spatial Analysis of Clinical and Molecular Parameters in Dextran Sodium Sulfate Induced Colitis." *PLoS ONE* 4, no. 6 (June): e6073.

Yang, Jian-Ping, M Hori, T Sanda, and T Okamoto. 1999. "Identification of a novel inhibitor of nuclear factor-kappaB, RelA-associated inhibitor." *Journal of Biological Chemistry* 274, no. 22 (May): 15662–15670.

Yang, Jian-Ping, Mayumi Hori, Naoko Takahashi, Takumi Kawabe, Hiroyuki Kato, and Takashi Okamoto. 1999. "NF-κB subunit p65 binds to 53BP2 and inhibits cell death induced by 53BP2." *Oncogene* 18, no. 37 (September): 5177–5186.

Yang, Qi, N A Bermingham, M J Finegold, and H Y Zoghbi. 2001. "Requirement of Math1 for secretory cell lineage commitment in the mouse intestine." *Science* 294, no. 5549 (December): 2155–2158.

Yin, Xiaolei, Henner F Farin, Johan H van Es, H Clevers, Robert Langer, and Jeffrey M Karp. 2013. "Niche-independent high-purity cultures of Lgr5+ intestinal stem cells and their progeny." *Nature methods* 11, no. 1 (December): 106–112.

Young, Madeleine, and Karen R Reed. 2016. "Organoids as a Model for Colorectal Cancer." *Current Colorectal Cancer Reports* (August): 1–7.

Yu, Hua, Heehyoung Lee, Andreas Herrmann, Ralf Buettner, and Richard Jove. 2014. "Revisiting STAT3 signalling in cancer: new and unexpected biological functions." *Nature reviews. Cancer* 14, no. 11 (November): 736–746.

Yu, Hua, Drew Pardoll, and Richard Jove. 2009. "STATs in cancer inflammation and immunity: a leading role for STAT3." *Nature reviews. Cancer* 9, no. 11 (November): 798–809.

Zak, J, V Vives, D Szumska, A Vernet, J E Schneider, P Miller, E A Slee, et al. 2016. "ASPP2 deficiency causes features of 1q41q42 microdeletion syndrome." *Cell death and differentiation* 23, no. 12 (December): 1973–1984.

Zgheib, Carlos, Fouad A Zouein, Rony Chidiac, Mazen Kurdi, and George W Booz. 2012. "Calyculin A Reveals Serine/Threonine Phosphatase Protein Phosphatase 1 as a Regulatory Nodal Point in Canonical Signal Transducer and Activator of Transcription 3 Signaling of Human Microvascular Endothelial Cells." *Journal of Interferon & Cytokine Research* 32, no. 2 (February): 87–94.

Zhang, Yong-Guo, Shaoping Wu, Yinglin Xia, and Jun Sun. 2014. "Salmonella-infected crypt-derived intestinal organoid culture system for host-bacterial interactions." *Physiological Reports* 2, no. 9 (September): e12147.

Zhao, Bin, Li Li, Qunying Lei, and Kun-Liang Guan. 2010. "The Hippo-YAP pathway in organ size control and tumorigenesis: an updated version." *Genes & development* 24, no. 9 (May): 862–874.

Zhao, Bin, Xiaomu Wei, Weiquan Li, Ryan S Udan, Qian Yang, Joungmok Kim, Joe Xie, et al. 2007. "Inactivation of YAP oncoprotein by the Hippo pathway is involved in cell contact inhibition and tissue growth control." *Genes & development* 21, no. 21 (November): 2747–2761.

Zhao, Jian, Guobin Wu, Fangfang Bu, Bin Lu, Anmin Liang, Lei Cao, Xin Tong, Xin Lu, Mengchao Wu, and Yajun Guo. 2010. "Epigenetic silence of ankyrin-repeat–containing, SH3-domain–containing, and proline-rich-region–containing protein 1 (ASPP1) and ASPP2 genes promotes tumor growth in hepatitis B virus–positive hepatocellular carcinoma." *Hepatology* 51, no. 1 (January): 142–153.

Zhao, Karen Tumaneng, and Kun-Liang Guan. 2011. "The Hippo pathway in organ size control, tissue regeneration and stem cell self-renewal." *Nature Cell Biology* 13, no. 8 (August): 877–883.

Zhu, Jinfang, and William E Paul. 2008. "CD4 T cells: fates, functions, and faults." *Blood* 112, no. 5 (September): 1557–1569.